Nearshore Topography and Bather Risk

By Reinier Wessel Geerlof
May 2017

TU Delft

Nearshore Topography and Bather Risk

M.Sc. Thesis

Reinier Wessel Geerlof

April 2017

Delft University of Technology
Faculty of Civil Engineering and Geosciences
Department of Hydraulic Engineering

Graduation Committee

Prof. dr. ir. S.G.J. Aarninkhof	Delft University of Technology, Chair
Prof. dr. ir. A.J.H.M. Reniers	Delft University of Technology
dr. ir. M.A. de Schipper	Delft University of Technology
ir. M. Radermacher	Delft University of Technology

This thesis was handed in for assessment by the graduation committee on May 2nd 2017

This thesis was uploaded to the TU Delft Repository on May 2nd 2017

Cover picture: Sand Motor February 16th 2016, by Jurriaan Brobbel/Rijkswaterstaat

Acknowledgements

I would like to thank my parents for supporting me and believing in me, especially in times when I was ill and progress on my study was halted. Thank you for believing in me, even in times I no longer believed in myself.

Secondly I would like to thank Karel Karsen for his help in getting my study back on the road after a difficult period of illness. Thanks to everyone in the study planning support group.

Max, I would like to sincerely thank you for giving me the opportunity to graduate under your guidance. I would have never learned as much about programming and the subjects handled in this theses if it weren't for you. Thank you for always being available when I needed you. Thank you for all the input given in the process of my thesis study, during committee meetings and on this document.

I would like to thank Mathieu de Shipper for all his input during committee meetings and especially on the comprehensive feedback he gave on almost every document I wrote during my time at the department of Hydraulic Engineering. As a dyslectic student, all the input you gave was very welcome and the efforts much appreciated.

I would like to thank Ad Reniers for making time for me, especially during times when he was not able to work full-time. Thank you for all the input on my modelling work and for all the input on my thesis report.

I would like to thank Stefan Aarninkhof for chairing my graduation committee. Thank you for all your input during committee meetings and for all your positive feedback.

I would like to thank my 'colleague' thesis students from the 'Afstudeerkamer'. I would like to thank everyone who was, directly or indirectly, a part of the process of me thesis work.

Finally I would like to thank my girlfriend for being such a positive distraction.

Summary

This document describes a study into the influence of alongshore bathymetric variability on currents which form a risk to bathers. Changes to coastal zone management along the Delfland Coast have given rise to questions on the influence of alongshore bathymetric variability on bather risk.

Extensive measurement data is available from two measurement projects, mapping the entire Delfland Coast. This data has been used to study the presence and development of alongshore bathymetric variability along the Delfland Coast. Subtidal variability was found to generally increase during the winter months, in accordance with literature. In the intertidal area variability was found to decrease in the winter months. Both intertidal and subtidal variability were found to be relatively low near the breakwater at Hoek van Holland. The range in measured variability along the Sand Motor was found to be very wide.

Using a parameterization of the alongshore variability, subsections of the Delfland Coast have been selected for a modelling study. Artificial bathymetries have been created, using the selected measurement data. These artificial bathymetries have been used as the basis of numerical models. These have been forced with linearized wave conditions, in order to investigate the relation between different levels of alongshore bathymetric variability and wave induced currents which might form a risk to bathers.

Good correlations were found between the alongshore variability and the wave induced currents, especially for the intertidal area. Alongshore bathymetric variability seems to be an important factor in generating wave induced currents which might form a risk to bathers. In order to be able to fully assess the influence of the bathymetry on such nearshore currents, the influence of the depth of the variable bar patterns, the distance between the subtidal bar and the intertidal bar and the phase differences between the subtidal and the intertidal bar need to be investigated further.

Content

ACKNOWLEDGEMENTS **V**

SUMMARY **VII**

1. INTRODUCTION **1**

1.1 The Delfland Coast 1
1.2 Coastal Zone Management and Alongshore Bathymetric Variability 2
1.3 Alongshore Variability and Swimmer Safety 3
1.3.1 Alongshore Variability and Rip Currents 4
1.3.2 Alongshore Variability and Bather Risk 4
1.4 Research Questions 7
1.5 Thesis Outline 7

2. METHODOLOGY DATA ANALYSIS **8**

2.1 Definition Alongshore Variability 8
2.2 Data Set 8
2.2.1 Interpolation 9
2.3 Quantifying Alongshore Bathymetric Variability 9
2.3.1 Alongshore Straightened Bathymetry 9
2.3.2 Alongshore Running Average Bathymetry 11
2.3.3 Difference Bathymetry 12
2.3.4 Local Alongshore Bathymetric Variability 13
2.3.5 Bulk Alongshore Variability 13
2.4 Conclusions Methodology Data Analysis 15

3. RESULTS DATA ANALYSIS **16**

3.1 Subtidal Zone 16
3.1.1 Time Stack of the Subtidal Bulk Alongshore Bathymetric Variability 16
3.1.2 Examples of Subtidal Alongshore Bathymetric Variability 17
3.1.3 Evolution of the Subtidal Alongshore Bathymetric Variability 21
3.2 Intertidal Zone 23
3.2.1 Time Stack of the Intertidal Bulk Alongshore Bathymetric Variability 23
3.2.2 Examples of Intertidal Alongshore Bathymetric Variability 24
3.2.3 Evolution of the Intertidal Alongshore Bathymetric Variability 27
3.2.4 The Influence of Groins 29
3.3 Spatiotemporal Relations in the Data 31
3.3.1 The Development of Alongshore Bathymetric Variability in Time 31
3.3.2 Trends of Alongshore Bathymetric Variability in Space 34
3.4 Reliability 38
3.5 Conclusions Data Analysis 38

4. METHODOLOGY MODELLING STUDY **39**

4.1 Model setup 39
4.1.1 Model bathymetry 39
4.1.2 Computational grid 41
4.1.3 Boundary conditions 42
4.1.4 Initial conditions 44
4.2 Validation 44
4.3 Calibration 44
4.4 Conclusions Methodology Model Study 45

5. RESULTS MODELLING STUDY **46**
5.1 OUTPUT ANALYSIS 46
5.2 CORRELATION STUDY 48
5.2.1 Velocity correlation *49*
5.2.2 Rip length correlation *64*
5.2.3 Correlation roller forces and bathymetry *70*
5.3 CONCLUSIONS MODELLING STUDY 71
6. DISCUSSION **73**
7. GENERAL CONCLUSIONS **75**
7.1 RECOMMENDATIONS 77
REFERENCES **78**
APPENDIX A1: INTERPOLATION- AND MEASUREMENT ERROR **81**
INTERPOLATION ERROR 81
Suggestion on Sand Motor Measurement Plan *82*
MEASUREMENT ERROR 83
APPENDIX A2: RUNNING AVERAGE LENGTH SCALES **85**
INTERTIDAL LENGTH SCALES 85
SUBTIDAL AREA 86
APPENDIX A3: COMPARING ACTUAL BATHYMETRY **87**
APPENDIX B1: MODEL BATHYMETRIES **100**

1. Introduction

This document is a Master thesis report, which tries to unveil the relation between bathymetric variability, and nearshore currents which form a risk to bathers along the Delfland Coast. If you do not have a clue as to what this actually means; do not despair. This introduction will explain what this first sentence actually means.

Starting off, this introduction will familiarise the reader with the Delfland Coast, and some of the man made the changes in this area, which made the coast looks the way it does today. After this an insight will be given into how these changes can affect bather risk. This section can be seen as both a general introduction to the problem of bathymetrically controlled rips for more general readers, as well as a literary review, in which the thesis student shows his mastery of the background knowledge of his thesis research.

1.1 The Delfland Coast

The Delfland Coast is a 18km long subsection of the Holland coast, separating the Netherlands from the North Sea. The Delfland coast starts at the breakwater, which protects the entrance to the Rotterdam harbour in the south, to the breakwater of the Scheveningen harbour (Near The Hague) in the north. This section of coastline is indicated by the blue colour in Figure 1.

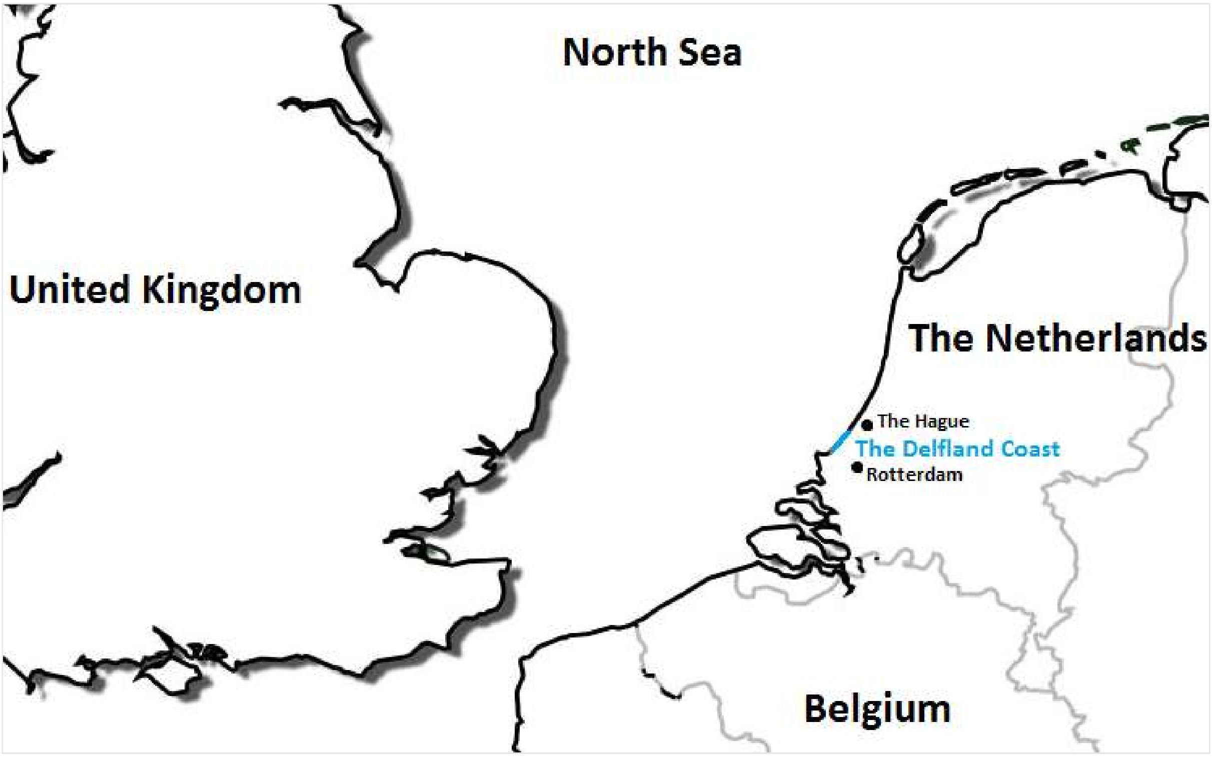

Figure 1: Southern North Sea basin, and the location of the Delfland Coast (Source: www.Freeworldmaps.net)

For the Dutch, the coastal area is more than an attractive recreational area. The coast, and in particular the dunes, also forms a crucial line of protection for the low-lying hinterland, against the destructive forces of the North Sea, and the elements. Since the eighteenth century, the Dutch have made efforts to protect this section of their sea defence against coastal erosion: a process which causes the coastline to recede inland, and the dunes to eventually disappear. This has resulted in the construction of the 'Delflandse Hoofden': coastal groins. These are small breakwaters of natural rock, which extend from the coastline out into sea, as can be seen in the left window of Figure 2.

In recent decades a new philosophy on coastal zone management has been developed in the Netherlands. The new idea was to no longer fix the position of the coastline with hard structures, such as coastal groins, dikes and seawalls, but to make sure that the coastal zone was nourished with enough sand, so as to counteract the effects of erosion, and to allow mother nature to do the rest.

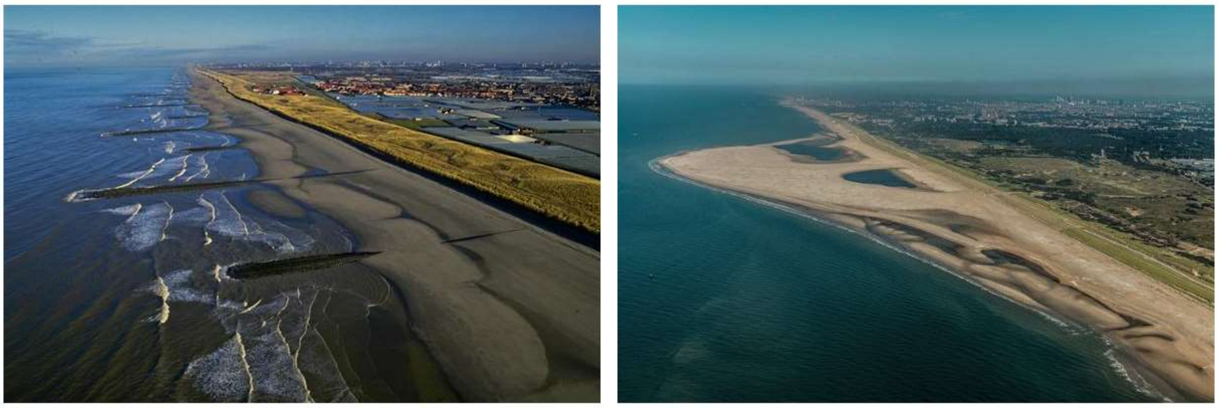

Figure 2: Development of coastal zone management along the Delfland Coast. The left window shows the old coastal groins (Delflanse Hoofden). The right window Shows the most modern iteration in beach nourishments: the Sand Motor. Both pictures are made near the village of Monster in 1993, and 2012 respectively. (Source: www.beeldbank.rws.nl)

The latest iteration of this nourishment philosophy are mega scale nourishments. The first of which is the Sand Motor, which can be seen in the right window of Figure 2 and in Figure 3. This nourishment was realised in 2011, essentially creating a peninsula by dumping 21Mm^3 of sand in front of the coast. The idea is to allow the tide, the waves and the wind to redistribute this sand along the Delfland Coast, bringing with it all sorts of ecological advantages.

Figure 3: The Delfland Coast with the Sand Motor in August 2014 (Source: Google Earth). The entrance to the Rotterdam harbour can be seen on the left, the Scheveningen harbour can be seen on the right. North is in the top right corner in the main picture.

1.2 Coastal Zone Management and Alongshore Bathymetric Variability

This change in coastal zone management has changed the way the Delfland Coast looks. The most obvious change is the fact that the coastline is no longer straight. It now has a wave like protrusion into the North Sea; the Sand Motor. The shape of the Sand Motor is constantly changing. Just after completion, the Sand Motor extended a kilometre out into the sea, and was two kilometres wide. Since than the overall shape has been diffusing; growing less pronounced, and ever wider. This process is a subject of ongoing study (Kaji [2013], de Schipper et al. [2016]).

Moving away from the use of hard structures, and toward ‘soft’ sand nourishments has other implications too. The groins stopped coastal erosion by reorientation the coastline to the dominant wave direction, stopping the alongshore transport of sediment. The new philosophy has liberated the sand, allowing it to freely migrate, and reshape the Dutch coast. This has caused the sand bars in the intertidal area in particular (the part of the coast which is submerged during flood, and which falls dry during ebb) to change radically. This new, dynamic situation brings with it new risks to bathers, and can be a challenge to lifeguards (de Zeeuw [2011]).

Research has shown that both the intertidal sand bars, as well as the subtidal sandbars (bars which are always submerged) also react directly to (shore face) nourishments. Research for different areas along the Dutch coast have shown different reactions to nourishments, with regard to the alongshore variability. For different locations the alongshore variability has been seen to increase (Grunnet and Ruessink [2005]), or not to be significantly affected (Ruessink et al. [2012]) by the presence of a nourishment.

Alongshore variability is the extent to which the bathymetry, the bottom topography, is different from the bathymetry directly to the right and left. For instance, at one location there might be a rip channel. Directly to the right and left of this channel are sand bars. In this example the deeper channel, forms a discontinuation of the more shallow bar. The channel is therefore a source of alongshore bathymetric variability. An example of such alongshore variably bathymetry is shown in Figure 4.

Figure 4: A picture of the coast north of Scheveningen in 2011. The intertidal bar is disrupted by several rip channels (Dutch: muien), and at several locations the bar has welded to shore filling in the bar trough (Dutch: zwin). This is an example of alongshore bathymetric variability. (Source: www.beeldbank.rws.nl)

Typical length scales for alongshore bathymetric variability along the Dutch coast are 1000m for subtidal bars and 200m for intertidal bars (Short [1991], Ruessink et al. [2012], van Enkevort and Ruessink [2003]).

1.3 Alongshore Variability and Swimmer Safety

Currents along the coast are the result of the interaction of the tide, the waves, the wind, and the bathymetry. So changes to the nearshore bathymetry cause changes to the currents in the nearshore area. The new shape of the coastline at the Sand Motor is related to several new flow patterns, previously unseen along the Delfland Coast (Radermacher [2017], Schlooz [2012]). These form a potential threat to bathers, but only locally at the Sand Motor. The focus of this study is the effect of the variability in the sand bars on rip currents. These sand bars have changed due to the modern coastal zone management approach along the entire Delfland Coast.

1.3.1 Alongshore Variability and Rip Currents

Rip currents are forced by alongshore variations in wave induced momentum flux, known in literature as radiation stress (Longuet-Higgins and Stewart [1964]), which result from alongshore variations in wave height. In short, these radiation stresses cause a set down in the water level outside the surf zone, due to the increase in wave height due to shoaling (a process by which waves grow higher due to interaction with the sea bed), and cause a set up in the water level inside the surf zone, due to the decrease in wave height caused by wave breaking. If there is no alongshore variation in the wave height (forcing), then the pressure gradient between inside and outside of the surf zone will induce an offshore-directed flow along the bed, called undertow.

In cases where there are alongshore variations in the wave height, there will be alongshore variations in this radiation stress, and alongshore water level (pressure) gradients. Outside the surf zone, the alongshore gradient in the water level, and the alongshore gradient in radiation stress are in balance. Inside the surf zone, however, these alongshore gradients work in the same direction. This causes a convergence of alongshore flow toward areas with lower waves, where the flow is directed out to sea, and exits the surf zone as a confined rip current (MacMahan et al. [2006]).

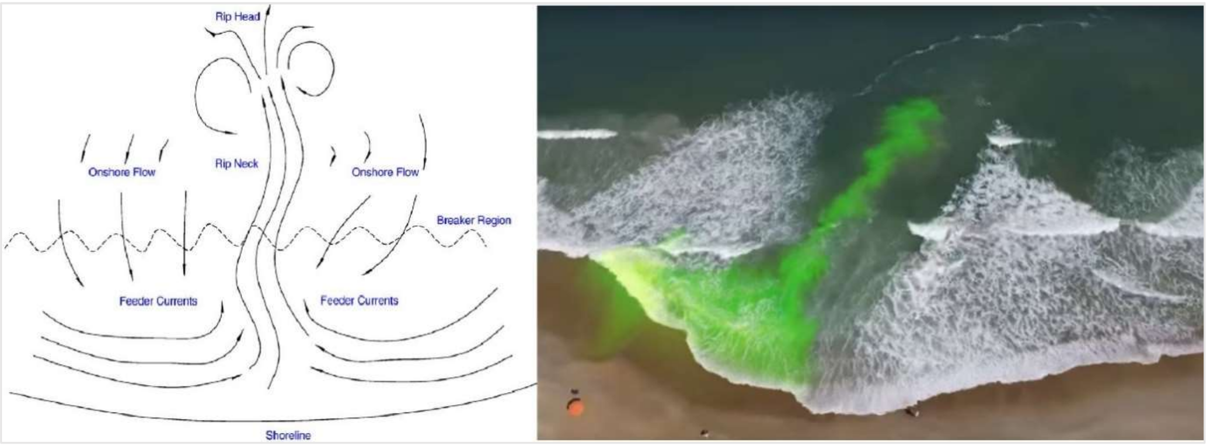

Figure 5: Bathymetrically controlled rip. Left window shows a schematization of a rip current (source: MacMahan [2006]). The right window shows green dye which has been released at the shoreline, and carried offshore by the rip current (source: www.youtube.com)

Figure 5 shows a schematization of a bathymetrically controlled rip in the left window. Incoming waves shoal as they move toward the relatively shallow bars, and finally break over the bars, forming rollers at the surface. These rollers act as an additional shear stress on the surface of the water in the surf zone, increasing the water level (pressure) gradients. The waves moving toward the deeper rip channel do not shoal, and remain stable. This causes feeder currents, which converge at the location of the rip channel, and flow out as a rip current.

The right window in Figure 5 shows white patches (the rollers) where the waves are breaking over the bars. Green dye, released near shore, is carried offshore by the rip current, revealing the location of the rip channel beneath.

1.3.2 Alongshore Variability and Bather Risk

Wright and Short [1984] classified these variable bar patterns as so called beach states. The more variable a beach state is, the stronger the bathymetrically controlled rip currents become. So, according to this classification system, the non-variable longshore bar and trough induce no rip currents, and the highly variable transverse bars and rips produce the strongest rip currents. An overview of these beach states can be found in Figure 6.

Wright and Short [1984] also found a direct relation between the incoming wave signal and the current beach state. High incoming wave energy, in particular when combined with fine graded sediment is associated with the dissipative extreme, whereas the reflective extreme is often associated with low-energy conditions, low-steepness (stable) waves and coarsely graded sediments. For more intermediate conditions, the bars tend to alternate between the highly variable intermediate bas states. This direct relation between the incoming wave signal and beach states, allowed Short and Hogan [1994] to come to a practical scheme for judging the safety for bathers at Australian beaches.

There are, however, a few problems with the classification as presented by Wright and Short [1984]. For the Dutch coast, the relation between the incoming wave signal, and the development in alongshore variability seems to be less direct. The development of variability also seems to be different. Increasing variability has in fact been associated with energetic storm events (de Schipper et al. [2013]), which is in direct opposition to the Wright and Short model. Next to that, the Dutch near shore area is defined by a system of multiple bars, rather than just one. Also, the classification system, using visual observation of bar states, is rather heuristic (Tan [2014]). This means that two different engineers, assessing the same beach, could come to different conclusions for the risks to bathers, according to the assessment scheme, presented by Short and Hogan [1994].

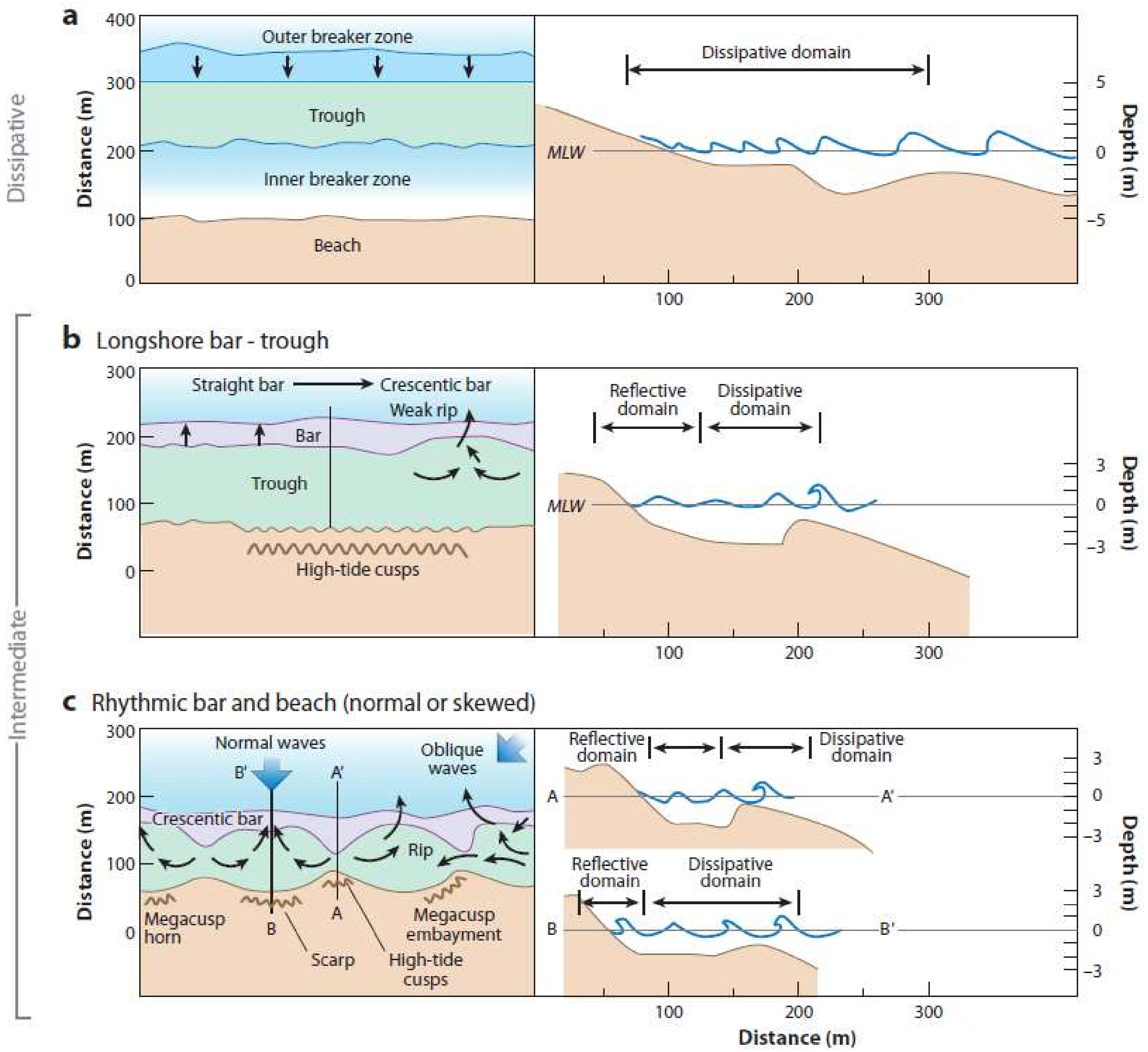

Figure 6: Beach states according to Wright and Short [1984], continues on next page (Source: Dalrymple et al. [2011])

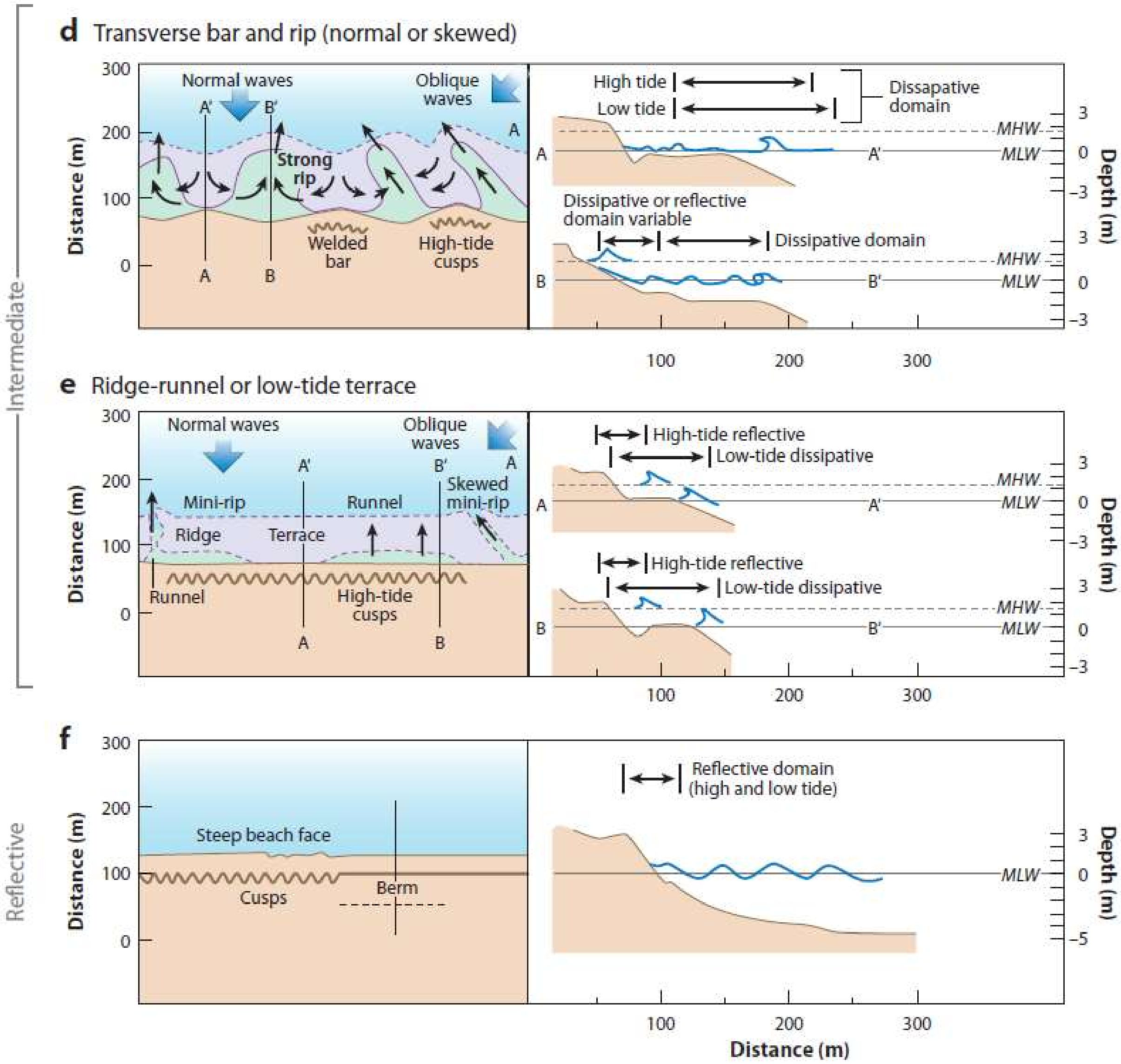

Figure 6 continued

The need for less heuristic, and more quantitative ways of assessing bathymetric variability has given rise to many mathematically sound judgement schemes (Tan [2014], de Schipper et al. [2013], and many others). Which begs the question: Can such a scheme be developed, in such a way that the potential risk to bathers along the Dutch coast, can be judged directly from this variability parameter? And since the new 'soft' nourishment philosophy on coastal zone management is known to affect the bathymetric variability along the Dutch coast, yet another question arises: Can such a scheme be used to quantify the effects of nourishment measures, such as the Sand Motor, to bather risk along the Delfland Coast? These questions are the main focus of this thesis.

The relevance of these questions is shown by the work of de Zeeuw [2011]. This work investigated both the new risks to bathers on nourished beaches, as well as the new challenges for lifeguards in doing their job. These questions become even more relevant in the light of recent media statements from the Dutch life brigade. In recent years they have seen a steady increase in the number of rescue operations, and more worryingly, a rise in the number of fatalities, related to a bathing accidents. In the summer of 2016, thirteen bathers lost their lives in waters guarded by the Dutch life brigade. These are not only coastal waters. And the Dutch life brigade makes no assumptions on the influence of coastal zone management on this trend. Rather, they see the decline in swimming ability as a main culprit. However, in the light of these numbers, it is now more relevant than ever, to assess the influence of the bathymetry on bather risk. And, in doing so, to see how we as engineers can be of help in this complex problem.

1.4 Research Questions

The main research questions which will be answered in this thesis report are the following:

1. Can a parameter be constructed, which is representative of the alongshore bathymetric variability along subsections of the Delfland Coast?
2. How does the alongshore bathymetric variability of the Delfland Coast develop during the studied period?
3. How can the (parameterized) alongshore variability be related to currents which form a risk to bathers?
4. Is the alongshore bathymetric variability an important indicator for nearshore currents which form a risk to bathers?

1.5 Thesis Outline

The first chapter has explained the background of this study. It described the research area, the Delfland Coast, and gave theoretical background on bathymetrically controlled rip currents. The upcoming chapters will take the reader through the analysis of nearshore bathymetry data, and a numerical modelling study, to conclusions on the relation between alongshore bathymetric variability and wave induced currents which form a risk to bathers. Each chapter will start with stating its goal and the main research question(s) that will be answered in that particular chapter.

The second chapter will explain the method used to investigate a data set of bathymetric measurements of the Delfland Coast.

The third chapter discusses the results of applying the method of chapter two to the measurement data set. Individual examples of (non-)variable bars will be shown, and subsequently general trends in the data will be discussed. Finally relations between the alongshore bathymetric variability and other parameters, such as the coastal orientation, will be investigated.

The fourth chapter discusses the method of the modelling study used to investigate the relation between the alongshore bathymetric variability and wave induced currents which can form a risk to bathers.

The fifth chapter discusses the results of the modelling study. Correlations are presented for the relation between intertidal- and subtidal alongshore bathymetric variability and the rip current velocity and rip current length. Subsequently causal relations for these statistical correlations are investigated using individual examples from the modelling data set. This chapter finishes by drawing conclusions on the relation between alongshore bathymetric variability and rip currents.

The discussion in chapter six will discuss the limits of the methods described in this document.

Chapter seven presents the general conclusions and recommendations.

2. Methodology Data Analysis

The objective of this section is to explain the scheme which has been used to quantitatively assess the alongshore bathymetric variability in the measured nearshore morphology of de Defland Coast. This is done not by looking at crest height, trough depth and other morphometric parameters, but by quantifying the alongshore bathymetric variability in both the intertidal- and subtidal zone separately. Finally an bulk parameter for the alongshore bathymetric variability is defined for 400m sections of coastline, which can be used to further understand the development of alongshore variability along the Delfland Coast. In Chapters 4 and 5 this bulk parameter will be used to select sections of nearshore bathymetry which are interesting for the modelling case study presented in chapters 4 and 5.

The main research question which will be answered in this chapter is research question one:

Can a parameter be constructed, which is representative of the alongshore bathymetric variability along subsections of the Delfland Coast?

2.1 Definition Alongshore Variability

The most general definition for the alongshore bathymetric variability is the degree to which the bed level at a certain location along the coast differs from the bed level directly left and right of this section. The definition of alongshore variability used in this document is analogous to de Schipper et al. [2013] and Tan [2014]: Alongshore variability is the deviation in bed level from an alongshore running average topography. This alongshore running average topography has been constructed by averaging the bed level at a certain cross-shore position, over a certain alongshore distance.

What this basically means is that a long, continuous, linear longshore bar will generate no alongshore variability, as the bed level at any cross-shore position does not change over a long alongshore length scale. Longshore bars which are interrupted by rip channels, rhythmic bars, transverse bars, etc. will generate varying amounts of alongshore variability. Note that the bar crest is not the only source of alongshore variability. Variation in the cross-shore position, depth and overall shape of the trough can also generates alongshore variability, as well as sudden variations of the coastal slope (visible at the Sand Motor in early stages of its development).

2.2 Data Set

Some steps of the method presented here concern issues related specifically to (the measurement dataset of) the Delfland Coast. Therefor this paragraph will introduce the reader to the dataset of bathymetric measurements of the Delfland Coast. The results of applying the method discussed in the upcoming paragraphs to this data set are discussed in chapter 3.

The bathymetric data used here, consists of RTK-DGPS measurements recorded for two different measurement projects. The first project handles data recorded in a measurement domain containing only the Sand Motor. Field measurements where recorded at least every month from August 2011 until July 2012. From then on measurements where recorded at least every two months. The second project, known as NeMo, handles data recorded in a measurement domain containing the entire coast and nearshore area in between the breakwater at Hoek van Holland and Scheveningen Harbour, except for the Sand Motor measurement domain. The NeMo project data of March 2012 has been made available, as well as bi-monthly data spanning the period of March 2013 to June 2015. Together these two projects map the entire Delfland Coast.

The data of both projects has been recorded using three methods. The subaqueous topography has been recorded using a Personal Water Craft (more commonly known as a jet ski) equipped with an echo sounder and a RTK-DGPS receiver. This measurement method leads to measurement errors in the order of 0.1m (van Son et al. [2009]). The subaerial topography has been recorder using a four wheel drive vehicle (more commonly known as a quadbike) equipped with a RTK-DGPS receiver. Finally, hard to access areas where measured using a GPS rolling-construction, basically a wheelbarrow equipped with a RTK-DGPS receiver. Performing the measurements using these methods usually takes about three to five days for the entire domain.

2.2.1 Interpolation

The measured data points have been interpolated to a regularly spaced 10m by 10m grid by means of linear interpolation. Along most of the Delfland Coast the original survey-tracks are mainly cross shore directed. In the Sand Motor measurement area a more complex measurement plan has been implemented, which involves a lot of intersecting alongshore- and cross shore directed survey-tracks. It has been found that this causes significant interpolation artefacts, especially in the intertidal area.

This issue has been addressed by subsampling the data before interpolation. Subsampling over a length scale slightly shorter than the distance between measurement cross-sections, results in a less dense point cloud, which looks more like a random scatter of data points. This solves the issues with interpolation artefacts without negatively affecting the resolution of the interpolated results, as the measurement cross-section spacing is leading in determining the level of detail of the interpolated results.

For more in depth information on the interpolations issues, and the solution to this problem can be found in appendix A1.

2.3 Quantifying Alongshore Bathymetric Variability

In order to extract the alongshore variability from the data set, a MATLAB algorithm has been written which handles the data in five steps, finally resulting in time stacks of the bulk alongshore variability for both the intertidal- and subtidal zones. This paragraph will discuss these steps in detail, so as to shed light on the how and why each step is taken.

The alongshore variability has been quantified in the following five steps:

1. Convert the curvy coastal bathymetry of the data set into an alongshore straightened coast
2. Determine an alongshore running average bathymetry for this alongshore straightened coast
3. Calculate the difference bathymetry by subtracting step 2 from step 1
4. Calculate the local alongshore variability by taking the absolute values of step 3
5. Isolate the intertidal- and subtidal zones, and calculate the bulk alongshore variability for both zones for sections of 400m

2.3.1 Alongshore Straightened Bathymetry

In quantifying the alongshore variability of the nearshore area, one is primarily interested in the comparing patterns in the sand bars to their direct neighbours left and right. Given the extreme curves in the measured coastline, especially around the Sand Motor, it is helpful to first obtain a different perspective on the bathymetric data. One which follows these curves in the coastline; the alongshore straightened bathymetry. This allows the algorithm to handle the data with greater ease.

Before generating the alongshore straightened bathymetry, all data points above +2.5m NAP and below -7m NAP have been removed so as to discard the dry beach and deep subtidal zones respectively. Data points concerning the Sand Motor dune lake and lagoon have also been disregarded, as well as the ‘North side’ of the Sand Motor before December 2011, the period when the spit had not developed yet. In doing so, only the nearshore bathymetric data was taken into account.

In order to extract an alongshore straightened bathymetry from this data, one must first obtain the macro scale shape of the Delfland Coast. This has been done by selecting an arbitrary depth contour, which follows all the macro scale curves of the coastline, and smoothing it over a certain length scale, so as to remove all small scale wiggles. After assessing the performance of different depth contours, it has been determined that for this data set the -1m NAP contour, smoothed over 300m, is an ideal candidate as it follows the macro scale shape of the Delfland Coast, without any cuts or any significant undulations on shorter length scales.

It is important to note that, as the Sand Motor changes shape, this smoothed contour line becomes shorter. In order to be able to compare the bulk alongshore variability from different measurements points on the smoothed contour line are paired to a reference line, and the alongshore distance has been set at zero at an arbitrary point near the tip. Coordinates of this point are [72538, 452791], in the Dutch RD (Rijksdriehoeksmeting) coordinate system. The result of this exercise is shown in Figure 7. for the measurement data of June 2015.

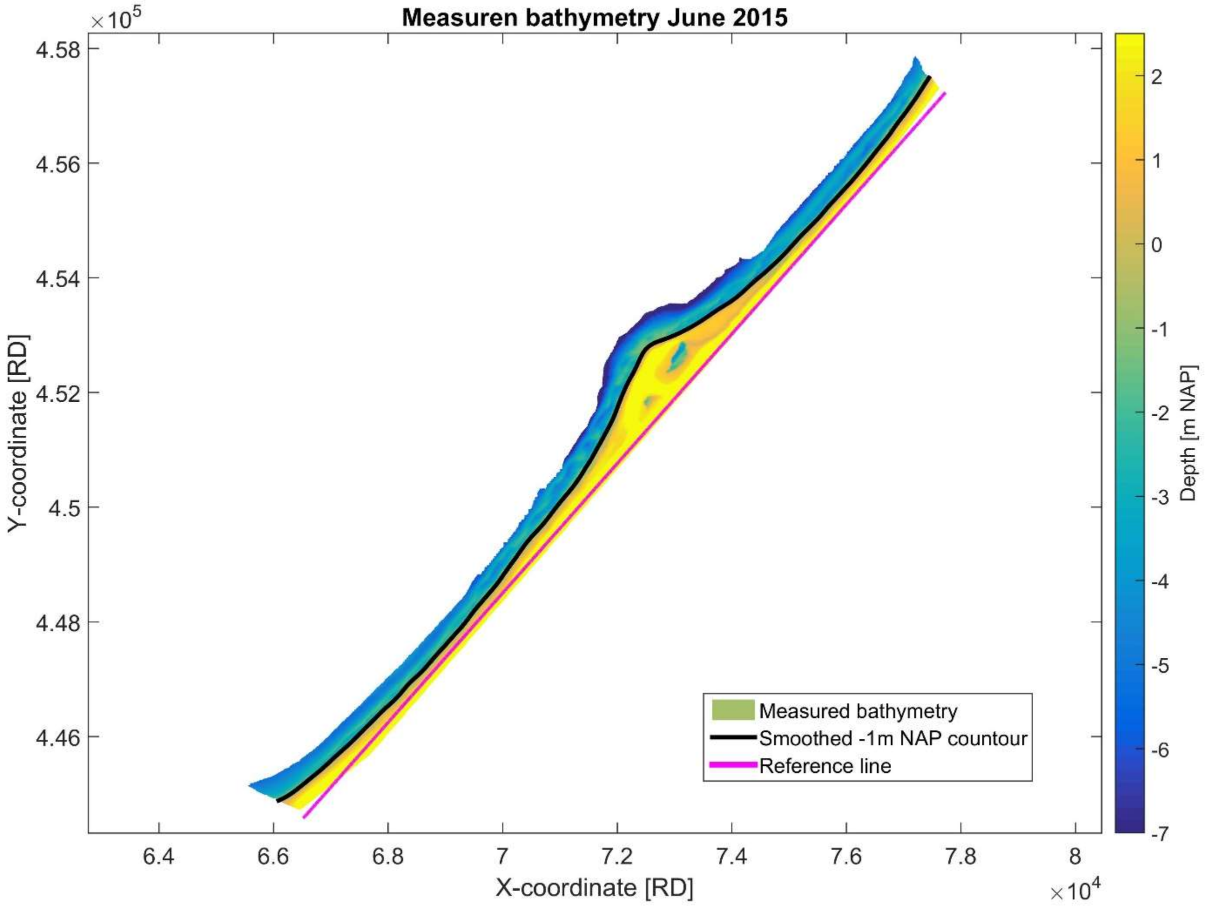

Figure 7: Measurement data for June 2015, the smoothed -1m NAP contour for the alongshore straightened bathymetry (black) and the reference line (purple)

In order to extract the alongshore straightened bathymetry, cross sections have been generated every ten meters along the smoothed contour, perpendicular to the smoothed contour. They extend 400m in shoreward direction and 500m in seaward direction. These cross sections are shown in Figure 8. Finally the bed level z_b is logged every two meters in each cross section. The points on the cross sections now effectively form a matrix of bathymetric data points, which can be plotted (and handled) as one matrix of data points. Such a plot is shown in the upper window of Figure 9 (see page 12) for the June 2015 data. This is the alongshore straightened bathymetry.

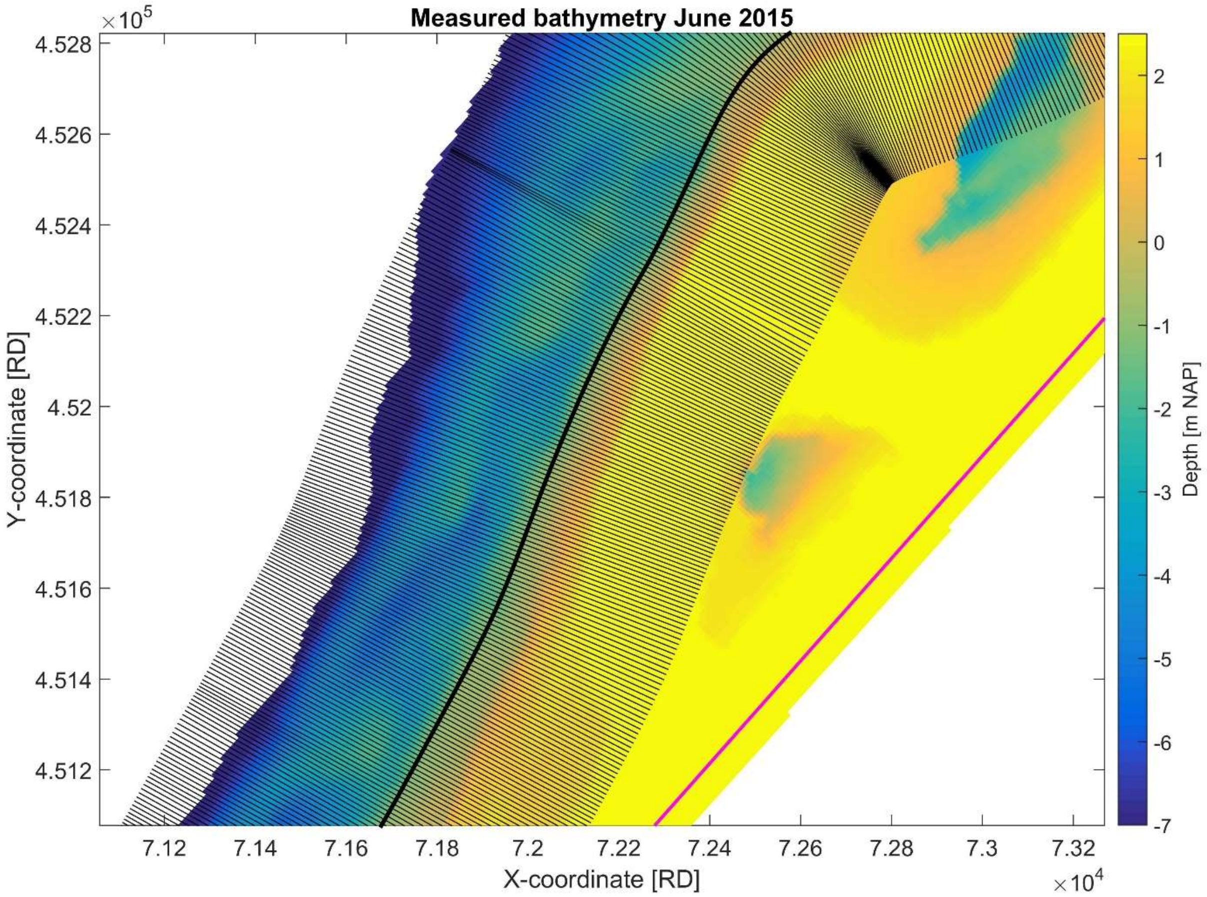

Figure 8: Cross sections (thin black lines) used to extract alongshore straightened bathymetry

2.3.2 Alongshore Running Average Bathymetry

Essentially, alongshore bathymetric variability is the deviation of the bed level from a certain alongshore mean. Here the alongshore mean will be determined as an alongshore running average bathymetry, analogous to Tan [2014]. In short, this running average bathymetry is obtained by smoothing the alongshore straightened bathymetry over a certain length scale.

The advantage of using this running average, is that various smoothing length scales can be used to construct various alongshore running averages. In doing so one can study bathymetric variability at different length scales. So bathymetric developments on a longer scale, for instance subtidal rhythmicity O(1000m), can be separated from shorter scale intertidal bar and rip features O(200m)[1] in the variability analysis.

For this study, two length scales have been defined for which the variability analysis has been performed. This choice has been made because of the difference in the dominant length scales in the subtidal and intertidal zones. The analysis of the intertidal area has been performed using an alongshore running average bathymetry constructed with a smoothing length scale of 200m. For the analysis of the subtidal region the length scale has been chosen at 1000m. For a more in depth discussion on these length scales, read appendix A2.

Tan [2014] proposed to construct a weighted alongshore running average, by using a Hanning window. Since this seems to yield no extra advantages, a simpler method is used. The alongshore straightened bathymetry is simply averaged out over the length scale of interest, without applying any extra weights. This result in the following computation for every point in the alongshore running average bathymetry matrix:

---

[1] For more information on these length scales please read the introduction of the thesis, or refer to other literature: Short [1991], Ruessink et al. [2012], Enkevoort and Ruessink [2002, 2003].

$$z_{ave}(x,y) = \frac{\int_{x-L/2}^{x+L/2} z_b(x,y)dx}{L}$$

Where z_{ave} is the alongshore running average bathymetry and z_b is the alongshore straightened bathymetry, x is the alongshore coordinate and y is the cross shore coordinate. This method has the drawback of losing half the length scale L at each boundary. The averaging length scale L should therefore not approach the order of size of the alongshore domain.

2.3.3 Difference Bathymetry

The difference bathymetry is now obtained by subtracting the running average bathymetry z_{ave} from the measured data, ignoring the data that lies outside of the running average domain.

$$z_{diff} = z_b - z_{ave}$$

The result of this exercise is shown in Figure 9 for the measurement data of June 2015, and a length scale of L=200m. The first window shows the alongshore straightened bathymetry. The second and third windows show the alongshore running average bathymetry and the difference bathymetry. Note that at first glance the upper two windows seem to be more or less equivalent. Since a relatively short length scale has been used to create the running average bathymetry, larger subtidal bars and coastline curves are not taken into consideration here.

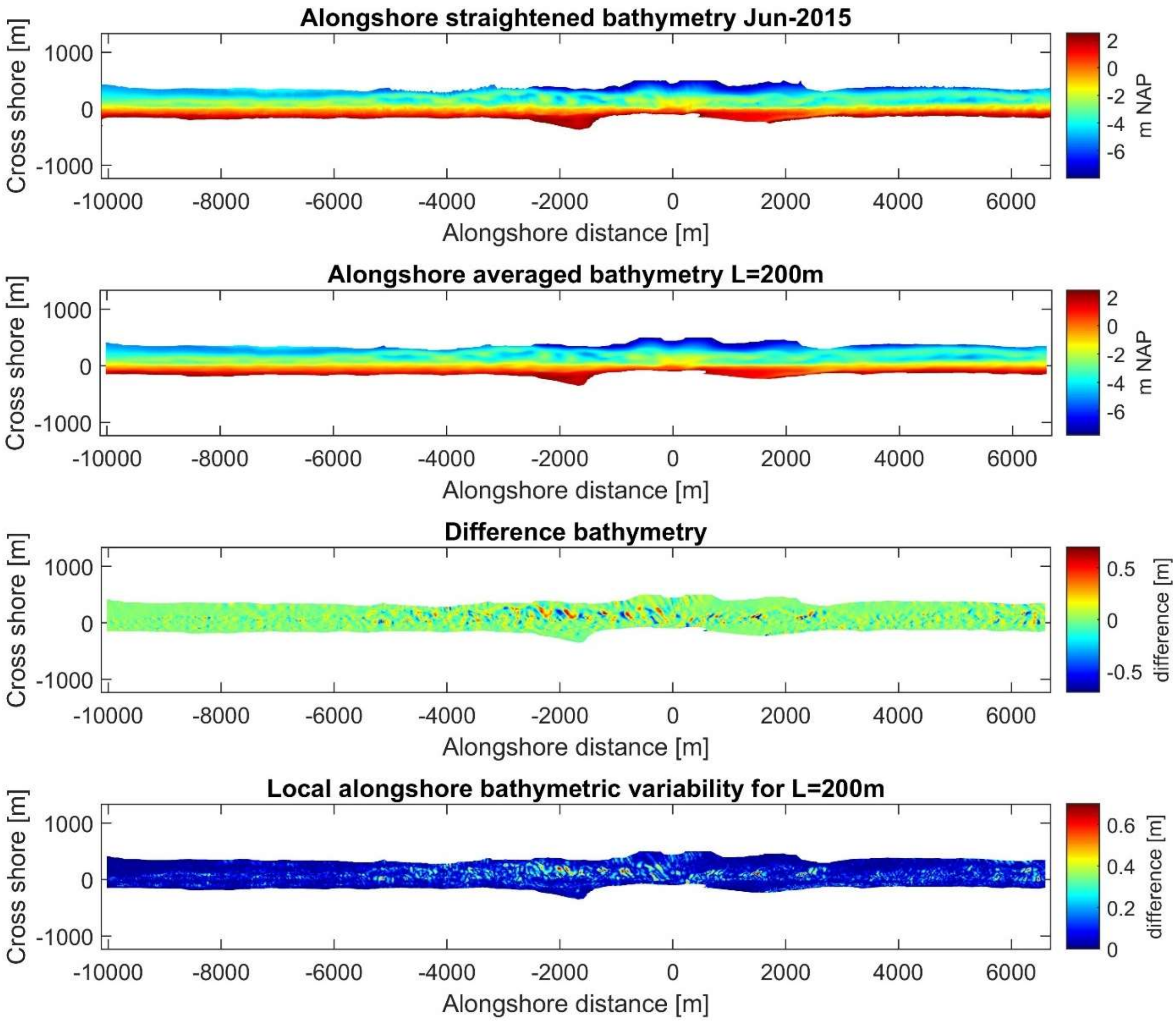

Figure 9: Alongshore straightened bathymetry (first window), alongshore running average (second window), difference bathymetry (third window) and local alongshore variability (fourth window) for measurement data of June 2015 and a length scale of L=200m

The difference bathymetry maps the deviations of the measured bathymetry, form the alongshore running average bathymetry. In other words, a relatively long, continuous, linear longshore bar and trough will result in a flat surface at 0m in the difference bathymetry z_{diff}. A rip channel in a longshore bar will result in a valley in the difference bathymetry, whilst a relatively narrow transverse bar will result in a hill.

2.3.4 Local Alongshore Bathymetric Variability

The local alongshore bathymetric variability z_{AV} is obtained by simply taking the absolute value of the values in the difference bathymetry z_{diff}. In doing so, the distinction between a negative and positive deviation of the alongshore running average disappears. All deviations have now become a certain level of variability.

$$z_{AV} = \left|z_{diff}\right|$$

The reason that the local alongshore bathymetric variability has not been defined as the squared values of the difference bathymetry, as in de Schipper et al. [2013], is that this has been found to generate too strong a bias toward extreme deviations, which can come to dominate the bulk alongshore bathymetric variability in an unrepresentative manner.

2.3.5 Bulk Alongshore Variability

The local alongshore variability contains the signal generated by every individual feature in the data set. Since the entire domain is about 17km long, and since the data set contains 34 sets of measurements, looking at the signal of every individual feature is hugely impractical. The end result will be very hard to make sense of. A bulk parameter can help to addresses these issues, by parameterising the local alongshore bathymetric variability for certain subsections of the Delfland Coast. Using the bulk alongshore bathymetric variability, one can easily spot trends in time for a certain subsection of nearshore bathymetry, or spot relations in variability between the intertidal and subtidal zones of certain subsections.

In generating the bulk alongshore variability, it is important to note that the signal generated in the intertidal zone differs from the signal in the subtidal zone. As stated earlier, the dominant alongshore length scales in both zones differ; O(200m) for the intertidal zoned and O(1000m) for the subtidal zone. This is why the analysis has been performed with two different length scales for the alongshore running average bathymetry z_{avg}. Next to that the bar amplitude in the subtidal zone can be an order of magnitude stronger than in the intertidal zone. In other words subtidal bars, troughs and rips are more pronounced than intertidal bars, troughs and rips, resulting in higher values for the subtidal bulk alongshore bathymetric variability.

By closely observing the alongshore straightened bathymetry data, it has been found that a sixty meter seaward offset of the smoothed -1m NAP contour is a good line to choose as a boundary between the subtidal and intertidal zones.[2] In generating the bulk intertidal- or bulk subtidal alongshore variability, only the data up to or above this this line of separation has been used.

The first step in generating the bulk alongshore variability is to average the local alongshore variability over the intertidal- and subtidal zones respectively, as shown in the formulae below. This basically transforms the 2D z_{AV} field, into a 1D vector.

$$z_{AV,sub}(x) = \frac{1}{L_{y,subtidal}} \int_{y_0}^{y_{max}} |z_{AV}(x,y)|\, dy$$

[2] From visual inspection of the data set, it has been determined that the real -2m NAP contour usually forms a good line of separation between the intertidal and subtidal zones. It would therefor seem obvious to use a smoothed -2m contour, rather than the smoothed -1m contour in the analysis. However, generating the smoothed -2m contour for this particular dataset is problematic. Persistent transverse bars at the tip of the Sand Motor, as well as rhythmic subtidal bars, connecting to the intertidal zone gave rise to these problems. No easy, general purpose solution has be found for such problems, but for this dataset, using the offset -1m NAP as described has proved an elegant and easy solution.

$$z_{AV,inter}(x) = \frac{1}{L_{y,intertidal}} \int_{y_{min}}^{y_0} |z_{AV}(x,y)|\, dy$$

The result of this exercise is shown in Figure 10 for the subtidal zone of the June 2015 measurement set. This signal, however, still has the same issues as the local alongshore bathymetric variability field (fourth window Figure 9), in that it is mostly produced by individual rip channels and other non-uniformities.

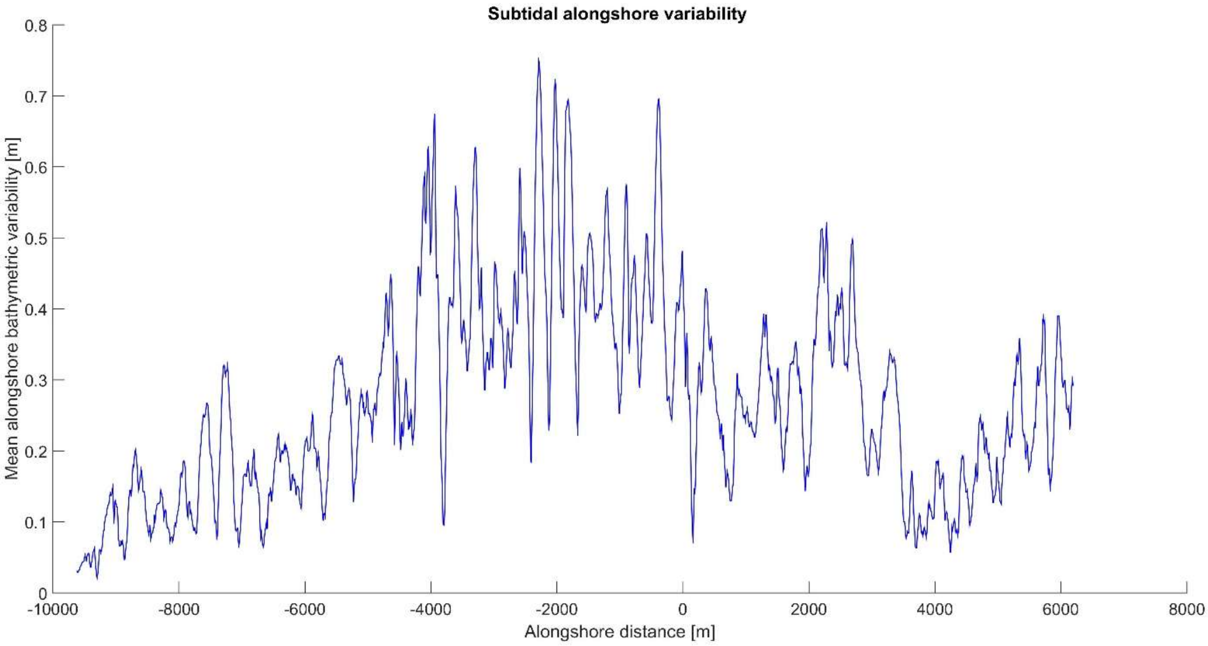

Figure 10: Subtidal alongshore variability for June 2015

The bulk alongshore variability is now calculated by first dividing the total alongshore length up into shorter subsections of a constant length L_{bulk}. Finally the signal shown in Figure 10 is averaged for each subsection. This is the bulk alongshore variability.

$$AV_{sub}(i) = \frac{1}{L_{bulk}} \int_{x_{min}+(L_{bulk}*(i-1))}^{x_{min}+L_{bulk}*i} z_{AV,sub}(x)\, dx\,, \qquad i = 1,2,\ldots, L_{total}/L_{bulk}$$

$$AV_{inter}(i) = \frac{1}{L_{bulk}} \int_{x_{min}+(L_{bulk}*(i-1))}^{x_{min}+L_{bulk}*i} z_{AV,inter}(x)\, dx\,, \qquad i = 1,2,\ldots, L_{total}/L_{bulk}$$

The result of this exercise for the subtidal zone of the June 2015 measurement set is shown in Figure 11. All in all, the bulk subtidal alongshore variability represents the overall trend in subtidal alongshore variability, shown in Figure 10. The bulk length scale used in this plot is 400m. This length scale has been chosen on practical grounds: one wants to create a more straight forward representation of the alongshore variability, without losing too much definition. After testing several different bulking length scales, it has been found that 400m is an optimal bulk length for this data set. The alongshore distance is measured along the dune foot, in a straight line from Hoek van Holland to Scheveningen (purple line in Figure 7), and has been set to zero at a point near the tip of the Sand Motor (see section 2.3.1).

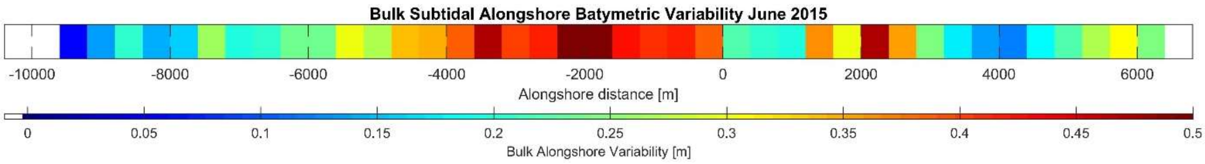

Figure 11: Bulk subtidal alongshore variability for June 2015. Bulk length scale is 400m. Hot colours indicate high variability, cold colours indicate low variability

This method has been performed for the entire dataset. The results, and interpretation of the results are handled in the next chapter.

2.4 Conclusions Methodology Data Analysis

This chapter is concluded by answering the main research question of this chapter; research question one:

Can a parameter be constructed, which is representative of the alongshore bathymetric variability along subsections of the Delfland Coast?

By using a five step scheme a bulk parameter for the alongshore bathymetric variability can be defined which is representative of the local alongshore bathymetric variability of 400m long subsections of the Delfland Coast, for both the intertidal zone and the subtidal zone. The five steps are listed below, in order of execution:

1. Convert the curvy coastal bathymetry of the data set into an alongshore straightened coast
2. Determine an alongshore running average bathymetry for this alongshore straightened coast
3. Calculate the difference bathymetry by subtracting step 2 from step 1
4. Calculate the local alongshore variability by taking the absolute values of step 3
5. Isolate the intertidal- and subtidal zones, and calculate the bulk alongshore variability for both zones for sections of 400m

3. Results Data Analysis

This chapter discusses the results of applying the method described in chapter 2, to the dataset of bathymetry measurements of the Delfland Coast (see paragraph 2.2). The results for the subtidal zone and intertidal zone are discussed separately. For each zone the results will be presented first, followed by some examples showing what generates low, medium and high output values for the bulk alongshore bathymetric variability. These examples will help the reader to better understand the relation between the original bathymetry and alongshore bathymetric variability and show the ability of the bulk parameter to represent the overall variability of a certain subsection of the Delfland Coast. Subsequently patterns in bulk alongshore bathymetric variability are discussed. After discussing the results for the subtidal- and intertidal zone separately, a correlation study will be presented.

The main research question which will be answered in this chapter is research question two:

How does the alongshore bathymetric variability of the Delfland Coast develop during the studied period?

3.1 Subtidal Zone

The dominant length scale of bathymetric features in the subtidal area is relatively long O(500m to 1000m). In generating the bulk parameters for the subtidal zone an alongshore averaging length scale of 1000m has been used and a bulk length scale of 400m, as is explained in paragraphs 2.3.2 and 2.3.5. The results of applying the method to the entire dataset have been combined to create a so called time stack, which gives insight into the development of the subtidal bulk alongshore bathymetric variability in time.

3.1.1 Time Stack of the Subtidal Bulk Alongshore Bathymetric Variability

Figure 12 shows the time stack of the subtidal bulk alongshore bathymetric variability. The time stack is a visual representation of the quantitative results for the bulk alongshore variability analysis of the subtidal zone, for the entire dataset. This plot has been generated by essentially stacking the individual results, such as presented in Figure 11, one on top of the other. In doing so, one can both observe the spatial patterns in bulk variability for each measurement, as well as study the development of the bulk variability for a certain section of coastline in time. The time series starts in August of 2011, presented on the top of the time stack, and finishes in January 2016 at the bottom.

It is important to note that a lot more data is available of the Sand Motor measurement area (roughly -2000m to +2000m in Figure 12), than of the NeMo measurement area. Sand Motor measurements are available from the time of completion of the Sand Motor in August 2011. While the NeMo area was first measured in March 2012. Subsequently, bi-monthly measurements have been performed from March 2013 onwards. However, the data from July 2015 onwards has not been included in this research. This explains the white patches in Figure 12. In the early stages of Sand Motor development, From August 2011 to December 2011, the spit of the Sand Motor was still forming. The Method could not yet be applied to the undeveloped spit area, which is why only a part of the Sand Motor domain shows results in this period.

A few things immediately stand out in Figure 12. The bulk alongshore bathymetric variability in March 2012 was a lot higher than it was in March 2013, over the entire domain. And the highest values are produced at the connection of the Sand Motor spit to the NeMo coastline in 2012, and the southern connection of the Sand Motor in 2012, whilst the lowest values are generated toward the southern end of the domain (ear the Hoek van Holland breakwater) from 2013 onwards.

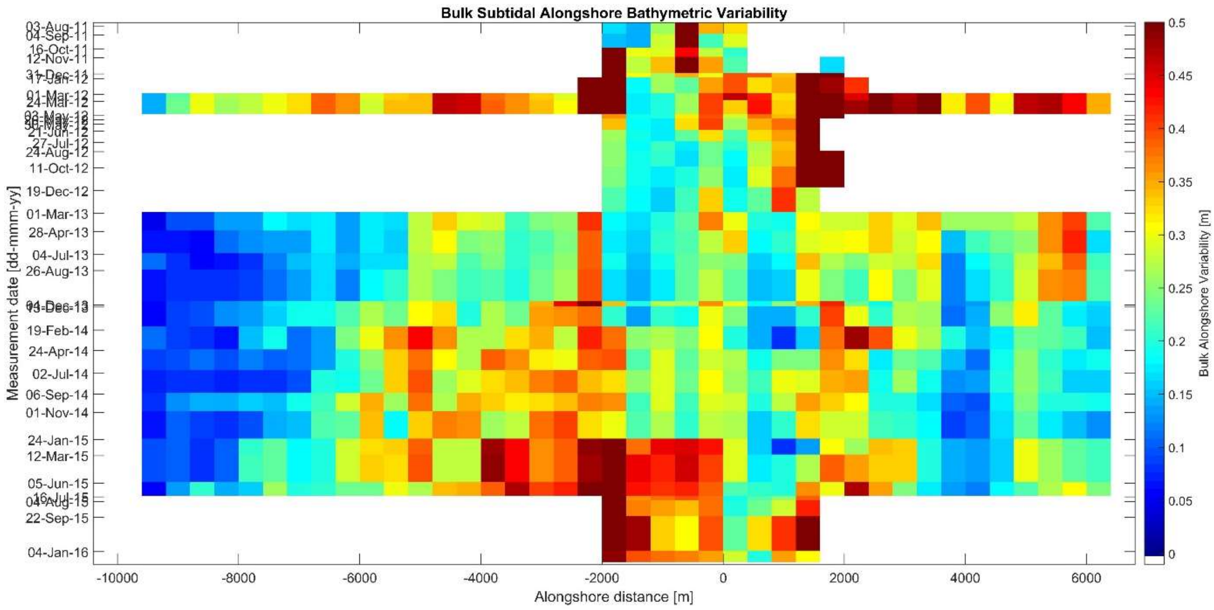

Figure 12: Time stack of the subtidal bulk alongshore bathymetric variability along the Delfland coast. Here the bulk AV values of the entire dataset are shown. The bulk length scale is 400m. This picture allows the reader to compare the variability of sections of subtidal bars, rather than comparing the AV signal produced by individual features.

In order to give the reader more insight into what generates these values and patterns, and to build trust that peaks are not generated by, for instance, mismatches of NeMo and Sand Motor data, some examples are presented, showing close up results of the analysis for some individual features. Afterwards the apparent patterns in Figure 12 will be discussed.

3.1.2 Examples of Subtidal Alongshore Bathymetric Variability

In this intermezzo three close up results will be discussed. These will show subtidal features which produce low-, medium-, and high levels of bulk subtidal alongshore bathymetric variability respectively. These close ups will also help the reader to gain confidence in the fact that the method is not generating false positives and/or false negatives, but that it generates reliable output.

First a section representative of low bulk alongshore bathymetric variability is presented. Figure 13 shows the local analysis around +4000m for the data of November 2014 (see next page). The time stack shows a low value in the bulk variability at this location on this date, which is persistent in time. The windows in Figure 13 show the alongshore straightened bathymetry, the longshore averaged bathymetry, the difference bathymetry and the local alongshore variability from top to bottom.

The longshore bar around +4000m is very linear. Both the bar crest and the bar trough show very little deviations in height or depth and there are no significant variations in the cross shore position of either the bar crest or the trough. There is clearly very little alongshore bathymetric variability in this section. The local alongshore bathymetric variability field (bottom window) shows cold colours, which represent a low output. This situation forms in late 2013, and persists until the end of the study period.

Around +3200m the bar gradually fades out, and a new subtidal bar starts to grow out from the intertidal area. This generates some medium alongshore bathymetric variability, represented by the green to yellow colours in the bottom window, around +3200m. Around +5000m, alongshore bathymetric variability in trough depth starts to increase, generating medium output in the bottom window. All in all, the output in both the bottom window of Figure 13 and the bulk parameter output in Figure 12 are a good representation of the measured data of November 2014.

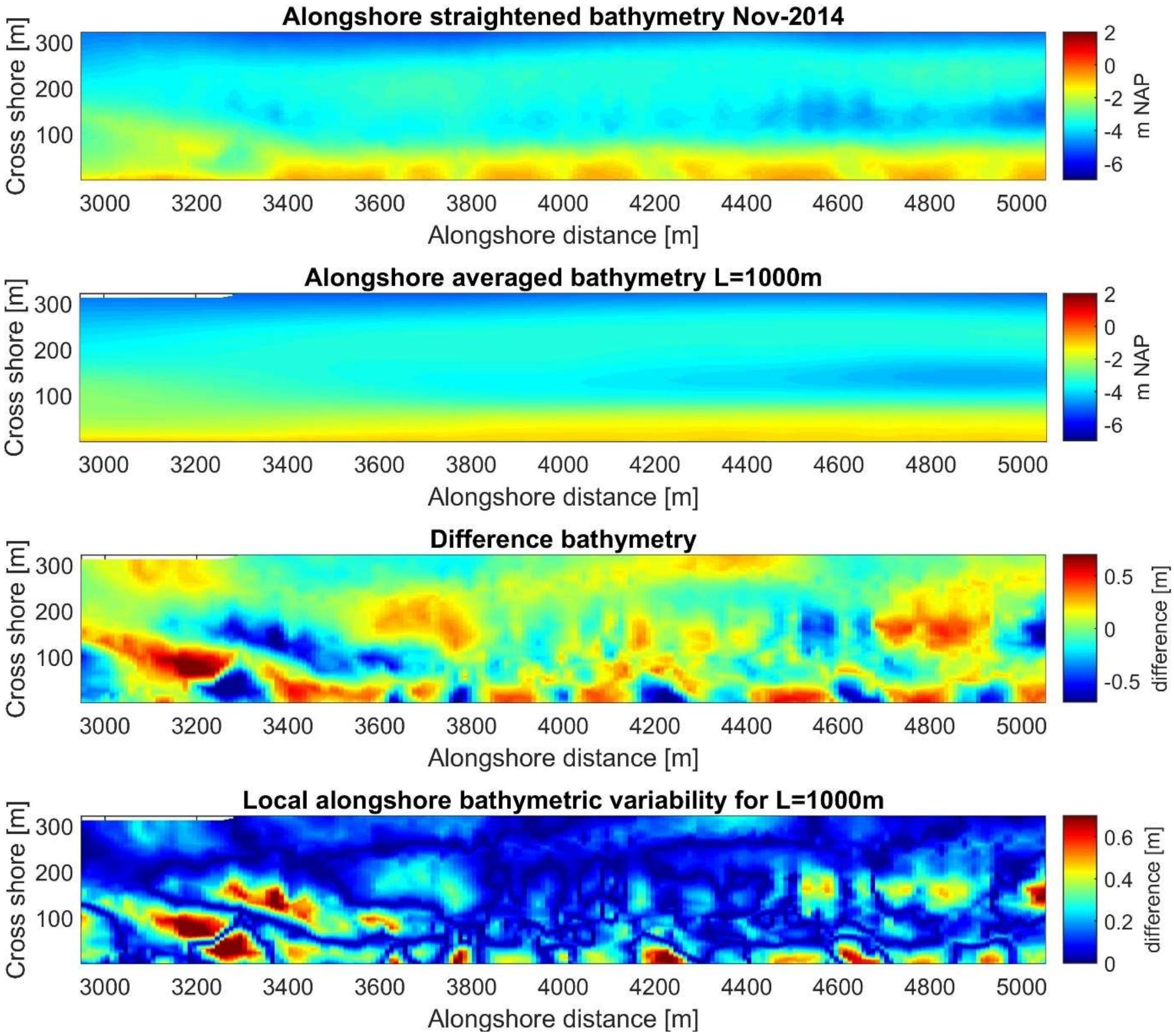

Figure 13: Zoom in analysis around +4000m, subtidal area for November 2014. This figure is representative of low bulk alongshore bathymetric variability. The windows show the alongshore straightened bathymetry, the alongshore averaged bathymetry, the difference bathymetry and the local alongshore bathymetric variability, from top to bottom

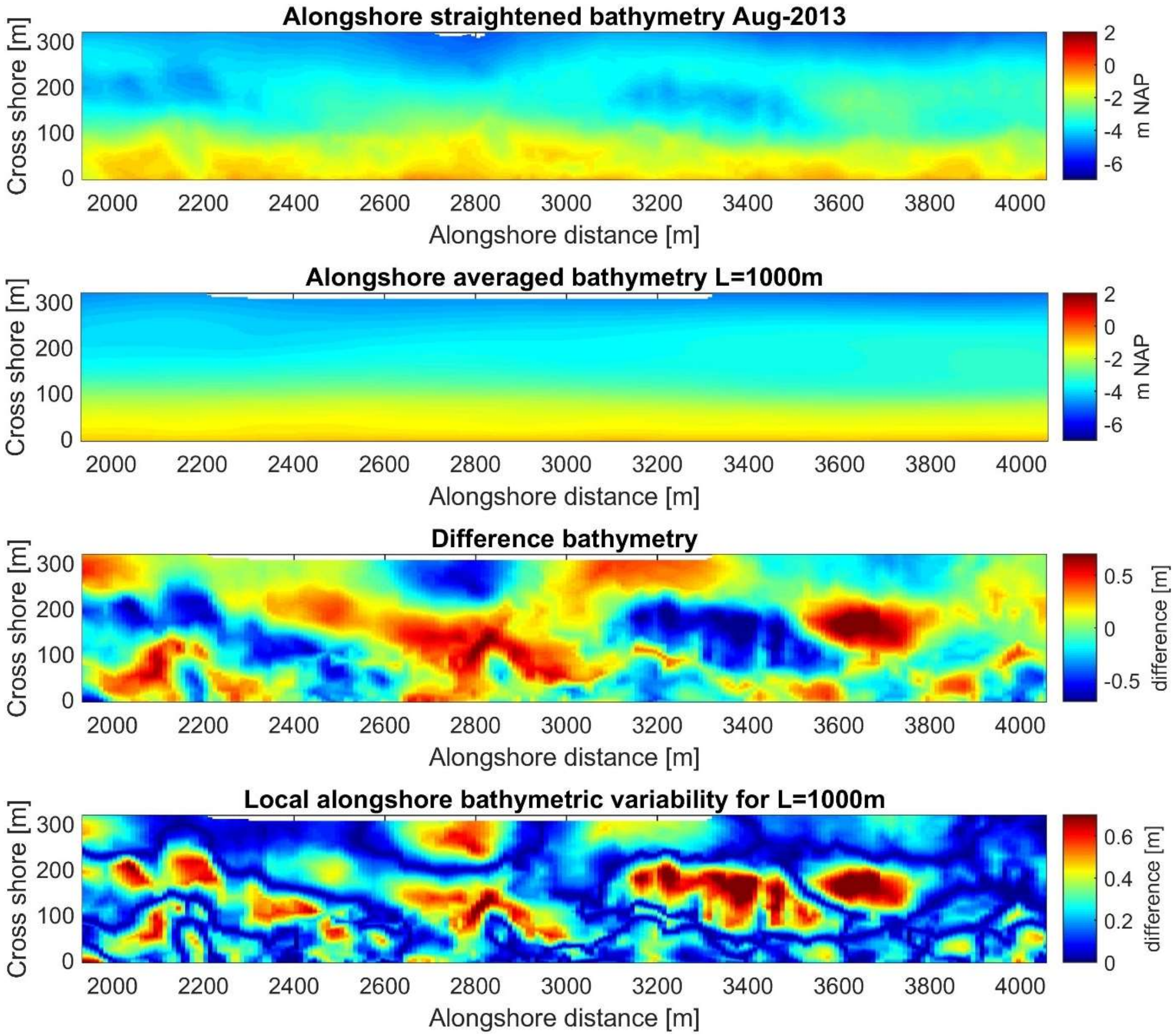

Figure 14: Zoom in analysis around +3000m, subtidal area for Augustus 2013. This figure is representative of medium bulk alongshore bathymetric variability. The windows show the alongshore straightened bathymetry, the alongshore averaged bathymetry, the difference bathymetry and the local alongshore bathymetric variability, from top to bottom

Figure 14 shows the local analysis around +3000m for the data of August 2013. The time stack shows yellowish colours, indicating medium values of bulk alongshore bathymetric variability at this location on this date. At this location the onset of rhythmic bar behaviour is visible. The upper window of Figure 14 shows the alongshore straightened bathymetry. Here one can clearly see that the cross shore position of the bar crest varies significantly in alongshore direction, to the point even where it interrupts the bar trough. Also quite some variation in crest height can be seen. The deepest points in the bar trough, as well as the rhythmic sections of the crest, which interrupt the bar trough produce the medium high signal at this location.

It should be pointed out that the alongshore variations in cross shore position of the bar crest are significant, but not extreme. The bed level difference between the crest and trough is also not too extreme for this case. A more extreme case is discussed below. All in all, the output in both the bottom window of Figure 14 and the bulk output in Figure 12 are a good representation of the measured data of August 2013.

Finally, Figure 15 (see next page) shows the local analysis around +2000m for the data of March 2012. The time stack shows very high values of bulk alongshore bathymetric variability at this location on this date, indicated by dark red colours. At this location the subtidal area of the Sand Motor spit connects to the subtidal area of the Delfland Coast. The subtidal bar around +2000m forms a link between the subtidal features in this area, and also bridges the difference in coastal slope between the Sand Motor and the Delfland Coast, which is still rather significant in March 2012.

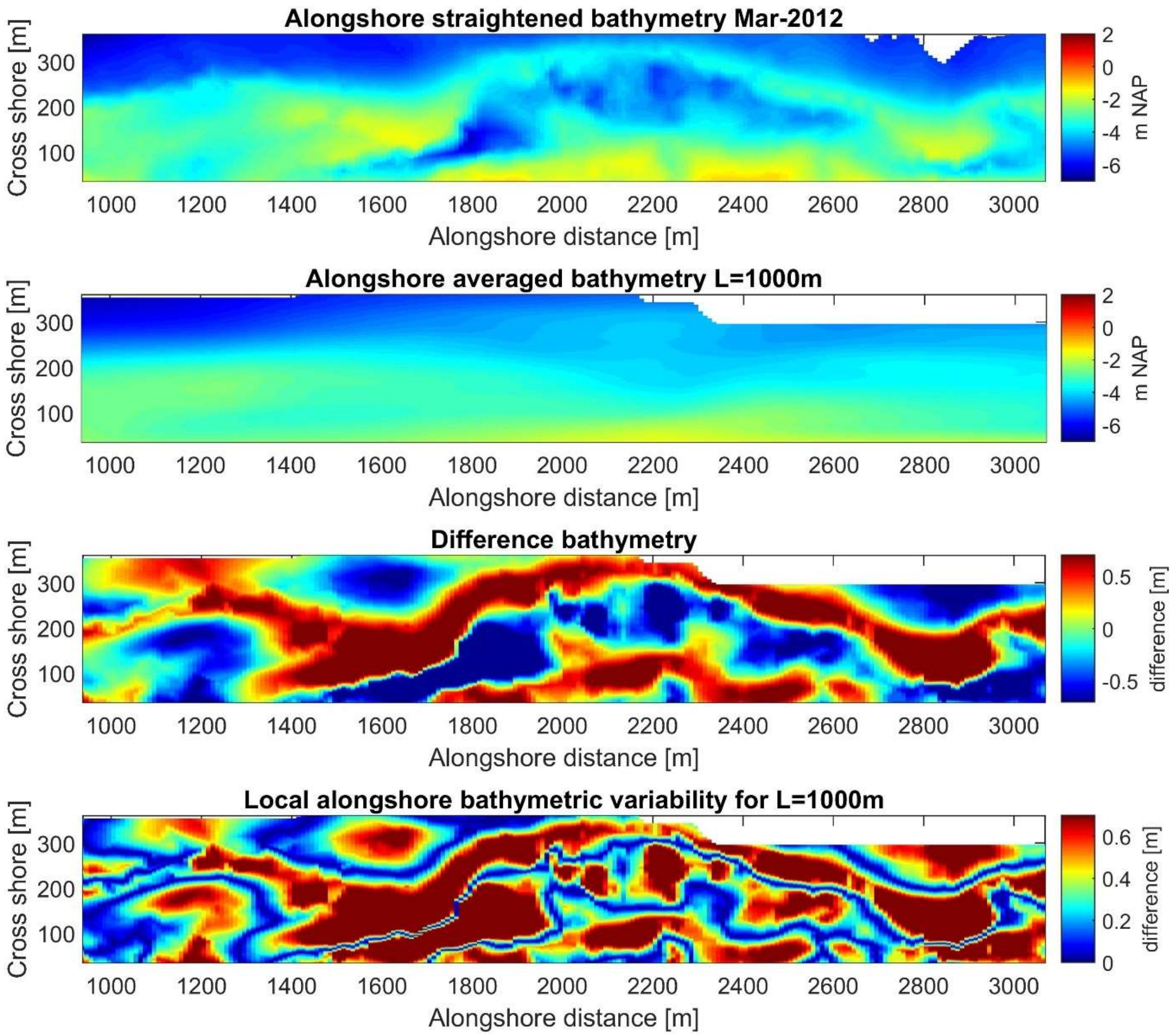

Figure 15: Zoom in analysis around +2000m, subtidal area March 2012. This figure ir representitiva of high bulk alongshore bathymetric variability. The windows show the alongshore straightened bathymetry, the alongshore averaged bathymetry, the difference bathymetry and the local alongshore bathymetric variability, from top to bottom

The upper window of Figure 15 shows extreme alongshore variation of the cross shore position of the bar crest for this case. The rhythmic sections of the bar crest which interrupt the bar trough, are so extreme that they form big shoals at the cross shore position, where normally the bar trough would be located for a linear, longshore bar. In particular the areas where the high sections of the bar crest interrupt the deep sections of the bar trough (around +1800m) generate extreme local alongshore variability. The section of the bar crest which bulges out seaward (around +2000m) also generates high values of local AV.

It should be pointed out that this subtidal feature is a real feature, and not a result of generating the alongshore straightened bathymetry. All in all, the output in both the bottom window of Figure 15 and the bulk output in Figure 12 are a good representation of the measured data of March 2012.

These three cases are exemplary for the rest of the data set. The bulk values in Figure 12 are a good quantitative representation of the subtidal features, visible in the measurement data. If one is interested in further understanding the relation of the bulk values presented in Figure 12 and the actual measured bathymetry, one can take a look at appendix A3, which contains more pictures of the measured bathymetry.

Relating the bulk values to the beach states, as defined by Wright and Short [1984], what stands out is that the lowest levels of bulk AV usually correspond to longshore bars. The highest levels, however, do not necessarily correspond to transverse bars. In fact, the highest levels in this data set correspond to two distinct rhythmic bars, as discussed later. What this tells us, is that the bulk parameter responds to the overall amplitude of the difference bathymetry, rather than any visually discernible patterns. As such, a very well defined rhythmic bar might generate higher values than a very faint transverse bar. Unlike the scheme presented by Tan [2014], the method used here cannot be used to identify beach states.

The next section will continue to interpret the apparent patterns in the results presented in Figure 12.

3.1.3 Evolution of the Subtidal Alongshore Bathymetric Variability

This section discusses the patterns that can be discerned from the bulk alongshore variability time stack, presented in Figure 12. The aim here is to gain insight in the development of alongshore variability in the research domain, and the possible effect the Sand Motor might have on the development of alongshore bathymetric variability along the entire Delfland Coast.

One major pattern which applies to the entire domain, is the overall decrease in bulk alongshore bathymetric variability values from March 2012 onwards, until December 2013. On December fifth a storm, nicknamed the Sinterklaas storm, hit the Netherlands. From this moment onward the bulk values start to increase between -7000m and +3000m, until the end of 2014 when something remarkable happens. Along the Southside of the Sand Motor and along the directly adjacent section of the Delfland Coast, a break point seems to have been reached in January 2015. The rhythmic, longshore directed bars have transformed into large, transverse bars, generating some of the highest bulk values of the entire dataset. This change is visualised in Figure 83 and Figure 84 in appendix A3.

The northern side of the Sand Motor behaves quite differently in January 2015. It becomes a lot more linear. The adjacent northern section of the Delfland Coast seems to react rather ambiguously. From +3000m onwards the subtidal area becomes less variable as a reaction to the Sinterklaas Storm in December 2013 and there seems to be no significant change in January 2015. In some other subsections, however, the bulk alongshore bathymetric variability increases.

Overall this observation seems to underline the conclusions of de Schipper et al. [2013]: that for the Holland coast, alongshore variability seems to increase in reaction to a single storm event, in contrast to the model proposed by Wright and Short [1984]. In addition to that, the data suggests that a large storm event, such as the Sinterklaas Storm, can change the overall dynamic of a system from overall decreasing alongshore bathymetric variability, to overall increasing alongshore bathymetric variability. The bulk values for the northern half of the domain in January of 2015, however, do not fit into this picture.

Some sections of the studied area are characterized by low bulk values, which persist over a long period of time. The breakwater at the Hoek van Holland border of the domain seems to force a situation, in which the subtidal bar shows more linear patterns than the rest of the Delfland Coast. Along the Southside of the Sand Motor, the subtidal area is dominated by a longshore linear bar from January 2012 until December 2013. After this period the longshore bar starts to become slightly more rhythmic, until January 2015 when it breaks up completely and is replaced by transverse bars. Finally a section of the subtidal area around +4000m is characterized by a longshore linear bar from April 2013 onwards.

Other sections of the studied area are characterized by high bulk values, which persist over a long period of time. From November 2011 until October 2012, extreme levels of variability persist in the areas where the Sand Motor connects to the Delfland Coast. In fact, these features generate the highest levels of bulk AV for this dataset. An example of such a feature can be seen in the upper window of Figure 15. Figure 71, Figure 73 and Figure 75 in appendix A3 give an overview of these connecting subtidal features for March 2012.

These connecting features are extreme bar shapes that connect the subtidal bars of the Sand Motor, with the subtidal bars of the adjacent Delfland Coast. The coastal slope around the Sand Motor still is a lot steeper in this stage of its development, than is the coastal slope at the Delfland Coast. This difference in coastal slope originates from the way the Sand Motor has been constricted, versus the natural slope of the of the Delfland Coast. These connecting features also seem to form a bridge between these two sections of significantly different coastal slope. From December 2012 onwards, these extreme connecting features are no longer visible.

This change might be explained by the changing shape of the Sand Motor. From its completion onwards the coastal slope of the Sand Motor constantly decreases during the study period. At the same time the sand from the Sand Motor is redistributed along the Delfland Coast, reshaping the Sand Motor into a less extreme perturbation of the straight Delfland Coast.

The most important source for the high bulk values for these connecting features are the two extremely deep bar troughs, indicated by the black circles in Figure 16 (also see the lower two windows in Figure 15). At each side of the Sand Motor a shoal has formed as part of the connecting subtidal feature. This shoal is accompanied by a deep trough, which points away from the Sand Motor.

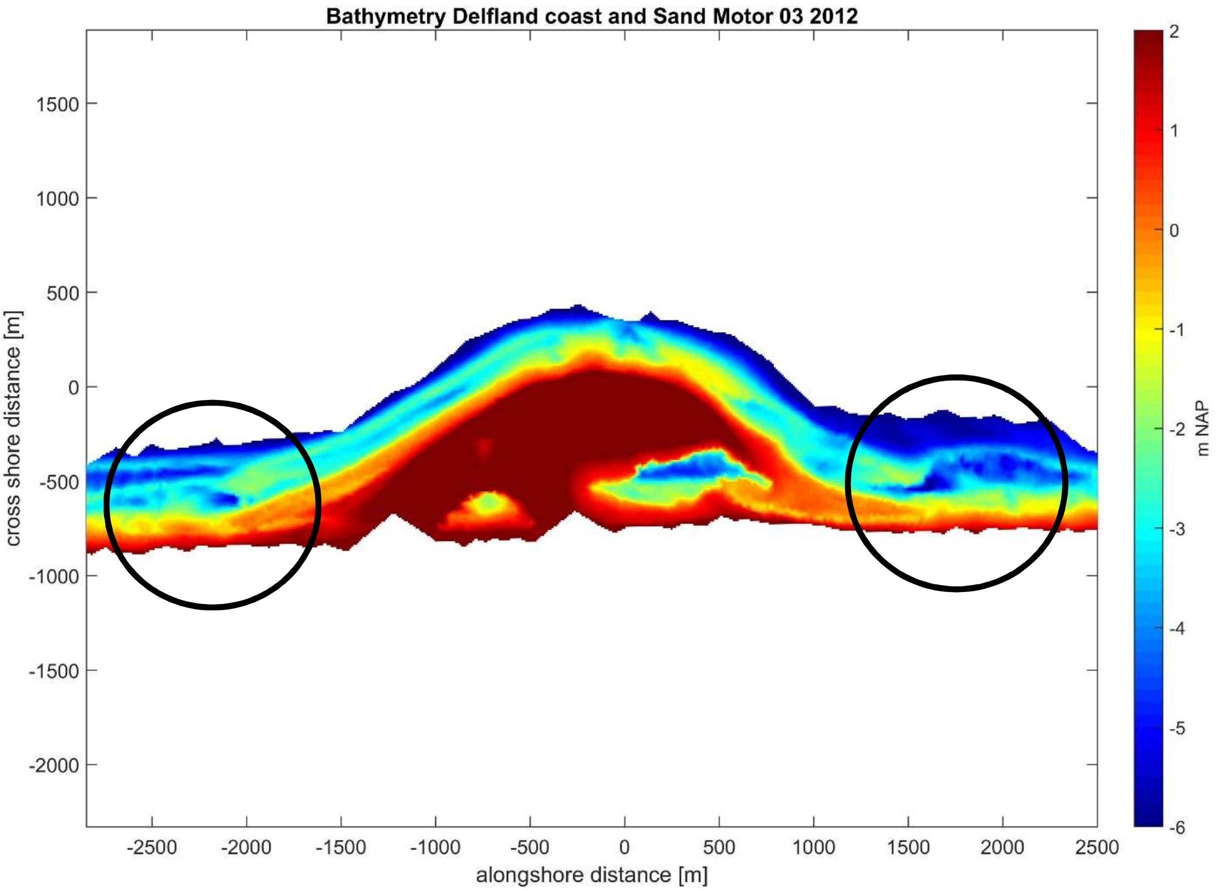

Figure 16: Sand Motor bathymetry for the March 2012 measurement set. The black circles indicate the high shoals and deep channels (pointing away from the Sand Motor), which generate the gighest bulk AV values of the dataset

The deep troughs first appeared in December 2011, indicating that they were generated by the same (series of) high energy event(s). They subsequently persist until they are filled in by some other process. The southern channel (left in Figure 16) disappears gradually during the summer of 2012, due to developments in the subtidal bars. These developments are also in line with the afore mentioned conclusions of de Schipper et al. [2013]. The northern channel disappears suddenly in December 2012, due to developments of the spit and lagoon channel, which fill in the subtidal channel with sediment.

Another source of persistent high bulk values are the transverse bars that form along the Southside of the Sand Motor and the directly adjacent coastline in January 2015. This period was characterized by energetic weather conditions. The combination of growing subtidal alongshore bathymetric variability and energetic weather seems to have been the trigger for this sudden dramatic change in bar patterns, and related increase in subtidal bulk values. This again underlines the afore mentioned conclusions of de Schipper et al. [2013]. This switch in bar states is visualised in Figure 81 to Figure 84 in appendix A3.

One event, however, is not in line with the conclusions of by de Schipper et al. [2013]. On the 21st of October 2014, the first storm of the season hit the Netherlands. The measurements of November 1st are representative of the effect of this storm on the bathymetry of the Delfland Coast. In Figure 12 the bulk variability along the Sand Motor in in the northern NeMo area has decreased. In the Southern NeMo area the results are more ambiguous; for some sections the bulk variability has increased, yet for others it has decreased. This is not in accordance with the conclusions of de Schipper et al. [2013], nor with those of Wright and Short [1984].

It seems that for the Delfland Coast variability usually increases due to a high energy event, yet it may also decrease. Looking at the differences between the different storms may give more insight into what causes this variation in morphological response of the nearshore system. In particular the angle of wave incidence during these storms could be of interest. Higher angles of incidence generate strong alongshore currents, which might eradicate alongshore bathymetric variable features. This, however, is outside of the scope of this report.

The subtidal zone at the tip of the Sand Motor is usually characterised by transverse bars. These bars are at times very large and well defined (March 2013), at other times these are very faint (August – October 2012). This generates varying levels of variability. From this we learn that the method for characterising alongshore bathymetric variability used here, is not able to differentiate between different bar states, as in Tan [2014]. Morphometric parameters, such as crest height, trough/rip depth and the cross shore extend (of rhythmicity), are leading in determining the level of variability for this method. The method used here is a good way to quantitatively asses the alongshore bathymetric variability, rather than a method for classifying bar states.

In the period of increasing bulk values (from December 2013 onwards), levels of high bulk alongshore bathymetric variability seem to be spreading away from the Sand Motor toward the boundaries of the Delfland Coast. This behaviour seems to be stronger in the southern NeMo section, where higher levels of bulk AV move more toward the Hoek van Holland boundary as the overall alongshore bathymetric variability increases in this period.

This south bound migration in the southern NeMo section is curiously not directly related to the migration of individual bars. Over the entire study period, bars migrate northward, toward the Scheveningen boundary of the Delfland Coast. The migration is quite slow and the total migration of bars if small over the study period (less than 400m, or one cell in the time stack). It is not clear what the relation between the migration of bulk AV and the migration of individual bars is.

3.2 Intertidal Zone

In the intertidal zone, the typical length scale of features is relatively short O(200m). In generating the bulk parameters for the intertidal zone, an alongshore averaging length scale of 200m has been used, and a bulk length scale of 400m, as is explained in paragraphs 2.3.2 and 2.3.5. The results have again been combined to create a so called time stack, which gives insight into the development of the intertidal bulk alongshore variability in time.

3.2.1 Time Stack of the Intertidal Bulk Alongshore Bathymetric Variability

Figure 17 shows the time stack of the intertidal bulk alongshore variability. The white patches in Figure 17 are caused by insufficient measurement data (see paragraph 3.1.1). Note these white patches are significantly shorter than in Figure 12. This is due to the different alongshore averaging length scales used for the different zones. For the subtidal zone this length scale is longer, which leads to disregarding of more data at boundaries and cuts.

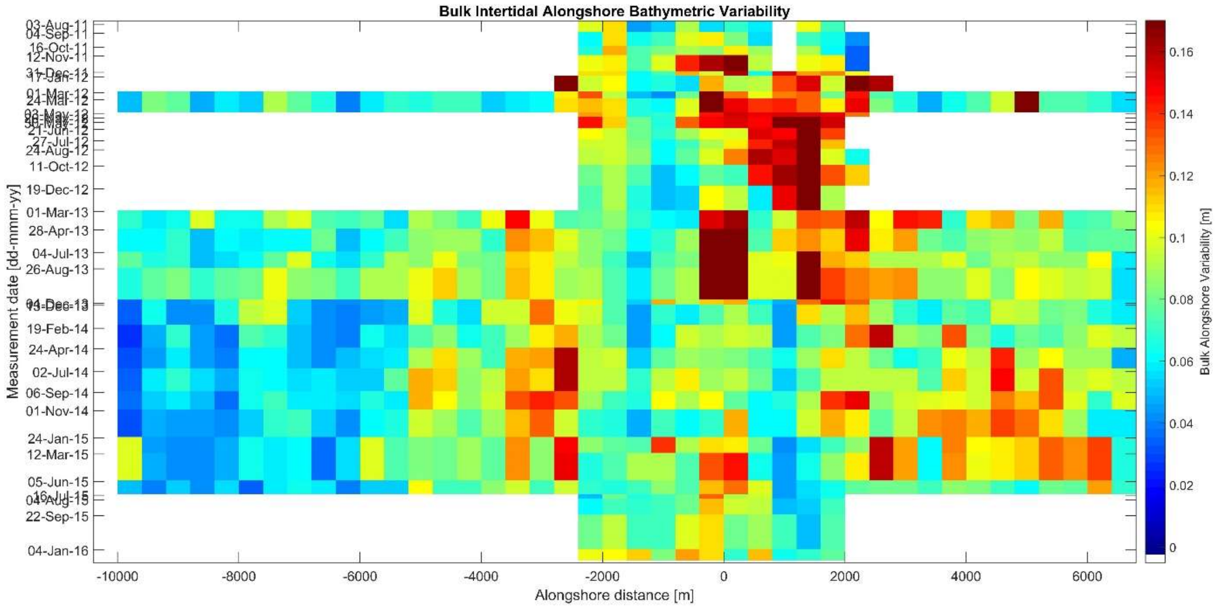

Figure 17: Time stack of the <u>bulk intertidal alongshore variability</u> along the Delfland coast. Here the bulk AV values of the entire dataset are shown. The bulk length scale is 400m.

A few things immediately stand out in Figure 17. Intertidal alongshore bathymetric variability along the Sand Motor (between -2000m and +2000m) shows large variations. For a single measurement some subsections might show high bulk values whilst others show very low values at the same time. The alongshore bathymetric variability of individual subsections along the Sand Motor also varies strongly in time. The intertidal zone along the spit, for instance, shows high amounts of bulk AV in 2012, yet very low bulk values in 2015. In between -5000m and -3000m, however, bulk values are always medium to high from March of 2013 onwards.

In order to give more insight in what generates these values and patterns, and to build trust that peaks are not generated by, for instance, false positives of false negatives, some examples are presented, showing close up results of the analysis for some individual features. After this the patterns in Figure 17 will be discussed.

3.2.2 Examples of Intertidal Alongshore Bathymetric Variability

This section discusses three close up results. These will show intertidal features which produce low-, medium-, and high levels of bulk intertidal alongshore bathymetric variability. These close ups will also help the reader to gain confidence in the fact that the method is not generating false positives and/or false negatives, but that it generates reliable output.

First a section representative of low bulk alongshore variability is presented. Figure 18 shows the local analysis around -1000m for the data of March 2012. The time stack shows a cold spot in the bulk variability at this location on this date. The neighbouring sections show more medium values, around -2000m, and very high values, around -100m. The windows in Figure 18 show the alongshore straightened bathymetry, the longshore averaged bathymetry, the difference bathymetry and the local alongshore variability from top to bottom.

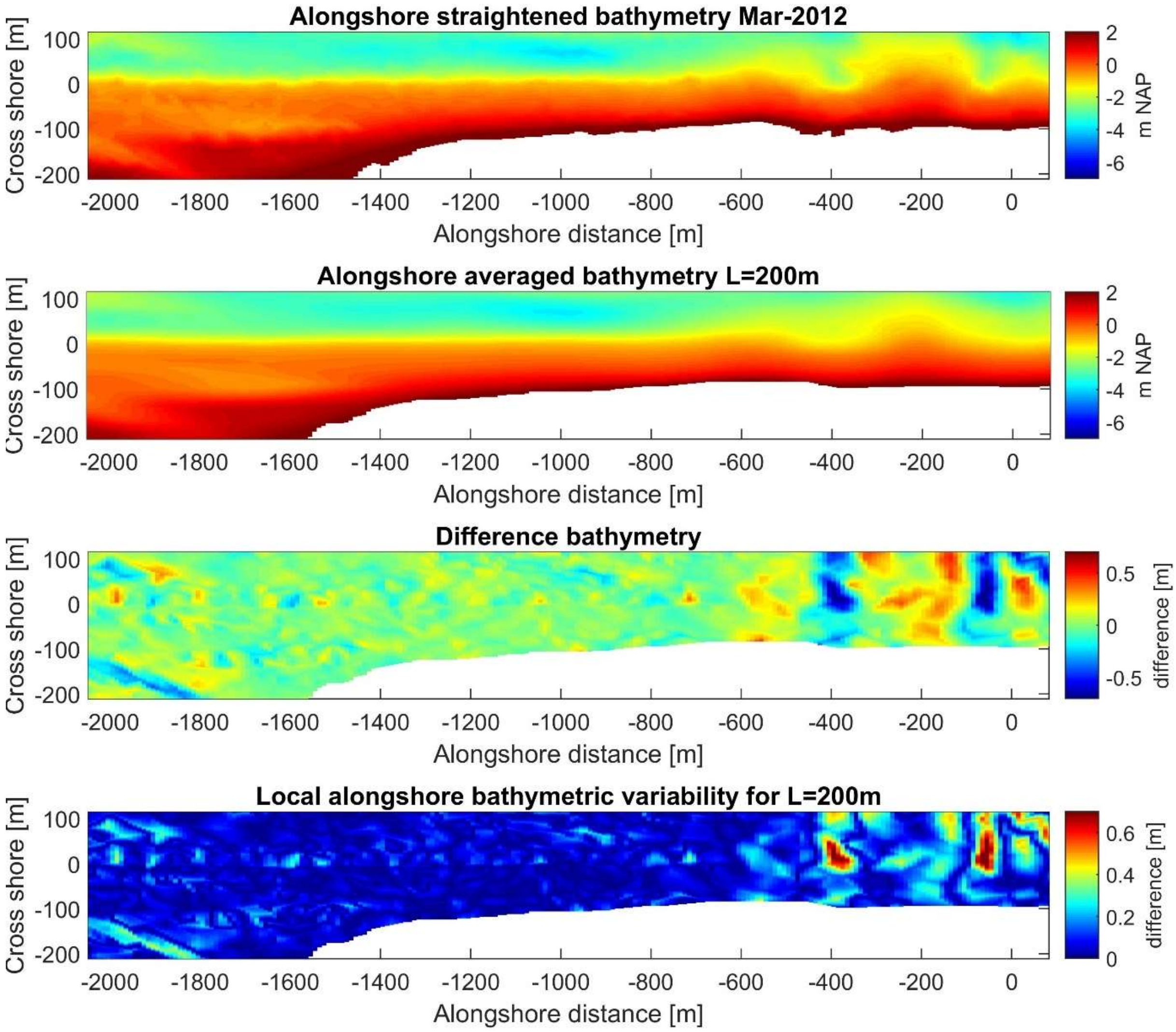

Figure 18: Zoom in analysis around -1000m, intertidal area March 2012. This figure is representative of low bulk alongshore bathymetric variability. The windows show the alongshore straightened bathymetry, the alongshore averaged bathymetry, the difference bathymetry and the local alongshore bathymetric variability, from top to bottom

Around the -1000m marker, the intertidal area is very linear. No distinct features, such as bars, troughs and rip channels, are visible. This section is located behind the longshore linear bar, which dominates the subtidal zone at this time. Clearly, there is very little alongshore variability in this area. The local alongshore bathymetric variability field (bottom window) shows a low output from the analysis, represented by the colder colours around -1000m.

Around -2000m the Sand Motor connects to the Delfland Coast. In March 2012 the connection has started to fill in with sediment, resulting in a wide intertidal area. The channel which allows water to drain from this area during falling tide, is the source of the medium high level of variability in this subsection. It can be identified as a greenish streak in the bottom window.

Near the tip of the Sand Motor, around -100m, large, transverse bars are visible. These run through the intertidal area, into the subtidal area, generating alongshore variability in both areas. They are present in some shape or form for most of the study period. On some dates they reside somewhat lower in the profile, generating higher values in the subtidal area. On March 2012, however, these transverse bars play a large role in the intertidal area, generating high levels of alongshore bathymetric variability, represented by the hot colours in the bottom window of Figure 18. From this it is clear that the output in both the bottom window of Figure 18 and the bulk output in Figure 17 are a good representation of the measured data of March 2012 around -1000m.

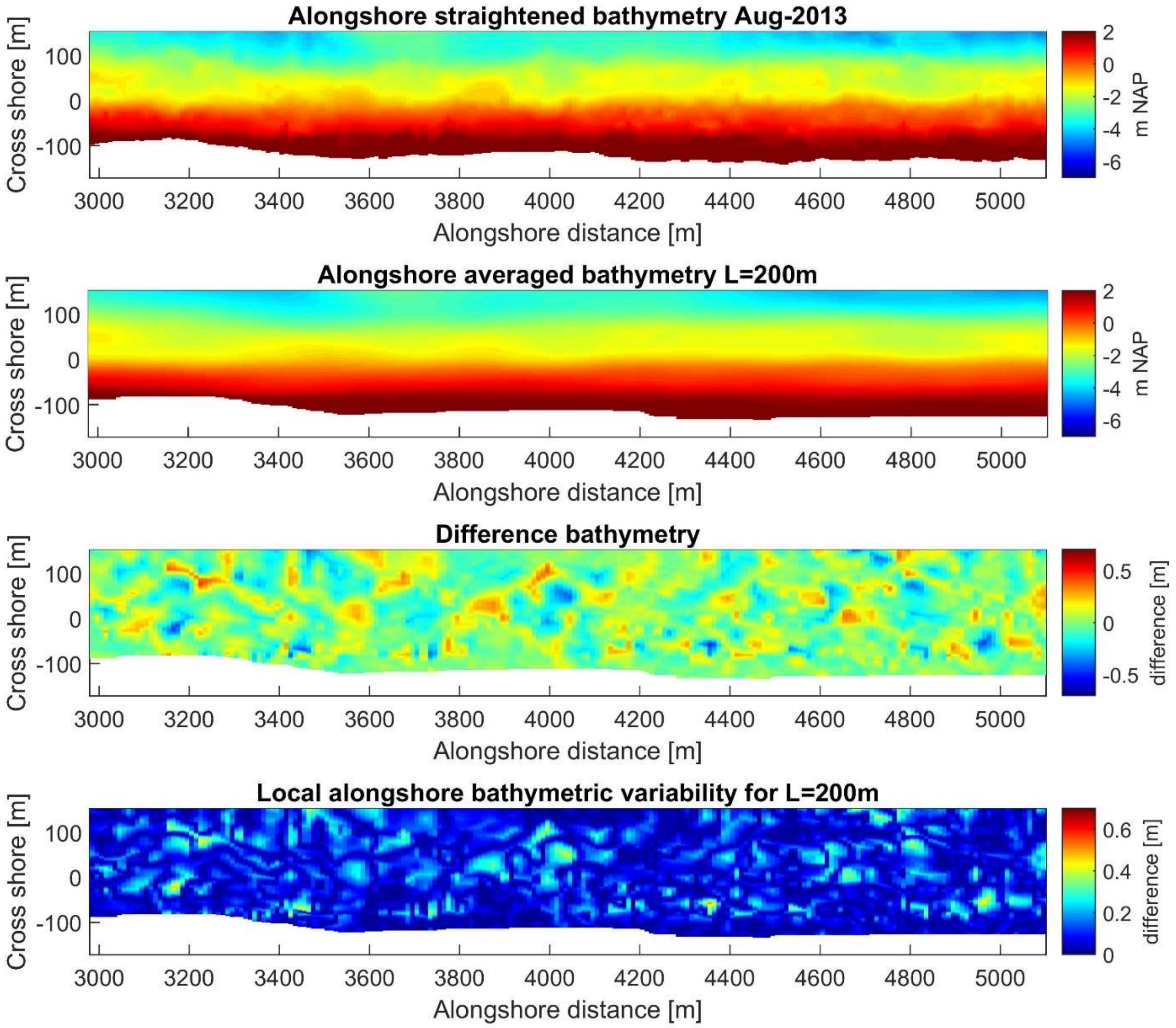

Figure 19: Zoom in analysis around +4000m, intertidal area August 2013. This figure is representative of medium bulk alongshore bathymetric variability. The windows show the alongshore straightened bathymetry, the alongshore averaged bathymetry, the difference bathymetry and the local alongshore bathymetric variability, from top to bottom

Figure 19 shows the local results around +4000m for the data of August 2013. The time stack shows green to yellow colours, indicating medium values of bulk alongshore bathymetry variability at this location on this date. At this location faint, irregular intertidal bars are visible.

In the upper window of Figure 19 one can clearly see the alongshore irregular bars, interrupted by rip channels. These features have a relatively small amplitude but they clearly are a source of alongshore variability. In the bottom window one can observe that the medium high output is generated by the highest parts of the bars, as well as the rip channels. This is indicated by the greenish patches of colour. The output presented in both the bottom window of Figure 19 and in Figure 17 are a good representation of alongshore bathymetric variability of the measured bathymetry of August 2013.

Finally, Figure 20 shows the local analysis around +3000m for the data of January 2015. The time stack shows high levels of bulk alongshore bathymetric variability, indicated by the dark red colours in Figure 17. In the top window of Figure 20 both the mouth of the lagoon channel, and some groin related rip channels are visible.

The mouth of the lagoon channel is visible at +2700m. The channel runs parallel to shore up to this point, then turns and connects to the sea. The mouth of the channel forms an abrupt break from the longshore continuous patterns that characterize the intertidal zone of the spit at this time. It is also relatively deep. This generates high levels of local alongshore bathymetric variability, indicated by the red patch in the bottom window of Figure 20 at +2700m, and a dark red tile in the time stack shown in Figure 17.

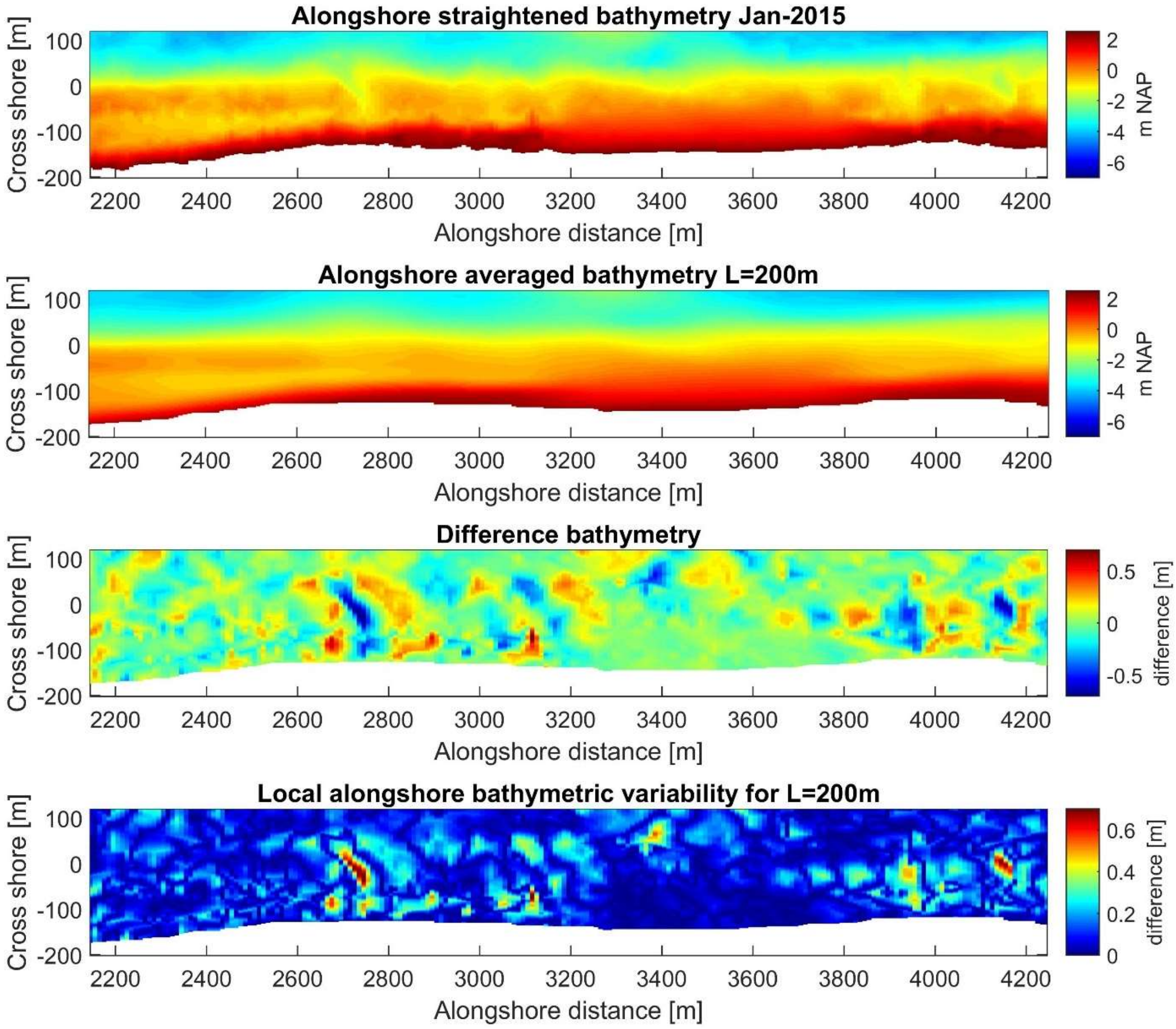

Figure 20: Zoom in analysis around +3000m, intertidal area January 2015. This figure is representative of high bulk alongshore bathymetric variability. The windows show the alongshore straightened bathymetry, the alongshore averaged bathymetry, the difference bathymetry and the local alongshore bathymetric variability, from top to bottom

In January 2015 all groins in the northern NeMo area have remerged from under the beach nourishments. Around +4000m, groins force well defined rip channels, as can be seen in the top window of Figure 20. These groins and rips are clearly a source of alongshore bathymetric variability, as is indicated by the warm colours in the bottom panel of Figure 20 and in the time stack shown in Figure 17.

These two sections of high bulk alongshore bathymetric variability are separated by a short, relatively linear section, without any distinct bathymetric features. This results in low alongshore bathymetric variability, represented by the cold colours in the bottom panel of Figure 20 and in Figure 17. All in all, the results shown in both the bottom window of Figure 20 and in Figure 17 are a good representation of the alongshore bathymetric variability of the measured bathymetry of January 2015.

These three cases are exemplary for the rest of the data set. The bulk values visualised in Figure 17 are a good quantitative representation of the intertidal features, visible in the measurement data. If one is interested in further understanding the relation of the values presented in Figure 17 and the actual measured bathymetry, one can take a look at appendix A3, which contains more pictures of the measured bathymetry. The next section will continue to interpret the patterns in the results presented in Figure 17.

3.2.3 Evolution of the Intertidal Alongshore Bathymetric Variability

The areas of extremely high bulk alongshore bathymetric variability stand out immediately from Figure 17. One such area is the tip of the Sand Motor, around 0m. The subtidal zone in this area is usually characterized by transverse bars. When the intertidal bulk values are high, for instance in from March to May in 2012, or from March to August in 2013, these transverse bars connected all the way up to the supratidal beach. This caused strong undulation in the depth contours, which is the source of the high alongshore bathymetric variability in this area. At other times the transverse subtidal bars where not as well defined (October 2012), or they did not reach the supra tidal beach, and therefore did not affect the alongshore bathymetric variability in the intertidal zone as much (2014).

The other area characterized by remarkably bulk values is the spit of the Sand Motor during 2012. Overall the spit is the most dynamic section of the entire research domain, in terms of gross morphological development. During 2012 the overall shape of the spit was very wavy, and changed rapidly. The lagoon channel usually had two or more branches, and flowed out into sea at two or more locations along the spit. The coastal slope was still very steep during this period, which might be one of the reasons why the subtidal bars connected to the intertidal area relatively often along the spit during 2012. These processes result in the extremely high bulk values for the intertidal zone along the spit of the Sand Motor during 2012.

From early 2013 onwards the spit becomes more linear in overall shape. Also, the coastal slope becomes less steep, which might be the reason why the subtidal bars no longer connect to the intertidal area as often. Finally, the lagoon channel stops having several branches. This is why the bulk values along the spit start to decrease from early 2013 onwards.

The intertidal bulk values decrease significantly for almost the entire domain on three occasions. The first is the December 2013 Sinterklaas Storm. Contrary to the subtidal bulk alongshore variability, the intertidal variability has decreased a lot after the storm. What is also striking, is the fact that the bulk values for the southernmost section of the southern NeMo area remain extremely low from December 2013.

The measurements of November 1st 2014 are representative of the influence of the storm of October 21st 2014. Here too an overall decrease of the bulk intertidal alongshore bathymetric variability can be observed for the southern NeMo area, as well as the Sand Motor. The Northern NeMo section, however, is characterised by an overall increase in bulk values. In the Southern NeMo area less (groin related) rip channels can be observed in November 2014 and the amount of alongshore bathymetric variability has decreased. The coastline along the Sand Motor has become more linear after the storm. In the Northern NeMo area, the groins, present in the entire area, have become more visible in the landscape. In particular the groin related rip channels have become deeper, and more well defined.

The third measurement for which the bulk values decreased overall, is the measurement of June 2015. The month of June was a relatively calm month. During the summer of 2015 a summer storm hit the Netherlands, but this was on July 24th, and its effects are therefore not reflected in this measurement. For this measurement set, a decrease in intertidal bulk values can be observed in the groin fields, between -5000m and -3000m in NeMo South, and the entire Northern NeMo area. What stands out from the measured data, is that the bar and rip patterns still are representative of strongly groin related patterns, just as in the measurement set of March 2015. However, the rip channels seem to have been filled in with sediment to a large extent. It might be that sedimentation of the rip channels has occurred during the calm summer month of June.

During the energetic winter month of January 2015, the intertidal bulk values do not decrease further, as they were already low after the October storm. In the areas with groin fields (-5000m to -3000m in NeMo South and the entire Northern NeMo area) the bulk levels slightly increase.

From these observations it seems that the response of the intertidal area to a storm event is different from that of the subtidal area. The overall reaction to a storm event is a decrease of alongshore variability. However, in areas where the intertidal area is dominated by groins, the alongshore variability can increase due to a storm event. During very calm months the alongshore variability might also decrease due to the sedimentation of the (groin related) rip channels.

3.2.4 The Influence of Groins

Another trend that can be spotted in Figure 17 is the re-emergence of coastal groins. These where covered by a shore face nourishment during the construction of the Sand Motor. In the Southern NeMo area the groins between -5000m and -3000m have reappeared by March 2013. As time develops these continue to become more dominant in shaping the intertidal bathymetry, causing medium high levels of variability. In the Northern NeMo area the first groin heads re-appear in March of 2013. From then on more and more groins re-appear from under the nourished sand. From September 2014 onward the become very dominant in shaping the intertidal bathymetry, resulting in medium high levels off variability.

Figure 21 gives more insight in the importance of the re-emerging coastal groins. In Figure 21 the local intertidal alongshore variability has been averaged over time. Hotspots in this picture show up at locations where high levels of local alongshore bathymetric variability have persisted over time. In areas where the local alongshore bathymetric variability has been (very) high occasionally, these single events of high local alongshore bathymetric variability average out over time and do not show up as hotspots in Figure 21.

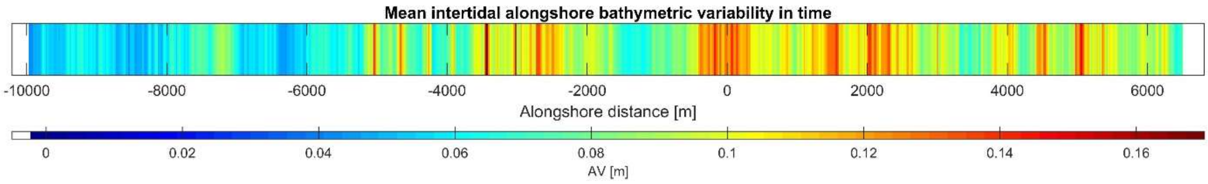

Figure 21: Average intertidal Alongshore Variability. Between -5000m and -3000m the long coastal groins clearly dominate the intertidal variability. From +3000m onwards the shorter coastal groins influence the alongshore variability, but zo not dominate it.

In Figure 21 seven thin lines of high time averaged local alongshore bathymetric variability are present between -5000m and -3000m. Blobs of high time averaged local AV are visible around 0m and 2000m. Between 3000m and 6000m again a few thin streaks of high local AV are visible.

The alongshore locations of the seven thin streaks of high time averaged local alongshore bathymetric variability (between -5000m and -3000m) coincide with the alongshore locations of seven re-emerging long coastal groins. Aerial photographs of some of these groins can be seen in Figure 22 (see next page). What this tells us, is that these seven groins are a dominating factor, shaping the intertidal bathymetry. They continuously force rip channels in their vicinity, and quite often a longshore bar is present in each groin cell in between the groin related rip channels. It does not seem likely that sediment coming from the Sand Motor will be able to cover these groins in the near future.

In contrast the coastal groins in the Northern NeMo area, between 3000m and 6000m, are not able to continuously play a leading role in the formation of bars and rip channels in the intertidal area. These groins can be seen in Figure 23 (see next page). Incidentally, however, they are able to do so. This is what generates the medium high bulk values in Figure 17 in this area. The groins in the Northern NeMo area are relatively short, compared to the seven long groins in the Southern NeMo area. Also, from the bottom left of Figure 23 the advancing spit of the Sand Motor can be seen in the form of well-developed short intertidal longshore bars. It seems very likely that this advancing spit will be able to cover the coastal groins in the Northern NeMo area in the coming months or years.

The blob of high time averaged local alongshore bathymetric variability around 0m shows the influence of the transverse bars in this area. They often play a very important role in shaping the coastline and intertidal area around the tip of the Sand Motor. As these transverse bars change shape constantly, and are not always in the exact same location, their influence shows as a blob medium to high time averaged values in Figure 21.

The blob of high time averaged values around the 2000m marker, shows the influence of the lagoon channel in this area. The mouth of the channel can cause high values of local (and bulk) alongshore bathymetric variability, especially at times when the channel has several branches and mouths. The channel is very dynamic and the mouth moves around a lot, which is why this shows as a blob of medium to high values in Figure 21.

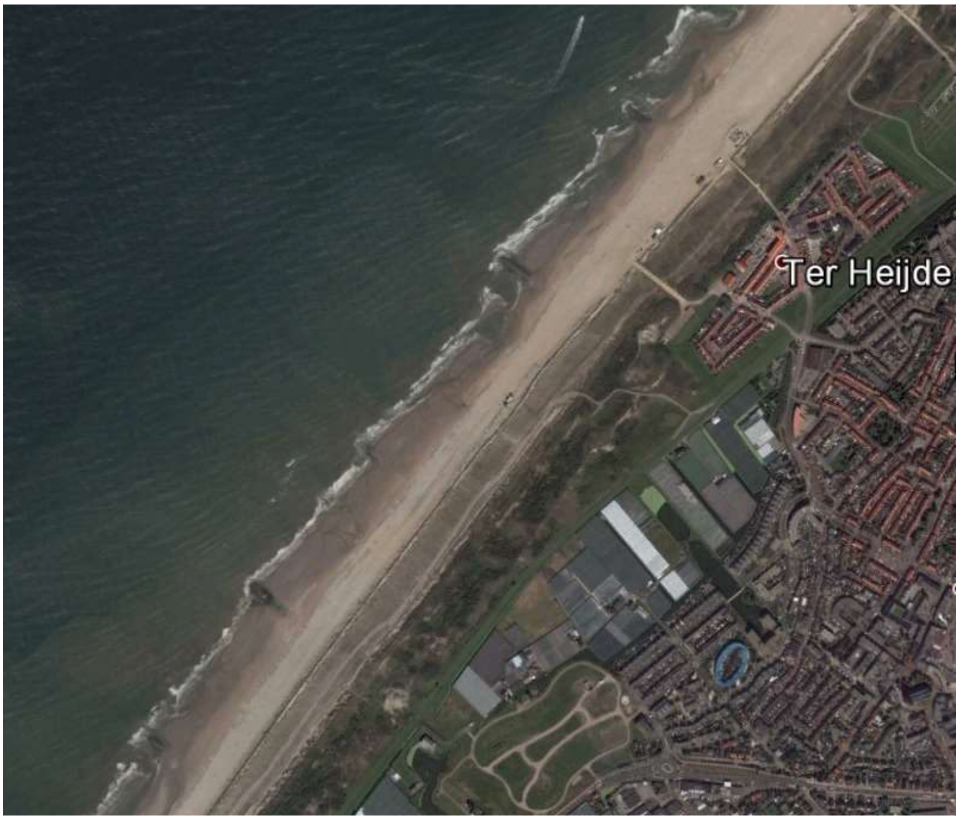

Figure 22: 'Long' groins between -5000m and -3000m for 27-8-2014 (source: Google Earth).

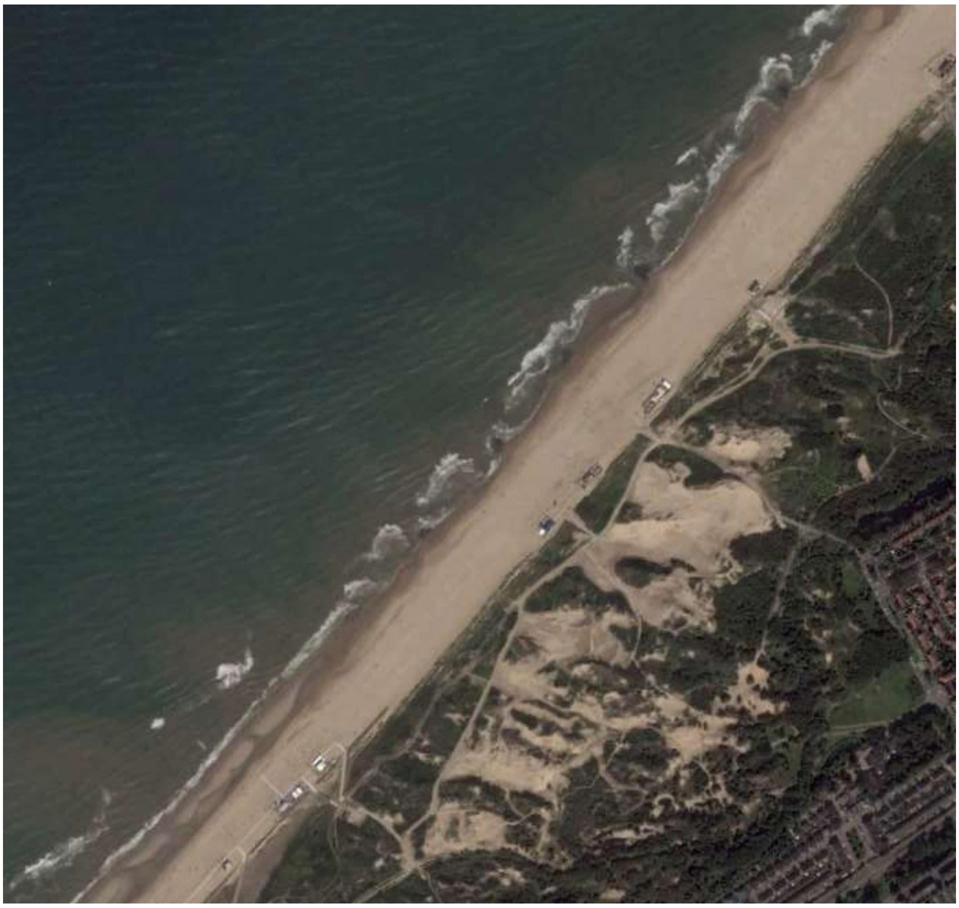

Figure 23: 'Short' groins around +3000m for 27-8-2014 (source: Google Earth). Some of the re-emerged groins are once again being covered with sediment from the advancing spit, visible in the bottom left.

3.3 Spatiotemporal Relations in the Data

This section looks at the bulk values from a different perspective. First data points of bulk alongshore bathymetric variability have been plotted for each measurement, to better study the trends in time. Secondly the bulk data points are studied for the location of each subsection to isolate the special trends from the data. Thirdly, a study of bulk values and the coastline orientation is presented. Finally the relation between subtidal- and intertidal bulk values is investigated.

3.3.1 The Development of Alongshore Bathymetric Variability in Time

Figure 24 shows the development in time of the subtidal- (upper window) and intertidal (lower window) bulk alongshore bathymetric variability in time. For each measurement a scatter of all bulk values for that measurement is shows. The Sand Motor and Southern- and Northern NeMo areas are shown in the colours red, blue and black respectively.

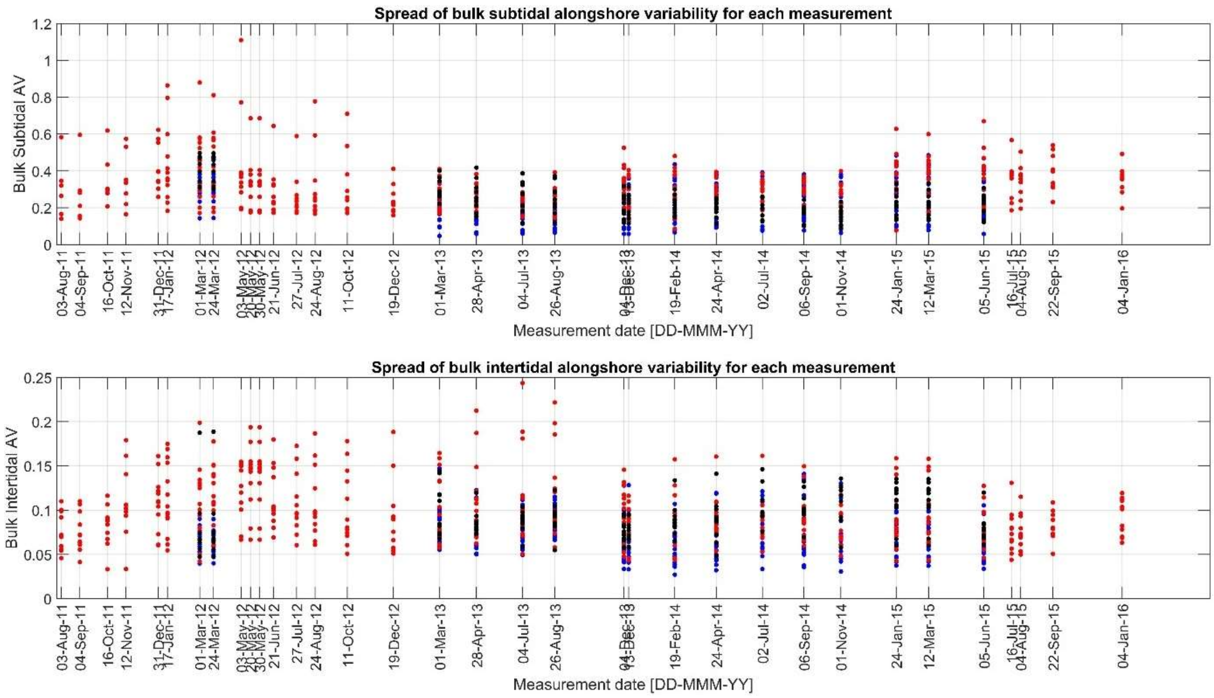

Figure 24: Spread of subtidal- (upper window) and intertidal (lower window) bulk alongshore variability values for each measurement. Blue dots represent data for the Southern NeMo area, red dots data for the Sand Motor area and black dots data for the Northern NeMo area.

In the upper window, the most important trend in subtidal bulk values is the overall increase of the bulk values in late autumn and in winter, supporting the conclusions of de Schipper et al. [2013] as stated earlier. Also visible are the high values produced by the connecting subtidal sandbars around the Sand Motor in 2012. However, in Figure 12 it was clear that different sections of the research domain behaved differently on several occasions. To shed more light on this, Figure 25, Figure 26 and Figure 27 show the data of the Sand Motor-, Southern- and Northern NeMo areas separately.

It is harder to identify such clear trends in the lower window. What is clearly visible, are the overall decreasing intertidal bulk AV values in late fall and in winter. In contrast to what is happening in the subtidal area, this is not in accordance with the conclusions of de Schipper et al [2013]. The overall decrease in bulk values for June 2015 is also visible in Figure 24.

Figure 25 (see next page) shows a spread of bulk values for each measurement, for both the subtidal- (upper window) and intertidal zone (lower window), for the Sand Motor measurement area. The subtidal bulk values are usually below 0.4m.Before December 2012 connecting bars at each side of the Sand Motor generate extreme values up to 1.1m. These decrease throughout 2012, and disappear in December 2012. In general subtidal bulk alongshore bathymetric variability increases for the Sand Motor area during the fall and winter, although there seems to be no reaction to the storm in October of 2014.

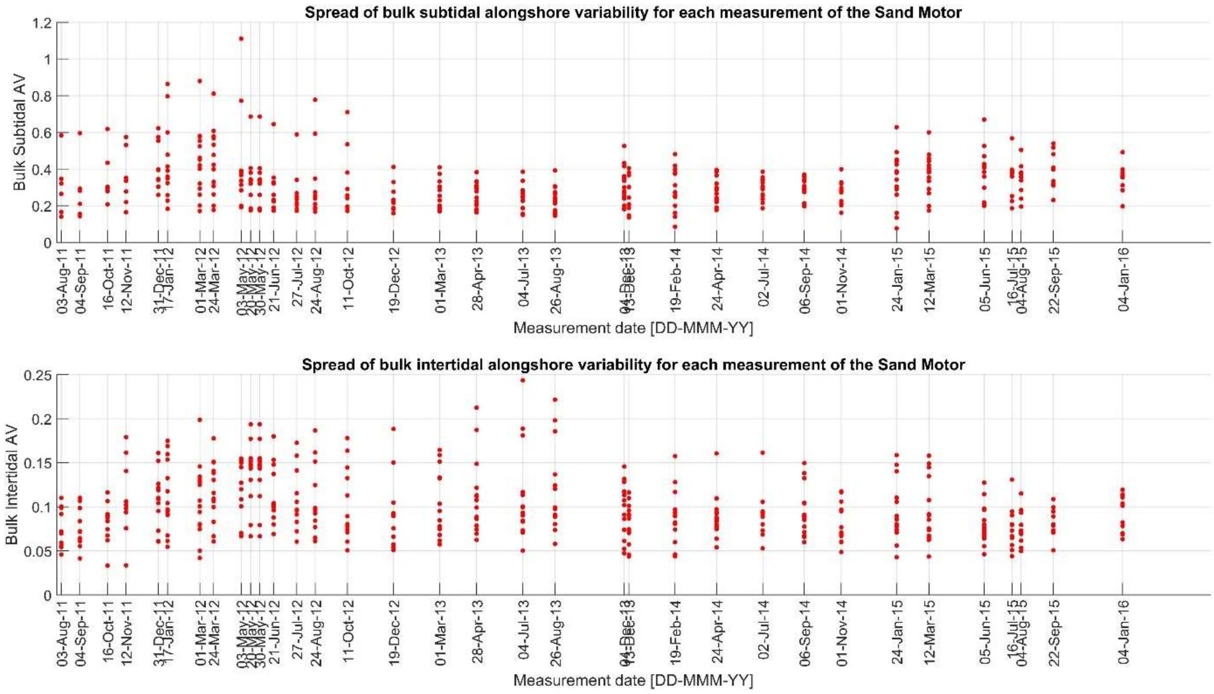

Figure 25: Spread of subtidal- (upper window) and intertidal (lower window) bulk alongshore variability values for each measurement for the Sand Motor area.

The intertidal bulk AV values are very high in the Sand Motor area until December 2013 (see the lower window in Figure 25). Values often reach above 0.15m, with a maximum of 0.25m. After the December 2013 Sinterklaas Storm, the alongshore bathymetric variability becomes very low. From this moment onward overall values are lower than before December 2013. In general intertidal bulk values decrease during the fall and winter seasons.

In Figure 26 a spread of bulk values for each measurement in the Southern NeMo area is shown. Just like in the Sand Motor area, subtidal variability increases in the fall and in winter. And there also seems to be no significant reaction of the subtidal zone to the fall storm in October 2014. During 2013 a clear and steady overall decrease of subtidal bulk AV is clearly visible, until the Sinterklaas Storm. Throughout 2014 subtidal bulk values remain more or less stable. Values are lower than those in the Sand Motor area, usually below 0.4m.

The lower window of Figure 26 shows the intertidal bulk values for the Southern NeMo area. Here one does not see extremes in alongshore bathymetric variability, such as around the Sand Motor. Usually a the maximum level is about 0.1m, which is consistent with the medium high variability related to groins. Overall the intertidal bulk values decrease in fall and winter, just as in the Sand Motor area.

Finally, the subtidal- and intertidal bulk AV values of the Northern NeMo area are depicted in the upper- and lower window of Figure 27 respectively. What stands out in the subtidal picture, is that the seasonality, so clearly visible in both the southern NeMo area and the Sand Motor area, is not present. Instead a steady overall decrease of subtidal bulk alongshore bathymetric variability shows, seemingly starting in March 2012 and lasting until November 2014. In January 2015 an increase in values is visible. Another thing that stands out, is that the spread in subtidal values is relatively narrow. Overall, the values are higher in the Northern NeMo area, than in the Southern NeMo area before the Sinterklaas Storm in December 2013. After this event, the values in the Southern NeMo area are higher on average. Subtidal bulk AV values are lower than those in the Sand Motor area.

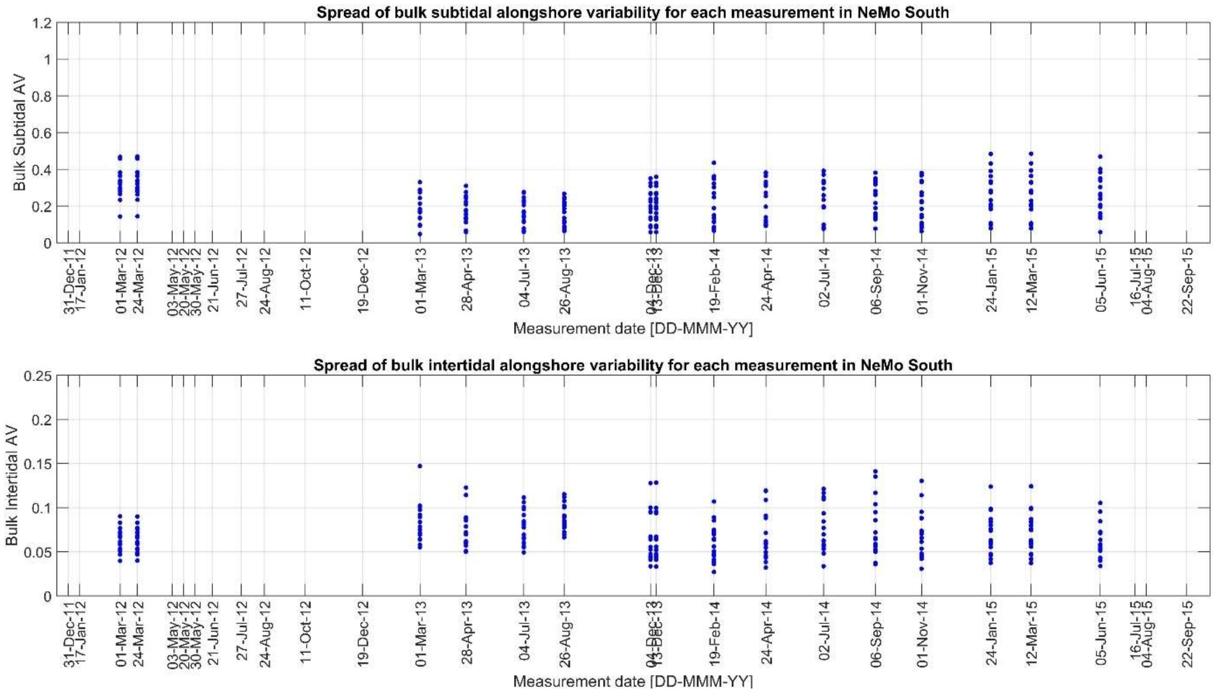

Figure 26: Spread of subtidal- (upper window) and intertidal (lower window) bulk alongshore variability values for each measurement for the Southern NeMo area.

The intertidal bulk values in the lower window of Figure 27, also do not show seasonal behaviour as strongly as in the other areas of the research domain. There is however a clear decrease in intertidal bulk values in December 2013. On average intertidal bulk values in the Northern NeMo area, are higher than those in the southern NeMo area, especially after the December 2013.

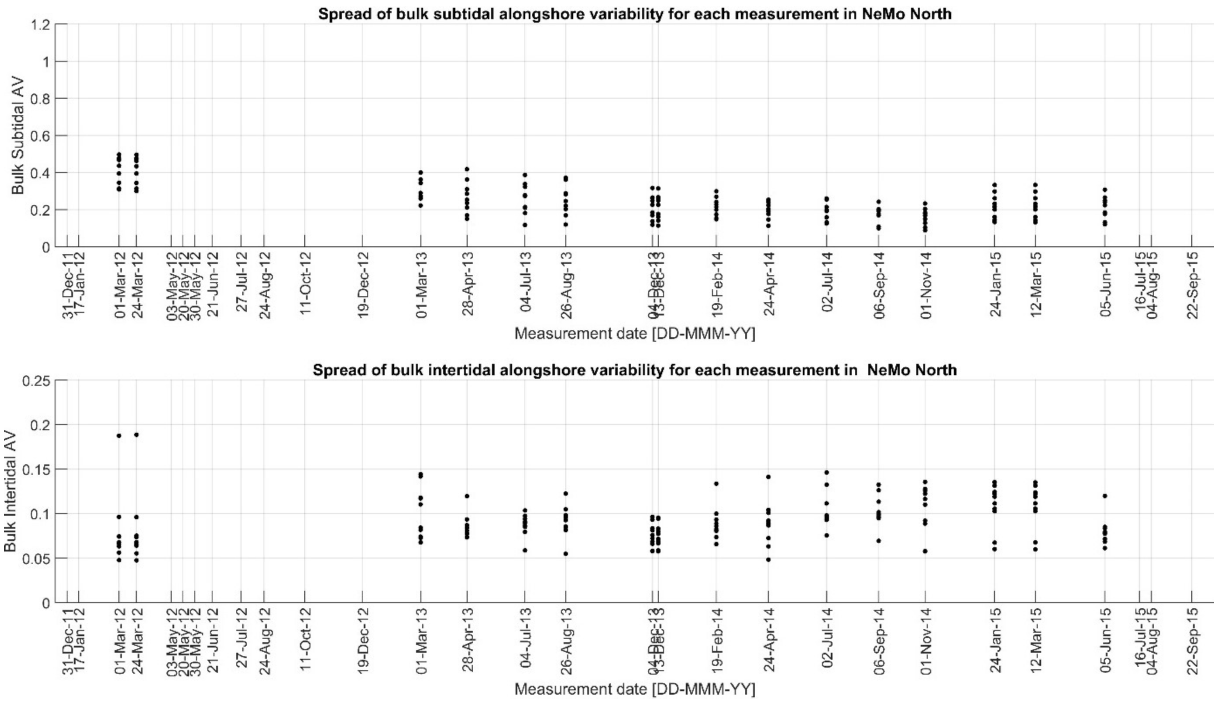

Figure 27: Spread of subtidal- (upper window) and intertidal (lower window) bulk alongshore variability values for each measurement for the Northern NeMo area.

3.3.2 Trends of Alongshore Bathymetric Variability in Space

In order to identify possible spatial trends of bulk alongshore bathymetric variability in the research domain, a plot of all bulk output values, for each 400m section of the research domain, is shown in Figure 28. The left window shows the subtidal bulk values and the right window shows the intertidal bulk values.

The extreme peaks in the subtidal bulk values around -2000m and 2000m are caused by the connecting bars in 2012. For the entire Sand Motor area, the spread of values is very large. The Sand Motor really stands out, both in terms of high and low subtidal bulk values. Both the Northern and Southern NeMo areas are characterized by relatively narrow spreads. In the Southern NeMo area, the presumed influence of the Hoek van Holland breakwater is clearly visible from -6000m onwards.

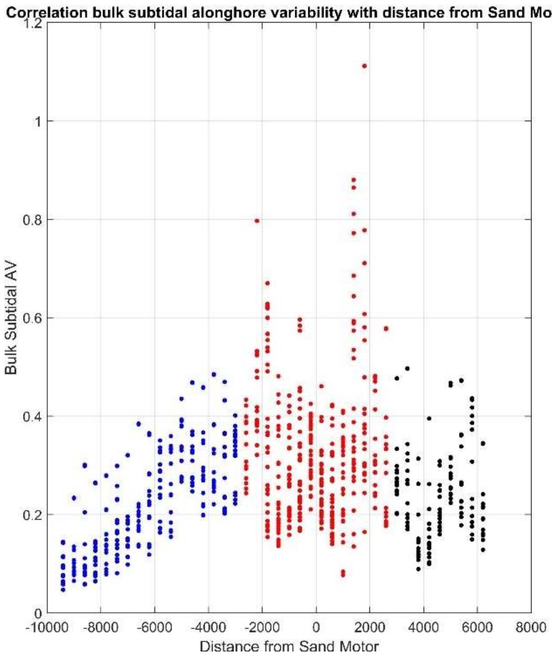

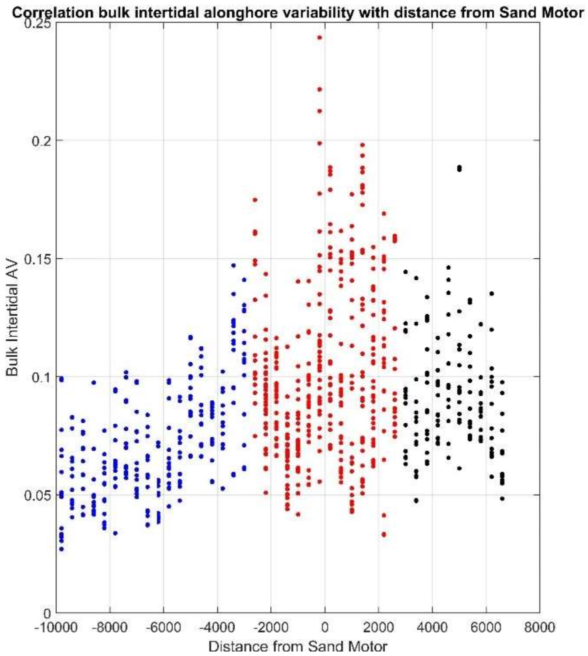

Figure 28: Left window: Subtidal bulk alongshore variability for each subsection and measurement in the dataset. Right window: Intertidal bulk AV for each subsection and measurement in the dataset. Bulk AV for subsections at the Sand Motor (red dots), NeMo-North (black dots) and NeMo-South (red dots) areas. Note different scaling for intertidal and subtidal windows.

Looking at the right window in Figure 28, again the intertidal bulk values at the Sand Motor stand out. The spread of values in the Sand Motor area is very large. What also stands out are the relatively low values around -1000m, an area which is dominated by a subtidal longshore bar for a long time. It seems that areas with less variable subtidal features, such as near Hoek van Holland, do not coincide with high intertidal alongshore variability. Highly variable subtidal features, such as transverse bars, can coincide with extremely high intertidal alongshore variability.

Medium high alongshore variability can also be related to groins, such as in the Northern NeMo area and in the Southern NeMo area from -3000m to -5000m. Even behind less variable subtidal features, such as the longshore bare around the +4000m marker. The lagoon channel, the influence of which is visible from 1000m to 2000m in the right window of Figure 28, can also generate higher intertidal bulk values. The sections of the Southern NeMo area which are not dominated by coastal groins have lower maxima in intertidal bulk values than sections of the NeMo area which are dominated by groins.

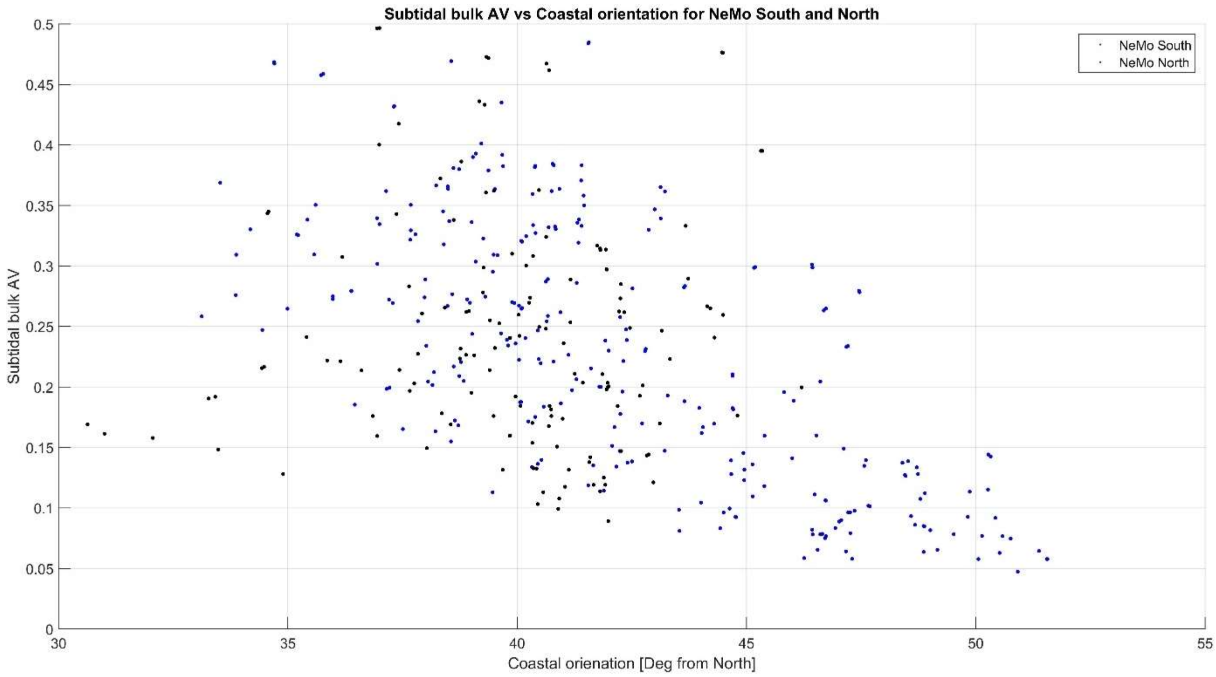

Figure 29: Scatter plot of subtidal bulk alongshore variability (vertical axis) vs coastline angle in degrees from North (horizontal axis). Blue dots represent data from the southern NeMo area, black dots represent data from the Northern NeMo area.

Figure 29 gives an overview of the relation between subtidal bulk alongshore bathymetric variability, and the coastal orientation, for both the southern-, and norther NeMo areas. Most data points in this figure are situated around the 40˚ to North (the 'normal' orientation of the Delfland Coast), and have quite a wide range in alongshore bathymetric variability. The data points around 50˚ to North are representative of sections that are influenced by the breakwater at Hoek van Holland. Here the presence of the breakwater seems to induce reorientation of the coast line, and cause a persistent decrease in the bulk alongshore bathymetric variability.

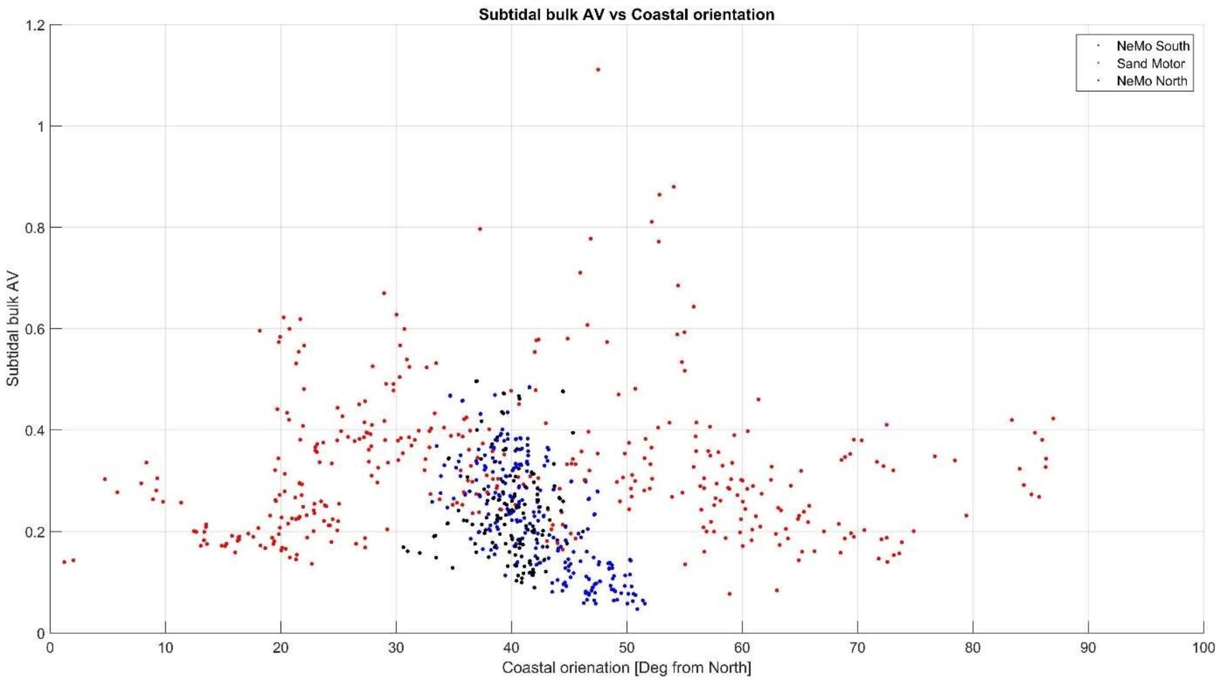

Figure 30: Scatter plot of subtidal bulk alongshore variability (vertical axis) vs coastline angle in degrees from North (horizontal axis). Blue dots represent data from the southern NeMo area, red dots represent data from the Sand Motor area and black dots represent data from the Northern NeMo area.

In Figure 30 the subtidal bulk values of the Sand Motor have been added to those of the NeMo area(see previous page). The range in orientations of the Sand Motor coastline is naturally much higher, than along the rest of the Delfland Coast. The spread in bulk values is also a lot higher along the Sand Motor, and this spread largest between 20˚ and 60˚ to North. A clear relation between the variability and coastal orientation does not seem to exist for the Sand Motor.

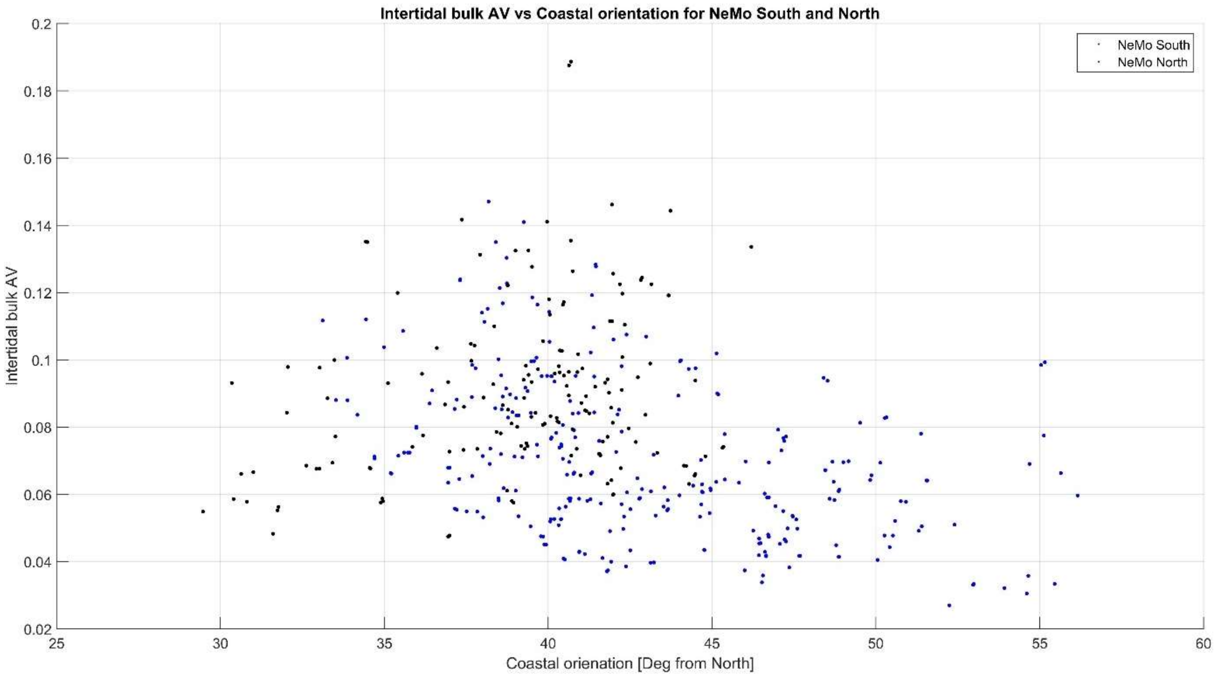

Figure 31: Scatter plot of intertidal bulk alongshore variability (vertical axis) vs coastline angle in degrees from North (horizontal axis). Blue dots represent data from the southern NeMo area, black dots represent data from the Northern NeMo area.

Figure 31 shows the relation between the intertidal bulk alongshore bathymetric variability, and the coastal orientation, for both the southern and northern NeMo areas. Here, the same general picture arises as in Figure 29, except that the spread in intertidal bulk values seems to be relatively small.

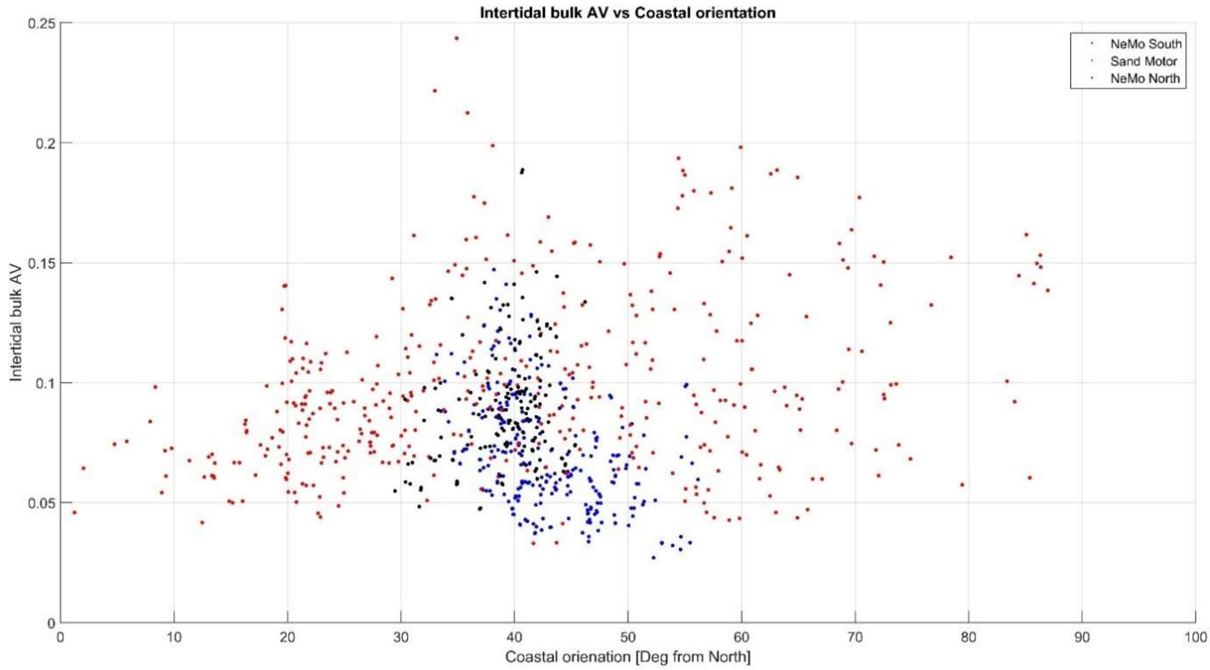

Figure 32: Scatter plot of intertidal bulk alongshore variability (vertical axis) vs coastline angle in degrees from North (horizontal axis). Blue dots represent data from the southern NeMo area, red dots represent data from the Sand Motor area and black dots represent data from the Northern NeMo area.

Figure 32 now includes the data points of the bulk alongshore bathymetric variability along the Sand Motor. A similar picture arises as in Figure 30, except for the fact that the extremely wide range in bulk values along the Sand Motor relates to a wider range in coastal orientation: from 30˚ to 90˚ to North.

All in all the 'normal orientation' along the Delfland Coast is around 40˚ to North, and sees a spread of low, to medium variability for both the subtidal-, and intertidal zones. The breakwater at Hoek van Holland seems to both cause a reorientation of the coastline, and a decrease in the spread in variability, resulting in mostly low alongshore bathymetric variability for both the subtidal-, and intertidal zones. The Sand Motor sees a very wide spread in variability, from low to high. There does not seem to be a clear relation between the variability and the coastal orientation of the Sand Motor.

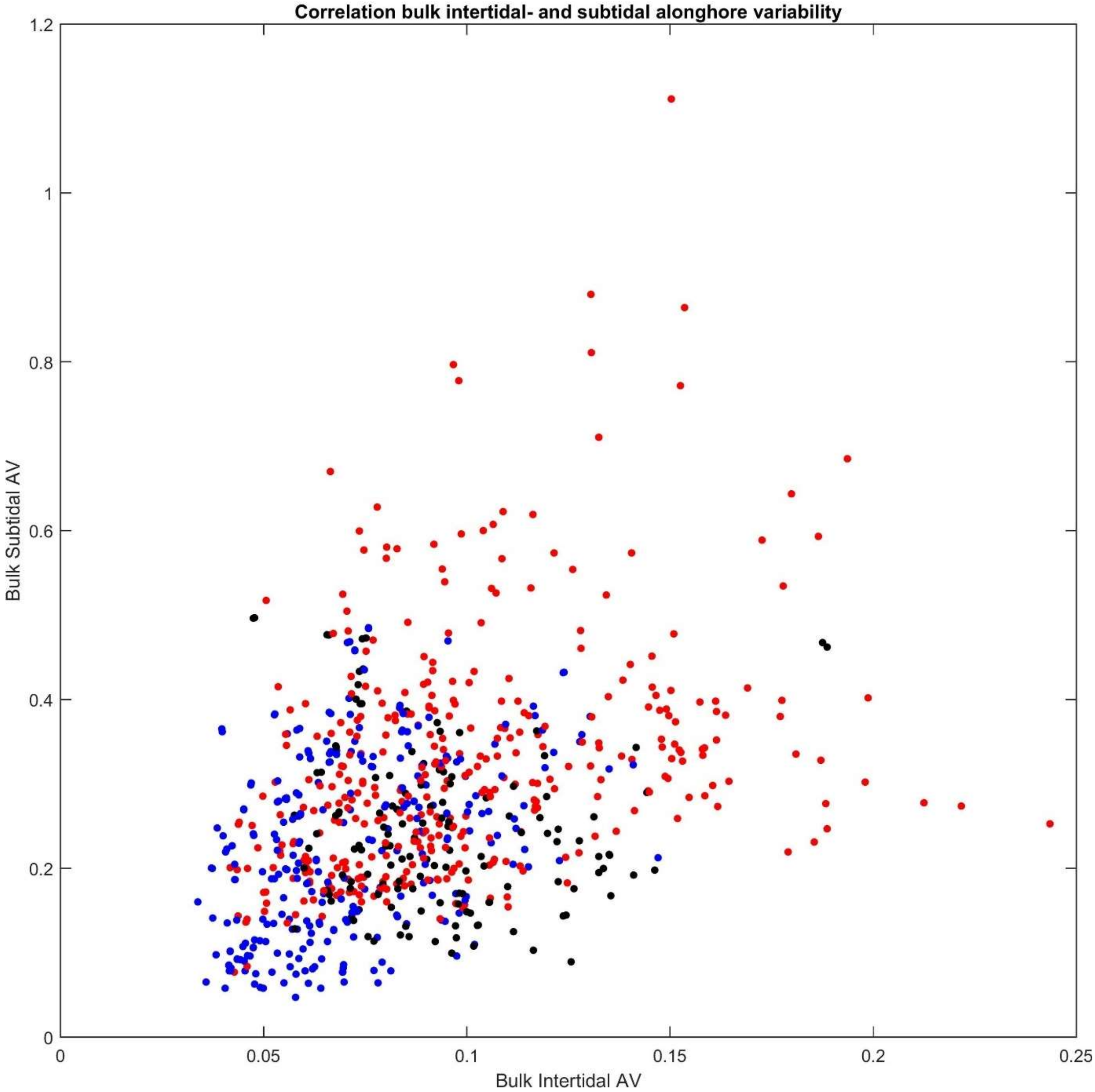

Figure 33: Correlation intertidal- and subtidal bulk alongshore variability for entire dataset. Comparing bulk AV values for the intertidal- and subtidal zones, for each 400m long subsection of coastline. Bulk AV for subsections at the Sand Motor (red dots), NeMo-North (black dots) and NeMo-South (red dots) areas

Figure 33 shows the relation between the subtidal bulk alongshore bathymetric variability on the vertical axis, and the intertidal bulk alongshore bathymetric variability on the horizontal axis. Most of the data points seem to be situated in the low, to medium variability region, and mostly relate to the NeMo area. The more extreme combinations of variability have almost always been generated along the Sand Motor.

For extremely low amounts of alongshore bathymetric variability, there seems to be a narrow spread in the relation between bulk subtidal-, and –intertidal values. So: extremely low subtidal variability, is almost always related to very low intertidal variability. Note that these data points are not only representative of the area near Hoek van Holland. For increasing bulk values the spread becomes rapidly wider. Especially along the Sand Motor, some extremely high values of variability relate to only medium high levels of intertidal variability. And some extremely high values of intertidal variability, seem to relate to quite low values of subtidal variability.

All in all extremely low values of alongshore bathymetric variability in one zone, only seem to match up with extremely low values in the other zone. For any level of variability above this, the spread becomes so wide, that a clear relation cannot be found, except for the fact that very high levels of variability in one zone, never match up with extremely low levels of variability in the other zone.

3.4 Reliability

It has been stated that the bulk parameter accurately represents the variability along a subsection of the Delfland Coast. Readers interested checking this claim, or interested in the bathymetric features which have generated the bulk values, can find an extensive overview of interesting bathymetry plots in appendix A3.

3.5 Conclusions Data Analysis

Here the main research question of this chapter is answered. This is research question two:

How does the alongshore bathymetric variability of the Delfland Coast develop during the studied period?

In accordance with de Schipper et al. [2013] the subtidal alongshore bathymetric variability along the Delfland Coast mostly decreases in the winter months when environmental conditions are more energetic. In the intertidal area the alongshore bathymetric variability usually decreases in the winter months, in contrast to the conclusions of de Schipper et al. [2013].

Very low levels of subtidal variability coincide with low levels of intertidal variability and vice versa. Very high levels of subtidal alongshore bathymetric variability coincide with a wide range of intertidal alongshore bathymetric variability, from low to very high.

The lowest levels of subtidal variability occur near the Hoek van Holland breakwater. In this area the intertidal alongshore bathymetric variability is usually low. The presence of groins can make the response of the intertidal area more complex. Groins can force the medium high levels of alongshore bathymetric variability, even when subtidal levels are low.

The highest levels of subtidal alongshore bathymetric variability are related to the sand bars which connect the subtidal area of the Sand Motor to that of the NeMo area in 2012. Subtidal variability can also be very high for transverse bars, at the tip of the Sand Motor for example. Here high levels of subtidal alongshore bathymetric variability are only associated with high intertidal levels if the bars run through the intertidal zone and connect to the supra tidal beach. If this is not the case than intertidal levels of alongshore variability can be can be quite low.

The highest levels of intertidal alongshore bathymetric variability are related to the lagoon channel. The lowest levels are related to the absence of any clear morphological features.

The low values of alongshore bathymetric variability near the breakwater at Hoek van Holland coincide with a coastal orientation of 50° to North. Other sections of the NeMo area see a higher spread of variability for a coastal orientation of about 40° to North. For the Sand Motor there seems to be no relation between the alongshore bathymetric variability and the coastal orientation.

4. Methodology Modelling Study

This Chapter discusses the method of the modelling study which tries to relate alongshore bathymetric variability to currents which form a risk to bather. This chapter mainly handles the model setup, the calibration and the validation of the model performance. This chapter will answer research question three:

How can the (parameterized) alongshore variability be related to currents which form a risk to bathers?

4.1 Model setup

The basic idea of the modelling setup explained here is similar to that used in Vargas Solis [2015]. The main differences with the modelling approach explained here are due to the differences in objective. The objective of the model approach, is to identify the relation between the bulk alongshore bathymetric variability, presented in the time stacks of the previous section, and wave induced currents which form a risk to bathers. Essentially this is an attempt to quantify the relation between bathymetrically controlled, wave induced currents, and variability in the bathymetry as described in literature (MacMahan [2006, 2008], de Zeeuw [2011]), for the situation of the Delfland Coast. Whereas Vargas Solis [2015] was interested in sediment transport, focussing on the subtidal bars.

In order to be able to relate alongshore bathymetric variability to certain flow velocities and flow structures, a set of model bathymetries have been generated using the alongshore straightened bathymetries of the previous section as a basis, covering a wide range of bathymetric variability. Together with the computational grid, initial- and boundary conditions, these model bathymetries have formed the basis of numerical model computations in Delft3D modelling software.

Before we dive into the details of the models used, it is insightful to tell something about the modules of Delft3D, which have been used. Two modules of the Delft3D modelling software have been used; the wave module and the flow module. The wave module uses SWAN, which calculates wave-bathymetry interactions (shoaling), wave-current interactions, wave induced setup, and depth induced wave breaking (breaking point). The flow module calculates the depth averaged current velocity and -direction. The roller model has been used in the flow module. After waves reach the breaking point (calculated by SWAN), a bore-like roller persists, and distributes the momentum due to wave breaking over a larger area than just the breaking point (Reniers, Roelvink and Thornton [2004]). The roller model accounts for this. (Delft3D-Flow user manual). Use of the roller model generally results in more realistic current patterns around the bars (Ruessink et al [2001], Morris [2001], Dykes, Hsu and Kaihatu [2003]).

4.1.1 Model bathymetry

The first step in generating the model bathymetries is to take a look at the bulk alongshore bathymetric variability time stacks in Figure 12 and Figure 17. To be able to relate the bathymetric variability of the Delfland Coast to certain flow parameters, the entire range of variability in both the intertidal and subtidal areas needs to be represented by the model bathymetries.

This essentially has been done by cutting a tile of nearshore bathymetry, out of the alongshore straightened bathymetries of the previous chapters. Such a tile should adequately represent the bulk alongshore variability of the corresponding cell in both the intertidal-, as well as the subtidal time stack. This tile has been pasted several side by side several times over, creating the model bathymetry for one case. In total over sixty such model bathymetries have been generated, covering the range in both time stack as good as possible.

After selecting a case from the time stacks, first the section of interest is cut from the relevant alongshore straightened bathymetry. When making such a cut, it is important to remember that the objective is to analyse the (offshore directed) wave driven rip currents. These will most likely flow through the rip channels. Therefore the cuts have been made on the bars rather than in the rips, in such a way that the dominant length scales are preserved.

Below in Figure 34 the top window shows the alongshore straightened bathymetry for the March 2013 Dataset, zoomed in around the Sand Motor area. A tile has been cut out, around the transverse bar and rip, focussing on the rip channel at +200m in the top window.

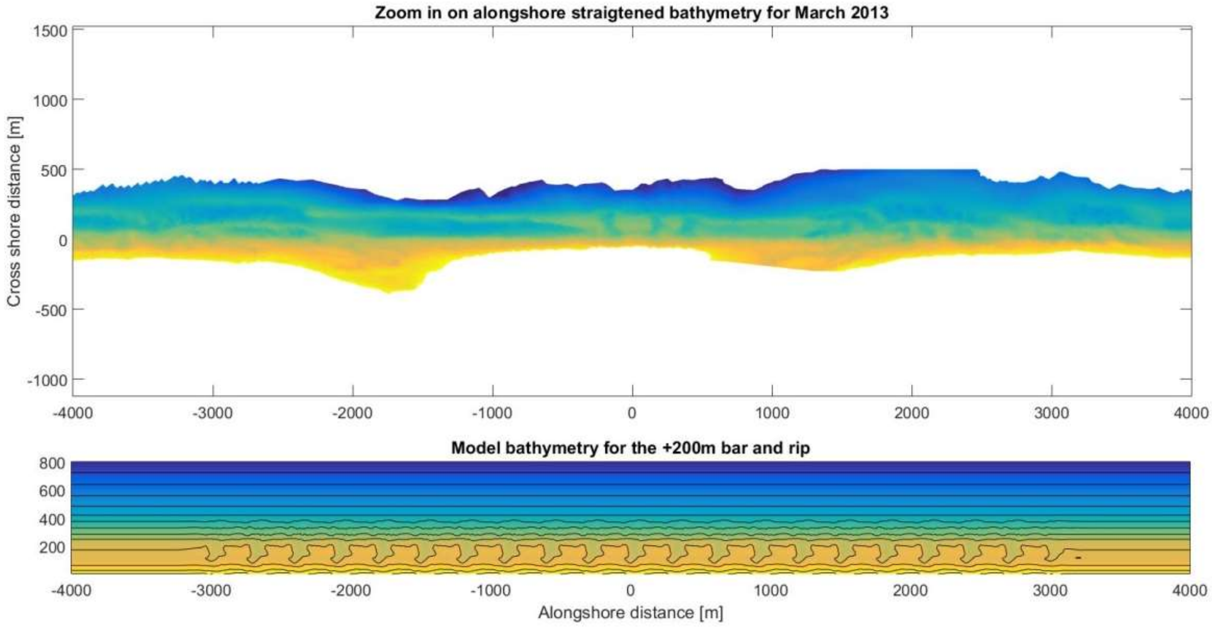

Figure 34: Alongshore straightened bathymetry around the Sand Motor for March 2013 (top window) and model bathymetry generated with a tile cut around the +200m rip (bottom window)

In the bottom window the repeating pattern of the tile can be seem between -3000m an +3000m. Toward the alongshore boundaries at -4000m and +4000m in the model bathymetry, an alongshore non-variable bathymetry has been generated, using the mean profile of the tile. The tile reaches to about 400m cross shore. From this point to the boundary at about 800m, a non-variable foreshore has been generated, with a constant slope, down to a depth of 12m NAP. In order to prevent the generation of artificial bathymetric variability, smoothing has been applied by means of crossfading the different bathymetries over a distance of 50m on all tile connections.

The next step is to determine the representative bulk alongshore bathymetric variability of the model bathymetry for both the intertidal and subtidal zone, and to compare this with the original values in the time stacks. The method for determining the bulk values of the model bathymetries is the same as presented in chapter 2. The results for both the intertidal- and subtidal bulk alongshore variability, with a bin size of 400m is shown in Figure 35.

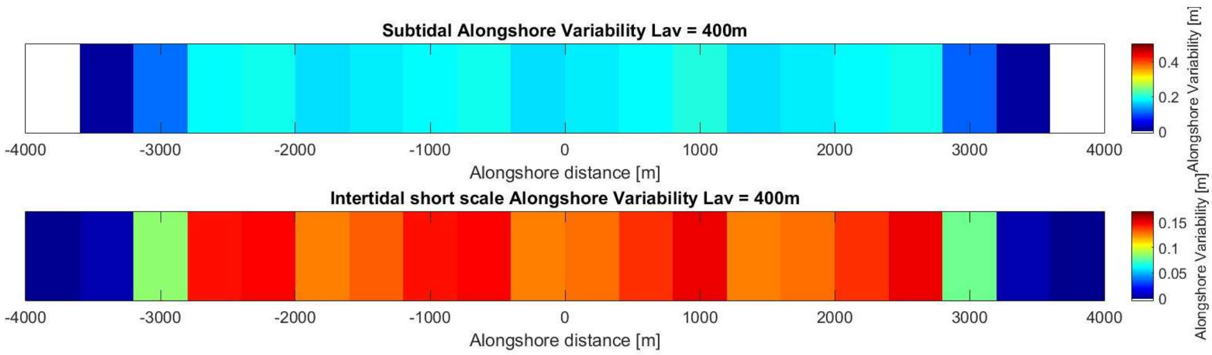

Figure 35: Bulk alongshore variability for the test model bathymetry in both the subtidal- (upper window) and intertidal zone (lower window)

As one can see in Figure 35, the bulk values vary somewhat as the edge locations of the bins vary over the variable bathymetric pattern. This is not a problem, as long as the values do not vary too much. A representative parameter is generated by taking the average of the bulk parameters generated between -2000m and +2000m.

Judging whether a generated model bathymetry is fit for use depends on three main questions:

- Is the difference between the computed bulk parameters and the bulk parameters from the time stacks less than 10%?
- Does the bulk alongshore variability show only minor differences between -2000m and +2000m?
- Does the generated bathymetry look alright, or has the process of cutting and pasting generated an artificial pattern, which is not representative of the original pattern observed in the field data?

The first question is the most important one. If something is wrong with the computed bulk parameter, it cannot be used for further analysis. The second question basically asks how representative the mean bulk parameter is for the bulk parameters generated between -2000m and +2000m.

The third question seems redundant. But cutting in the wrong location can, in practice, generate patterns which might have the correct level of bulk variability, but that simply do not represent a real bar and rip situation anymore. For instance, cutting a rhythmic bar in half, might generate the needed level of bulk variability, but it also generates a bathymetry with repeating, unconnected, skewed bars, rather than a longshore continuous string of rhythmic bars. This will generate flow patterns which simply will not have any relation to the real situation. This should be avoided at all time.

The parameter check for the example shown here reads as following:

Intertidal bulk AV = 0.13449

Real intertidal bulk AV = 0.1645

Agreement intertidal bulk AV = -18.244%

Subtidal bulk AV = 0.17777

Real subtidal bulk AV = 0.30293

Agreement subtidal bulk AV = -41.3166%

Clearly this example does not make the grade. By going back to the original plots made during the computation of the bulk parameters in the time stacks, more insight can be gained in which features originally generated the bulk variability in the time stacks. By making sure all these features are included, a good representation of the real world can be made.

A possible solution is shown in Figure 36. Here the adjacent rip channel has been included, to come to a better representation of the real world.

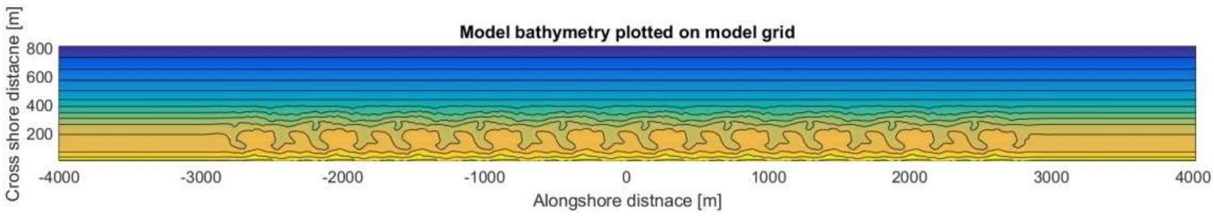

Figure 36: Improved model bathymetry for March 2013

4.1.2 Computational grid

For Delft3D to be able to run, the domain needs to be discretised to a finite number of computational cells. This is done by means of a computational grid. The finer the grid resolution, the closer the computational grid approaches the real world. However, including more cells mean more computational time. In order to speed up the computational process varying grid cell sizes have been used. In this way, a high resolution can be obtained in the area of interest (over the bars), while toward the boundaries the resolution decreases.

The fine area of the grid has a resolution of 10m alongshore and 5m cross shore. The fine area of the grid reaches from -3000m to +3000m alongshore, and from 0m to 400m cross shore. Over a length of 200m in both the cross shore and alongshore directions, the grid becomes coarser until the grid resolution becomes 20m by 20m in the far offshore corners of the grid. Note that for the offshore grid cells in between -3000m and +3000m, the alongshore resolution remains 10m, and for the nearshore grid cells beyond these extremes the cross shore resolution remains 5m.

As stated earlier, Delft3D essentially will run two modules: a flow module and a wave module. Each will need a computational grid. For the model approach used in this thesis research, the same grid has been used for both models. This will lead to 'shadowing effects' if the direction of the waves specified at the offshore boundary is not perpendicular to shore (and the offshore boundary). If the angle stays within 30 degrees, this shading effect will fall inside the longshore non-variable section of bathymetry, near the lateral boundaries. For the model approach used here, this is sufficient. The wave conditions are discussed in greater detail in the next subparagraph on the boundary conditions.

4.1.3 Boundary conditions

Both the flow module and the wave module require boundary conditions. For the flow module boundaries have been specified on the two lateral boundaries of the computational grid, and on the offshore boundary. The offshore boundary condition has been specified as a water level boundary condition (Dirichlet type), setting the water level to 0m NAP at the offshore boundary in the flow module. On the lateral boundaries a Neumann boundary condition has been used, setting the water level gradient to zero. This boundary condition is needed to limit the effects of pressure gradients near the boundary, which can induce (accelerated) flow, something which is especially important when using the roller model (Dykes, Hsu and Kaihatu [2003]). The model bathymetry essentially forms the fourth, closed boundary at the shoreline.

In order to be able to understand the choices made in generating the boundary conditions for the wave module, it is good to go back to the objective of this modelling approach. The objective of this modelling approach is to relate alongshore bathymetric variability to potentially dangerous currents in the nearshore area. However, dangerous, wave induced currents in the nearshore can also be generated, without the need for bathymetric variability (Johnson and Pattiaratchi [2006], Reniers et al [2007]). These so-called transient rips are, simply put, generated by the natural variability in a wave signal and are not caused by or bound to topographical features. However Delft3D applies wave averaging in its calculations, and therefore it cannot resolve long waves or very large frequency motions, which force flash rips. Using a wave condition with a tight directional spreading, the influence of the bathymetric variability on nearshore (rip)currents can be isolated.

The wave module requires a wave condition. This wave condition has been specified at the offshore boundary. All models used for this thesis research have been forced with a similar, simple wave condition: a significant wave height of 1.5m and a peak wave period of 6s. The only thing which has been varied from model to model is the incoming wave angle. Figure 37 can help explain this choice.

The peaks in Figure 37 indicate that during the summer, waves mostly come in from the South West and the North. Everything up to the yellow bands in the bars are representative of wave heights up to 1.5m. Not only are waves higher than 1.5m rare in the summertime, such extreme conditions are not favourable for bathing. The 1.5m wave height can be seen as an upper extreme for bathing conditions. This wave height is also likely to cause wave breaking over the subtidal bar. Note that this exceeds the 1m wave height scenario, described as especially dangerous for bathers by Scott et al. [2014].

The main objective of looking at different incoming wave angles, rather than only the shore normal direction, is to find the incoming wave angle, for which the longshore current starts to dominate, and the rip channels are being bypassed. The shore normal direction (perpendicular to the shoreline) in Figure 37, is at about 313° to North. From Figure 37 one can see that the peaks in the figure occur at about 70° to 80° from shore normal. However, as stated in the subparagraph on the computational grids, due to the choice of the computational grid for the wave module, a 30° angle from shore normal is the maximum for this model approach. In the next chapter it will be shown that this suffices.

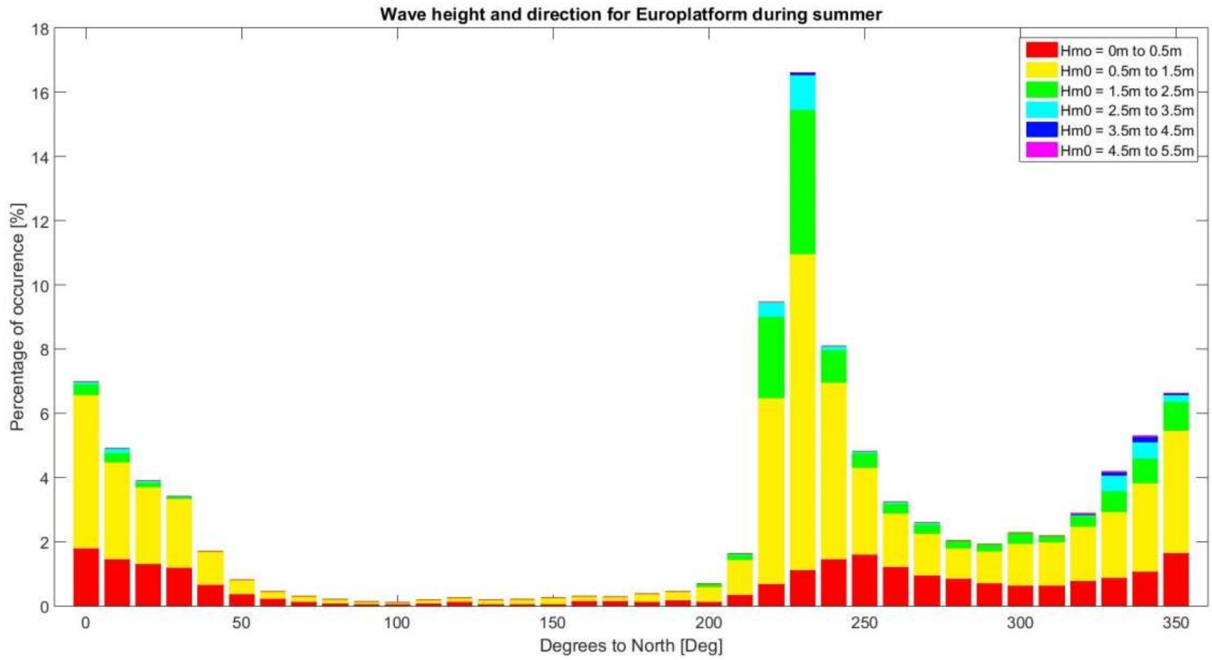

Figure 37: Summer wave rose for the Europlatform measurement station (Long year wave statistic in the months June - September)

So the wave module has been forced with a single wave condition on the offshore boundary. The significant wave height has been set at 1.5m, and the peak period at 6s. The direction is varied from model to model for each model bathymetry, from -30° to +30° to shore normal with increments of 5°. This means that each model bathymetry has been used in thirteen different models, each being forced with a different incoming wave angle. This means that for this model study, a total of 819 model runs have been executed.

One thing which is clearly missing from the boundary conditions is the tide. The tide causes water level fluctuations, causing water to flow in and out of the nearshore area due to the volume effect. This volume of water will preferably leave through existing channels in the nearshore area such as rip channels. The magnitude of currents related to the volume effect is typically an order of magnitude smaller than the magnitude of wave induced currents in the nearshore along the Delfland Coast. So not accounting for this effect will not lead to extreme underestimation of the nearshore currents.

The tide, however, does not only cause significant variations in water level at the Delfland Coast, it also generates (mostly longshore directed) currents. These currents can induce earlier rip bypassing, than caused by the wave driven longshore current alone. This cannot be accounted for in the modelling approach used here.

Scott et al. [2014] described a relation between the moment of mean low water, and bather risk[3]. Unfortunately such detailed rescue data is not available for the Dutch Coast. However, Dutch life guards have often pointed out that rips in the intertidal area are a very important factor affecting bather risk along the Dutch coast (de Zeeuw [2011]). This could fall in line with the notion of 'active morphology' in Scott et al. [2014], where the water level elevation determines which part of the bathymetry is actively interacting with the incoming wave signal. Therefor a water level elevation of 0m has been chosen, leading to water depths in the order of 1m to 2m over the intertidal area.

[3] Note that due to continuity the current velocities related to the volume effect are at a minimum around mean low-, and mean high water, as the rate of water level change is at a minimum for these moments. This observation supports the assumption that the influence of the volume effect is negligible.

4.1.4 Initial conditions

The time timeframe for the computations was two hours of simulated time (virtual time inside the models) for waves coming in at -5°, 0° and 5° to shore normal. For the other computations the timeframe was three hours of simulated time. This is because the larger wave angles generate a longshore current. This current needs some more spin up time than the cross shore directed rip currents, and hence needs some more simulation time, before the modelled flow becomes stable.

A time step of 6s has been used. This does not lead to stability issues, leads to a sufficiently accurate answer, and does not blow up the computational time (real world time, needed to run the models).

Finally the communication between the flow and the wave module has been specified every 15 minutes of simulated time, and the output of the flow module has been stored every 15minutes of simulated time.

4.2 Validation

Unfortunately, there was no data available for model validation. But what does this mean for the reliability of the model output? The other physical- and numerical parameters have been obtained from other, well validated numerical models of the Holland coast (see Radermacher [2017]). So the order of scale of the model behaviour can be seen as representative for the Delfland Coast. The relative behaviour of the output of the different model runs can also be seen as being representative. So features inducing strong wave breaking, and/or strong rip currents will also do so in real life. The exact velocities themselves, however, should be handled with some caution as there is no data available to verify them. This should be kept in mind when handling the results of the model runs.

4.3 Calibration

As stated earlier, most of the physical- and numerical parameter values have been obtained from well validated models of the Holland coast. The only calibration parameters remaining in this model approach, are the incoming wave angle, the wave height and -period, and the water level.

The wave angle is an object of study. So the response of the model output to changes in wave angle will be handled in the next paragraph on the model results. As stated in the sub paragraph on the boundary conditions, the chosen wave height is seen as an upper limit for recreational conditions. An increase in wave height, will lead to an increase in the driving forces of the wave induced currents. However, such cases are not of interest for this study into recreational safety. Using a lower wave height has the opposite effect. Small variations to the wave height do not lead to significant differences in the wave induced currents in this model. So the currents calculated by these models can be seen as representative for the upper limit of recreational conditions.

The water level has been set at 0m NAP. Changing the water level can have some significant consequences for the model output. Lowering the water level to a level representative for mean low water in the tidal signal, will mean that the intertidal zone will largely be situated above the water level, and therefor will not be part of the modelling study. It will also mean that the waterline is a considerable walking distance away from the beach, which may have consequences when it comes to analysing swimmer safety. Wave breaking over the subtidal bar will intensify, and possible rip currents in the subtidal area will grow stronger. Increasing the water level will decrease the wave breaking over the subtidal bar.

Even slight changes in water level can affect the model output significantly. Especially in the intertidal zone, where the relation between the flow velocity and the water depth is highly non-linear, small changes in water level, can lead to significant changes in rip velocities. This is a shortcoming of this modelling approach and one which will have to be accounted for in processing the results.

The water level set at 0m NAP means that the intertidal bathymetry is included in the study. This also means that dangerous currents may exist relatively close to the beach. The subtidal bar will also induce some wave breakage, allowing for the possibility of an intertidal rip current to flow out into a subtidal rip current, creating a situation in which bathers can be transported a very large distance away from the beach. This can be seen as a worst case scenario.

4.4 Conclusions Methodology Model Study

Here the main research question for this chapter is answered; Research question three:

How can the (parameterized) alongshore variability be related to currents which form a risk to bathers?

This can be done by means of a numerical model analysis. Model bathymetries can be created with tiles of nearshore bathymetry which have been cut out of the alongshore straightened bathymetries, generated during the data analysis. Judging whether a generated model bathymetry is fit for use depends on three main questions:

- Is the difference between the computed bulk parameters and the bulk parameters from the time stacks less than 10%?
- Does the bulk alongshore variability show only minor differences between -2000m and +2000m?
- Does the generated bathymetry look alright, or has the process of cutting and pasting generated an artificial pattern, which is not representative of the original pattern observed in the field data?

If a bathymetry is approved it can be loaded to a computational grid with variable cell spacing. Over the intertidal and subtidal bars the cell dimensions are 10m alongshore and 5m cross shore. In areas which aren't of interest to the modelling study, he cell size increases to 20m by 20m.

The water level is now set to 0m NAP. The numerical models are forced with simple wave conditions, which vary from model to model. The significant wave height is set at 1.5m, which can be seen as an upper limit for recreational conditions. The peak period is set at 6s. The angle of wave incidence is varied from model to model. The angle of wave incidence is varied from -30° to +30° to shore normal, with 5° increments. This results in 13 models per model bathymetry. In doing so the influence of the bathymetric variability on nearshore (rip)currents can be isolated.

In total 63 model bathymetries have been created, resulting in 819 model runs. The results of these computations can be used to relate the alongshore bathymetric variability to the computed flow velocities and flow structures.

5. Results Modelling Study

This chapter discusses the results of the model study. For the purpose of this model study the 63 model bathymetries have been tested for 13 different incoming wave angles each. A list of the 63 model bathymetries can be found in appendix B1. The results of the numerical model runs have been analysed to try and find relations between the wave induced currents and the bulk alongshore variability.

The direct results of the modelling efforts are over 177GB of output data. In order to be able to look into any relation between computed flow, and alongshore bathymetric variability, this data has been reduced to parameters which are representative of the flow in the subtidal, and intertidal region. This chapter will explain how these parameters have been obtained, and why they are relevant. Subsequently a correlation study will be presented, using these parameters, and the previously determined bulk alongshore bathymetric variability parameters.

The main research question which will be answered in this chapter is research question four:

Is the alongshore bathymetric variability an important indicator for nearshore currents which form a risk to bathers?

In parameterizing the output of the modelling efforts, this chapter also further answer research question three:

How can the (parameterized) alongshore variability be related to currents which form a risk to bathers?

5.1 Output analysis

The first parameter to be determined is related to the forcing of the rip currents. Part of the model output are the roller forces. These are 2D fields of the computed surface shear stress induced by the wave rollers on the water surface. As explained in the introduction, these roller forces are part of the forcing mechanism of rip currents. The alongshore variability in the forcing (a measure for the alongshore gradients in roller forces), caused by the alongshore variability in the bathymetry, force the bathymetrically controlled rip currents.

Both the roller forces and the local alongshore variability in roller forces are shown in Figure 38, for the case of normally incident waves over model bathymetry artif_bathy_03. The upper window shows a zoom in on the model bathymetry. The second window shows the difference bathymetry for a length scale of 1000m. The bottom window shows the roller forces. The third window shows the local alongshore differences in wave forces. These are calculated in a similar way as the difference bathymetry for the model bathymetry with the same length scale of 1000m.

From the top and bottom windows of Figure 38 one can already get a qualitative sense of the relation between the subtidal- and intertidal bars and breaking waves. The middle two windows give a qualitative sense of the relation between alongshore bathymetric variability and the alongshore variability in rip forcing.

From the 2D fields of shear stress, such as presented in the bottom window of Figure 38, the bulk parameters for the alongshore variability in the roller forces can now be computed, in much the same way as the bulk alongshore bathymetric variability has been computed. Using the same length scales, and the same line of separation for the intertidal-, and the subtidal zone, bulk parameters have been computed for the alongshore variability in roller forces. This is a representation of the alongshore gradients in rip forcing. This parameter can be used to test relations between the alongshore bathymetric variability, the rip current parameters, and the alongshore variability in the wave forcing.

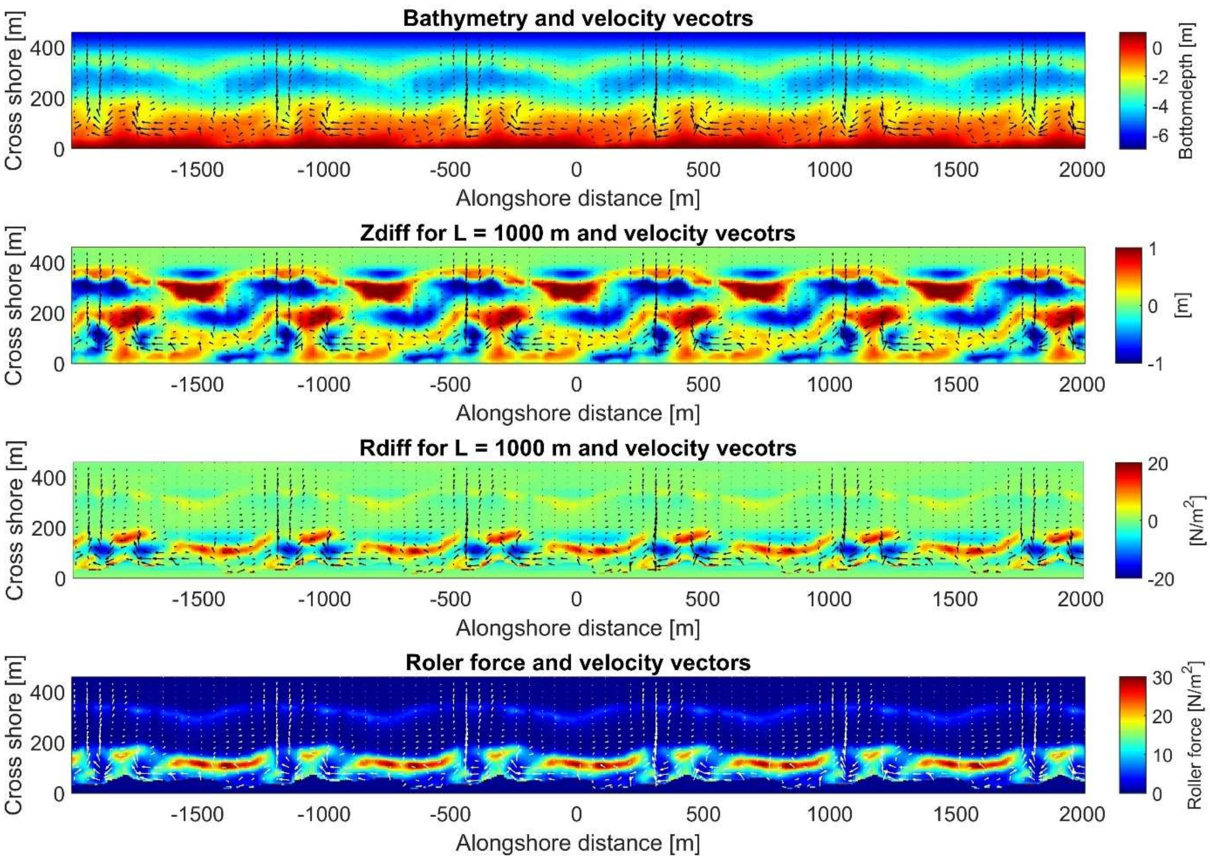

Figure 38: Roller force variability calculation for the case of normally incident waves over artif_bathy _03. Top window: zoom in on the model bathymetry. Second window: zoom in on the long-length scale difference bathymetry. Third window: Long-length scale differences in the roller forces. Bottom window: Roller forces

Subsequently the flow files have been studied. These are 2D fields of the depth averaged current velocities, computed in a Eulerian frame of reference. Two such fields have been computed by the Delft3D software: one containing the cross-shore directed velocities, and one containing the alongshore directed velocities. These two fields together form a vector notation of the current output calculated for every velocity point.

Using statistics on swimming ability both Schlooz [2012] and de Zeeuw [2011] determined velocity thresholds, for which currents in the nearshore start to form a risk to bathers. Since the exact velocities calculated here should be used with some degree of caution, given the lack of validation data, the suggestion made by de Zeeuw [2011] is followed, classifying offshore directed currents with velocities of at least 0.25m/s as a safe lower limit for currents which start to form a risk to bathers.

Using this threshold patches of high cross shore directed velocity can now be detected in the flow fields. If the average depth under these patches of cross shore flow velocity is 1m or deeper, and if these patches are not too close to the model boundaries, than the patches are approved as a rip, and used for further analysis.

Figure 39 shows an example of the rip detection (see next page). This figure has been zoomed in on the central 4 kilometres of the model bathymetry. The top window shows white velocity vectors, over a bathymetry with a repeating rhythmic subtidal bar. The black contours are approved rip currents, and used in further analysis. For these rips, the 90 percentile cross-shore velocity, the mean bottom depth and the cross-shore length of the rip are logged. The magenta contours show rips which have been discarded, in this case for being too shallow.

A recurring pattern of rips can be seen, over the recurring patterns in the bathymetry. From the velocity vectors, and from the ross-shore magnitudes, it is clear that all rips present over the intertidal bathymetry (intertidal rips) communicate with the rips over the subtidal bathymetry (subtidal rip). The central intertidal rip communicates so strongly, that one, elongated rip is formed over both the intertidal, and the subtidal bathymetry.

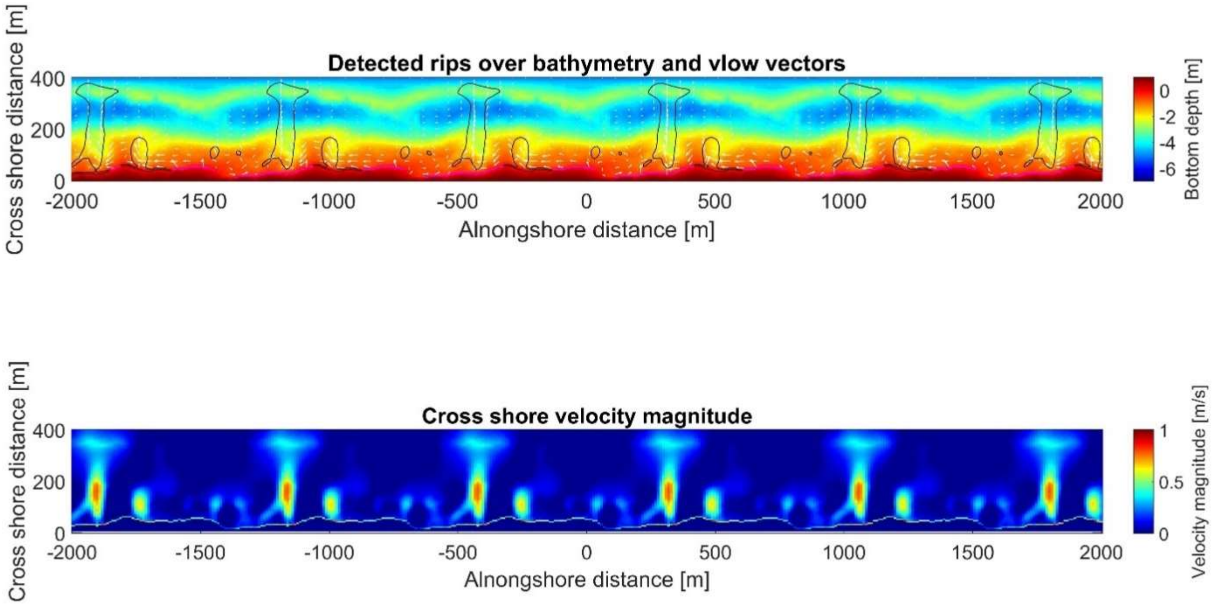

Figure 39: Rip detection in model output of artif_bathy_03 for the case of normally incident waves. The top window shows the velocity vectors (white) over an example bathymetry with rhythmic subtidal bars. Black contours are approved rips, magenta contours are discarded rips. The bottom window shows the cross-shore velocity magnitude

For further analysis, only the rips in the central kilometre, from -500m to +500m alongshore, are considered. These rips are furthest away from the lateral model boundaries, and far away from possible shadowing effects. Therefore, these rips are presumed to give the most accurate representation of reality. Inside this region, the rip with the highest 90 percentile cross-shore velocity is selected, over both the subtidal, and the intertidal bathymetry. The parameters belonging to these rips are used in the correlation study in the next paragraph.

There is one big drawback to this contour line approach, in detecting risky currents. In selecting a lower limit, all currents below this lower limit are discarded. This artificially bands the range for which a correlation study can be executed using these rip parameters. Setting a lower threshold has a big drawback. As this threshold approaches 0m/s, the patch size approaches infinity, or in a practical case, the entire model area.

5.2 Correlation study

The rip parameters, derived from the modelling output, are now studied as one group per incoming wave angle. For these groups, three categories of rips have been studied separately: rips over the intertidal bathymetry, rips over the subtidal bathymetry, and so called 'big rips', where the intertidal and the subtidal rips have lined up, to form one big rip over both the subtidal- and the intertidal bathymetry. First statistical correlations are presented, then causal relations will be explored.

By using a threshold velocity of 0.25m/s it is possible that for low-variable model bathymetries no rips will be found. So for these levels of variability, the rip velocity has been artificially set to 0m/s. This is quite a far-reaching action. So ideally, these cases with artificially low rip velocity are disregarded in computing correlation parameters. In order to be able to do so, however, one must first prove that the two groups in the data are significantly different. If they are than they can be handled as two separate groups. This would justify disregarding the cases in which the rip velocity has been artificially set to zero.

In order to prove that these two groups in the data are significantly different, an adaptation of the Student t-test has been used, as proposed by Welch [1947]. This test can be used to test the null hypothesis that two populations have equal means. In other words; if two groups of data have a similar distribution. Welch's t-test is more reliable then the Student t-test when two samples have unequal variances and unequal group sizes. Since it is expected that particularly the low-variable bathymetries will generate zero velocity, this seems a good assumption.

However, rip-bypassing might also cause higher-variable bathymetries to generate zero rip velocities, for larger angles of wave incidence. In such a case, the variance of the two samples might be the same. First testing the (in)equality of variances, before selecting either Welch's t-test or the Student's t-test, is known to generate errors (Zimmerman [2004]). And since Welch's test preforms aptly for samples with equal variances (Ruxton [2006]), always using the Welch's t-test is sound.

So Welch's t-test is used to justify disregarding of the group of rips for which the velocity has been artificially set to zero due to the threshold of 0.25m/s, from the group of rips with detected velocities. The t-statistic for the Welch's t-test is calculated as follows:

$$t = \frac{\bar{X}_1 - \bar{X}_2}{\sqrt{s_1^2/n_1 - s_2^2/n_2}}$$

Here $\bar{X}_i$ is the group mean, n_i is the group size, and s_i^2 is the unbiased estimator of the group variance calculated with:

$$s_i^2 = \frac{1}{n_i - 1}\sum_{j=1}^{n}\left(X_j - \bar{X}\right)^2$$

A critical value for *t* can now be derived from the Student's t-distribution, using a level of degree of confidence *p*, and the degrees of freedom of the distribution. A degree of confidence of *p=95%* has been used. The degrees of freedom can be calculated with:

$$d.f. = \frac{\left({s_1^2}/{n_1} + {s_2^2}/{n_2}\right)^2}{{(s_1^2/n_1)^2}/{(n_1 - 1)} + {(s_2^2/n_2)^2}/{(n_2 - 1)}}$$

If the absolute value of *t* is larger than the critical value for *t*, the null hypothesis can be discarded, and the two groups can be considered to be significantly different.

If this test discards the null hypothesis, the group for which the rip velocities have artificially been set to zero and the group of rips with velocities above 0.25m/s are significantly different, and can be studied separately. If so, the correlation parameters can now de calculated for the group with rip velocities of 0.25m/s or higher.

A correlation quantifies the degree to which two parameters are statistically related. If good enough correlations can be found, than this relation can be quantified using a linear regression line. Essentially this is a best fit for a linear relation through a scatterplot of the two variables. The quality of this fitted relation can be quantified with the coefficient of determination, denoted as R^2. This coefficient can be calculated as follows:

$$R^2 = 1 - \frac{\sum(y_i - f_i)^2}{\sum(y_i - \bar{y})^2}$$

In which y_i represents the scattered data, f_i represents the corresponding values on the linear regression line and $\bar{y}$ represents the mean of the scattered data. In short, R^2 tells how successful the linear regression line is in predicting the actual data points. A value of 1 if excellent, whilst a value of 0 very poor.

5.2.1 Velocity correlation

In order to give some insight into the dataset created with the model runs, Table 1 presents the mean-, maximum- and minimum rip velocity per wave angle. The strongest rip currents of the data set are found over the intertidal bathymetry for an incoming wave angle of 5°. Both the maxima- and the mean velocities of rips over the subtidal bathymetry are lower than velocities of rips over the intertidal bathymetry.

INTERTIDAL RIPS			SUBTIDAL RIPS		BIG RIPS	
WAVE ANGLE	Mean velocity	Max velocity	Mean velocity	Max velocity	Mean velocity	Max velocity
330	0,29	0,82	0,06	0,51	0,41	0,59
335	0,33	0,87	0,06	0,40	0,44	0,66
340	0,35	0,89	0,06	0,44	0,49	0,73
345	0,40	0,93	0,10	0,61	0,56	0,74
350	0,41	0,99	0,14	0,60	0,59	0,73
355	0,41	0,86	0,29	0,84	0,59	0,79
0	0,42	0,91	0,24	0,62	0,57	0,79
5	0,42	0,97	0,14	0,50	0,54	0,66
10	0,37	0,96	0,13	0,56	0,42	0,59
15	0,32	0,84	0,10	0,50	0,43	0,55
20	0,31	0,80	0,09	0,47	0,39	0,50
25	0,29	0,76	0,09	0,46	0,36	0,40
30	0,26	0,74	0,09	0,43	0,35	0,39

Table 1: Mean-, maximum- and minimum velocity for the intertidal-, subtidal- and big rips

Figure 40 gives an overview of all the detected rips in the data set. The left window shows the subtidal results and the right window shows the intertidal results (blue data points). The big rips are shown in both widows (red data points). The 90 percentile velocity for all rips in shown, for all combinations of model bathymetries and wave direction.

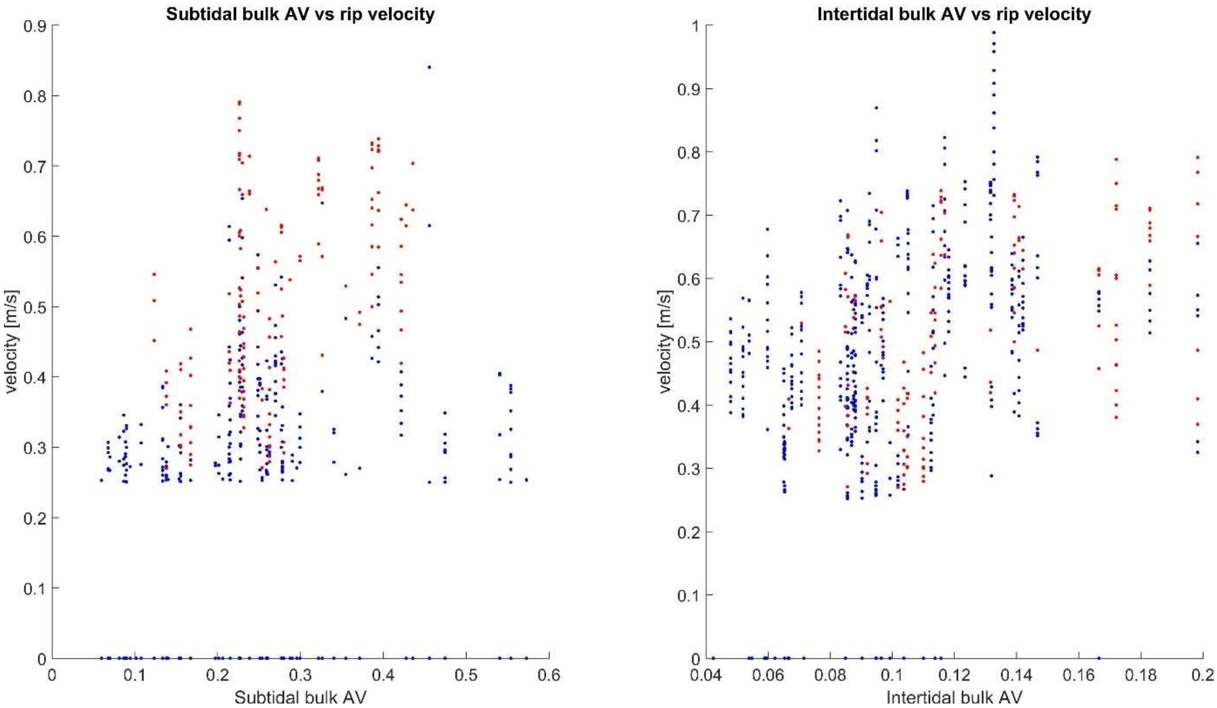

Figure 40: Overview of al rips in the data set for all combinations of model bathymetries and wave direction. Left window shows the subtidal data. Right window shows the intertidal data. The red data points are big rips and are shown in both windows

Table 2 gives an overview of the results for the different tests. In this table the intertidal rip velocities have been correlated with the bulk alongshore bathymetric variability, and the bulk alongshore variability in the roller forces. Only the correlations with 95% certainty are shown.

CORRELATION WITH THE INTERTIDAL VELOCITY

WAVE ANGLE	Bathymetric AV	Forcing AV	Group size	t-test	R^2
-30	0,4053	0,5614	33	1,20	0,1643
-25	0,3454	0,4985	35	2,18	0,1193
-20	0,4220	0,5320	33	2,13	0,1781
-15		0,4026	34		
-10	0,4230	0,6099	32	3,32	0,1789
-5	0,4311	0,5971	33	3,53	0,1858
0	0,6357	0,6438	29	3,85	0,4041
5	0,4778	0,5164	37	4,33	0,2283
10	0,4751	0,5920	38	2,48	0,2258
15	0,4312	0,5518	35	2,10	0,1859
20	0,4403	0,4922	36	2,22	0,1939
25		0,4707	36		
30		0,4202	35		

Table 2: Correlation of the intertidal 90 percentile rip velocities, with the intertidal bulk bathymetric variability (second column) and bulk variability in roller forces (third column), for each wave angle of incidence. Only correlations with 95% certainty or more are shown. Column three represents the number of rips, with velocities of at least 0.25m/s. Column 5 gives the result of the t-test (positive output, means that it was justified to discard zero velocity rips). R^2, the last column, gives the coefficient of determination for calculated linear regression lines

Some of the first things that stand out, are that the correlation with the alongshore variability in roller forces is somewhat higher than the alongshore bathymetric variability, and that the correlations for normally incident waves (wave angle of 0°) is highest for both bulk parameters. Before diving deeper into what causes these numbers, the results for the subtidal rips and the big rips are presented.

Table 3 gives an overview of the results for the subtidal rips. Again, only the correlations with a certainty of at least 95% are shown. The first thing that stands out is that very few correlations are significant. For a large part this has to do with the low number of subtidal rips that have been found. The second thing that stands out, is that the correlation of the rip velocities with the alongshore bathymetric variability for normally incident waves, is much lower than it was for intertidal rips. Note that the t-test has failed for this case, indicating that disregarding the group with zero velocities was not justified.

CORRELATION WITH THE SUBTIDAL VELOCITY

WAVE ANGLE	Bathymetric AV	Forcing AV	Group size	t-test	R2
-30			10		
-25			10		
-20			9		
-15			14		
-10			19		
-5			34		
0	0,3773		29	-1,37	0,1423
5		0,6073	22		
10		0,6287	20		
15		0,6702	16		
20		0,6985	15		
25		0,7136	15		
30		0,6555	15		

Table 3: Correlation of the subtidal 90 percentile rip velocities, with the subtidal bulk bathymetric variability (second column) and bulk variability in roller forces (third column), for each wave angle of incidence. Only correlations with 95% certainty or more are shown. Column three represents the number of rips, with velocities of at least 0.25m/s. Column 5 gives the result of the t-test (positive output, means that it was justified to discard zero velocity rips). R^2, the last column, gives the coefficient of determination for calculated linear regression lines

The results for so called big rips are depicted in Table 4. Since the big rips extend out over both the intertidal-, as well as the subtidal bathymetry, correlations for both the bulk parameters have been computed. Again, only the correlations with a certainty of at least 95% are shown.

CORRELATION WITH THE BIG RIP VELOCITY

	Bathymetric AV		Forcing AV		
WAVE ANGLE	Subtidal	Intertidal	Subtidal	Intertidal	Group size
-30	0,6495		0,7094		10
-25			0,7497		11
-20	0,6527		0,7079		13
-15		0,6216	0,7083		15
-10	0,5655	0,5035	0,7292		18
-5		0,7127	0,7005		17
0		0,7260	0,6361		21
5		0,5677	0,6599		13
10			0,8712		6
15			0,8575		8
20			0,8023		8
25					5
30					5

Table 4: Correlation of the 90 percentile rip velocities, with the subtidal and intertidal bulk bathymetric variability (second and third column) and bulk variability in roller forces (fourth and fifth column), for each wave angle of incidence. Only correlations with 95% certainty or more are shown.

In order to better understand the values presented in the tables, some interesting results are highlighted, starting with the data for normally incident waves. The correlation with the intertidal rip velocities in Table 2 is strongest for these normally incident waves. Since rip-bypassing is known to occur for larger incident waves, when the longshore current pics up, this is not a surprise. The correlations of the subtidal rips for normally incident waves do not perform as well as the correlations for the intertidal area. Since most of the waves break over the intertidal bars, the number of rips in the subtidal group will probably be less. This might explain the pour performance of the correlations for subtidal rips.

Figure 41 shows the data for normally incident waves. The left window shows the results for the subtidal rips, the right window shows the results for the intertidal rips (blue dots in both windows). For both groups, a regression line is plotted. As stated earlier, this regression line is calculated for the rips with a velocity of at least 0.25m/s. So the dots on the horizontal axis are not represented by this regression line. The data for the big rips is plotted in both windows, in order to try to identify how these should be studied. Looking at the datapoints that represent zero velocity rips, it becomes clear why the Welch's t-test failed for the subtidal data, and succeded for the intertidal data. The points on the horizontal axis in the left window of Figure 41 have a similar spread as the data points in the pointcloud. Where as the data points on the horizintal axis in the right window, are densly concentrated around low values for the bulk intertidal alingshore bathymetric variability.

This is due to the fact that the subtidal bars might not generate rip currents for two reasons. They can be to invariable to cause rip currents and they might be situated too deep down in the water, which means that waves simply do not break over this bar. If waves do not break over the bar, they only continue to shoal, and there is no forcing mechanism which can generate rip currents.

The linear regression line in for the intertidal data, in the right window of Figure 41, does a relatively good job in predicting the trend in the scattered data. Most of the data points lie in a band of about 0.1m/s around the regression line, whilst the line itself has a relatively steep slope over the presented range of alongshore bathymetric variability values. The regression line for the subtidal data does not do as good a job. The data can vary 0.15m/s from this line whilst the slope is very mild. This explains the difference in the coefficients of determination. Since the regression lines for the subtidal data do not perform well, they are no longer shown.

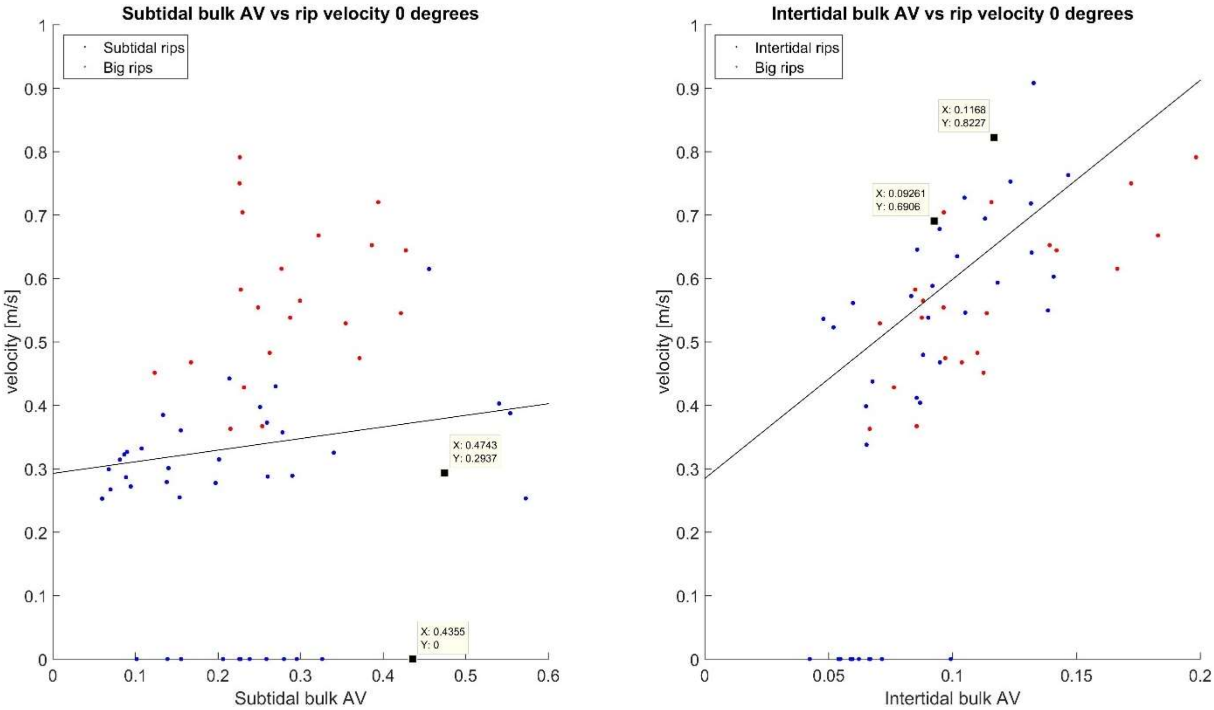

Figure 41: Scatter of the 90 percentile rip velocities, and the corresponding bulk alongshore bathymetric variability. The left window shows the data for the subtidal rips, the right window for the intertidal rips (blue data points). The data for the big rips is incorporated in both windows (red data points). The regression lines have been calculated for the blue data points in the point cloud. The big rip data points and the zero velocity data points (on the horizontal axes) have been ignored in calculating the regression line.

The data of the big rips (the red dots) follows the intertidal data very well. As it turns out, the maximum velocities for these rips are generated over the intertidal bathymetry. This explains why the big rip data points seem to form a separate point cloud in the left window of Figure 41.

Now the focus is turned to the spread in the data points. What causes this spread? In both windows, the results for two artificial bathymetries are highlighted. For the intertidal data they are in the upper edge of the point cloud following the overall trend of the regression line. For the subtidal data, both have a relatively high amount of alongshore bathymetric variability. Yet one is producing subtidal rip currents, which are only just above the threshold value, and the other is not producing any rip current at all. So what is going on here?

NAME	SUBTIDAL VARIABILITY	SUBTIDAL VELOCITY	INTERTIDAL VARIABILITY	INTERTIDAL VELOCITY	DATE	LOCATION
ARTIF_BATHY_60	0.4355	0	0.1168	0.82	Jan-2015	-3281
ARTIF_BATHY_61	0.4743	0.29	0.0926	0.69	Jun-2015	-3326

Table 5: Highlighted cases

Table 5 shows the details of the highlighted cases. Both bars where located just south of the Sand Motor. The first one was measured in January 2015, and the other was measured in June 2015. Figure 42 shows the result of the rip detection for the case of normally incident waves over artif_bathy_60, the case that did not generate a subtidal rip (see next page).

The subtidal bar is very far away from the beach, and is situated very deep. This means that little wave breakage actually takes place over this bar. If there is (almost) no forcing to begin with (see the bottom window in Figure 43, see next page), then there will be (almost) no alongshore variability in the forcing (third window from the top in Figure 43), and therefore no rips will be generated over the subtidal bar.

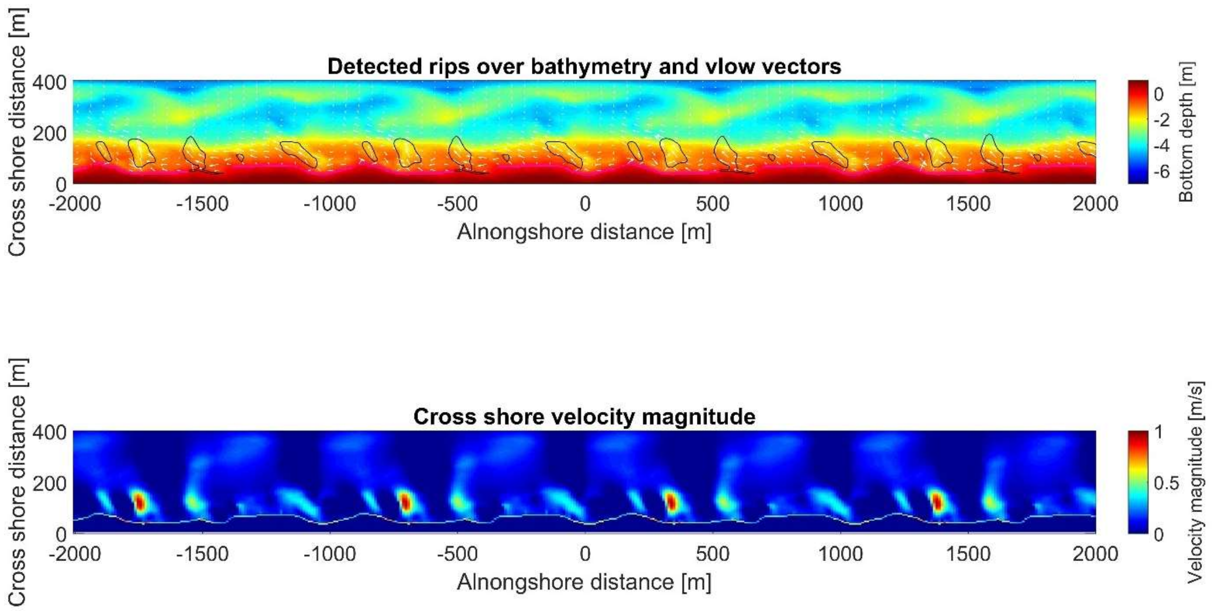

Figure 42: Rip detection for normally incident waves over artif_bathy_60. The black contours in the upper window represent the detected rips. The lower window shows the magnitude of the cross-shore directed velocity

Looking at Figure 43, a very variable bar can be seen in the subtidal area (upper two windows). However, since it is too deep, very little roller forces are generated, due to interactions with this bar. (lower two windows). Looking at the intertidal area it is clear that almost all of the wave breaking takes place over the intertidal bars, leading to longshore differences in the forcing which generate the rips in Figure 42.

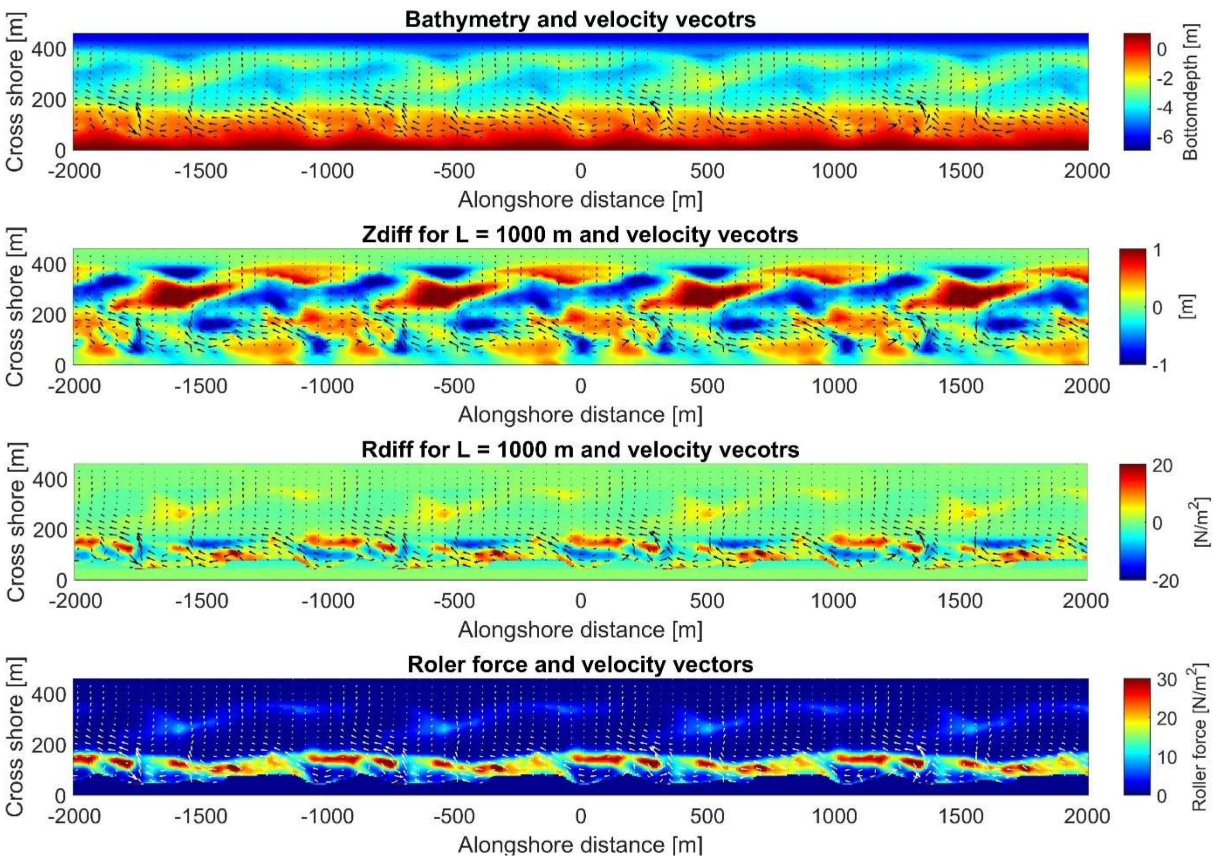

Figure 43: The case of normally incident waves over artif_bathy _60. Top window: zoom in on the model bathymetry. Second window: zoom in on the long-length scale difference bathymetry. Third window: Long-length scale differences in the roller forces. Bottom window: Roller forces

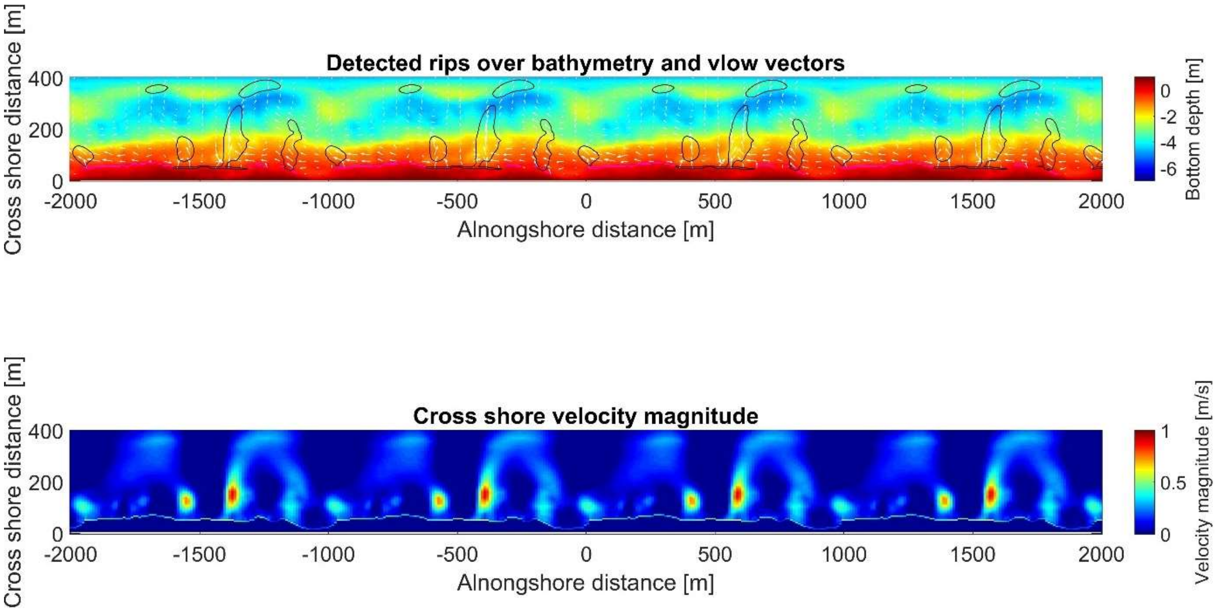

Figure 44: Rip detection for normally incident waves over artif_bathy_61. The black contours in the upper window represent the detected rips. The lower window shows the magnitude of the cross-shore directed velocity

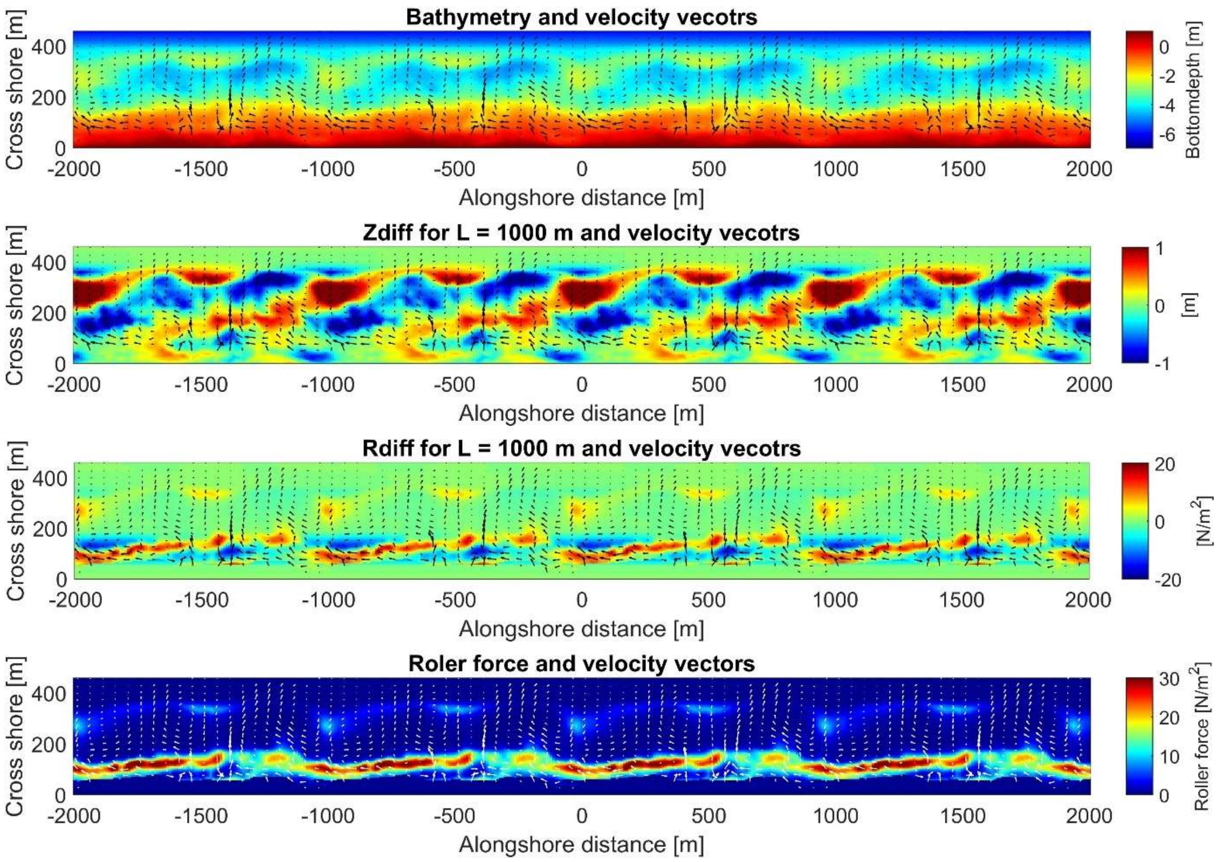

Figure 45: The case of normally incident waves over artif_bathy _61. Top window: zoom in on the model bathymetry. Second window: zoom in on the long-length scale difference bathymetry. Third window: Long-length scale differences in the roller forces. Bottom window: Roller forces

Six months later, the bar is relatively unchanged, which is unsurprising given the fact that most waves do not interact strongly with this bar. The crest height, has increased somewhat. This means that more waves now break over this bar, generating stronger forces related to wave breaking. This means that the alongshore variability in the forces is larger, generating rip currents over the subtidal bar. It should be pointed out, however, that this bar still is very deep. Therefore only a relatively mild rip is generated. This is more clearly shown in Figure 45.

This then explains the difference in correlation with the alongshore bathymetric variability, and the alongshore variability in roller forces. The alongshore bathymetric variability is not the only parameter influencing the generation of rip forces. The actual depth at which this bathymetric variability is located also plays an important role. This could appears to be in line with the notion of 'active morphology' as used by Scott et al. [2014].

A lot more can be said about these pictures. But for now, data of another angle of wave incidence will be highlighted, in order to attempt to better understand the correlation values.

Figure 46 shows the scattered data for the model runs where the incoming waves had an angle of incidence of 5° (clockwise). Again the left window shows the subtidal rips (blue) and big rips (red), and the right window shows the intertidal rips (blue) and big rips (red). This time the linear regression line is only plotted in the window for intertidal rips. The performance of this regression line can now be compared to that of the line in Figure 41.

The linear regression line for the intertidal rips preforms worse than the line for normally incident waves. The line does seem to represent an overall trend in the point cloud, but the trend is weaker than it was for normally incident waves. The spread of the data points around the line is wider, and the slope of the line is milder. This line is not that good in predicting the actual data, explaining the value for the coefficient of determination in Table 2. From now on regression lines will no longer be plotted, as they do cannot tell that much about the data, for increasing angles of incidence.

Looking at the zero rip data points, the points on the horizontal axis, a similar picture rises as for normally incident waves. For the intertidal rips these points are concentrated at the low end of the intertidal variability range. For the subtidal rips the data points lay spread out along the horizontal axis. This explains the results for the Welch's test. Note that the correlation for the subtidal data was deemed not to be significant, and therefore the results are omitted in Table 3.

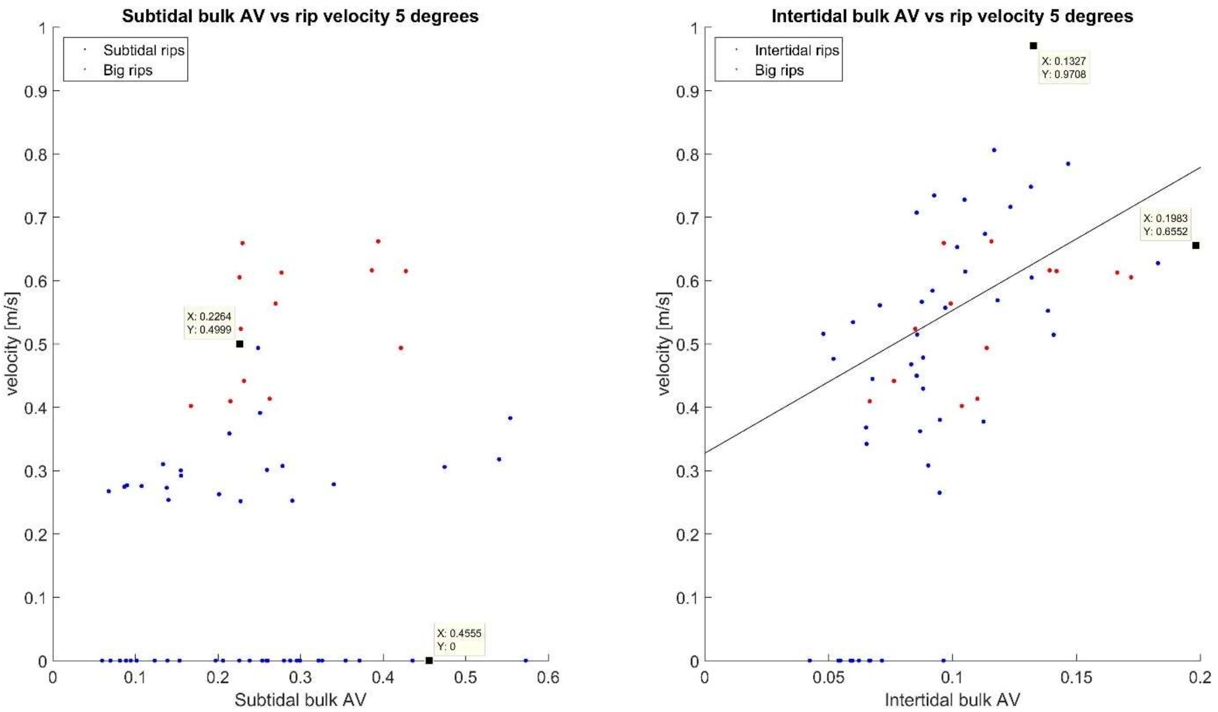

Figure 46: Scatter of the 90 percentile rip velocities, and the corresponding bulk alongshore bathymetric variability. The left window shows the data for the subtidal rips, the right window for the intertidal rips. The data for the big rips is incorporated in both windows.

Again the data of the big rips (the red dots) follows the intertidal data very well. As it turns out the maximum velocities for these rips are generated over the intertidal bathymetry. This explains why, just like in Figure 41, the big rip data points seem to form a separate point cloud in the left window of Figure 46.

The focus now is turned to the spread in the data points. In both windows, the results for two artificial bathymetries are highlighted. For the intertidal data, both have a rather high amount of variability. One is quite close to the regression line, whilst the other forms a far extreme in the point cloud. For the subtidal data, one has a somewhat higher bathymetric variability but no rip, whilst the other has somewhat low bathymetric variability and a rather strong rip current. Table 6 shows the details of the highlighted cases.

NAME	SUBTIDAL VARIABILITY	SUBTIDAL VELOCITY	INTERTIDAL VARIABILITY	INTERTIDAL VELOCITY	DATE	LOCATION
ARTIF_BATHY_62	0.4555	0	0.1327	0.97	Jan-2015	-1045
ARTIF_BATHY_32	0.2264	0.50	0.1983	0.66	Aug-2013	42

Table 6: Highlighted cases

The first case is representative of a bar measured in January of 2015, along the south side of the Sand Motor, and has quite a considerable distance between the sub tidal-, and intertidal bars. The second case represents transverse bars, connecting from the subtidal zone all the way up to the supra tidal beach, measured in August of 2013 near the tip of the Sand Motor.

Figure 47 depicts the results of the rip detection for the case of 5° incident waves, over artif_bathy_62. Two rips are detected. In looking at the lower window in Figure 47, it becomes clear that these are rips relating to the two intertidal rip channels, as their velocity maximum lies in these intertidal rip channels. The subtidal bar is, for the most part, quite deep and quite far away from the intertidal area. Some wave breaking occurs over the shallower end of the bar. This induces some minor circulation but it is not enough to generate significant subtidal rips currents.

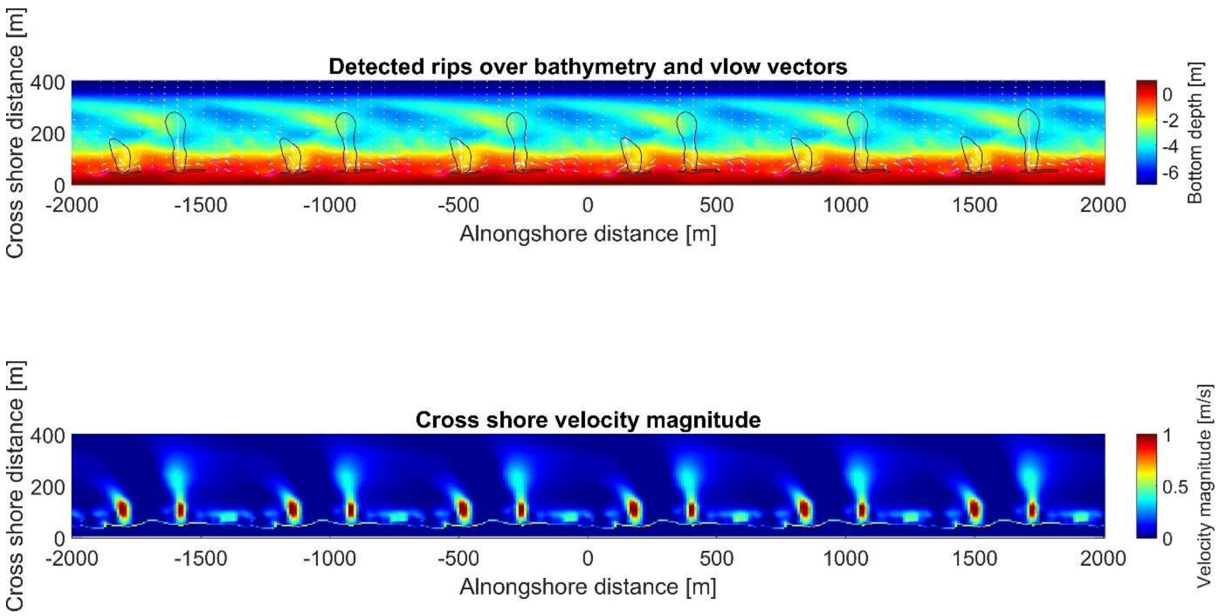

Figure 47: Rip detection for waves with an angle of incidence of 5° over artif_bathy_62. The black contours in the upper window represent the detected rips. The lower window shows the magnitude of the cross-shore directed velocity

Looking at Figure 48 (see next page), it becomes clear that the alternating shallow end of the subtidal bar and deep, oblique subtidal trough are highly alongshore variable (upper two windows of Figure 48). Yet they are simply too deep to cause significant alongshore variability in wave breaking (Lower two windows of Figure 48). Again most of the waves break over the intertidal bars, leading to longshore variability in wave breaking at the intertidal rip channels. This than leads to the gradients in forces which drives the intertidal rips.

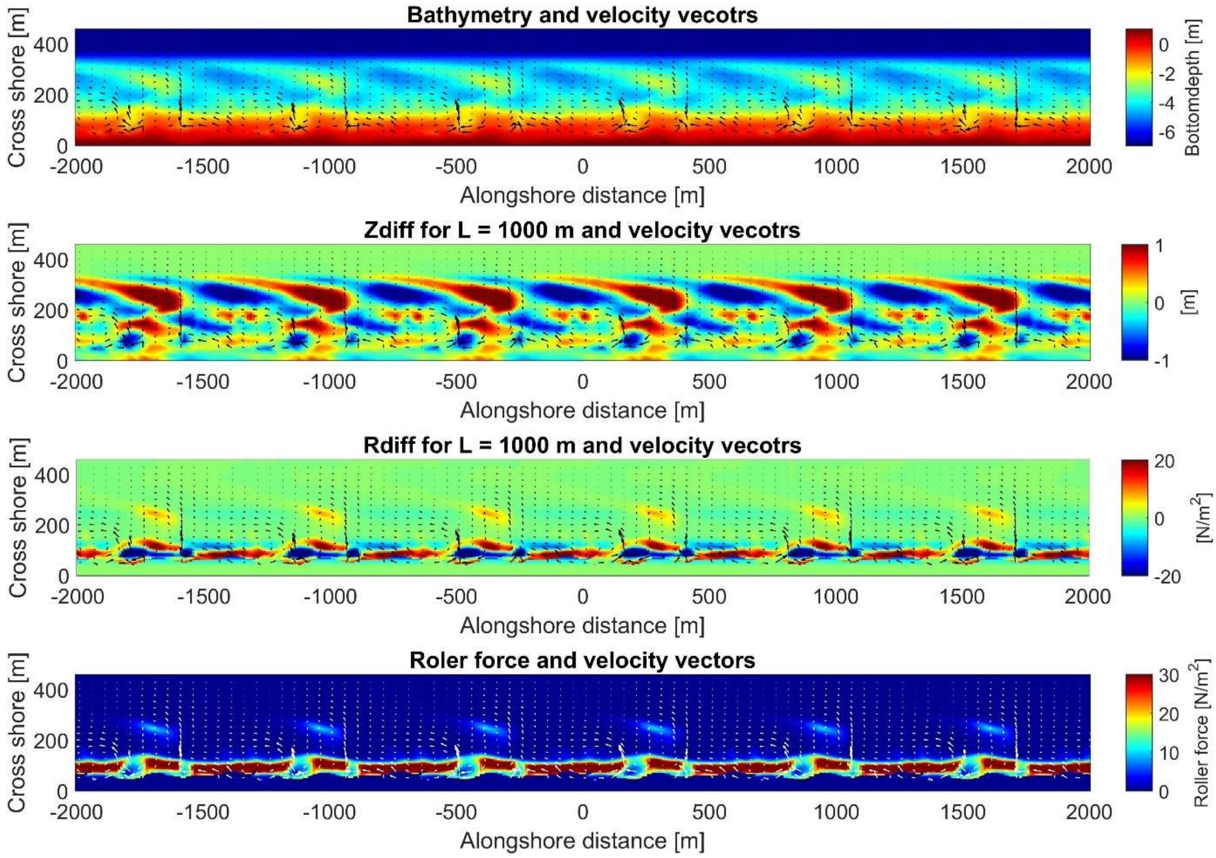

Figure 48: The case of waves with an angle of incidence of 5° over artif_bathy_62. Top window: zoom in on the model bathymetry. Second window: zoom in on the long-length scale difference bathymetry. Third window: Long-length scale differences in the roller forces. Bottom window: Roller forces

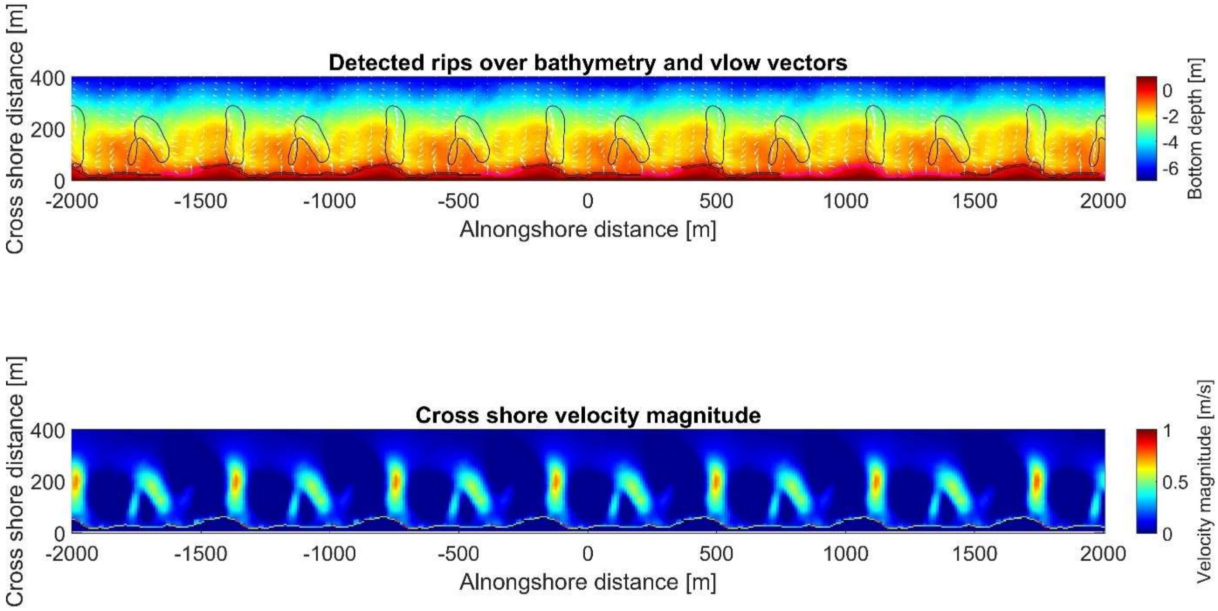

Figure 49: Rip detection for waves with an angle of incidence of 5° over artif_bathy_32. The black contours in the upper window represent the detected rips. The lower window shows the magnitude of the cross-shore directed velocity

Moving to the case of 5° incident waves over artif_bathy_32 the bars look very different (see Figure 49). The subtidal bar has connected with the intertidal bar all the way up to the supratidal beach, forming large bars which Wright and Short [1984] classified as transverse bars and rips. Wright and Short [1984] linked these bars to the strongest observed rip currents. The transverse bars now alternate with rip channels which are not all that wide or deep. This generates the somewhat underwhelming amount of subtidal bathymetric variability, as these patterns are generally seen as the most variable. For intertidal features these patterns are strongly variable, relative to other intertidal bar and rip patterns.

Long rips are detected, stretching from close to the waterline, all the way out over the subtidal part of the bars. The maximum velocity is measured at about 200m from the shoreline, over the subtidal part of the bathymetry. Studying Figure 50, it is clear that all waves break over the transverse bar. This leads to strong alongshore differences in the forces related to wave shoaling, and breaking. These gradients in the forces now drive one big rip cell.

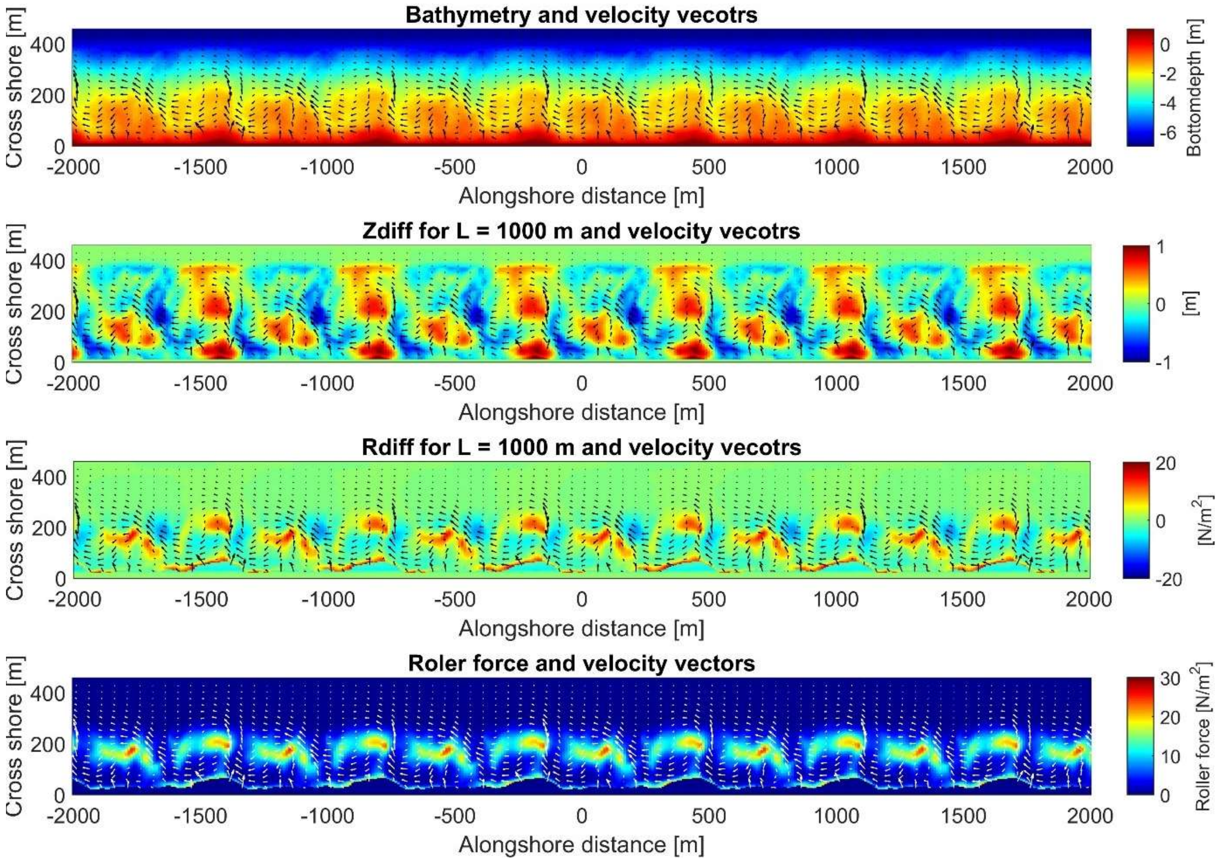

Figure 50: The case of waves with an angle of incidence of 5° over artif_bathy_32. Top window: zoom in on the model bathymetry. Second window: zoom in on the long-length scale difference bathymetry. Third window: Long-length scale differences in the roller forces. Bottom window: Roller forces

It appears that yet another important bathymetric variable can be identified for the generation of rip currents. Apart from the variability and the depth, the distance between the subtidal- and the intertidal bars seems to be of importance. If there are two bars, and if waves break over both of these bars, then two circulating rip cells are generated. The closer together these subtidal- and intertidal cells are, the stronger they communicate, increasing the chance that big rips are formed, which can drag bathers very far away from the coast. When the distance becomes zero, and the subtidal bar and the intertidal bar become one big transverse bar, all of the waves break over this one bar forming one big circulating rip cell which can form a very big risk to bathers.

Note that in Figure 50 the subtidal and intertidal bathymetry are in phase with each other. This is an important observation. Not only the distance between the bars, but also the fact that the intertidal- and subtidal bars are in or out of phase is an important factor which can determine the strength of interaction between intertidal- and subtidal rip currents. Returning to Figure 39, one can observe that one intertidal rip channel is in phase with the subtidal rhythmic bar. The current generated if this intertidal rip channel links up with the subtidal rip current, forming one uninterrupted rip interrupted rip current. For more on phase (differences) in (multi) barred beaches, refer to literature (for instance Quartel [2009]).

Note also that the distance between the subtidal and intertidal bars, and the depth of the subtidal bar are somewhat interconnected. If a subtidal bar is close to the intertidal bars it is higher up the coastal slope and therefore in a shallower part of the nearshore area. This means that more waves will break over the subtidal bar, generating stronger subtidal rips. This also means that there already is an alongshore difference in wave height for the waves that approach the intertidal bars. At some sections, these waves have dissipated part of their energy over the subtidal bars, whilst at other sections they moved unhindered through the subtidal rip channels. This may also increase the forcing for intertidal rip currents. Note that this might lead o additional positive feedback when the intertidal- and subtidal bars are in phase.

Perhaps the influence of these additional morphometric parameters can help explain why the correlations for the big rips suggest a stronger relation with the intertidal bathymetric variability (Table 4), than is the case for the intertidal rips (Table 2). Perhaps for these big rip cases the morphometric parameters, such as the depth of the variability, are more ideal than for the other rips, allowing the waves to better interact with the longshore variable bars.

For higher angles of wave incidence a longshore current starts to dominate the nearshore area. This longshore current can cause bypassing of rip channels. As an example, Table 7 gives an overview of the angles of incidence for which bypassing occurs in the four cases which have been used as an example so far, along with one additional case in which the bar patterns where very linear (so low-variable).

	SOME INITIAL BYPASSING		DOMINANT LONGSHORE CURRENT	
NAME	intertidal	subtidal	intertidal	subtidal
ARTIF_BATHY_60	-20° , +10°	-	-25° , +15°	-10° , +5°
ARTIF_BATHY_61	-15° , +15°	-	-20° , +15°	-10° , +20°
ARTIF_BATHY_62	-20° , +15°	-	-30° , +15°	-10° , +10°
ARTIF_BATHY_32	-20° , +10°	-	-30° , +15°	-
ARTIF_BATHY_18	-	-	-	-10° , +5°

Table 7: Occurrence of rip bypassing. Second and third column depict the angles of incidence for which some rip bypassing occurs. The fourth and fifth column depict wave angles for which all rips are bypassed

It can be concluded that the longshore current starts to dominate the subtidal area for angles of incidence of at least -10° and +20°. The longshore current starts to dominate the intertidal area for angles of incidence of at least -30° and +20°. The difference in the occurring of bypassing for positive and negative angles of wave incidence points to an influence of asymmetry in the bathymetric patterns on the onset of rip bypassing. In the model bathymetries one can observe that most of the (subtidal) rip channels have a counter clockwise orientation, representative of a due SSW orientation in the original bathymetry. This might explain the differences in the onset of rip bypassing.

Figure 51 depicts the scattered data for the limits at which the intertidal area should be dominated by a longshore current. Figure 52 depicts the same situation for the subtidal limits. Surprisingly enough, quite a few cross shore currents are detected. But these can't be rip currents, as these should be bypassed. So what is going on here?

In order to better understand these outcomes, two specific cases are highlighted. The details of these cases are shown in Table 8. The new case represents a linear bar, along the southside of the Sand Motor, measured in March of 2013.

NAME	SUBTIDAL VARIABILITY	SUBTIDAL VELOCITY	INTERTIDAL VARIABILITY	INTERTIDAL VELOCITY	DATE	LOCATION
ARTIF_BATHY_18	0.1549	0.26 , 0	0.0664	0 , 0	Mar-2013	-1229
ARTIF_BATHY_32	0.2264	0.72, 0.46	0.1983	0.37 , 0.57	Aug-2013	42

Table 8: Highlighted cases. The two velocities in columns 3 and 5 are the relevant velocities for each limiting case

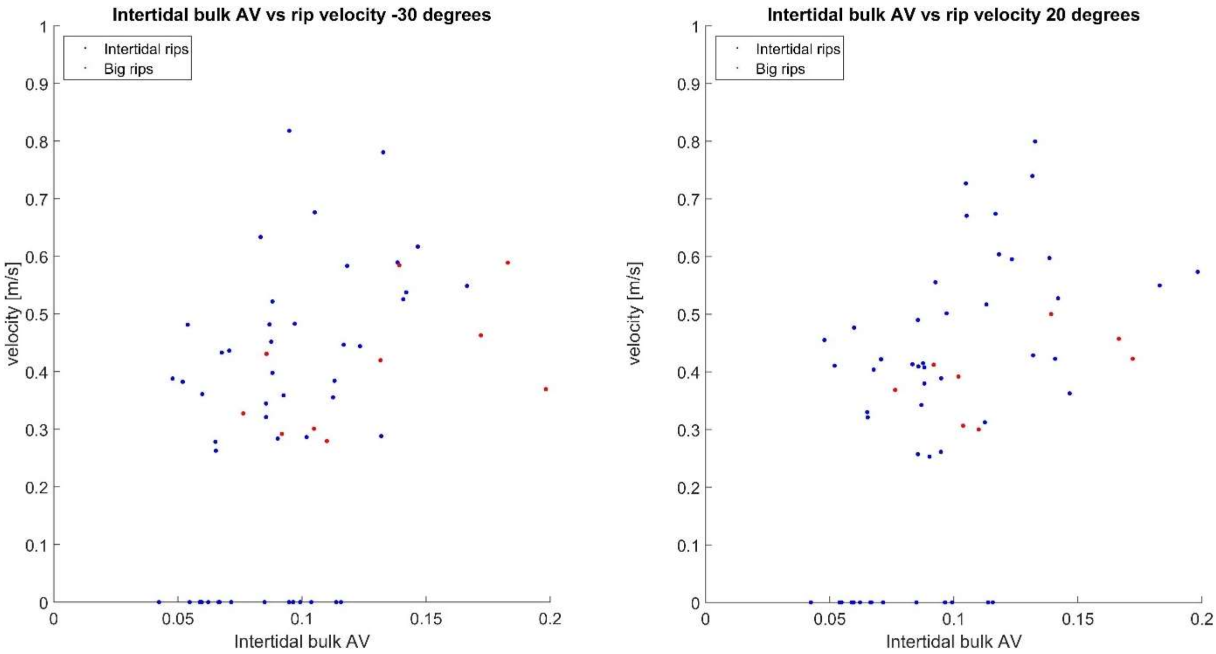

Figure 51: Scatter of intertidal velocity data for the limits at which the longshore current dominates the intertidal area. Left window: cases for the -30° limit (counter clockwise). In the right window: cases for the +20° limit (clockwise)

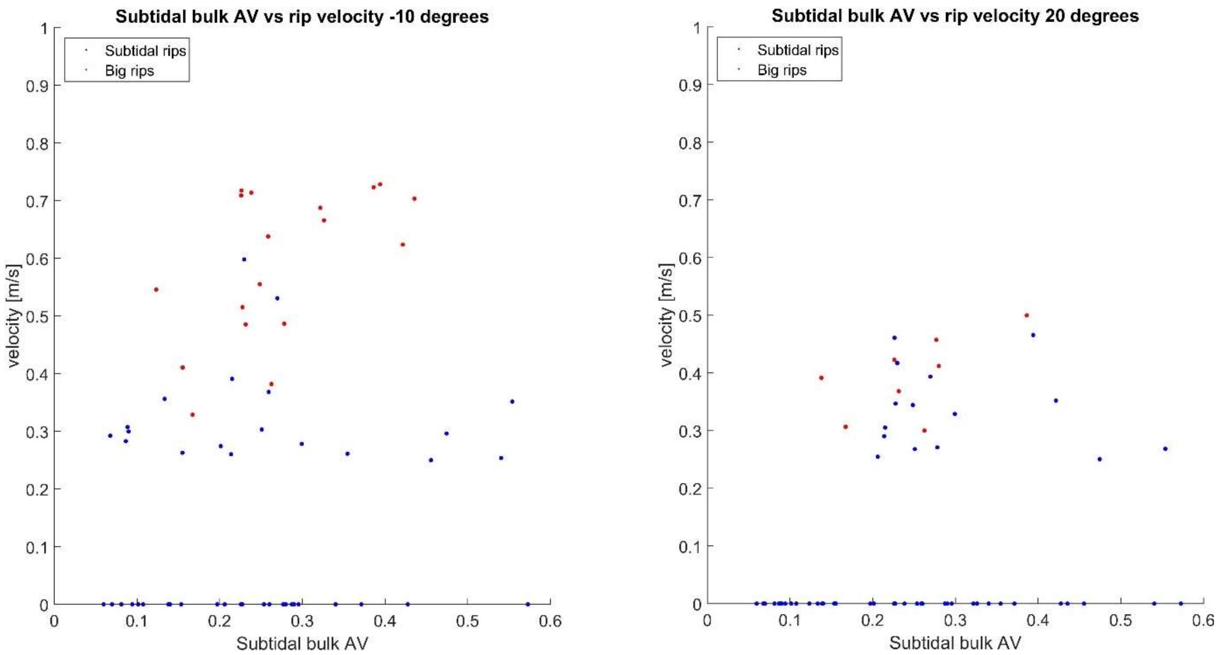

Figure 52: Scatter of intertidal velocity data for the limits at which the longshore current dominates the subtidal area. Left window: cases for the -10° limit (counter clockwise). In the right window: cases for the +20° limit (clockwise)

Figure 53 shows the rip detection for -10° incident waves over artif_bathy_18 (see next page). Rips seem to be detected over small differences in crest height over the longshore subtidal bar. No rips are detected over the intertidal bathymetry. However, in studying the flow field it becomes clear that we are looking at a longshore current. There are no circulating rip cells in the flow field. The rip detection scheme is picking up on the slight meandering of the longshore current, associated with the minor variability in the subtidal bar.

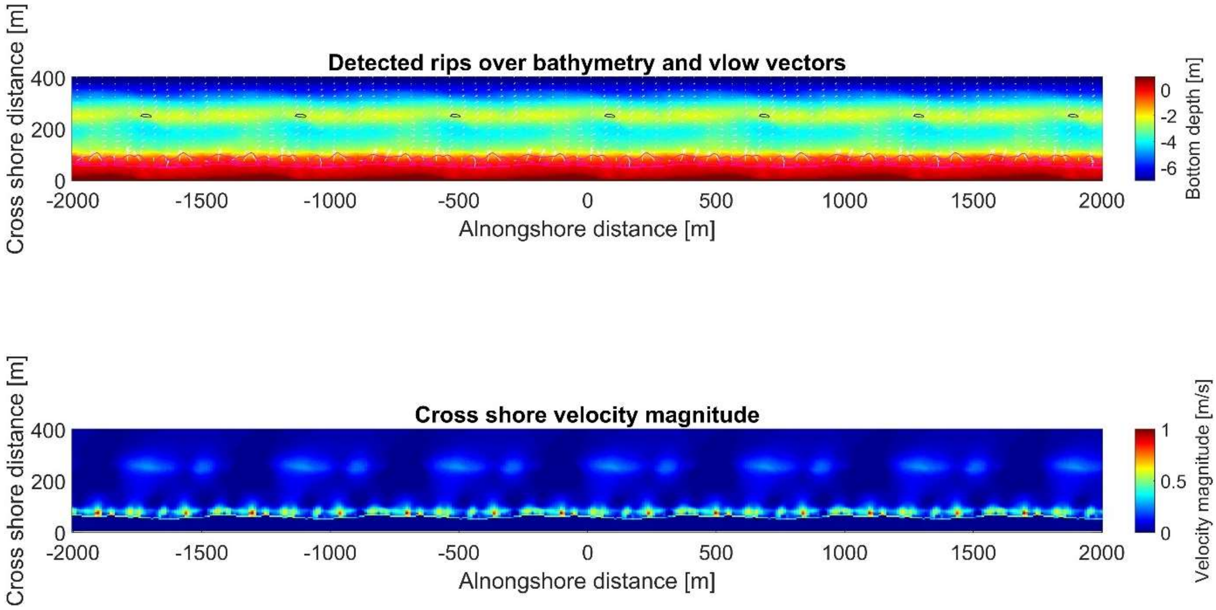

Figure 53: Rip detection for the case of -10° incident waves over artif_bathy_18. The black contours in the upper window represent the detected rips. The lower window depicts the cross-shore directed velocity magnitude.

This becomes even more clear when looking at the lower two windows of Figure 54. Almost no variability in the forces is visible. However, looking at the top two windows it is clear that the meandering is related to the variability in the subtidal bar.

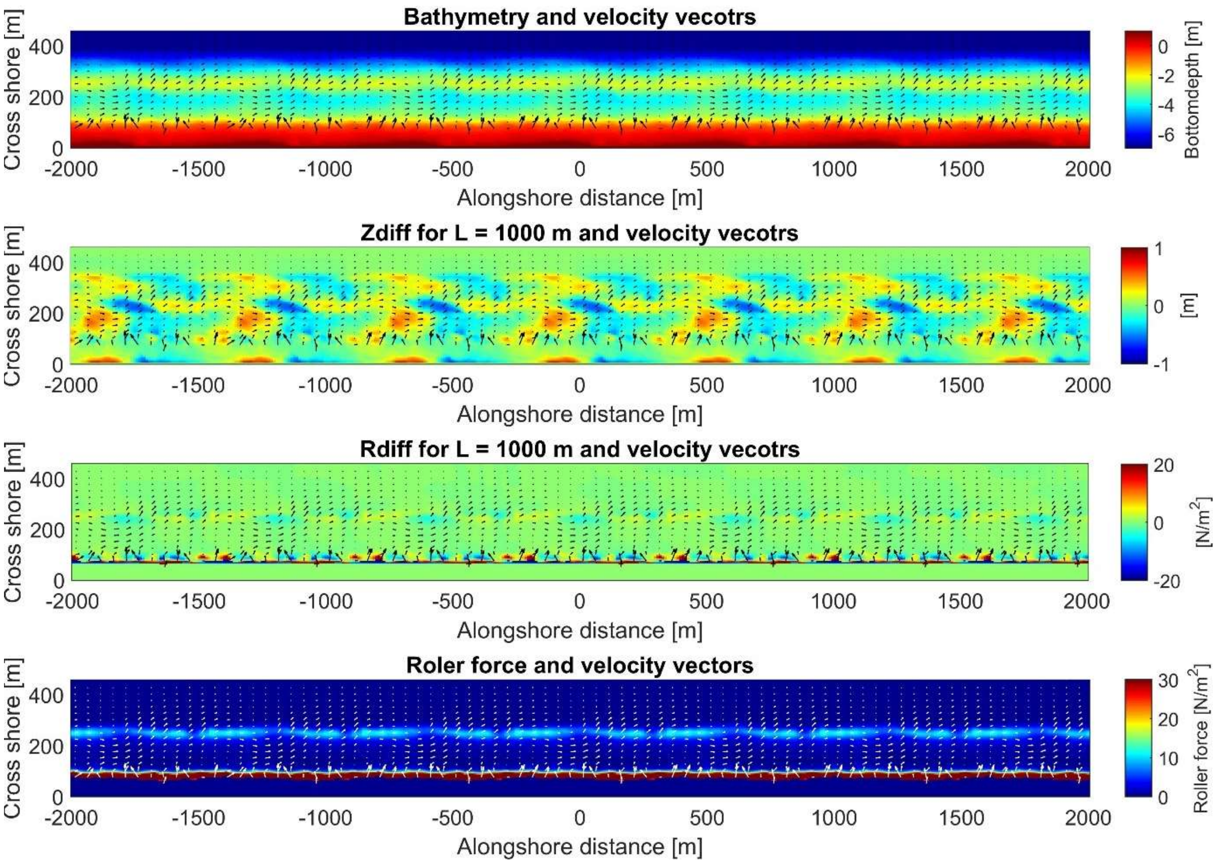

Figure 54: The case of waves with an angle of incidence of -10° over artif_bathy_18. Top window: zoom in on the model bathymetry. Second window: zoom in on the long-length scale difference bathymetry. Third window: Long-length scale differences in the roller forces. Bottom window: Roller forces

This is not a false positive. De Zeeuw [2011] concluded that these meandering longshore currents are known to cause bathers to panic. Therefore these meandering currents are relevant wave induced currents for bather risk, and should be accounted for. For this case, however, this meandering takes place in a very small area, about 300m from the waterline. This is something that a possible bather risk model should account for.

Figure 55 shows the rip detection for -30° incident waves over artif_bathy_32. Cross shore currents are detected close to the transverse bars as can be seen in the upper window. These currents are representative of the strong meandering of the longshore current related to the variability in the bars. This time the meandering takes place over a very large area only about 100m from the beach.

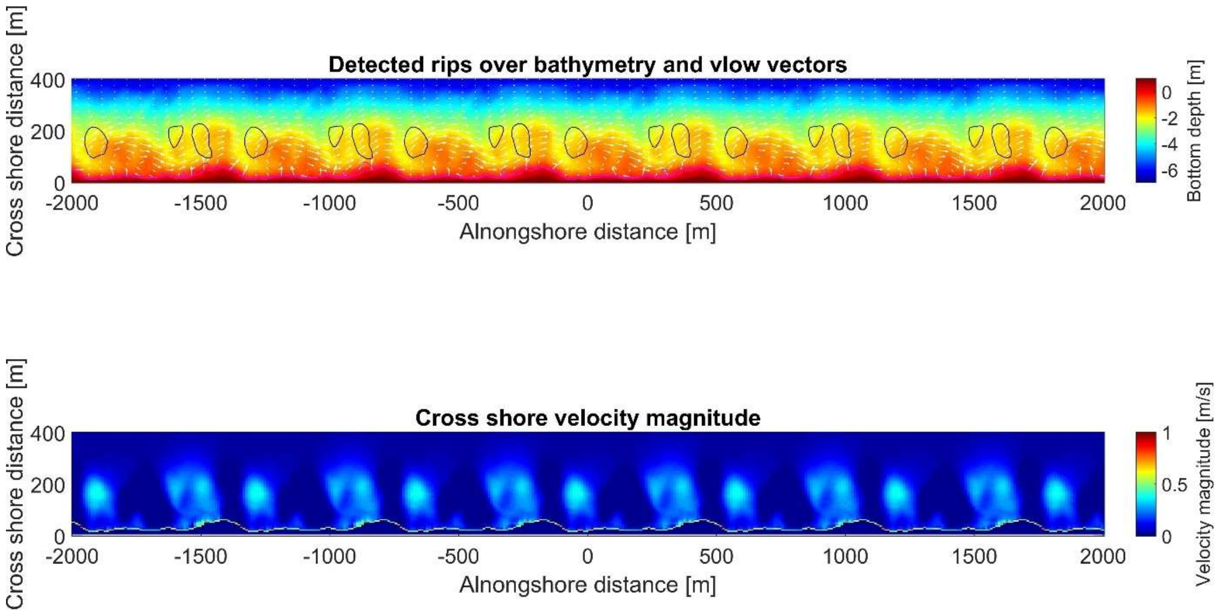

Figure 55: Rip detection for the case of -30° incident waves over artif_bathy_32. The black contours in the upper window represent the detected rips. The lower window depicts the cross-shore directed velocity magnitude.

The relation between the alongshore bathymetric variability and the meandering becomes all the more clear when looking at Figure 56 (see next page). The upper two windows show a longshore current which tends to avoid the shallower part formed by the transverse bars. It is clear that the bathymetry of artif_bathy_32 is a lot more variable than that of artif_bathy_18. However, due to the influence of the morphometric parameter mentioned earlier, the depth of the features and the distance between the intertidal bars and the subtidal bars, no clear relation between these meandering velocities and the alongshore bathymetric variability can be found.

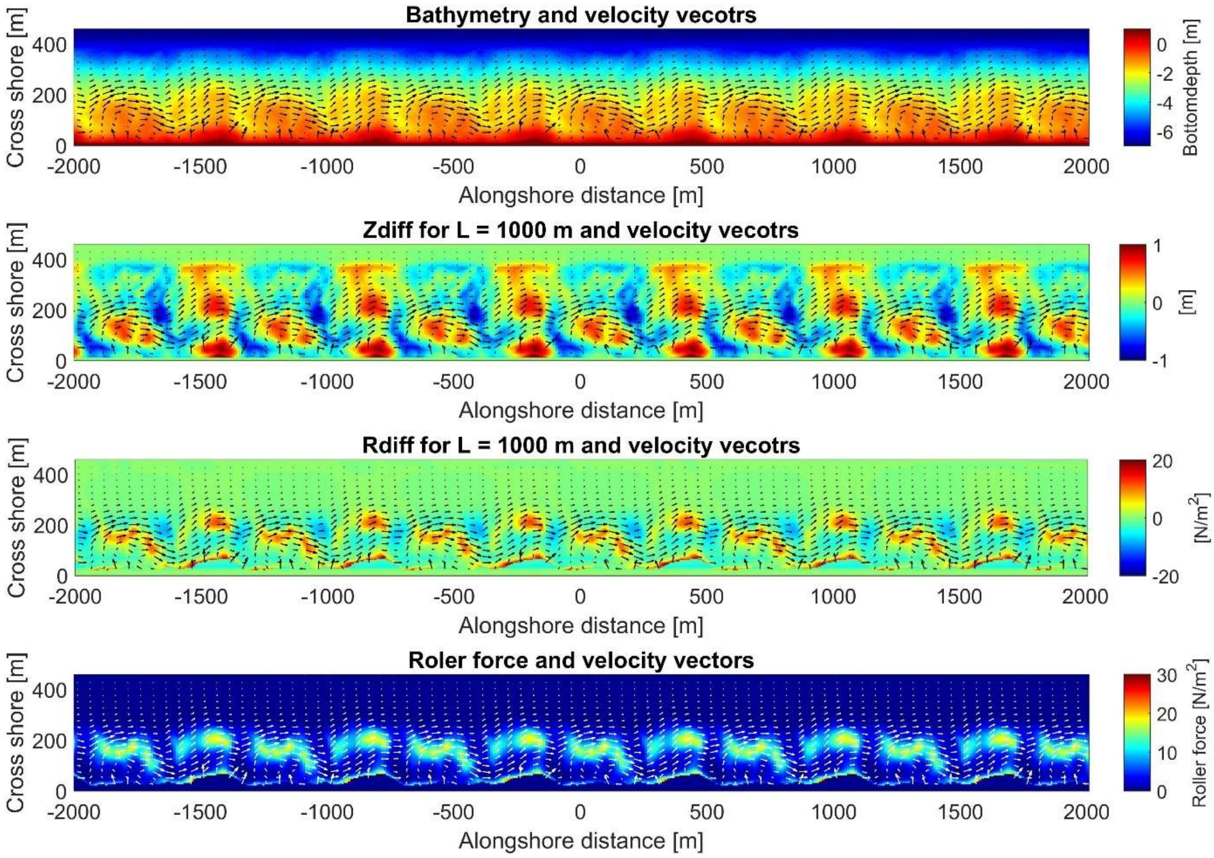

Figure 56: The case of waves with an angle of incidence of -30° over artif_bathy_32. Top window: zoom in on the model bathymetry. Second window: zoom in on the long-length scale difference bathymetry. Third window: Long-length scale differences in the roller forces. Bottom window: Roller forces

5.2.2 Rip length correlation

The primary factor of importance for bather risk is the rip velocity. If a current is not strong enough, there simply is no risk. Of secondary importance is the rip length. It should be kept in mind that the flow structures represent the rip currents in a Eulerian sense, not in a Lagrangian sense. So if there is even a slight alongshore directed current, it is unlikely that a drifter deployed in a rip will travel the entire extent of the rip length detected here.

Table 9 shows the correlation of the cross shore length of the intertidal rip currents, with the intertidal bathymetric variability and the intertidal variability in roller forces. Again only the correlations with a certainty of at least 95% are shown.

CORRELATION WITH THE INTERTIDAL RIP LENGTH

WAVE ANGLE	Bathymetric AV	Forcing AV	Group size
-30	0,6622	0,5237	33
-25	0,6786	0,5467	35
-20	0,7078	0,5277	33
-15	0,5547	0,3659	34
-10	0,5631	0,4445	32
-5		0,3759	33
0	0,5535	0,4395	29
5	0,6409		37
10	0,7438	0,3401	38
15	0,7738	0,4264	35
20	0,7538	0,3772	36
25	0,6667	0,4241	36
30	0,6537	0,3740	35

Table 9: Correlation of the intertidal rip lengths, with the intertidal bulk bathymetric variability (second column) and bulk variability in roller forces (third column), for each wave angle of incidence. Only correlations will 95% certainty of more have are shown. Column three represents the number of rips, with velocities of at least 0.25m/s.

What stands out is that these correlations seem to be performing better for more extreme wave angles, than was the case with the intertidal velocity (see Table 2). Also, the correlation with the bathymetric variability is better than with the variability in roller forces.

This might be explained by the fact that these cases are really meandering longshore currents. The cross shore amplitude of these meanders seems to relate to the cross shore amplitude of the variability in the bars as can be seen in Figure 55.

Table 10 and Table 11 show the correlations for the length of subtidal rips and big rips respectively. Again the correlations seem to perform better than those for the velocities in Table 3 and Table 4. In contrast with the intertidal rip currents the correlations of the rip length with the subtidal variability in roller forces are quite good for both the subtidal rips and the big rips.

CORRELATION WITH THE SUBTIDAL RIP LENGTH

WAVE ANGLE	Bathymetric AV	Forcing AV	Group size
-30	0,8924	0,7024	10
-25		0,6989	10
-20			9
-15			14
-10			19
-5	0,5308	0,3817	34
0	0,6076		29
5	0,5412	0,6080	22
10	0,5110	0,7082	20
15		0,7226	16
20		0,7154	15
25		0,7007	15
30		0,6938	15

Table 10: Correlation of the intertidal rip lengths, with the subtidal bulk bathymetric variability (second column) and bulk variability in roller forces (third column), for each wave angle of incidence. Only correlations will 95% certainty of more have are shown. Column three represents the number of rips, with velocities of at least 0.25m/s.

It is not all that obvious what the causal relation for this statistical correlation could be. Perhaps it is again representative of the relation with the depth. In Figure 54 and Figure 56 the longshore current seems to avoid the shallower parts of the bars. It seems likely that for deeper, highly variable bars the longshore current will not interact as strongly, and therefor meander less.

CORRELATION WITH THE BIG RIP LENGTH

	Bathymetric AV		Forcing AV		
WAVE ANGLE	Subtidal	Intertidal	Subtidal	Intertidal	Group size
-30	0,6398	0,7002	0,8802		10
-25	0,7745		0,8916		11
-20	0,8364		0,8514		13
-15	0,5721		0,7732		15
-10	0,5798	0,4978	0,8616		18
-5	0,7099		0,7687		17
0	0,6783		0,6631		21
5	0,6504		0,6866		13
10			0,9350		6
15			0,8777		8
20	0,7408		0,8814		8
25		0,9221	0,9021		5
30		0,9220	0,8892		5

Table 11: Correlation of the big rip lengths, with the subtidal bulk bathymetric variability (second column) and bulk variability in roller forces (third column), for each wave angle of incidence. Only correlations will 95% certainty of more have are shown. Column three represents the number of rips, with velocities of at least 0.25m/s.

In order to gain a better understanding of the numbers presented in the correlation tables the results for normally incident waves are studied. Figure 57 shows a scatterplot of the intertidal rip lengths in the right window, and the subtidal rip lengths in the left window. Again the big rips have been plotted in both windows (red dots), in order to be able to study them relative to the other rips.

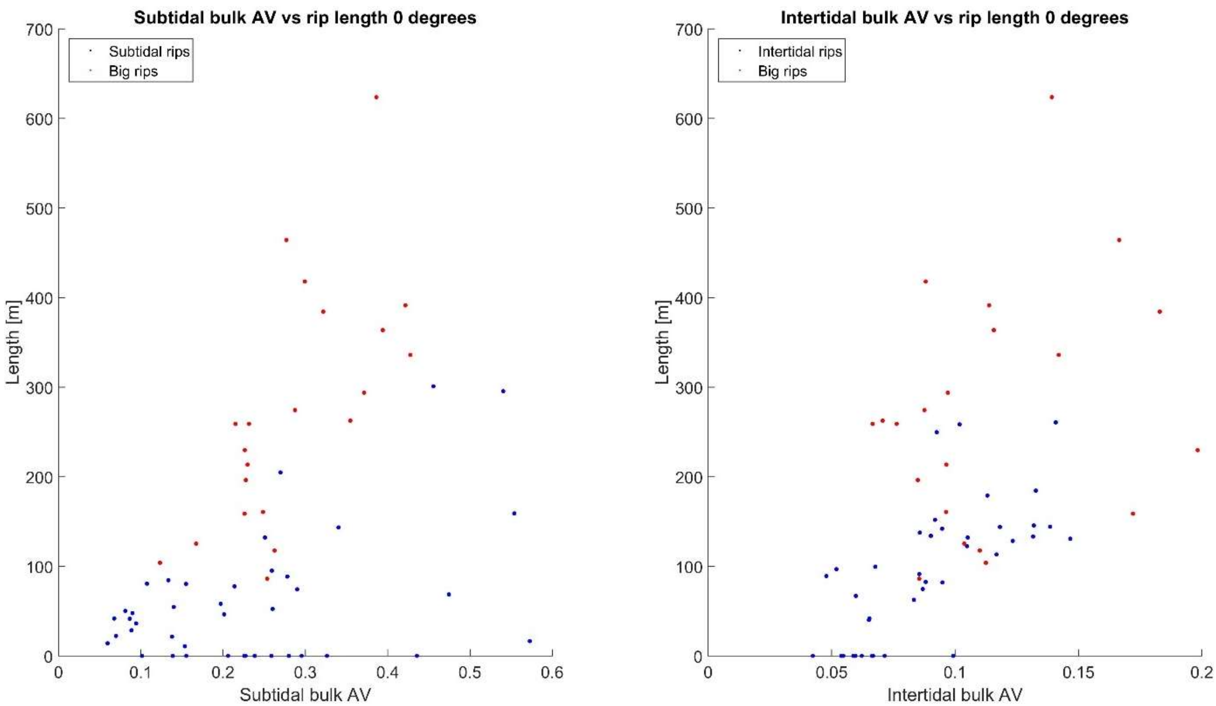

Figure 57: Scatter of the rip length, and the corresponding bulk alongshore bathymetric variability. The left window shows the data for the subtidal rips, the right window for the intertidal rips. The data for the big rips is incorporated in both windows.

In contrast with the point clouds for the intertidal velocity in Figure 41 and Figure 46, the big rip data points no longer fall in line with the general behaviour of the intertidal rip data points. In both windows of Figure 57 the big rips form a separate point cloud representing the far extremes in length. Another difference with the velocity plots that stands out is the fact that the relation with the intertidal rip length and the intertidal alongshore bathymetric variability seems to be a lot milder than the relation with the intertidal rip velocity and intertidal alongshore bathymetric variability (see Figure 41).

The rough trend in both windows seems to be that very low variability will cause short rip lengths, and higher levels will cause either somewhat longer rip lengths or very extreme rip lengths. The spread in the lengths for the higher amounts of variability might again be caused by the influence of the depth at which the bathymetric variability occurs, as well as the cross shore distance between the intertidal bars and the subtidal bars.

In order to gain better insight into this spread, two specific cases are highlighted. The details of these two cases are listed in Table 12. Both cases have a medium high amount of subtidal variability and a relatively high amount of intertidal variability. Yet the difference in rip length is extreme. The first case is representative of bars measured in the northern NeMo area in March of 2013. The second case is representative of bars measured at the tip of the Sand Motor two years later, in March 2015.

NAME	SUBTIDAL VARIABILITY	SUBTIDAL LENGTH	INTERTIDAL VARIABILITY	INTERTIDAL LENGTH	DATE	LOCATION
ARTIF_BATHY_19	0.2782	0	0.1467	131	Mar-2013	+3044
ARTIF_BATHY_55	0.3861	624	0.1392	624	Mar-2015	-82

Table 12: Highlighted cases

Figure 58 shows the results of the rip detection for normally incident waves over artif_bathy_19. In the upper window, a rhythmic subtidal bar is visible. The intertidal bars are well developed and are groin related. This explains why they weld to the shoreline at more or less regular intervals. Rip currents are only detected in the intertidal rips. From the lower window, it becomes clear that only very low offshore directed flows are present over the subtidal bar. This flow is very diffuse, as it occurs over a relatively wide area.

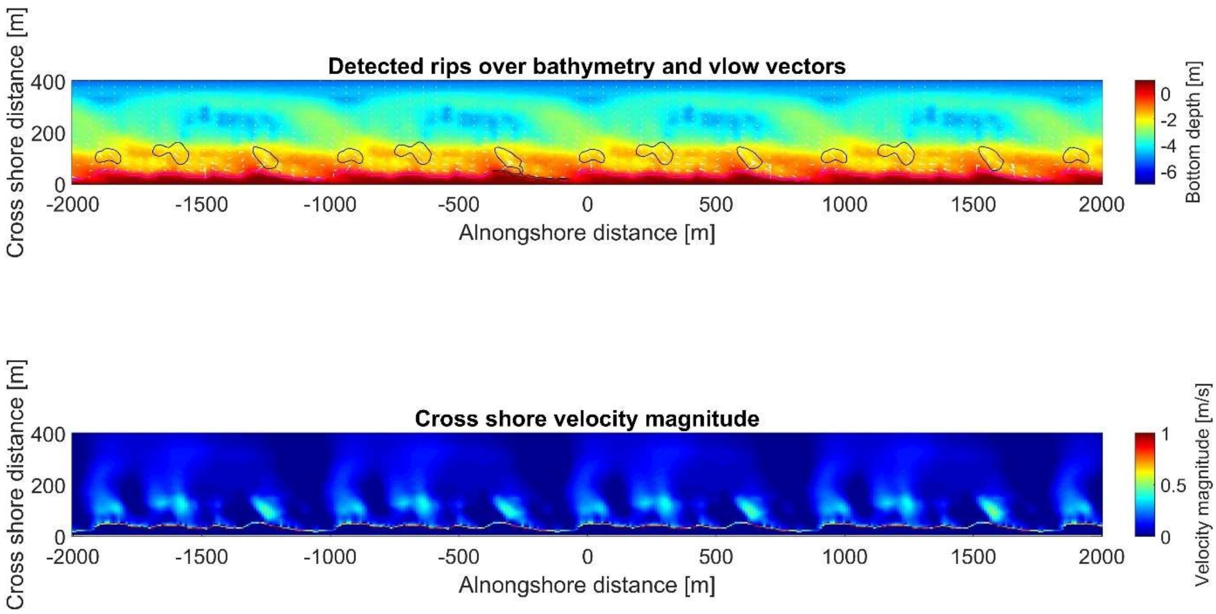

Figure 58: Rip detection for normally incident waves over artif_bathy_19. The black contours in the upper window represent the detected rips. The lower window shows the magnitude of the cross-shore directed velocity

In Figure 59 one can see that the rhythmicity in the subtidal bar generates some serious alongshore bathymetric variability (see next page). However, the bar is too deep to cause significant wave breaking. The intertidal bars on the other hand, cause most waves to break generating alongshore variability in the related forces in the area of the intertidal rip channels, which generates the rip currents.

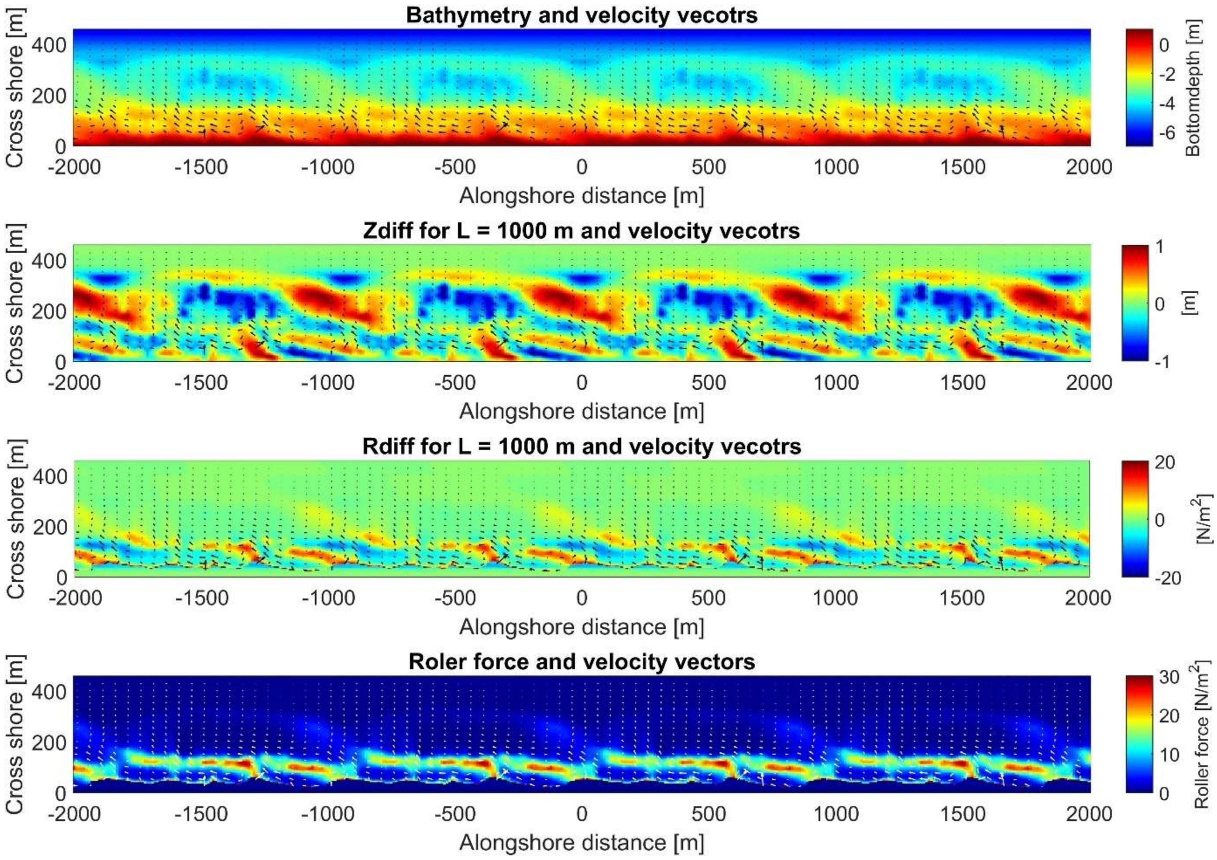

Figure 59: The case of normally incident waves over artif_bathy _19. Top window: zoom in on the model bathymetry. Second window: zoom in on the long-length scale difference bathymetry. Third window: Long-length scale differences in the roller forces. Bottom window: Roller forces

Again the depth at which bathymetric variability occurs seems to cause the difference in flow behaviour between the intertidal and the subtidal zones. But why then are the rips so much shorter than for the case of artif_bathy_55 which has comparable amounts of variability? Figure 60 helps to answer that question.

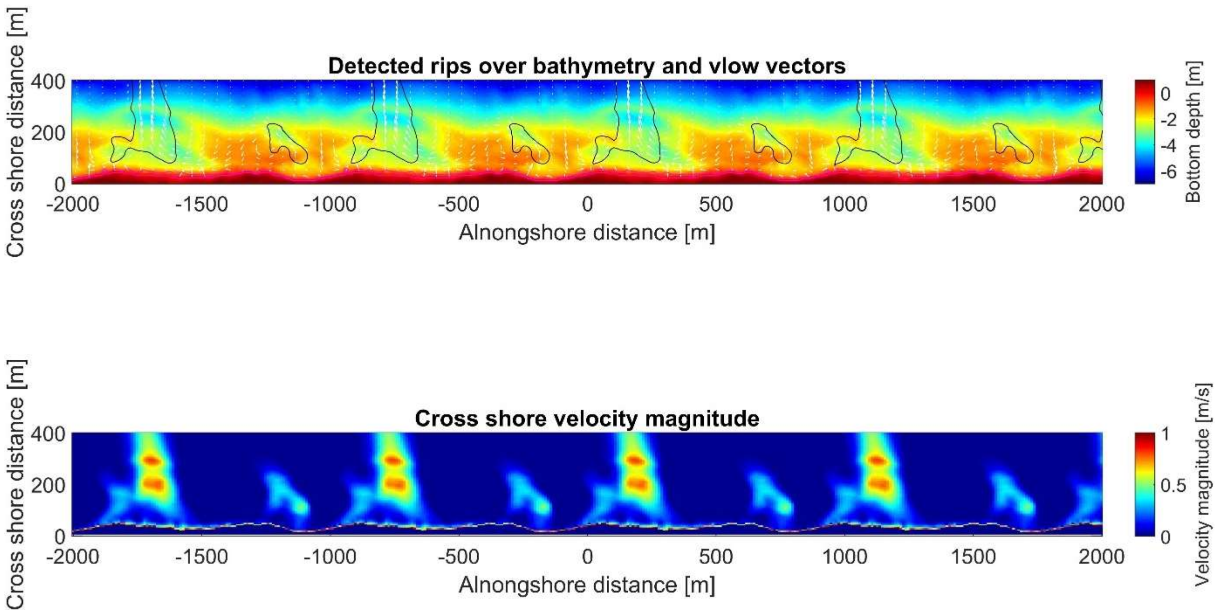

Figure 60: Rip detection for normally incident waves over artif_bathy_55. The black contours in the upper window represent the detected rips. The lower window shows the magnitude of the cross-shore directed velocity

Figure 60 shows the results of rip detection for normally incident waves over artif_bathy_55. The black contours representing the detected rips extend all the way out of the picture forming a big rip. The upper window shows rips generated over transverse bars which connect all the way up to the supratidal beach. Two rip channels can be observed. One is relatively narrow and not that much deeper or wider than the rip channels in artif_bathy_19. This rip channel is somewhat reminiscent of the rip channels in the other bathymetry with transverse bars and rips highlighted earlier (artif_bathy_32, see Figure 50). The other rip, however, is absolutely huge. It is a lot wider and very deep and remains so until it reaches the waterline. A lot of sediment must have been moved around to create this large rip. Some of it seems to have been deposited in a rip delta at the offshore end of the rip channel. The velocity in this rip remains high over a long cross shore distance. Both rip channels are oblique, pointing somewhat to the left.

In Figure 61 it is clear that in particular the alternation between the transverse bars and the wide, deep rip channel generates a lot of bathymetric variability. This signal is clearly stronger than that in Figure 50. All waves approaching the bars, break over the bars, whereas the waves approaching the rip remain stable, and do not break until they reach the shoreline. This generates one extremely large rip cell.

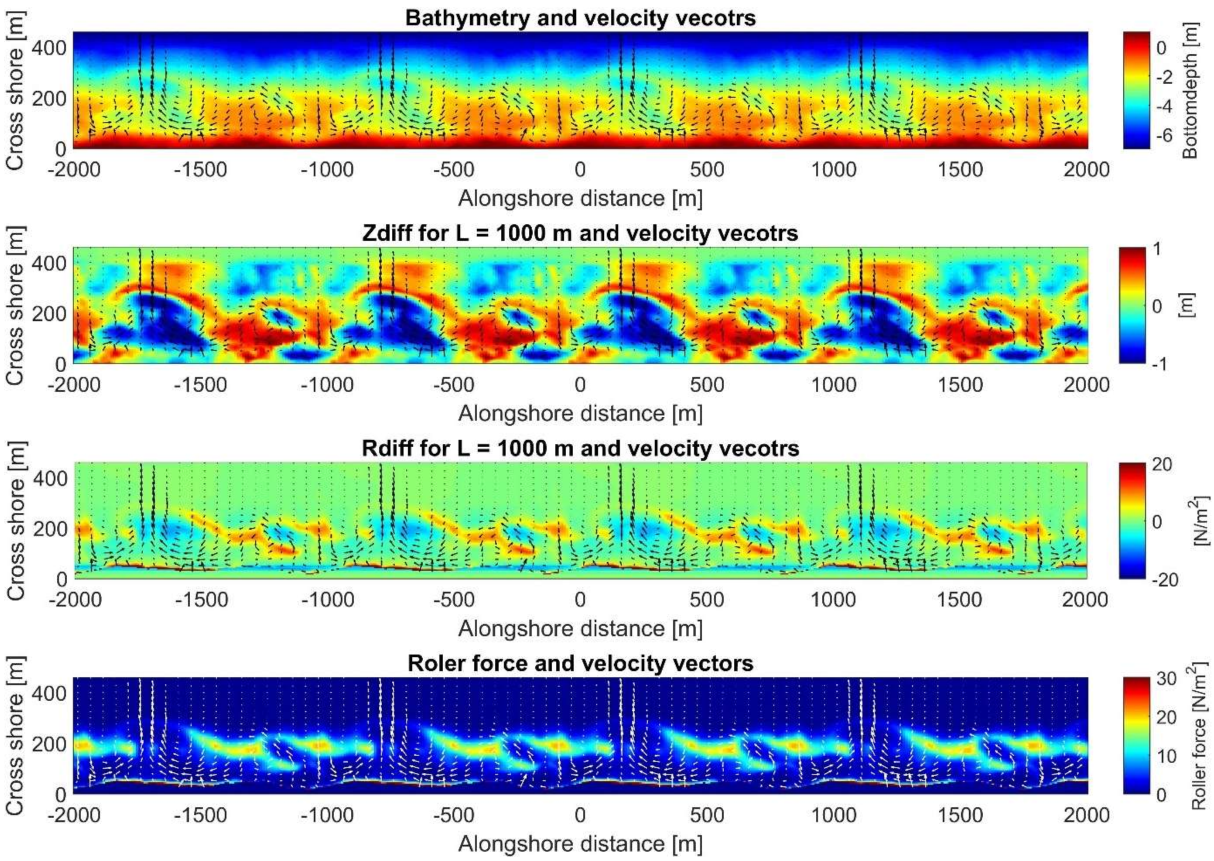

Figure 61: The case of normally incident waves over artif_bathy _55. Top window: zoom in on the model bathymetry. Second window: zoom in on the long-length scale difference bathymetry. Third window: Long-length scale differences in the roller forces. Bottom window: Roller forces

From this it is clear that not only the variability is important when it comes to generating rip currents with a certain length. Again the depth of the variability and the distance between the intertidal bars and the subtidal bars turn out to be important. However, the width and depth of the channel also seem to be of importance in explaining the difference in behaviour between the earlier presented case of artif_bathy_32 and the case of artif_bathy_55 presented here. However, from the upper two windows in Figure 61 it seems that the morphometric parameters of the rip channel (width and length) are well represented in the alongshore bathymetric variability signal. Therefore, unlike the depth and cross shore distances, these morphometric parameters do not have to be quantified in another way.

The alongshore length scale of the transverse bars in Figure 61 and Figure 56 is different. In Figure 56 the alongshore length scale is about 250m. In Figure 61 this is about 500m. Castelle, Reniers and McMahan [2014] concluded that differences in the alongshore length scale of bars induces differences in surf zone retention. When the rip spacing is smaller than the surf zone width retention rates increase to 100% and rip current velocities maximize. When the rip spacing is larger than the surf zone width, retention rates and rip current velocities quickly decline. In both figures presented here, the surf zone is about 250m wide. This means that for increasing rip spacing the rip current velocities seem to grow (see Figure 61), at least for these cases of transverse bars. This is in contrast to the conclusions of Castelle, Reniers and McMahan [2014]. Retention rates of numerical drifters cannot be computed here because processes critical for surf zone retention, such as Stokes drift and VLF's, are not represented in the models used here. Intuitively, however, the extreme length of the rip current presented in Figure 60 seems to indicate that this rip would cause a decrease in surf zone retention, as the detected rip extends outside the surf zone.

Before concluding the correlation study for the rip lengths the meandering longshore current is studied. Figure 62 depicts the relation between the cross shore length of detected flow structures and the subtidal bathymetric variability in the left window, and the intertidal bathymetric variability in the right window. This is done for a wave angle of incidence of -30°.

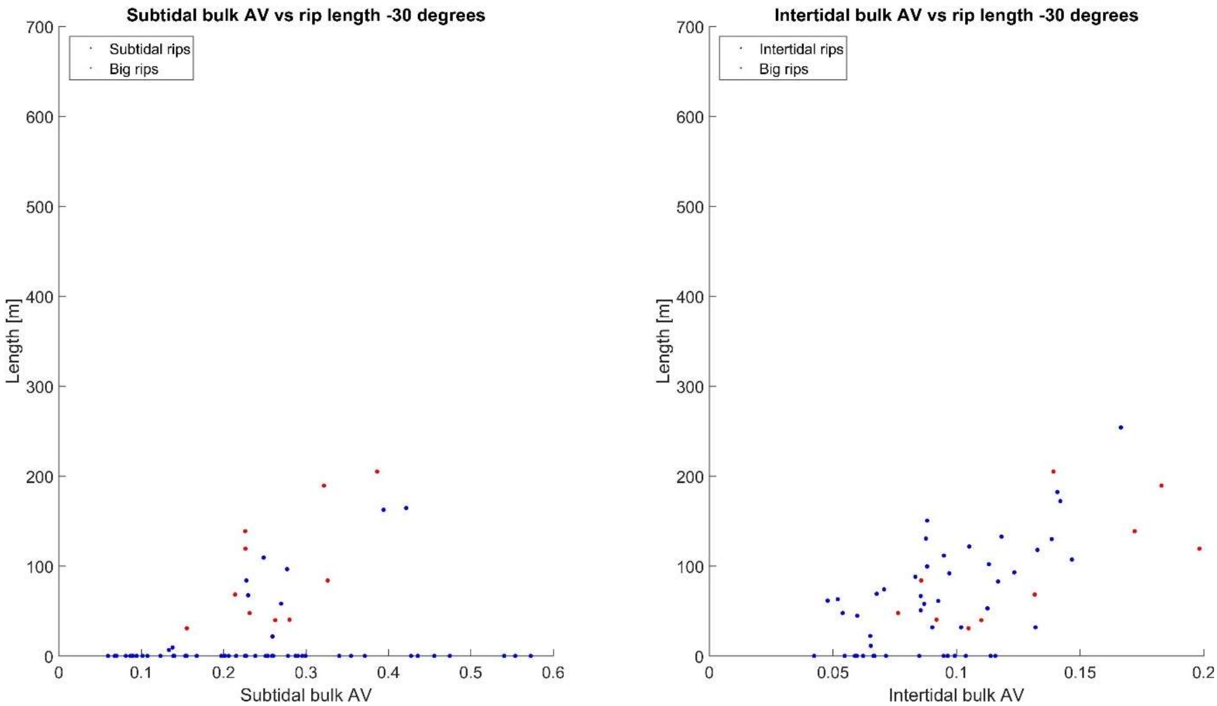

Figure 62: Scatter of the rip length, and the corresponding bulk alongshore bathymetric variability. The left window shows the data for the subtidal rips, the right window for the intertidal rips. The data for the big rips is incorporated in both windows.

In these cases a strong longshore current has picked up, bypassing the rip cahnnels. However, this longshore current meanders due to the influence of the bathymetric variability. Comparing the length scales found here with those for normally incident waves in Figure 57, it is clear that the amplitude of these meanders is a lot less than the more extreme lengths the rip currents can have. Yet the overall trend seems to be the same: low amounts of variability induce little meandering whilst higher amounts of variability can induce stronger meandering in the longshore current, as long as these features are not too deep for the longshore current to interact with.

5.2.3 Correlation roller forces and bathymetry

Finally the relation between the alongshore bathymetric variability and the alongshore variability in roller forces is studied. Table 13 shows the correlation between the alongshore variability in the bathymetry and the roller forces grouped per wave angle for every model run, regardless of rip detection results. All shown values have a certainty of more than 95%.

Here again the relation between the depth of the bathymetric features and the bathymetric variability shows itself. The correlation for the shallower intertidal area is a lot stronger than for the deeper subtidal area

CORRELATION BETWEEN THE BATHYMETRIC AV AND FORCING AV

WAVE ANGLE	Intertidal	Subtidal
-30	0,6919	0,5518
-25	0,6857	0,5456
-20	0,6822	0,5386
-15	0,6778	0,5291
-10	0,6737	0,5152
-5	0,6703	0,4972
0	0,7169	0,5054
5	0,7117	0,5211
10	0,7069	0,5337
15	0,7011	0,5426
20	0,6963	0,5489
25	0,6946	0,5519
30	0,6895	0,5501

Table 13: Correlation of the bulk bathymetric variability and bulk variability in roller forces for the intertidal area (second column) and the subtidal area (third column), for each wave angle of incidence.

This table shows that there is a significant relation between the alongshore bathymetric variability, and the driving forces which cause rip currents, as long as the variable bar patterns are at a depth where a significant portion of the waves break over them. If the bulk alongshore bathymetric variability is used as a parameter to predict the presence of dangerous rips than the relation with the depth of the variable patters clearly needs to be quantified as well.

5.3 Conclusions Modelling Study

This chapter ends by answering the research questions of this chapter. The main research question which has been answered in this chapter is research question four:

Is the alongshore bathymetric variability an important indicator for nearshore currents which form a risk to bathers?

Significant relations between alongshore bathymetric variability and the alongshore variability in roller forces, rip current velocity and rip current length have been found. Especially for normally incident waves there seems to be a good relation with the intertidal alongshore bathymetric variability and the rip velocity of rips over the intertidal area. The length of big rips and intertidal rips also correlates well with the alongshore bathymetric variability, in particular for larger angles of incidence. The cross shore length scale of meandering of the longshore current also relates to alongshore bathymetric variability. The relation between the alongshore bathymetric variability is not a one in one relation. Other parameters also play a role in determining rip velocity and length. Is a bather risk model where to be created the alongshore bathymetric variability is an important factor which should be included in this model.

Bypassing of rip channels due to the influence of the longshore current has also been observed. It can be concluded that the longshore current starts to dominate the subtidal area for angles of incidence of at least -10° and +20° relative to shore normal. The longshore current starts to dominate the intertidal area for angles of incidence of at least -30° and +20° relative to shore normal.

Qualitative observations made in answering this question are the following. Apart from the alongshore bathymetric variability three other parameters appear to act as controls on the rip current velocity and length. The depth at which the variable patterns are situated determines the extent to which the variable bathymetry and the waves are able to interact. This could appears to be in line with the notion of 'active morphology' as used by Scott et al. [2014].

The second factor is the distance with between the intertidal bar and the subtidal bar. When waves break over both bars, a circulating rip cell is generated over each bar. The closer these two bars are situated to one another, the stronger the interaction between these two circulations seems to be. This might cause long rip currents.

The third parameter which seems to influence the rip current parameters is the is the phase difference between the intertidal and the subtidal bar. When both bars are in phase, the circulating rip cells over the intertidal- and subtidal bar seem to interact stronger. This might cause long rip currents.

In short rip currents are expected to be strong if both the intertidal- and the subtidal alongshore bathymetric variability are high, waves break over the bars the distance between the subtidal- and intertidal bars is minimal and the subtidal- and intertidal bars are in phase. A good example of this are transverse bars which connect from the subtidal bathymetry, through the intertidal bathymetry to the supratidal beach, with wide, well defined bars and with deep, relatively wide, well developed rip channels.

This chapter also further answered research question three:

How can the (parameterized) alongshore variability be related to currents which form a risk to bathers?

In order to compare model performance for different levels of alongshore bathymetric variability, the model output needs to be parameterised. The alongshore variability on roller forces, representative of alongshore gradients in the forces related to wave breaking which a part of the driving forces of rip currents, can be computed with the same multi step process as the bulk alongshore bathymetric variability for model bathymetries. First an alongshore running average roller force field is computed using the same length scales as for the bathymetric alongshore running average. Local alongshore differences can be computed by subtracting this alongshore running average roller force field from the roller force field output of the model computation. By taking the absolute values of the local alongshore difference field, the local alongshore variability in roller forces can be computed. This can be used to compute bulk parameters for the alongshore variability in roller forces over the intertidal bathymetry and the subtidal bathymetry.

From the 2D field of cross shore velocity output, patches of dangerous current can be detected. If a threshold value of 0.25m/s is exceeded and if the depth of a rip current is at least 1m and if the current is sufficiently far away from the lateral boundaries, than the detected current is approved as a risky rip current. From these currents, the strongest current is used for further study. For this detected current patch the 90 percentile velocity and the rip length in cross shore direction are studied as these parameters are relevant for bather risk. This is done for rips over the intertidal bathymetry (intertidal rips), rips over the subtidal bathymetry (subtidal rips) and rips which run over both the intertidal- and subtidal bathymetry (big rips).

Using this peak over threshold detection scheme entails that for current velocities lower than 0.25m/s the rip parameters have artificially been set to zero. Ideally one would like to exclude these artificial data points from the rest of the data. Justifying this choice can be done by means of Welch's t-test. If the null hypothesis of this test is discarded, the choice to discard the zero rips was justified. The relation between bulk alongshore bathymetric variability and the rip parameters can now be quantified by means of the correlation and coefficient of determination.

6. Discussion

A number of assumptions have been made in the process of this thesis research which affect the conclusions made in this report. Not incorporating water level variations has limited the ability to assess the relation between the water depth, alongshore bathymetric variability and rip currents. For coasts which, like the Delfland Coast, see significant water level differences due to the tide, it is known that rip current velocity and the nature of rip circulation at large can change significantly for different water level elevations (Scott et al. [2014]).

For the longer rips detected in the modelling study, not incorporating the tidal currents might also have significant consequences. The longest rips detected in the modelling output reach hundreds of meters outside the surf zone. In this area these currents no longer have a direct, local relation to bathymetric patterns or the wave forcing. Their existence far outside the surf zone is probably mostly due to inertia effects. In reality, however, the currents outside the surf zone will be dominated by the horizontal tide along the Delfland Coast. Interaction between the horizontal tide and these long rip currents probably will not influence the rip current (velocities) inside the surf zone significantly. But for the part which extends outside the surf zone, the interaction will cause changes which can have implications for the length of these rip currents.

Qualitatively there are a lot of examples of phase differences between the intertidal bar and the subtidal bar in the data set of modelling bathymetries. These phase differences have, however, not been quantified, as phase differences have not been an object of study in this thesis study. This limits the extent to which this study can draw conclusions on the influence of phase differences between the intertidal bar and the subtidal bar on rip current velocity and length.

The same can be said for the distance between the intertidal bar and the subtidal bars. Again, a lot of examples with different bar spacing can found in the data set. Yet it has not been an object of study here. Also quantifying the cross shore position of a bar is not as trivial is it might seem at first. The local cross shore position of a rhythmic bar can vary over 100m in this data set. Aside from that there is a relation between the cross shore position and the depth of a bar. A bar which lies close to shore is situation higher up the coastal slope and therefore lies in a shallower part of the foreshore. These relations between the different parameters which influence rip currents are at first glance rather complex and need more in depth study before hard conclusions can be drawn.

Using a peak over threshold approach in detecting dangerous rip currents has resulted in discarding a part of the modelling data set. Arguably, if one were interested in using this approach for a more energetic wave condition, more problems would arise. More energetic wave conditions are likely to induce stronger return currents. This could mean that the 0.25m/s threshold will be exceeded for most of the domain, rather than highlighting dangerous areas in rip circulations. Both problems can possibly be overcome by calculating the expected return current for the used wave condition, assuming that only undertow takes place. If this threshold is exceeded (by some margin) a rip current is detected. This can lead to a variable threshold. Judging weather a certain current forms a risk to bathers can be done by using some velocity statistic of this detected rip, such as the 90 percentile velocity.

By cutting tiles of variable patterns out of the measured bathymetry, transitions from one level of alongshore bathymetric variability to another are not represented in the modelling study. In the case where a section of non-variable bathymetry transitions into a more variable section of bathymetry, more rip bypassing might occur over the more variable part of the bathymetry than is found in this study. If oblique wave attack occurs and a longshore current develops, it might gain more momentum over the non-variable part of the bathymetry than is seen in this modelling study. This might mean that at these transitions a stronger alongshore current might be present over a bathymetry with significant alongshore bathymetric variability, than is suggested by the modelling study. This stronger longshore current might locally induce rip bypassing for smaller angles of wave incidence than this study would suggest.

In the study presented here the morphodynamics have been disregarded. In the data set of model bathymetries, there are a lot of examples of bathymetric patterns which were measured well outside the summer season (June to September). Yet the wave conditions used in the modelling study are seen as representative of the upper limit of bathing conditions. These conditions one would typically expect in the summer period. These choices might seem in contrast to one another, as nearshore bathymetric patterns are in part dependant on the current local hydrodynamic conditions (Smit, Reniers and Stive [2012]). However the object here was to relate real world examples of bathymetric variability to currents which might form a risk to bathers. The data analysis has shown that, though clear overall patterns can be discerned, wide varieties of alongshore bathymetric variability can be found along the Delfland Coast, even in the summer months. This seems to justify the choice of incorporating the measurement data which was recorded outside the summer months, without accounting for the morphodynamics in the modelling study, as long as one is solely interested in the relation between alongshore bathymetric variability and the wave induced current which could form a risk to bathers. Assessing the chance of occurrence of certain levels of (intertidal and/or subtidal) alongshore bathymetric variability coinciding with environmental conditions favourable for bathers is outside of the scope of this study.

In this study has highlighted a large variety of rip currents for sections of bathymetry of the Delfland Coast. Some were rather weak and small. Other rips wehe very strong and big. Rips associated with the more extreme form of transverse bars at the tip of the Sand Motor can generate strong currents over a large area (see chapter 5). One example, shown in Figure 60, shows a rip current with an alongshore width of about 200m. If a bather would follow the rip escape strategy presented on the website of the Dutch life brigade, one could swim 100m in alongshore direction and still not have escaped the dangerous rip current, whilst being transported a significant offshore during the time it would take to swim this distance. Qualitatively, the observations made in this study seem to underline the conclusions of McCarroll et al. [2014] that a single escape strategy safety message, such as presented on the website of the Dutch life brigade, is inappropriate.

The results of this study can be used for a possible bather risk model. Two main audiences can be identified; the life brigade, who would use it as an aid in their day to day operations, and policy makers, who would us it to better justify investments in safety measurements. The life brigade would mainly be of interest in the potential risk level itself for a given bathymetry, whilst policymakers would want to know possible effects of certain decisions/actions.

In assessing the possible risk level, one would ideally like to know what levels of risk one can expect, give the current alongshore bathymetric variability, and the range in tidal elevations and wave conditions expected for a certain day. With the measured bathymetric data, and the wave forecast in hand, the life brigade would be able to assess the needed preventive measures and ‘rescue capacity’ needed for each subsection of the Delfland Coast. Note that the presence of bathers also plays a crucial role here. The results of this study do not lead to such a model directly, given the previously mentioned restraints on this study, but the results presented here should be used as input.

In assessing possible changes to the risk level, given certain decisions/actions of policymakers, more factors play a role. Here especially the influence of human behaviour in the nearshore area and crowd flow on the beach are of importance. Given the infrastructure offered to tourists on and near the beaches of the Delfland Coast (parking lots, beach entrances, boulevards, on-beach catering facilities, etc.), large groups of bathers might be steered towards, or away from certain sections of the coast. If these sections are known to be associated with especially risky currents, than this is significant for bather risk. Coming to a model which would be able to describe all this, the expertise of other experts is needed as these topics lie outside the field of expertise of civil engineers. The results of this study do form valuable input for such a model.

7. General Conclusions

Here the conclusions and observations regarding this Master thesis research are listed. First each research question is expressed in bold, followed by the conclusions.

Research question one: Can a parameter be constructed, which is representative of the alongshore bathymetric variability along subsections of the Delfland Coast?

By using a five step scheme a bulk parameter for the alongshore bathymetric variability can be defined which is representative of the local alongshore bathymetric variability of 400m long subsections of the Delfland Coast, for both the intertidal zone and the subtidal zone. The five steps are listed below, in order of execution:

1. Convert the curvy coastal bathymetry of the data set into an alongshore straightened coast
2. Determine an alongshore running average bathymetry for this alongshore straightened coast
3. Calculate the difference bathymetry by subtracting step 2 from step 1
4. Calculate the local alongshore variability by taking the absolute values of step 3
5. Isolate the intertidal- and subtidal zones, and calculate the bulk alongshore variability for both zones for sections of 400m

Research question two: How does the alongshore bathymetric variability of the Delfland Coast develop during the studied period?

In accordance with de Schipper et al. [2013] the subtidal alongshore bathymetric variability along the Delfland Coast mostly decreases in the winter months when environmental conditions are more energetic. In the intertidal area the alongshore bathymetric variability usually decreases in the winter months, in contrast to the conclusions of de Schipper et al. [2013].

Very low levels of subtidal variability coincide with low levels of intertidal variability and vice versa. Very high levels of subtidal alongshore bathymetric variability coincide with a wide range of intertidal alongshore bathymetric variability, from low to very high.

The lowest levels of subtidal variability occur near the Hoek van Holland breakwater. In this area the intertidal alongshore bathymetric variability is usually low. The presence of groins can make the response of the intertidal area more complex. Groins can force the medium high levels of alongshore bathymetric variability, even when subtidal levels are low.

The highest levels of subtidal alongshore bathymetric variability are related to the sand bars which connect the subtidal area of the Sand Motor to that of the NeMo area in 2012. Subtidal variability can also be very high for transverse bars, at the tip of the Sand Motor for example. For this data set high levels of subtidal alongshore bathymetric variability are only associated with high intertidal levels if the bars run through the intertidal zone and connect to the supra tidal beach. If this is not the case than intertidal levels of alongshore variability can be can be quite low.

The highest levels of intertidal alongshore bathymetric variability are related to the lagoon channel. The lowest levels are related to the absence of any clear morphological features.

The low values of alongshore bathymetric variability near the breakwater at Hoek van Holland coincide with a coastal orientation of 50° to North. Other sections of the NeMo area see a higher spread of variability for a coastal orientation of about 40° to North. For the Sand Motor there seems to be no relation between the alongshore bathymetric variability and the coastal orientation.

How can the (parameterized) alongshore variability be related to currents which form a risk to bathers?

This can be done by means of a numerical model analysis. Model bathymetries can be created with tiles of nearshore bathymetry which have been cut out of the alongshore straightened bathymetries, generated during the data analysis. Judging whether a generated model bathymetry is fit for use depends on three main questions:

- Is the difference between the computed bulk parameters and the bulk parameters from the time stacks less than 10%?
- Does the bulk alongshore variability show only minor differences between -2000m and +2000m?
- Does the generated bathymetry look alright, or has the process of cutting and pasting generated an artificial pattern, which is not representative of the original pattern observed in the field data?

The significant wave height in the model is set at 1.5m, which can be seen as an upper limit for recreational conditions. The peak period is set at 6s. The angle of wave incidence is varied from model to model. The angle of wave incidence is varied from -30° to +30° to shore normal, with 5° increments.

In order to compare model performance for different levels of alongshore bathymetric variability, the model output needs to be parameterised. The alongshore variability on roller forces, representative of alongshore gradients in the forces related to wave breaking which a part of the driving forces of rip currents, can be computed with the same multi step process as the bulk alongshore bathymetric variability for model bathymetries.

From the 2D field of cross shore velocity output, patches of dangerous current can be detected. If a threshold value of 0.25m/s is exceeded and if the depth of a rip current is at least 1m and if the current is sufficiently far away from the lateral boundaries, than the detected current is approved as a risky rip current. From these currents, the strongest current is used for further study. For this detected current patch the 90 percentile velocity and the rip length in cross shore direction are studied as these parameters are relevant for bather risk.

Is the alongshore bathymetric variability an important indicator for nearshore currents which form a risk to bathers?

Significant relations between alongshore bathymetric variability and the alongshore variability in roller forces, rip current velocity and rip current length have been found. Especially for normally incident waves there seems to be a good relation with the intertidal alongshore bathymetric variability and the rip velocity of rips over the intertidal area. The length of big rips and intertidal rips also correlates well with the alongshore bathymetric variability, in particular for larger angles of incidence. The cross shore length scale of meandering of the longshore current also relates to alongshore bathymetric variability. The relation between the alongshore bathymetric variability is not a one in one relation. Other parameters also play a role in determining rip velocity and length. Is a bather risk model where to be created the alongshore bathymetric variability is an important factor which should be included in this model.

Bypassing of rip channels due to the influence of the longshore current has also been observed. It can be concluded that the longshore current starts to dominate the subtidal area for angles of incidence of at least -10° and +20° relative to shore normal. The longshore current starts to dominate the intertidal area for angles of incidence of at least -30° and +20° relative to shore normal.

Qualitative observations made in answering this question are the following. Apart from the alongshore bathymetric variability three other parameters appear to act as controls on the rip current velocity and length. The depth at which the variable patterns are situated determines the extent to which the variable bathymetry and the waves are able to interact. This could appears to be in line with the notion of 'active morphology' as used by Scott et al. [2014].

The second factor is the distance with between the intertidal bar and the subtidal bar. When waves break over both bars, a circulating rip cell is generated over each bar. The closer these two bars are situated to one another, the stronger the interaction between these two circulations seems to be. This might cause long rip currents.

The third parameter which seems to influence the rip current parameters is the is the phase difference between the intertidal and the subtidal bar. When both bars are in phase, the circulating rip cells over the intertidal- and subtidal bar seem to interact stronger. This might cause long rip currents.

In short rip currents are expected to be strong if both the intertidal- and the subtidal alongshore bathymetric variability are high, waves break over the bars the distance between the subtidal- and intertidal bars is minimal and the subtidal- and intertidal bars are in phase. A good example of this are transverse bars which connect from the subtidal bathymetry, through the intertidal bathymetry to the supratidal beach, with wide, well defined bars and with deep, relatively wide, well developed rip channels.

7.1 Recommendations

In order to better understand the influence of the nearshore topography on currents which might form a risk to bathers, it is recommended to further investigate the influence of the depth at which alongshore bathymetric variability is situated, the distance between the subtidal bar and the intertidal bar and the phase differences between the subtidal bar and the intertidal bar on such currents.

References

Castelle, B., Reniers, A.J.H.M. and MacMahan, J. [2014] Bathymetric control of surf zone retention on a rip-channelled beach. Ocean Dynamics, Vol. 64, 121-1231

Dalrymple, R.A. [1978] Rip Currents and their causes. In Proceedings 16th International Conference Coastal Engineering, pp. 1414–27. Washington, DC: ASCE

Dykes, J.D., Hsu, Y.L. and Kaihatu, J.L [2003] Application of Delft3D in the nearshore zone. Proc. 5th AMS Coastal Conf

van Enckevort, I.M.J. and Ruessink, B.G. [2002] Video observations of nearshore bar behaviour. Part 1: alongshore uniform variability. Continental Shelf Research 23 (2003) 501-512

van Enckevort, I.M.J. and Ruessink, B.G. [2003] Video observations of nearshore bar behaviour. Part 2: alongshore non-uniform variability. Continental Shelf Research 23 (2003) 513-532

Grunnet, N.M and Ruessink, B.G. [2005] Morphodynamic response of nearshore bars to a shoreface nourishment. Coastal Engineering 52 (2005) 119-137

Haller, M.C. [2002] Experimental study of nearshore dynamics on a barred beach with rip channels. Journal of Geophysical Research, Vol. 107, NO. C6, 306 (2002)

Johnson, D. and Pattiaratchi, C. [2006] Boussinesq modelling of transient rip currents. Coastal Engineering 53 (2006) 419-439

Kaji, O.A. [2013] Assessment of the variables influencing sediment transport at the Sand Motor (Master Thesis)

Longuet-Higgins, M.S., Stewart, R.W. [1964] Radiation stress in water waves; a physical discussion, with applications. Deep-Sea Research, 1964, Vol. 11, pp. 529 to 562.

McCarroll, R.J., Brander, R.W., MacMahan, J.H., Turner, I.L., Reniers, A.J.H.M., Brown, J.A., Bradstreet, A. and Sherker, S. [2014] Evaluation of swimmer-based rip current escape strategies. Nat Hazards (2014) 71:1821-1846

MacMahan, J.H., Thornton, E.B. and Reniers, A.J.H.M. [2006] Rip current review. Coastal Engineering, 53 (2006) 191-208

MacMahan, J.H., Thornton, E.B., Reniers, A.J.H.M., Stanton, T.P. and Symonds, G. [2008] Low-energy rip currents associated with small bathymetric variations. Marine Geology, 255 (2008) 156-164

Plant, G.N, Holland, K.T. and Puleo, J.A. [2002] Analysis of the scale errors in nearshore bathymetric data. Marine Geology, Vol. 191 (2002) 71-86

Quartel, S. [2009] Temporal and spatial behaviour of rip channels in a multiple-barred coastal system. Earth Surface Processes and Landforms, Vol. 34, Issue , 163-176, February 2009

Radermacher, M., de Schipper, M.A., Swinkels, C., MacMahan, J.H. and Reniers, A.J.H.M. [2017] Tidal flow separation at protruding beach nourishments. Journal of Geophysical Research: Oceans, Vol. 122

Reniers, A.J.H.M., Roelvink, J.A. and Thornton, E.B. [2004] Morphodynamic modelling of an embayed beach under wave group forcing. Journal of Geophysical Research, Vol. 109 (2004)

Reniers, A.J.H.M, MacMahan, J.H, Thornton, E.B. and Stanton, T.P. [2007] Modelling of very low frequency motions during RIPEX. Journal of Geophysical Research, Vol. 112, 2007

Ruessink, B.G., Miles, J.R., Feddersen, F., Guza, R.T. and Elgar, S. [2001] Modelling the alongshore current on barred beaches. Journal of Geophysical Research, Vol. 106, October 15th 2001

Ruessink, B.G., van der Grinten, R.M., Vonhögen-Peeters, L., Ramaekers, G. and Lodder, Q.J. [2012] Nearshore evolution at Noordwijk (NL) in response to nourishments, as inferred from Argus video imagery. Jubilee Conference Proceedings, NCK-Days 2012

Ruxton, G.D. [2006] The unequal variance t-test is an underestimated alternative to Student's t-test and the Mann-Whitney U-test. Behavioural Ecology, 17 May 2006

de Schipper, M.A., de Vries, S., Ranasinghe, R., Reniers, A.J.H.M and Stive, M. [2013] Alongshore topographic variability at a nourished beach. Coastal Dynamics 2013, paper no.049

de Schipper, M.A., de Vries, S., Ruessink, G., de Zeeuw, R.C., Rutten, J. ,van Gelder-Maas, C., Stive, M.J.F. [2016] Initial spreading of a mega feeder nourishment: Observations of the Sand Engine pilot project. Coastal Engineering 111 (2016) 23-38

Schlooz, G. [2012] Convex coastline induced rip currents at the Sand Engine. (Master Thesis)

Scott, T, Masselink, G., Austin, M.J. and Russel, P. [2014] Controls on macrotidal rip current circulation and hazard. Geomorphology 214 (2014) 198-215

Short, A.D. [1991] Beach systems of the central Netherlands coast: Processes, morphology and structural impacts in a storm driven multi-bar system. Marine Geology, 107 (1992) 103-137

Short, A.D. and Hogan, C.L. [1994] Rip currents and beach hazards: Their impact on public safety and implications for coastal management. Journal of Coastal Research Special Issue No. 12: Coastal Hazards, pp. 197-209 (1994)

Smit, M.W.J, Reniers, A.J.H.M and Stive, M.J.F. [2012] Role of morphological variability in the evolution of nearshore sandbars. Coastal Engineering, Vol 69, 19-28

van Son, S.T.J., Lindenbergh, R.C., de Schipper, M.A., de Vries, S. and Duijnmayer, K. [2009] Using a Personal Watercraft for monitoring bathymetric changes at storm scale. In Proceedings of the International Hydrographic Conference, November 10-12 2009, Cape Town, South Africa

Tan Y.C. [2014] Assessment of beach states at the Sand Motor on the basis of alongshore variability in bathymetry data. (Master thesis)

Vargas Solis, A. [2015] Impact of beach states in net longshore sediment transport. (Master thesis)

Welch, B.A. [1947] The generalization of the 'Stundent's' problem when several different population variances are involved. Biometrika, Vol. 34, No. ½ (January 1947) 28-35

Wright, L.D. and Short, A.D. [1984] Morphodynamic variability of surf zones and beaches: A synthesis. Marine Geology, 56 (1984) 93-118

de Zeeuw, R.C. [2011] Nearshore currents and swimmer safety in the Netherlands. (Master thesis)

Zimmerman, D.W. [2004] A not on preliminary tests of equality of variances. British Journal of Mathematical and Statistical Psychology (2004), 57, 173-181

Appendixes

Appendix A1: Interpolation- and measurement error

The raw data of the NeMo- and Sand Motor measurement project has been interpolated to a 10m by 10m grid before the method described in this document has been applied to the measurement data. In doing so, two possible errors can affect the data: measurement error and interpolation error. This appendix will highlight examples of both error types, and discuss the way the interpolation error has been addressed and what this means for the resolvable length scales. A lot of quantitative research has been done into errors in nearshore bathymetric data (Plan, Holland and Puelo [2002]). This appendix will stick to qualitative examples of the data set used for the study described in the main document.

Interpolation Error

The measurement plan for the NeMo area is pretty straight forward. The bathymetry has been measured every two meters, on cross shore directed measurement tracks spaced 30 to 40m apart. In the Sand Motor measurement area, the measurement plan is a lot more complex. There are measurement tracks directed in both the alongshore direction, as well as the cross shore direction. These tracks are spaced about 30m apart.

Especially the crossing measurement track seem to generate interpolation errors. These errors are particularly problematic in the intertidal area, where the dominant length scales are relatively short and the amplitudes are relatively small. Figure 63 Shows an example of linearly interpolated data of the March 2015 at a location on the spit of the Sand Motor. The measurement points are represented by the white markers. At this moment faint longshore bars and rips with an alongshore length scale in the order of 50m to 100m where present. This, however, is not the picture which rises form the linearly interpolated data.

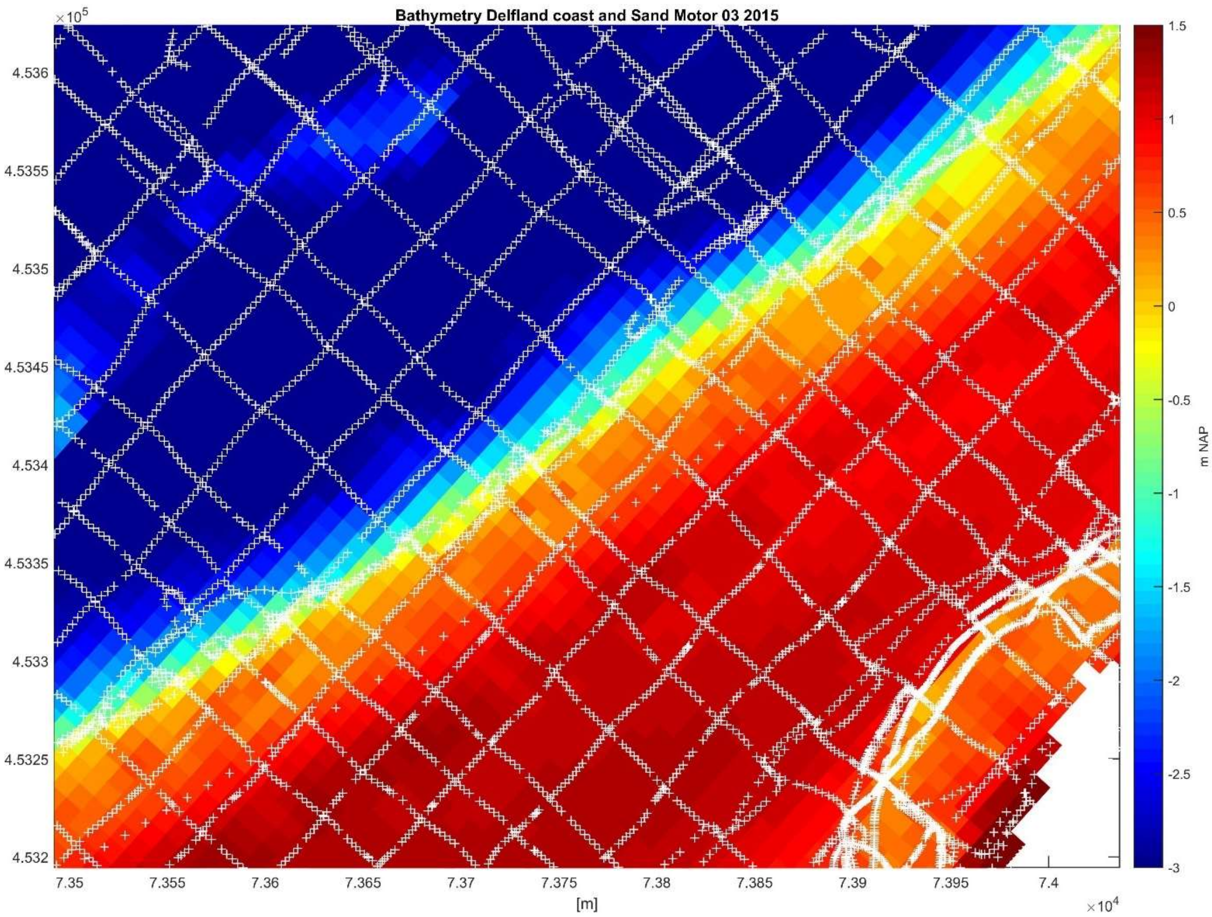

Figure 63: Measurement points (white markers) and linearly interpolated data at the Sand Motor spit, for March 2015

Instead of longshore bars, the intertidal area in Figure 63 is characterized by a lot of noise related to the crossing measurements tracks. Clearly, the original patterns are under resolved by the measurement plan and lead to interpolation errors when interpolated by means of linear interpolation. It was found that locally, these interpolation artefacts significantly influence the alongshore bathymetric variability computation. Another example of such interpolation artefacts at crossing measurement tracks in shown in

These interpolation artefacts have been addressed by means of subsampling. The data has been subsampled with subsampling diameter slightly less than the measurement track spacing. A sampling spacing of 25m has been used. This effectively reduces the structured measurement point cloud to a less dense, unstructured point cloud which is more suitable for linear interpolation. This is shown in Figure 64.

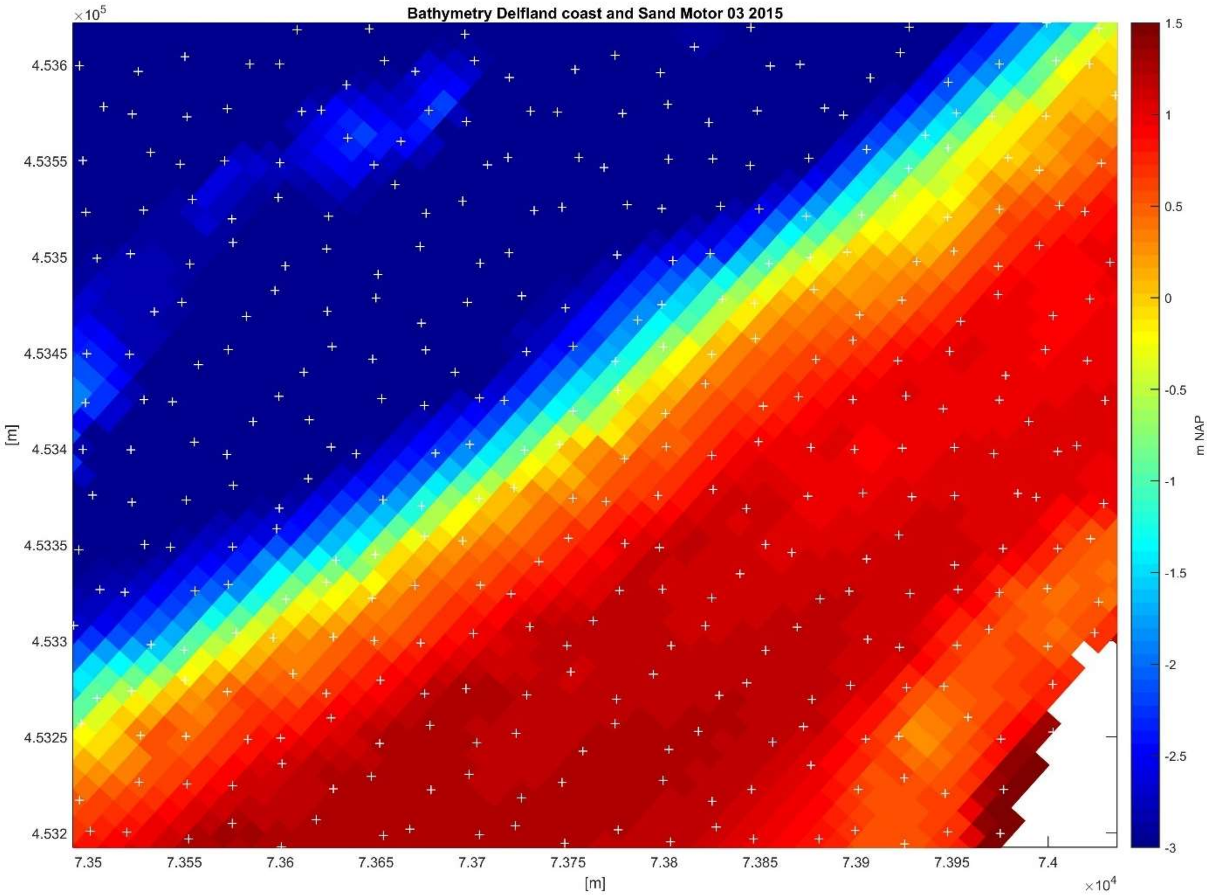

Figure 64: Subsampled data points (white markers) and linearly interpolated data at the Sand Motor spit, for March 2015

Subsampling has clearly reduced the number of data points used by the linear interpolation scheme. The total effect is that the interpolated data has been smoothed. This reduces the noise without reducing the resolved length scales in the alongshore and cross shore direction, since these where effectively determined by the measurement track spacing in the original situation. The shortest length scale handled in the main document (200m in alongshore direction) is well resolved by this scheme.

Suggestion on Sand Motor Measurement Plan

Any measurement plan cannot resolve bathymetric features with an alongshore length scale shorter than the measurement track spacing. Feature length scales with the same order of size as the measurement interval are usually under resolved. These features can be a source of interpolation error, as in the above example. Currently a lot of extra effort is made in taking additional measurements of the Sand Motor bathymetry. However, with respect to the NeMo measurement plan, the resolved length scales do not decrease. The additional data points likely increase the certainty at the resolved length scales, but the smallest resolved length scale as such is still determined by the measurement track spacing of about 30m.

The observation of interpolation errors around the Sand Motor has led to the suggestion that a different measurement plan might be more appropriate for the Sand Motor measurement area. Simply increasing the frequency of the cross shore directed measurement tracks would make the most out of the additional measurement effort. In such a case the measurement track spacing would decrease to about 15m in the Sand Motor measurement area. Some form of subsampling or smoothing will most likely still be needed in order to prevent interpolation errors (see Plant, Holland and Puelo [2002]). However the of subsampling- or smoothing length scale can now be shorter for the Sand Motor data (note that for the NeMo data this length scale would remain unchanged). This would decrease the shortest resolved length scale around the Sand Motor.

Arguably, the suggested measurement plan simpler to execute than the current, more complex measurement plan. The suggested measurement plan could arguably reduce the chance of potential measurement errors in the Sand Motor measurement area.

Measurement error

Figure 65 shows the interpolated data for March 2015 near a few groins in the southern NEMO area. The grey lined represent the groins. This figure contains more of the same type of interpolation error as mentioned above, in the bathymetric features in between the groins. However, it also shows measurement error at the upper right groin. For some reason the measurement team was not able to take measurements of this groin. This measurement error clearly causes a significant error in the interpolated data. It is important to note that errors of this nature are rare. This is the only groin which the measurement team was not able to measure during the session of March 2015. Next to that, the measurement team was able to measure the surrounding bathymetry, which was heavily influenced by the presence of the groin.

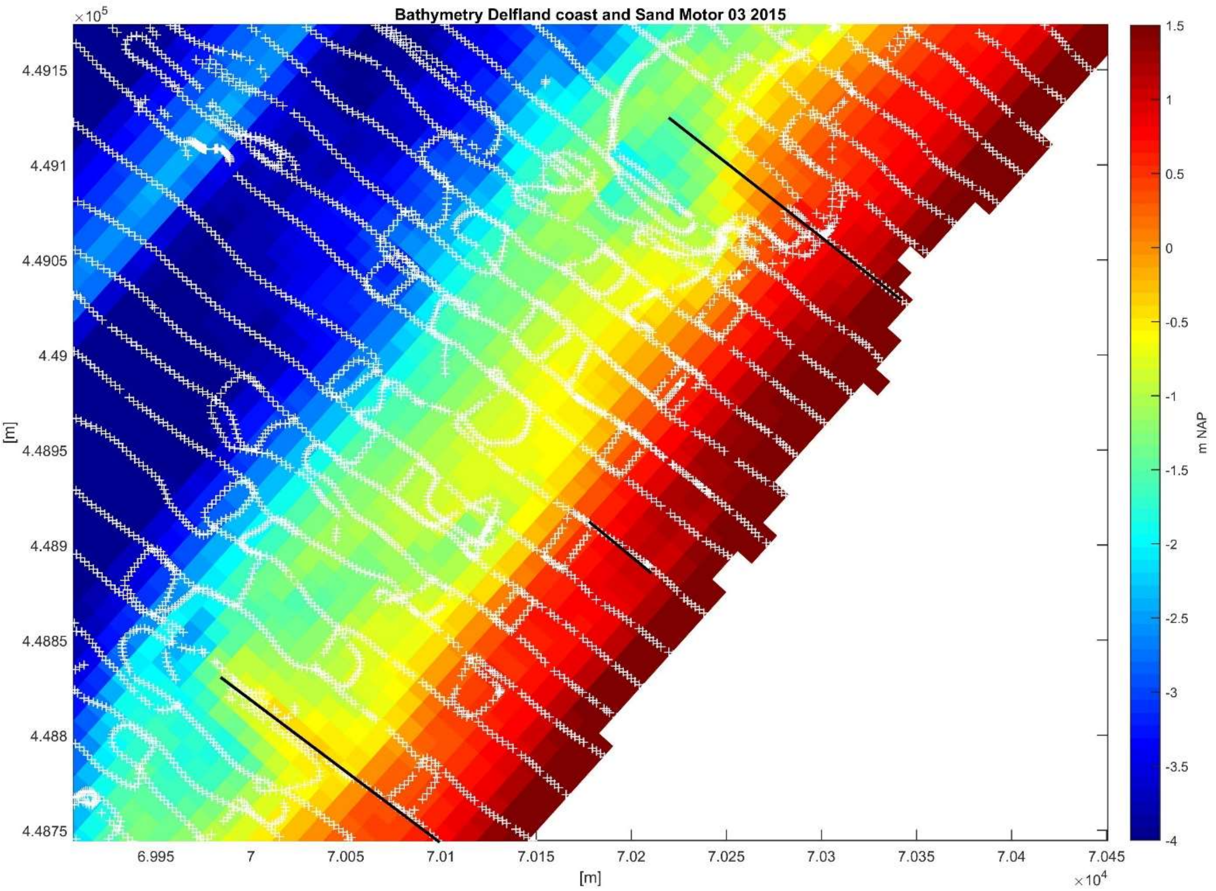

Figure 65: Measurement points (white markers) and interpolated data at the groin field in the southern NEMO section, for March 2015

Figure 66 shows the alongshore variability analysis for this section of coast. The absence of the groin around -4400m in the data is clearly visible. However the level of local alongshore bathymetric variability is of the same order as for the correctly measured groin. Clearly the efforts to correctly measure the surrounding area paid off. These rare measurement errors do not significantly affect the conclusions made in the main document.

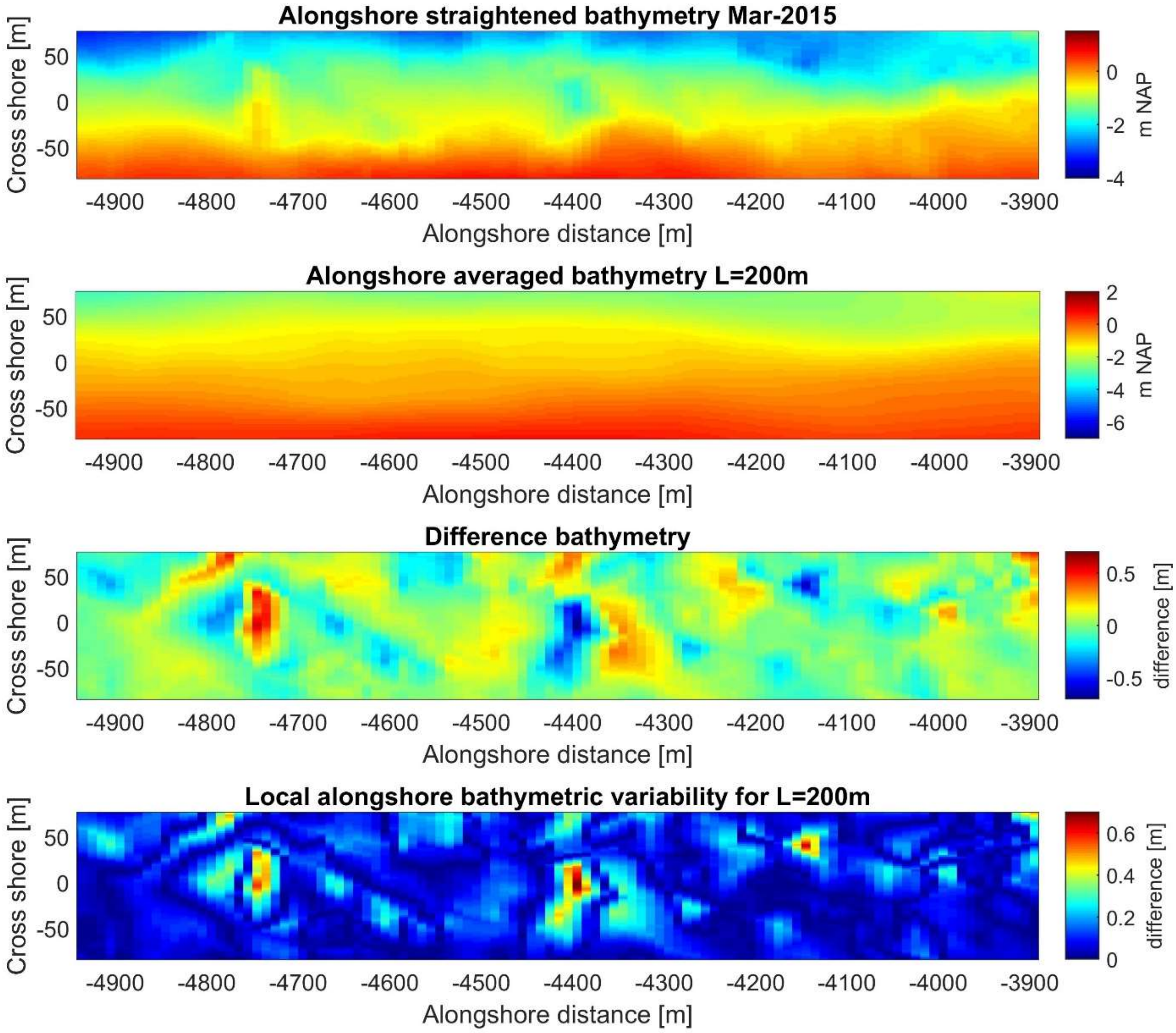

Figure 66: Alongshore bathymetric variability analysis around groin measurement error. Note that here, subsampling has been applied

Appendix A2: Running average length scales

Here the performance of different running average length scales for determining the alongshore bathymetric variability is assessed. A range of relevant length scales will be asessed, resulting in two length scales at which the data will be assessed; 200m for the intertidal area and 1000m for the subtidal area.

Intertidal length scales

The intertidal area largely consists of sections of coastline dominated by 'free' bar-rip bathymetry, and sections dominated by groin related bathymetry. In Figure 67 the performance of the analysis is shown for four length scales. The plotted lines represent the intertidal alongshore variability at each alongshore location. Note that the scaling of the vertical axes varies for the different.

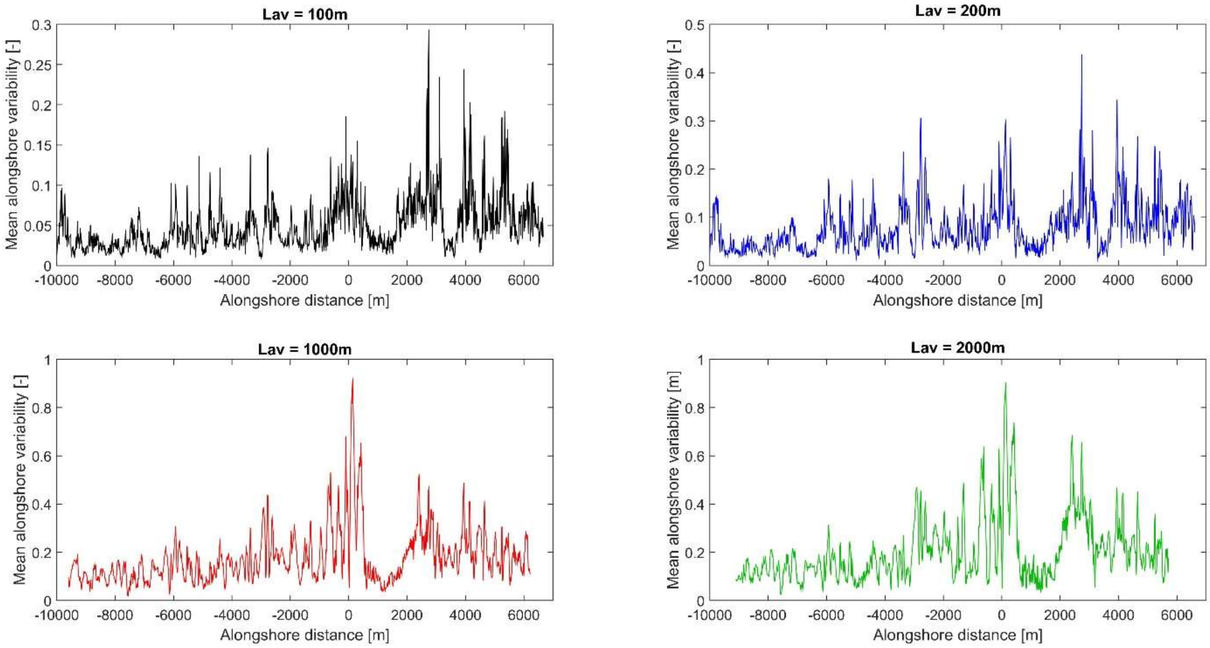

Figure 67: Intertidal performance of the analysis at four alongshore running average length scales, for measurement data from March 2015. Top left: 100m, top right: 200m, bottom left: 1000m, bottom right: 2000m

Looking at the line plots in Figure 67, it becomes clear that there is a big difference between the two larger length scales, and the two shorter ones. At 1000m and +2000m not only the intertidal bar-rip patterns are taken into account. Also longer scale undulations of the coastline produce a strong signal. In particular in the 2000m plot, the signal coming of these undulations seems to be stronger than the bar-rip signal, which is the signal of interest. Basically the bar-rip signal 'drowns' in the signal produced by other features at longer length scales, making it impossible to discern a groin dominated section of coastline from a 'free' bar-rip section of coastline. Next to that, the longer length scales seem to generate excessive peaks at local features, such as the lagoon channel mouth, between +2000m and +3000m alongshore.

The upper two windows in Figure 67 seem to do a better job at representing bar-rip related alongshore variability. Between -6000m and -3000m and +4000m and +6000m, both show peaks at the areas of groin related rip topography. And at the spit, around +1000m, and near Hoek van Holland, -10,000m to -6000m, the signal is distinctly les prominent than at the groins, apart from peaks produced by a few individual features. Strangely, however, the 100m signal seems to be a lot larger for the groins in NEMO north, than in NEMO south. Also, the difference in prominence of the signal at a section of groins and a 'free' bar-rip section seems to be larger for the 200m signal, making the output easier to judge. The overall strength of the signal (numbers on the vertical axis) also strongly indicates that the analysis for 200m is doing a better job.

All in all the analysis of the intertidal area seems to be working best for an alongshore running average length scale of 200m.

Subtidal area

In general subtidal bars longer than in the bars in the intertidal area. But to help better understand the performance of the analysis, output for the subtidal area is shown in Figure 68, a the same length scales as studied for the intertidal area. Note that the scaling on the vertical axes varies for the different windows.

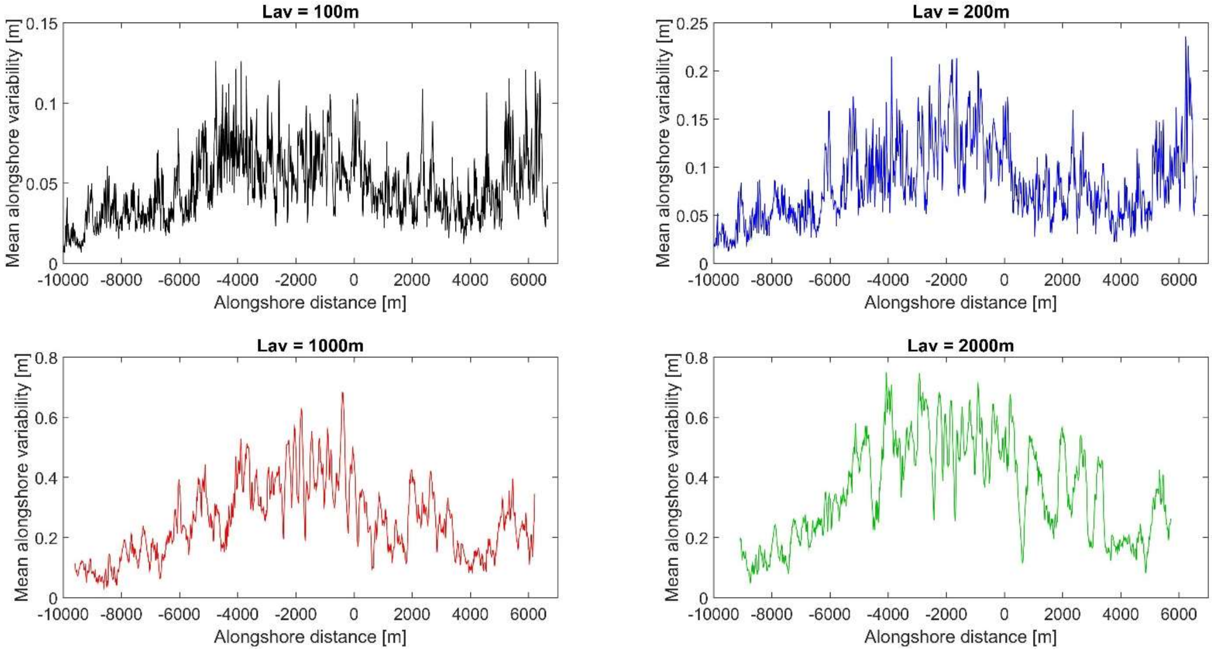

Figure 68: Subtidal performance of the analysis at four alongshore running average length scales, for measurement data from March 2015. Top left: 100m, top right: 200m, bottom left: 1000m, bottom right: 2000m

The two shorter length scales, shown in the upper windows of Figure 68, generally seem to record ‘noise’ generated by bed forms (also look at the overall signal strength).

The longer length scales, shown in the bottom windows of Figure 68, both produce better results. Both signals have a high amplitude at rhythmic features and TBR-like features, -6000m to -1000, and +2000m to +4000m. The section of the TBR-like ‘broccoli’ features (-2500m to -1000m), however, has a higher peak density in both signals, which will generate extra ‘heat’ in the bulk parameter analysis. Sections of more or less alongshore continuous bars, -10,000m to -6000m and +4000m to +5500m, generate very little peak prominence.

All is all, results are very similar. However, the overall trend in the 2000m plot is very high along the Sand Motor area. This is indicative of the fact that the alongshore differences in the coastal slope play an important role in generating the signal at this length scale. This is a false positive. All in all the analysis of the subtidal area seems to be working best for an alongshore running average length scale of 1000m.

Appendix A3: Comparing actual bathymetry

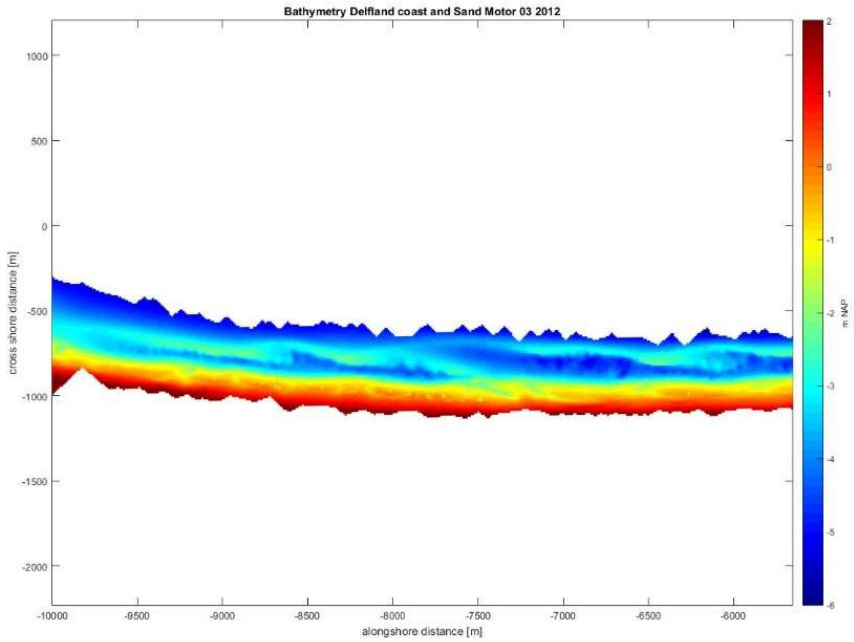

Figure 69: Southernmost section of the NEMO measurement area (Hoek van Holland is just to the right of this picture) for <u>March 2012</u>. Subtidal bars (blue hues) show increasing rhythmicity from south to north. Intertidal bars (yellow to orange hues) show a linear bar-rip pattern from -10,000m to -7500m. Between -7500m and -7000m the subtidal bar and intertidal bar are linked, forming a distinct transverse bar in the intertidal area. From -7000m onwards patterns are hard to describe, but rip channels are clearly visible.

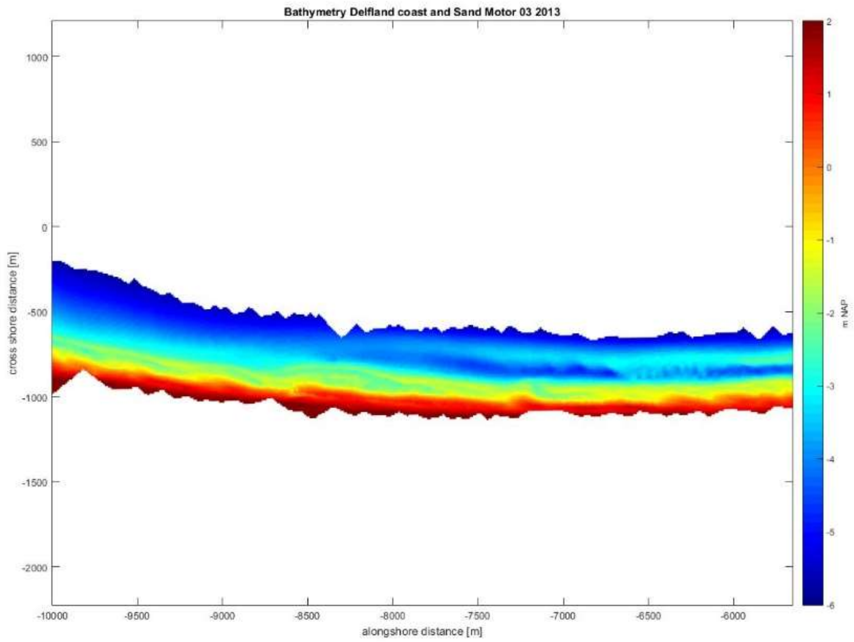

Figure 70: Southernmost section of the NEMO measurement area (Hoek van Holland is just to the right of this picture) for <u>March 2013</u>. The subtidal bar (blue hues) does not seem to exist between -10,000m and -8000m. From -8000m onwards, a linear subtidal bar is visible, with some short scale variability. Intertidal bars (yellow hues) show hard to describe patterns, but rip channel-like features are visible.

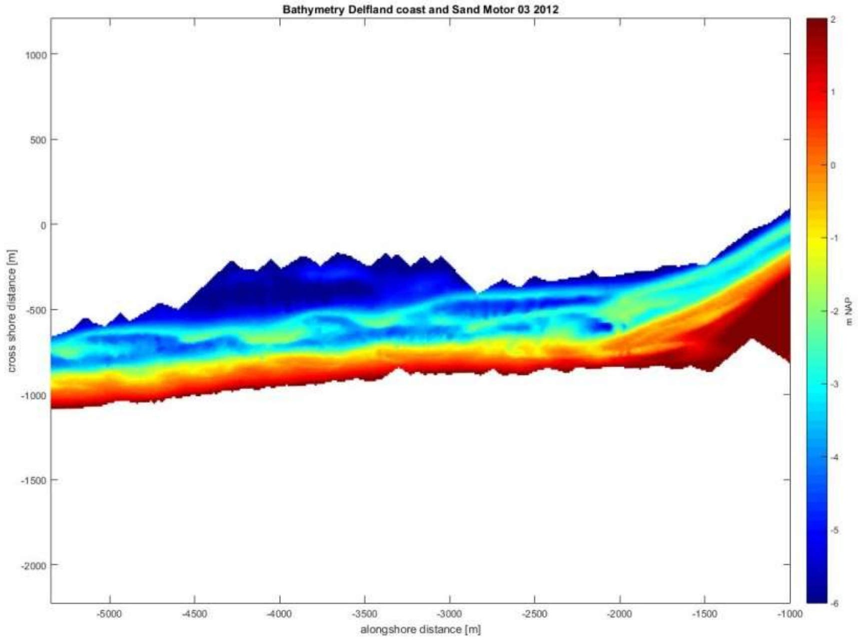

Figure 71: Section of the NEMO measurement area just south of the Sand Motor, for March 2012. Subtidal bars (blue hues) show a distinct rhythmic pattern, and are well defined (high crests and deep troughs). Near the Sand Motor a double bar system is visible. These bars connect to the subtidal bar of the Sand Motor, forming a large shoal. Intertidal bars (yellow to orange hues) show hard to describe patterns. Close to the Sand Motor these seem to become more extreme.

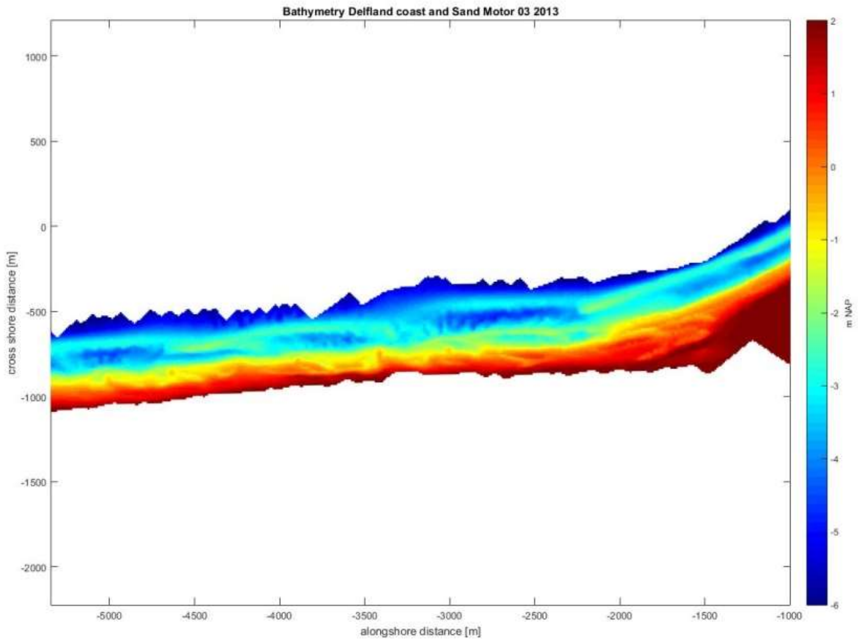

Figure 72: Section of the NEMO measurement area just south of the Sand Motor, for March 2013. Subtidal bars (blue hues) show a weakly rhythmic pattern, and are rather faint. Near the Sand Motor the remains of double bar system are faintly visible. The connection to the subtidal bar of the Sand Motor is now dominated by the latter. In the intertidal area (yellow to orange hues), between -5000m and -3000m, coastal groins have re-emerged. These force the existence of rip channels near the heads of these groins. Close to the Sand Motor patterns are hard to describe and rather faint.

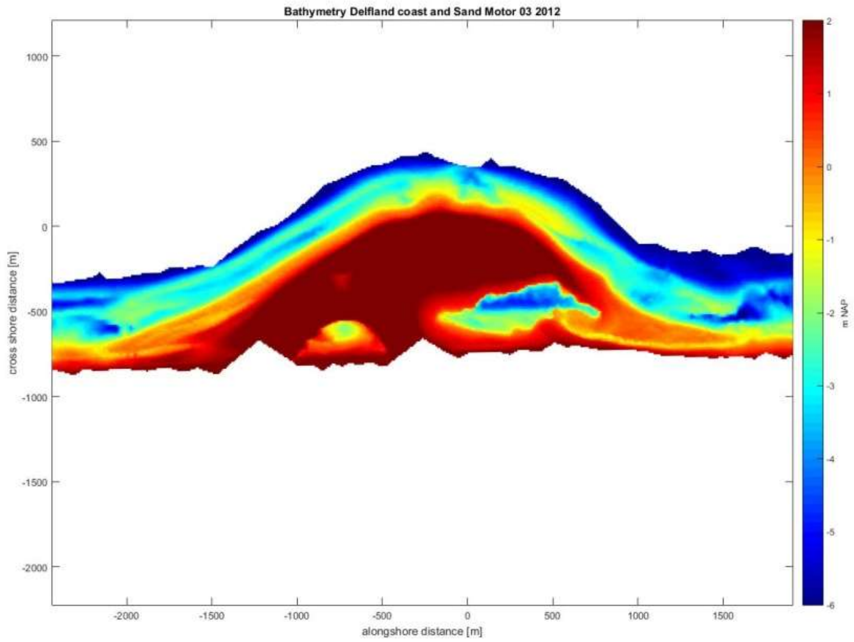

Figure 73: Sand Motor measurement area, for March 2012. Subtidal bar (blue to green hues) along the south side is continuous and linear. The tip of the Sand Motor shows mushroom-like transverse bars, which connect to the intertidal area, causing a wavy coastline. The subtidal area along the North side is hard to describe and rather faint. The intertidal area (yellow to orange hues) along the south side is very linear. Along the tip, the intertidal area is dominates by strong undulations caused by the subtidal bars. Along the northern end, the intertidal area shows longer-scale undulations. The mouth of the lagoon channel is a very sudden break in this pattern.

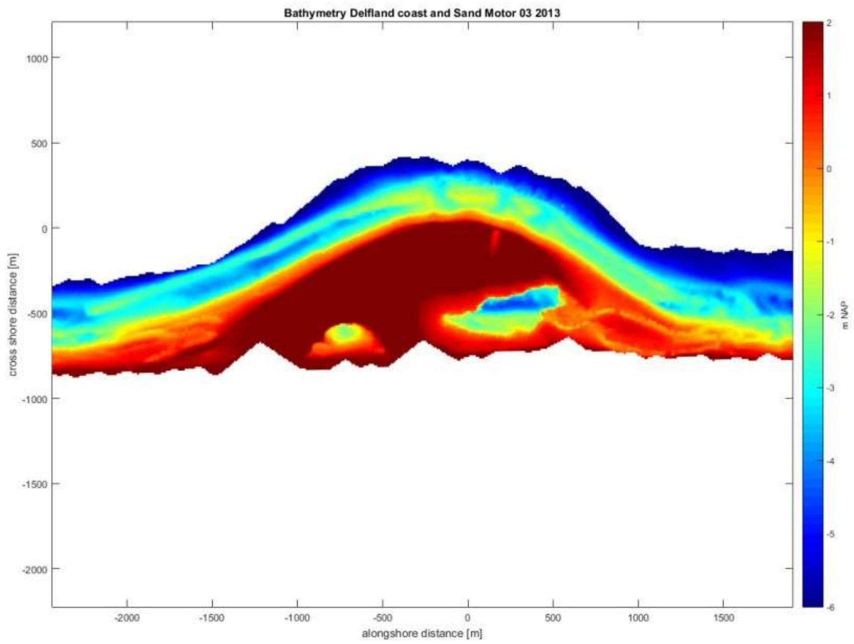

Figure 74: Sand Motor measurement area, for March 2013. Subtidal bar (blue to green hues) along the south side is continuous and linear. The tip of the Sand Motor shows mushroom-like transverse bars, which connect to the intertidal area, causing a wavy coastline. The subtidal area along the North side characterized by a linear bar with a very shallow trough. The intertidal area (yellow to orange hues) along the south side is very linear. Along the tip, the intertidal area is dominates by undulations caused by the subtidal bars. Along the northern end, the spit has developed considerably. The intertidal area has become linear. The lagoon channel has several mouths which form a very sudden break in this linear pattern.

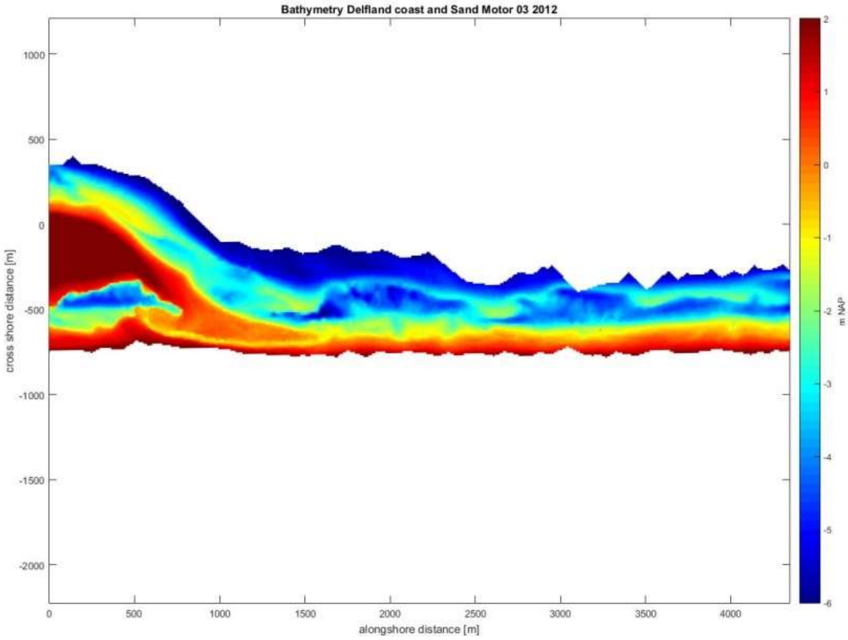

Figure 75: Section of the NEMO measurement area just north of the Sand Motor, for <u>March 2012</u>. Subtidal bars (blue to green hues) show a distinct rhythmic pattern, and are well defined (high crests and deep troughs). Near the Sand Motor the most extreme rhythmic bar, with a very deep trough, can be observed. Intertidal bars (yellow hues) show hard to describe patterns. Directly next to the channel opening two extreme rip channels are visible.

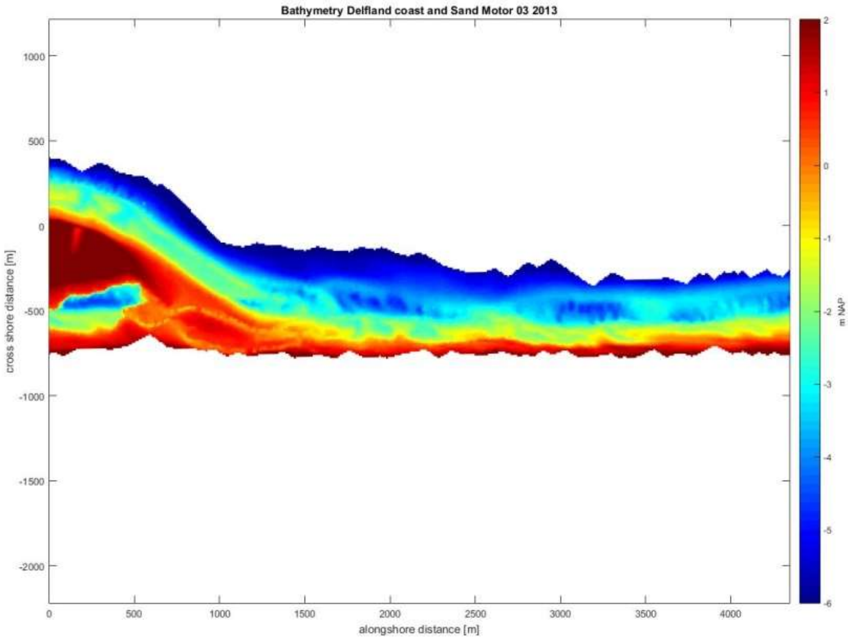

Figure 76: Section of the NEMO measurement area just north of the Sand Motor, for <u>March 2013</u>. Subtidal bars (blue hues) are faint, and show a weakly rhythmic pattern. The bar near the Sand Motor no longer stands out from the others. Intertidal bars (yellow hues) show hard to describe patterns. A lot of rip channels are visible, which seem to be more well defined nearer to the Sand Motor.

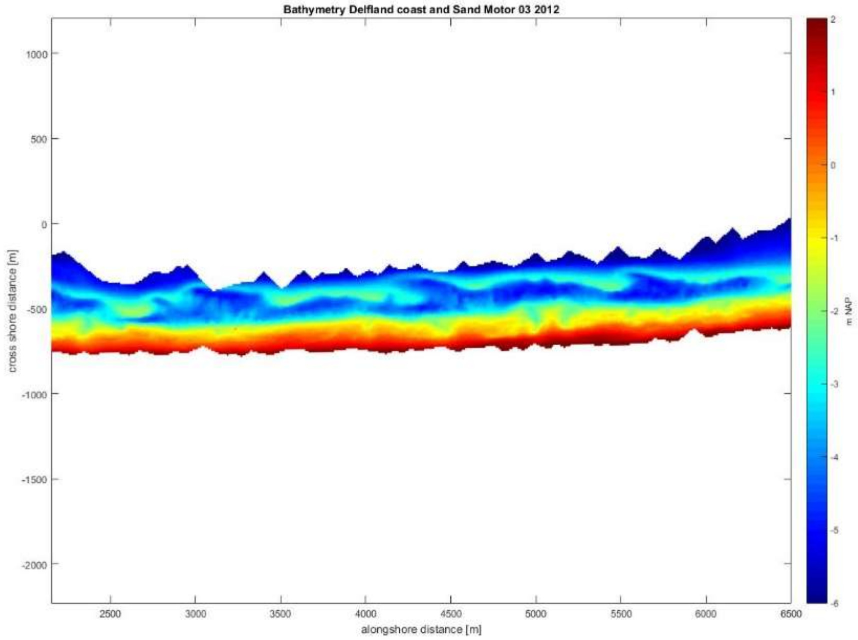

Figure 77: Northern most section of the NEMO measurement area (Scheveningen harbour is just to the right in this image), for March 2012. Subtidal bars (blue to green hues) show a distinct rhythmic pattern, and are well defined (high crests and deep troughs). Intertidal bars (yellow hues) show varying patterns, from linear sections of coastline to transverse bars.

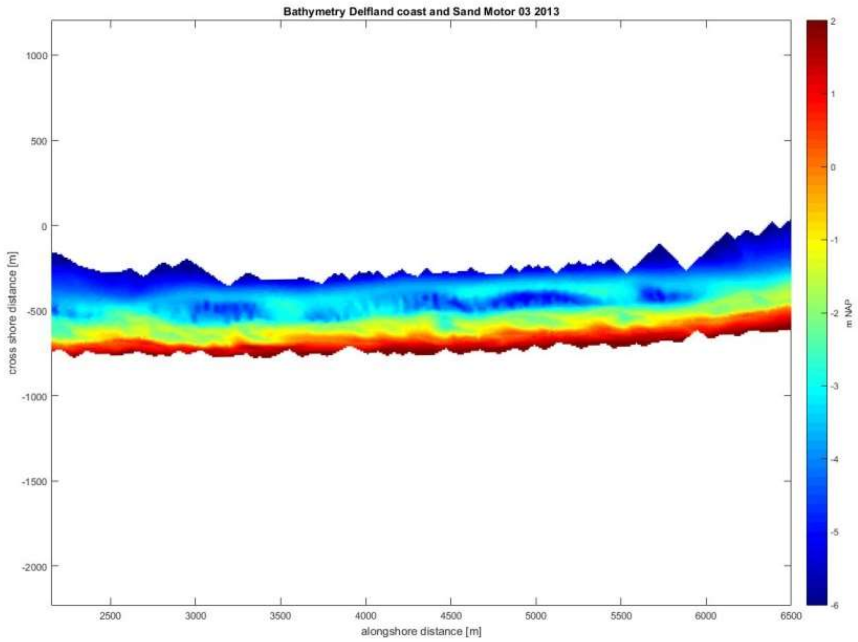

Figure 78: Northern most section of the NEMO measurement area (Scheveningen harbour is just to the right in this image), for March 2013. Subtidal bars (blue to green hues are faint, and show a weakly rhythmic pattern. Near the breakwater at Scheveningen, the subtidal bar links up to the intertidal area, and ceases to exist. In the intertidal area (yellow hues), the first groin heads have re-emerged. A lot of transverse patterns are visible, with a lot of rip channels. (yellow hues)

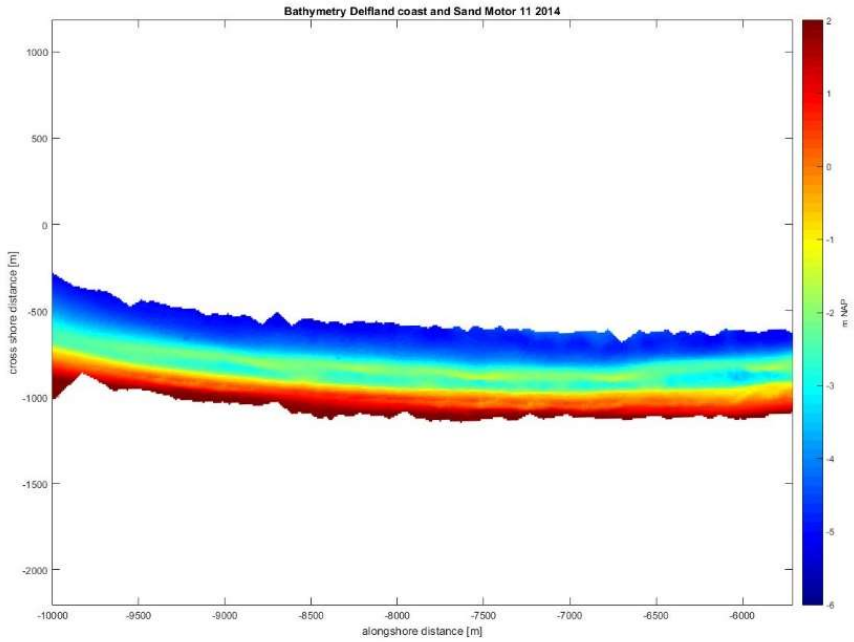

Figure 79: Southernmost section of the NEMO measurement area (Hoek van Holland is just to the right of this picture) for <u>November 2014</u>. Subtidal bar (blue to green hues) is more or less longshore linear. Some variability in crest height is visible, which seems to increase around -6500m. Intertidal bars (yellow to orange hues) show faint linear bar-rip pattern around -7400m. In other areas intertidal patterns are very faint and hard to describe.

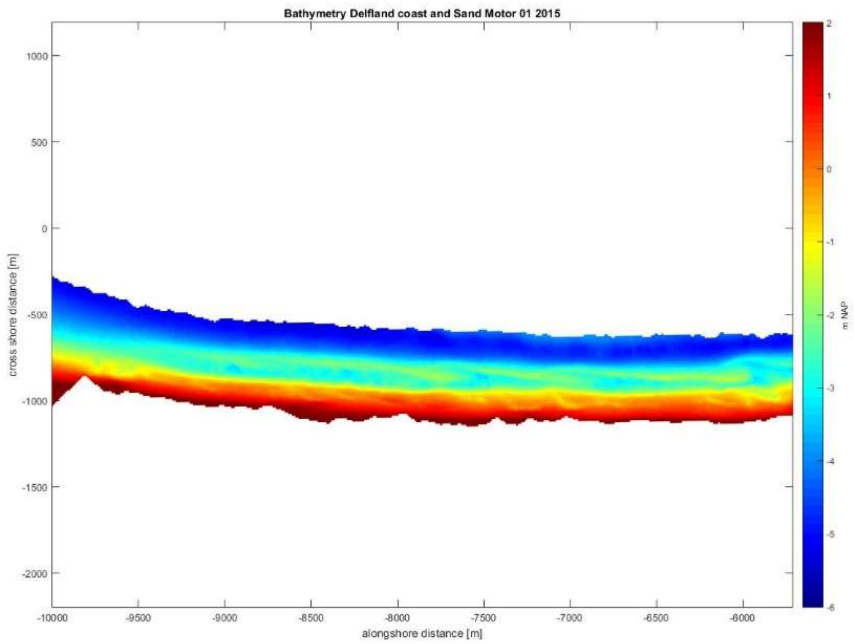

Figure 80: Southernmost section of the NEMO measurement area (Hoek van Holland is just to the right of this picture) for <u>January 2015</u>. From -9000m onwards the subtidal area (blue to green hues) shows rhythmic bars, which become slightly more rhythmic toward -6000m. Intertidal bars (yellow to orange hues) shows varying amounts of variability. Some well-defined rip channels are visible.

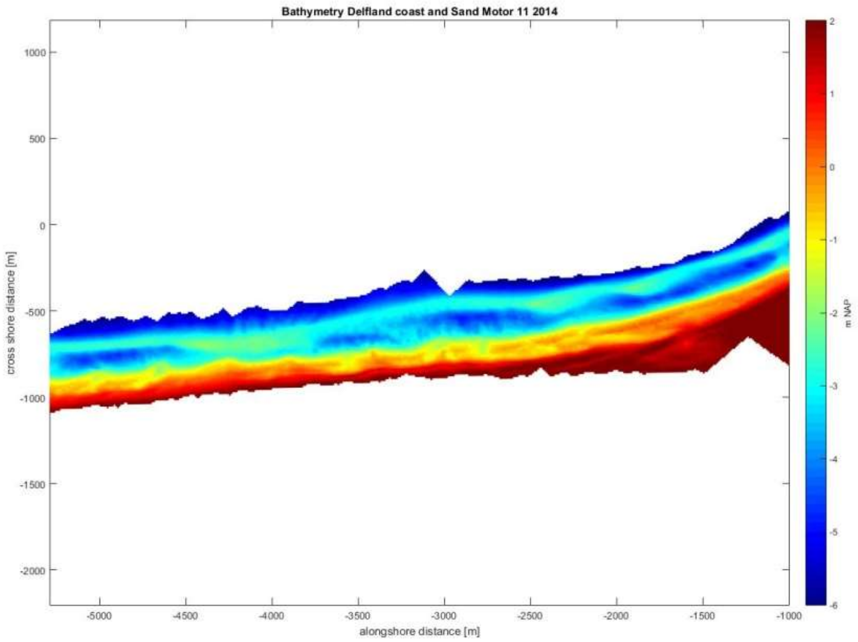

Figure 81: Section of the NEMO measurement area just south of the Sand Motor, for November 2014. Subtidal bars (blue hues) show a distinct rhythmic pattern, and are well defined (high crests and deep troughs). Near the Sand Motor, between -2500m and -1000m, the longshore length scale of the rhythmicity's decreases. Intertidal area (yellow to orange hues) is strongly influenced by the re-emerged coastal groins, forcing very distinct rip channels. From -2500m onwards, this pattern abruptly stops. From there on a more linear bar-rip pattern is visible.

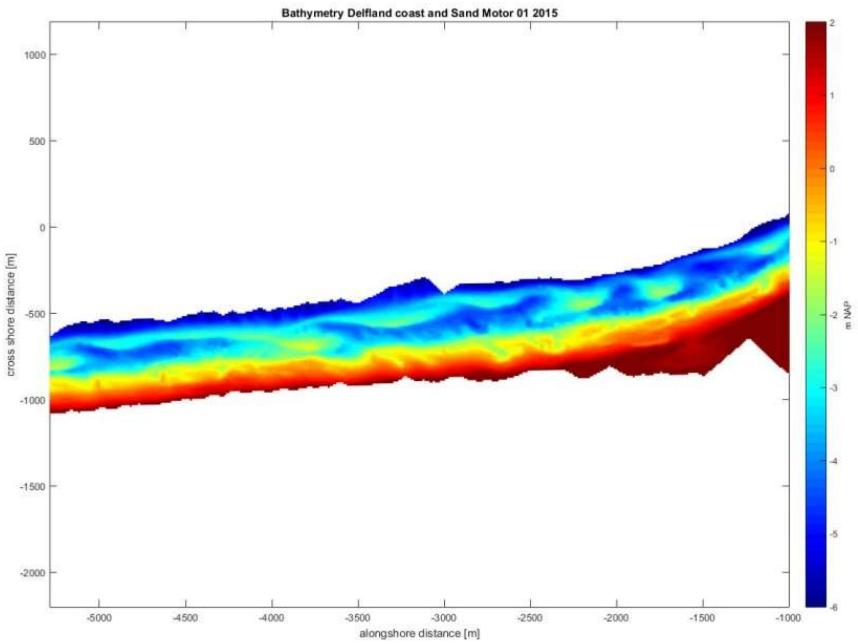

Figure 82: Section of the NEMO measurement area just south of the Sand Motor, for January 2015. Subtidal bars (blue hues) are strongly rhythmic bars. This pattern becomes more extreme toward the Sand Motor. Intertidal area (yellow to orange hues) is strongly influenced by the re-emerged coastal groins, forcing very distinct rip channels. From -2500m onwards, this pattern abruptly stops. From there on the variability develops freely.

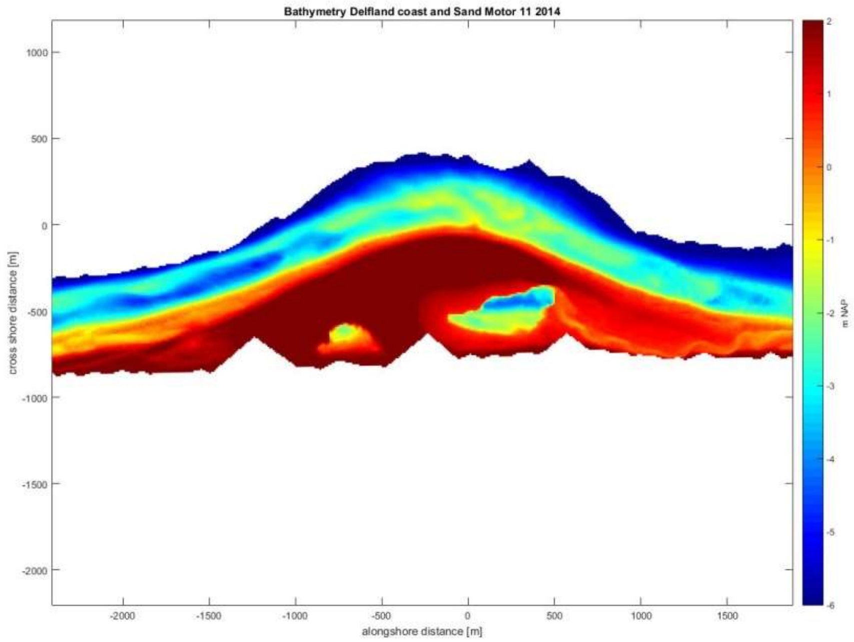

Figure 83: Sand Motor measurement area, for <u>November 2014</u>. Subtidal bar (blue to green hues) along the south side is mildly rhythmic. The tip of the Sand Motor shows cloud-like bars, which sometimes connect to the intertidal area. The subtidal area along the North side show hook-shaped bars, which connect to the intertidal area, and rather faint. The intertidal area (yellow to orange hues) along the south side and tip is quite linear. Along the northern end, there seem to be some faint intertidal features along the spit. The mouth of the lagoon channel is a very sudden break in this pattern.

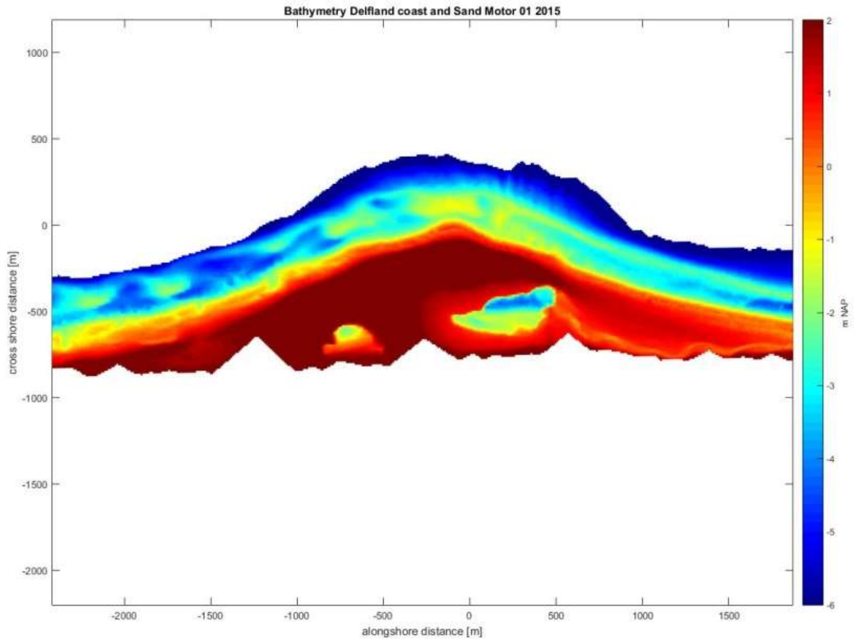

Figure 84: Sand Motor measurement area, for <u>January 2015</u>. Subtidal bar (blue to green hues) along the south side continue to show extremely variably patterns, which continue toward the tip of the Sand Motor. The subtidal area along the North side is dominated by a longshore bar. The trough behind this bar becomes deeper toward the mouth of the lagoon channel. The intertidal area (yellow to orange hues) along the south side and tip shows a very wavy coastline, caused by the variably subtidal features in this area. Along the northern end, there seem to be some faint intertidal features along the spit. The mouth of the lagoon channel is a very sudden break in this pattern. Note that the channel opening lies well outside the Sand Motor measurement area.

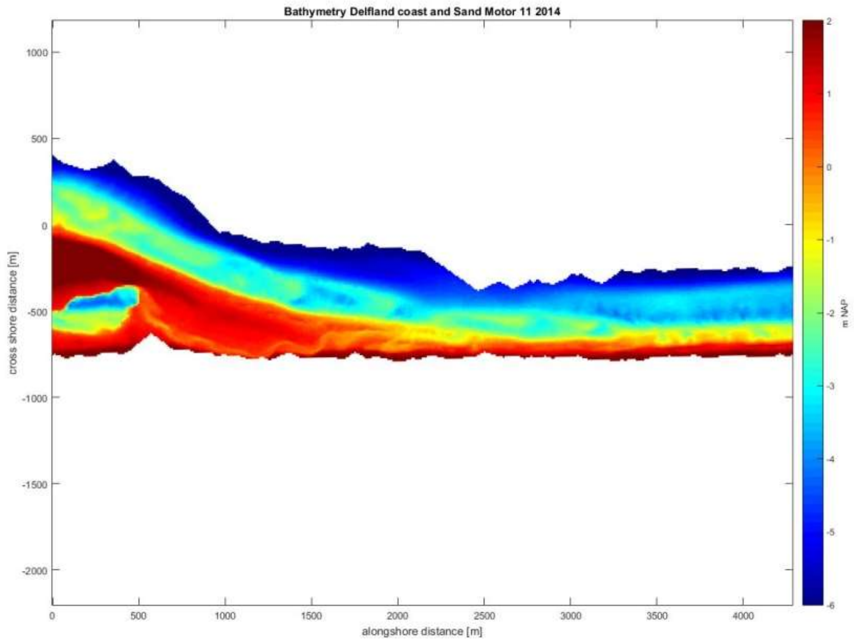

Figure 85: Section of the NEMO measurement area just north of the Sand Motor, for November 2014. At the connection with the Sand Motor, subtidal bars (blue to green hues) continue to show a pattern of hook shaped bars. At +3000m, this pattern stops. Intertidal area (yellow to orange hues) behind the subtidal hook shaped bars shows very faint patterns.

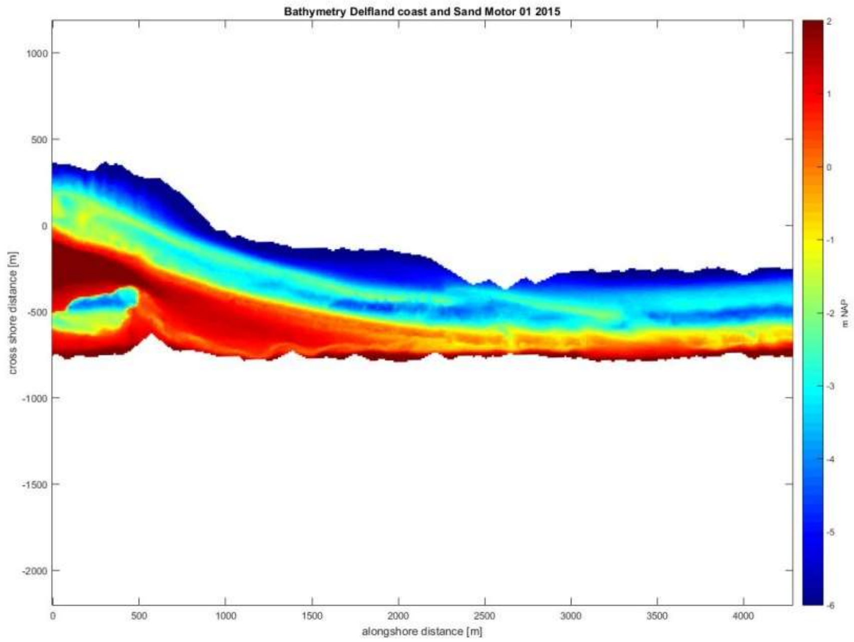

Figure 86: Section of the NEMO measurement area just north of the Sand Motor, for January 2015. At the connection with the Sand Motor, subtidal bar (blue to green hues) has formed a disconnected oblique section between +2000m and +3500m (in front of the lagoon channel opening). The intertidal area (yellow to orange hues) is dominated by well-defined longshore bars.

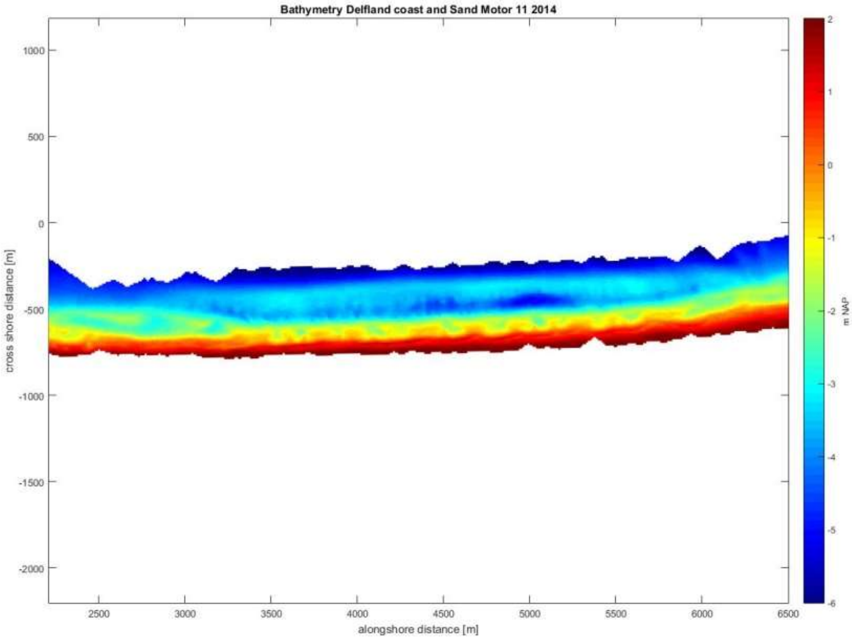

Figure 87: Northern most section of the NEMO measurement area (Scheveningen harbour is just to the right in this image), for November 2014. Subtidal area (blue to green hues) show a faint longshore bar, which is not connected to the hook shaped bars near the Sand Motor. The intertidal area (yellow to orange hues) show transverse bars and rip channels, which seem to be forced by the re-emerging heads of coastal groins.

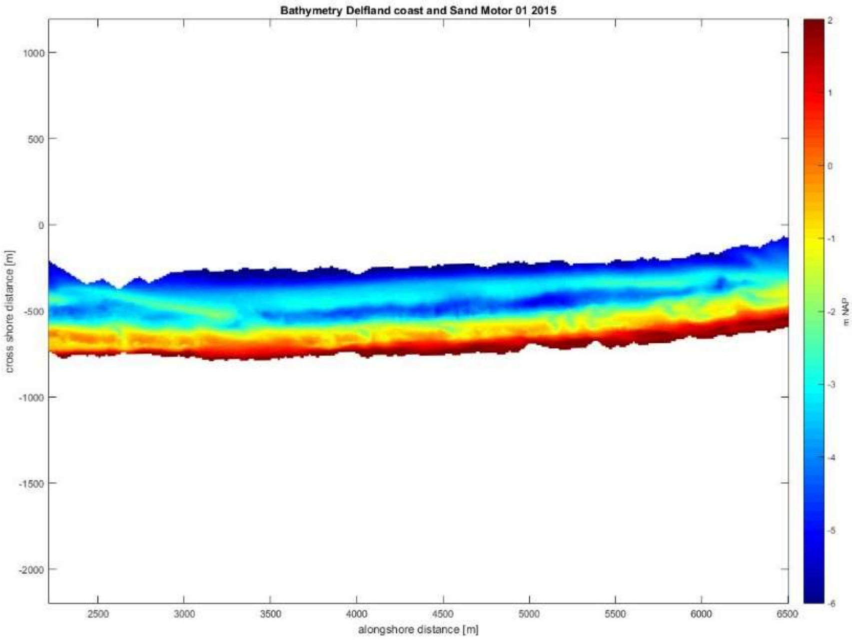

Figure 88: Northern most section of the NEMO measurement area (Scheveningen harbour is just to the right in this image), for January 2015. Subtidal area (blue to green hues) is dominated by a longshore bar. The intertidal area (yellow to orange hues) show transverse bars and rip channels, which seem to be related to the re-emerging heads of coastal groins.

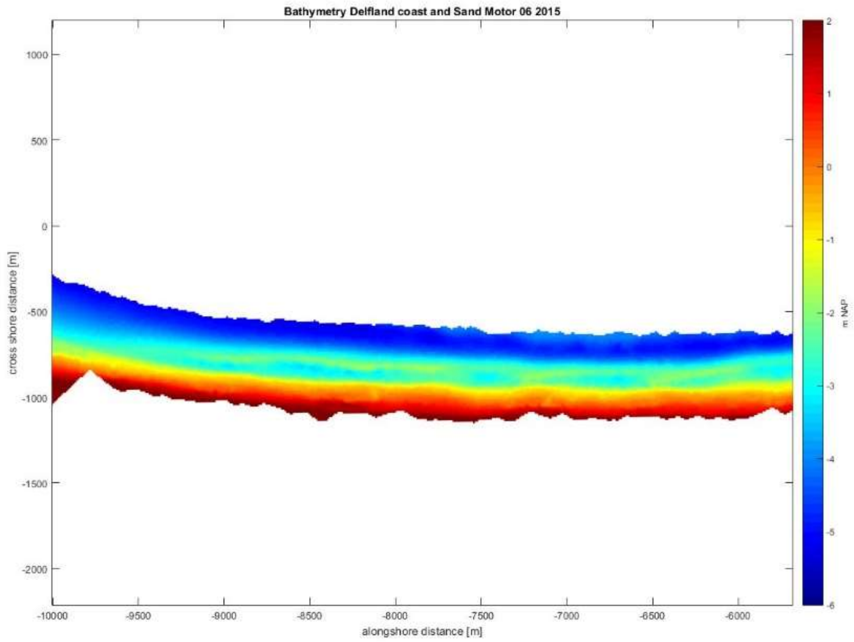

Figure 89: Southernmost section of the NEMO measurement area (Hoek van Holland is just to the right of this picture) for <u>June 2015</u>. From -9000m to -6000m onwards the subtidal area (blue to green hues) shows rhythmic bars. Intertidal bars (yellow to orange hues) does not show well developed patterns. Some faint rip channels are visible.

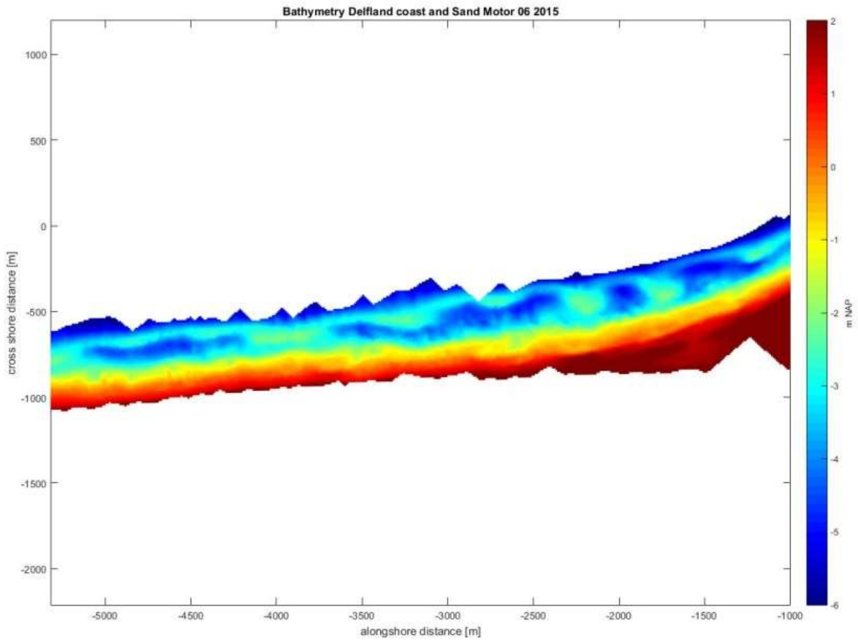

Figure 90: Section of the NEMO measurement area just south of the Sand Motor, for <u>June 2015</u>. Subtidal bars (blue hues) are strongly rhythmic bars (variation in crest height somewhat less than in January). This pattern becomes more extreme toward the Sand Motor. Intertidal area (yellow to orange hues) is influenced by the re-emerged coastal groins, forcing some rip channels, but overall the intertidal area is a lot more linear than it was in January. From -2500m onwards, this pattern abruptly stops. From there on the variability develops freely.

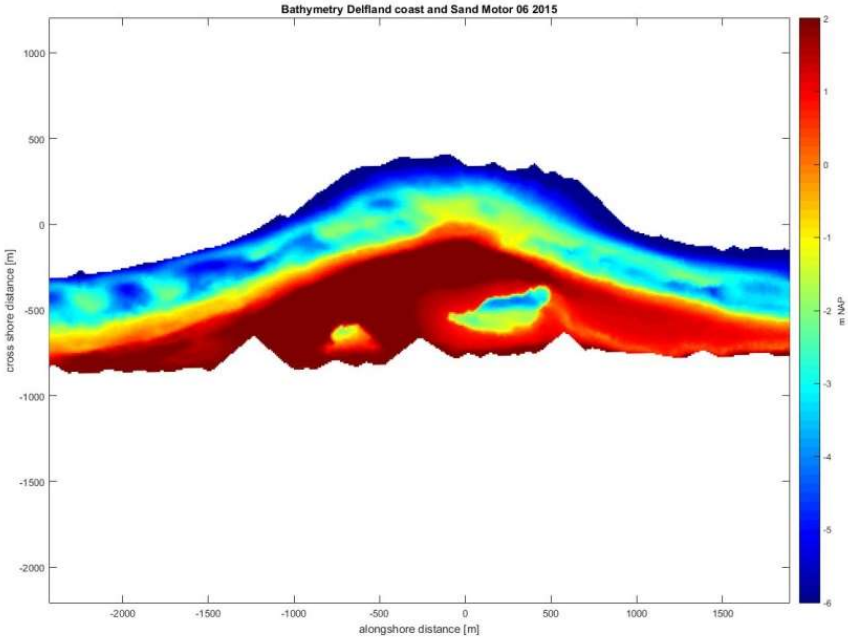

Figure 92: Sand Motor measurement area, for June 2015. Subtidal bar (blue to green hues) along the south side continue to shows extremely variably patterns. At the tip of the Sand Motor these subtidal features connect to shore. Along the north side the subtidal bar is quite linear. The intertidal area (yellow to orange hues) along the south side shows some undulation, related to the variably subtidal features in this area. Along the northern end the intertidal area is linear.

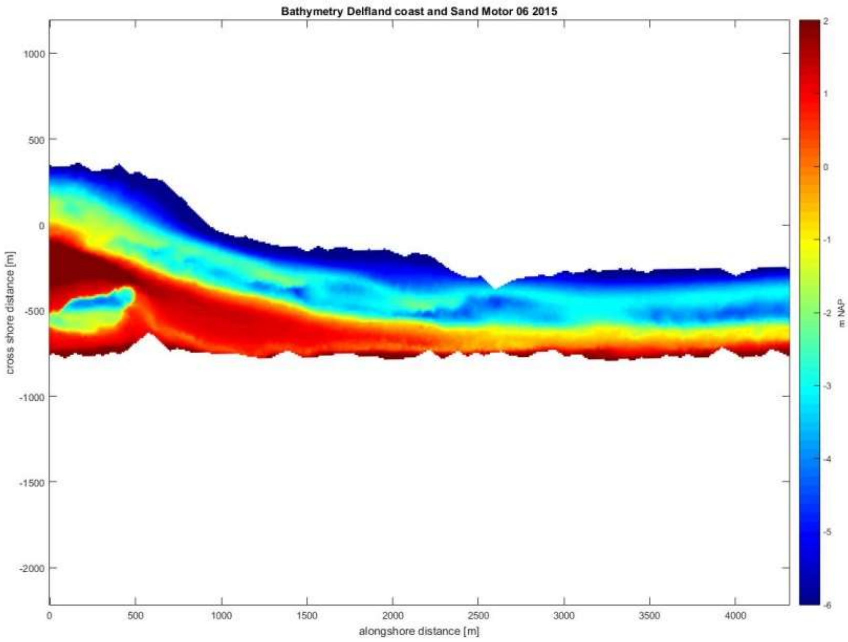

Figure 91: Section of the NEMO measurement area just north of the Sand Motor, for June 2015. At the connection with the Sand Motor, subtidal bar (blue to green hues) is rhythmic. The intertidal area (yellow to orange hues) is dominated by coastal groins.

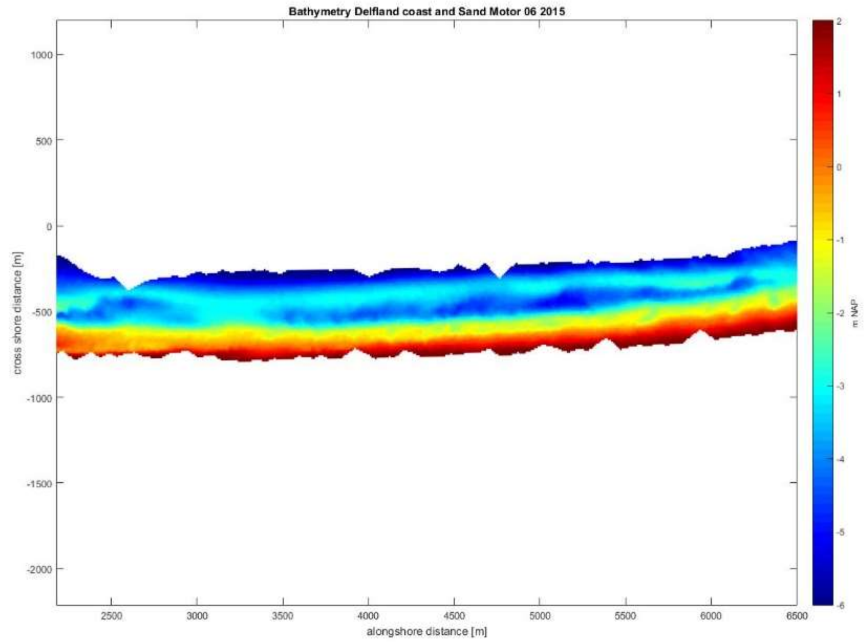

Figure 93: Northern most section of the NEMO measurement area (Scheveningen harbour is just to the right in this image), for June 2015. Subtidal area (blue to green hues) is dominated by a longshore bar with variable crest height. The intertidal area (yellow to orange hues) is dominated by the re-emerging heads of coastal groins.

Appendix B1: Model Bathymetries

MODEL BATHY ID	DATE	AV SUB	CHECK SUB	AV INTER	CHECK INTER	ALONGSHORE [M]
ARTIF_BATHY_01	24-mar-2012	0,2899	11,1251	0,1385	5,5161	5331
ARTIF_BATHY_02	24-mar-2012	0,3546	5,5861	0,0707	6,759	-4844
ARTIF_BATHY_03	24-mar-2012	0,4275	-7,4371	0,142	-24,7314	5074
ARTIF_BATHY_04	24-mar-2012	0,1074	-38,8988	0,0715	7,1765	-1267
ARTIF_BATHY_05	24-mar-2012	0,3218	-2,4257	0,1829	21,5405	66
ARTIF_BATHY_06	2-jul-14	0,0897	7,6274	0,0622	-0,0609	-7794
ARTIF_BATHY_07	2-jul-14	0,2138	7,9962	0,1316	-9,9745	4772
ARTIF_BATHY_08	2-jul-14	0,1233	-1,4159	0,1125	0,8773	3959
ARTIF_BATHY_09	6-sep-14	0,2591	-7,934	0,0598	7,4441	-6182
ARTIF_BATHY_10	6-sep-14	0,1335	-9,4125	0,0668	-6,9806	-7568
ARTIF_BATHY_11	6-sep-14	0,2698	-6,9418	0,0992	-4,3738	-47
ARTIF_BATHY_12	6-sep-14	0,2059	5,5226	0,1319	-0,3956	5286
ARTIF_BATHY_13	6-sep-14	0,1016	2,1369	0,1051	9,0682	4059
ARTIF_BATHY_14	6-sep-14	0,0697	5,0875	0,0547	-9,2157	-9402
ARTIF_BATHY_15	1-mrt-13	0,1552	-8,5585	0,1048	7,6805	-6959
ARTIF_BATHY_16	1-mrt-13	0,3401	2,9439	0,0869	3,8812	-4547
ARTIF_BATHY_17	1-mrt-13	0,2767	-8,6459	0,1665	1,203	93
ARTIF_BATHY_18	1-mrt-13	0,1549	-7,8067	0,0664	-2,3009	-1229
ARTIF_BATHY_19	1-mrt-13	0,2782	-3,9488	0,1467	1,628	3044
ARTIF_BATHY_20	1-mrt-13	0,2586	-0,437	0,1131	-4,16	4501
ARTIF_BATHY_21	1-mrt-13	0,2537	-7,3698	0,0855	4,6076	5039
ARTIF_BATHY_22	8-apr-13	0,2601	6,6578	0,0855	-3,5492	-4112
ARTIF_BATHY_23	8-apr-13	0,1399	-13,9268	0,0593	-4,8208	-1424
ARTIF_BATHY_24	8-apr-13	0,2626	-7,8958	0,11	-8,0729	3030
ARTIF_BATHY_25	8-apr-13	0,2272	-3,8079	0,0947	8,6854	4577
ARTIF_BATHY_26	4-jul-13	0,2872	5,429	0,0876	3,6485	-4988
ARTIF_BATHY_27	4-jul-13	0,0677	-12,0068	0,0596	-14,1093	-8942
ARTIF_BATHY_28	4-jul-13	0,1388	-5,5751	0,0902	-8,0634	-6989
ARTIF_BATHY_29	4-jul-13	0,1533	2,9232	0,0539	7,3203	-1366
ARTIF_BATHY_30	4-jul-13	0,2259	-8,5154	0,1721	-8,7571	83
ARTIF_BATHY_31	4-jul-13	0,2781	0,6512	0,0919	-2,2959	5155
ARTIF_BATHY_32	26-aug-13	0,2264	-2,1309	0,1983	6,8863	42
ARTIF_BATHY_33	26-aug-13	0,2261	1,5587	0,0965	5,9066	-450
ARTIF_BATHY_34	26-aug-13	0,197	-9,2526	0,0881	-1,108	-4009
ARTIF_BATHY_35	26-aug-13	0,1671	9,05	0,1037	4,6659	669
ARTIF_BATHY_36	13-dec-13	0,1378	-0,6659	0,1018	8,5501	-7758
ARTIF_BATHY_37	13-dec-13	0,0596	3,1524	0,0653	1,7661	-9457
ARTIF_BATHY_38	13-dec-13	0,2276	-6,8828	0,0849	-5,4542	81
ARTIF_BATHY_39	13-dec-13	0,3263	3,7658	0,0857	-9,065	5070
ARTIF_BATHY_40	19-feb-14	0,0942	9,5328	0,0651	-6,6971	-9006
ARTIF_BATHY_41	19-feb-14	0,2509	-7,919	0,0595	-0,4088	-1071

ARTIF_BATHY_42	19-feb-14	0,2314	1,7884	0,0764	3,9167	5374
ARTIF_BATHY_43	24-apr-14	0,2014	2,6945	0,0519	4,3888	-6149
ARTIF_BATHY_44	24-apr-14	0,0887	-22,3456	0,0479	-2,3648	-6919
ARTIF_BATHY_45	24-apr-14	0,3713	-2,0037	0,097	6,9876	-4952
ARTIF_BATHY_46	2-jul-14	0,2483	-4,8127	0,0963	4,0154	125
ARTIF_BATHY_47	2-jul-14	0,0865	6,7024	0,0588	-5,1952	-7379
ARTIF_BATHY_48	1-nov-14	0,2151	2,6036	0,0666	11,1669	862
ARTIF_BATHY_49	1-nov-14	0,2257	-2,8522	0,1234	-3,333	5116
ARTIF_BATHY_50	24-jan-15	0,2993	-8,2412	0,0881	-9,6454	-5909
ARTIF_BATHY_51	24-jan-15	0,0812	5,4078	0,0424	-0,9088	1041
ARTIF_BATHY_52	24-jan-15	0,2953	-0,664	0,1182	6,0099	5024
ARTIF_BATHY_53	24-1-2015	0,394	-7,2917	0,1157	4,8027	-376
ARTIF_BATHY_54	16-6-2015	0,4215	9,6543	0,1138	-0,3539	-176
ARTIF_BATHY_55	12-3-2015	0,3861	-4,2145	0,1392	3,2496	-82
ARTIF_BATHY_56	5-6-2015	0,4973	-5,257	0,0681	-1,904	-2106
ARTIF_BATHY_57	16-jul-15	0,5404	-4,7326	0,0833	3,9608	-1839
ARTIF_BATHY_58	5-6-2015	0,5537	5,5027	0,0676	-2,6167	-2061
ARTIF_BATHY_59	22-sep-15	0,5728	6,1581	0,0948	0,3162	-1725
ARTIF_BATHY_60	24-1-2015	0,4355	0,9001	0,1168	-5,545	-3281
ARTIF_BATHY_61	5-6-2015	0,4743	1,0667	0,0926	-2,9153	-3326
ARTIF_BATHY_62	24-1-2015	0,4555	3,2267	0,1327	-5,3597	-1045
ARTIF_BATHY_63	30-may-12	0,2382	-7,9615	0,1407	-7,3433	63

Table 14: Overview of model bathymetry information. First column: ID, second column date of original measured bathymetry. Second column: subtidal bulk alongshore bathymetric variability of model bathymetry. Third column: check with measured Bulk variability. Fourth column: intertidal bulk variability for model bathymetry. Fifth column: check with measured bulk variability. Sixth column: original alongshore coordinate of the tile.

BATHY ID	SUBTIDAL	INTERTIDAL	REMARKS
ARTIF_BATHY_01	Mild RBB	Well defined rips; LBT to TBR like	High variability in intertidal region and mild variability in subtidal area was reason for cutting
ARTIF_BATHY_02	RBB	Trough and rip: LBT to RBB	Well defined subtidal rhythmicity in combination with mild short scale variability in intertidal
ARTIF_BATHY_03	RBB	One well defined TBR	Intertidal variability is hugely underestimated. Locally the TBR feature is present, but instead of filling up one bin in the matrix, it is now averaged with local variability of adjacent intertidal area, which can't be cut off due do subtidal feature
ARTIF_BATHY_04	LBT	Linear	Subtidal is hugely underestimated: Var is low, so small changes result in large relative differences
ARTIF_BATHY_05	TBR	TBR	Intertidal is overestimated, due to the subsequent repeating of the TBR feature, which doesn't happen in reality
ARTIF_BATHY_06	LBT	Linear beach	Low in both sub and inter
ARTIF_BATHY_07	Mild RBB	RBB to TBR	Low in sub and very high inter
ARTIF_BATHY_08	LBT to mild TBR	Groin related medium var	Low in sub and medium high inter
ARTIF_BATHY_09	RBB	LBT ish, short length scale	Long, mild RBB n subtidal, some faint rip channels in intertidal
ARTIF_BATHY_10	Very mild RBB	LBT ish, short length scale	Intertidal comparable to run 09, subtidal smaller bar, less variable
ARTIF_BATHY_11	TBR ish	TBR ish	Very patchy bars dominating both subtidal and intertidal areas near the tip
ARTIF_BATHY_12	LBT to mild RBB	nice (groin related) rip channels	Quite low subtidal and medium intertidal
ARTIF_BATHY_13	LBT	LBT ish,	Very low subtidal and medium intertidal
ARTIF_BATHY_14	LBT to mild RBB	Linear beach	
ARTIF_BATHY_15	LBT	LBT: One well defined rip channel	Low subtidal vs medium intertidal
ARTIF_BATHY_16	Mild RBB	Groin related medium var	Low subtidal vs medium (groin related) intertidal
ARTIF_BATHY_17	TBR	TBR	Three TBR rips, running through subtidal and intertidal
ARTIF_BATHY_18	LBT	Linear beach	Low in both sub and inter
ARTIF_BATHY_19	RBB	LBT to TBR	Medium variable sub-, highly variable intertidal
ARTIF_BATHY_20	RBB	TBR ish	Medium variable sub-, medium high variable intertidal

ARTIF_BATHY_21	RBB	LBT ish	Medium variable sub-, medium variable intertidal
ARTIF_BATHY_22	RBB	Groin related medium var	Medium var in sub- and intertidal
ARTIF_BATHY_23	LBT	linear beach	Low var in subtidal and intertidal. Note that the low absolute values blow up the relative check for the subtidal region
ARTIF_BATHY_24	RBB	LBT to TBR	Medium high subtidal with medium high intertidal; some very nice intertidal rips
ARTIF_BATHY_25	RBB	LBT to TBR	Medium var in sub- and intertidal
ARTIF_BATHY_26	RBB	Groin related medium var	Medium var in sub- and intertidal
ARTIF_BATHY_27	LBT	LBT - linear beach	Low var in subtidal and intertidal. Note that the low absolute values blow up the relative check
ARTIF_BATHY_28	LBT to mild RBB	LBT	Low subtidal, medium intertidal var. Some nice rips in intertidal area
ARTIF_BATHY_29	LBT	Linear beach	Low var in subtidal and intertidal. Note that the low absolute values blow up the relative check
ARTIF_BATHY_30	TBR	TBR	Medium subtidal var, very high intertidal var. TBR running through intertidal into subtidal
ARTIF_BATHY_31	RBB	LBT	Medium high in subtidal, medium in intertidal. Two very nice intertidal rips, one will probably link up with subtidal rip!!
ARTIF_BATHY_32	TBR	TBR	Transverse bars running through the intertidal into the subtidal
ARTIF_BATHY_33	TBR ish	Linear beach/TBR	Hook shaped transverse bar, not much else in intertidal
ARTIF_BATHY_34	RBB	Groin related medium var	Medium low subtidal var, medium intertidal
ARTIF_BATHY_35	TBR ish	TBR ish	Low subtidal, medium intertidal var. Small TBR northern side SM => Link to Astrid!
ARTIF_BATHY_36	Fading LBT	Very asymmetric TBR	Low subtidal, medium intertidal; Well developed, very asymmetrical TBR in intertidal
ARTIF_BATHY_37	LBT LBT	LBT to TBR	Low subtidal: Double bar, LBT. Medium low intertidal; one rip channel
ARTIF_BATHY_38	TBR	TBR	Medium var subtidal, medium var intertidal, And yet: TBR
ARTIF_BATHY_39	RBB	LBT to TBR	Medium var subtidal and intertidal
ARTIF_BATHY_40	LBT	LBT	Low subtidal, medium low intertidal var. Scarp in supratidal, second (non-significant) bar subtidal
ARTIF_BATHY_41	LBT	LBT	Mildly variably LBT in subtidal, small features in intertidal
ARTIF_BATHY_42	RBB	Groin related LBT	Medium to medium low in both subtidal and intertidal
ARTIF_BATHY_43	Mild RBB	Linear beach	Medium low var subtidal, low var intertidal

ARTIF_BATHY_44	LBT	Linear beach	Low in subtidal and intertidal. Check mis match in subtidal due to small absolute differences
ARTIF_BATHY_45	RBB	Groin related rips	Medium to high subtidal variability, medium intertidal variability
ARTIF_BATHY_46	TBR	TBR	Medium var in sub- and intertidal, TBR running through the intertidal into the subtidal
ARTIF_BATHY_47	LBT	LBT	Low subtidal and intertidal
ARTIF_BATHY_48	RBB	LBT	Intertidal check is too high, but absolute difference is ok
ARTIF_BATHY_49	RBB	Groin related	Medium subtidal var, medium high intertidal
ARTIF_BATHY_50	RBB	Groin related	
ARTIF_BATHY_51	LBT	Linear beach	LBT northern side SM
ARTIF_BATHY_52	RBB	Groin related rips	Medium high subtidal and intertidal var
ARTIF_BATHY_53	TBR	TBR	Large TBR running through intertidal and subtidal. Very asymmetric
ARTIF_BATHY_54	TBR	TBR	Large TBR running through intertidal and subtidal. Very asymmetric
ARTIF_BATHY_55	TBR	TBR	Large TBR running through intertidal and subtidal. 2 rips, both very asymmetric
ARTIF_BATHY_56	TBR	LBB	Very high subtidal var, low intertidal var
ARTIF_BATHY_57	Extreme RBB	LBT ish	Very high subtidal var, medium intertidal var Some months after 'storm' event
ARTIF_BATHY_58	TBR	LBT ish	Very high subtidal var, low intertidal var. Some months after 'storm' event
ARTIF_BATHY_59	Extreme RBB	LBT ish, one rip channel	Very high subtidal, medium intertidal. Long time after 'storm event'
ARTIF_BATHY_60	Extreme RBB	TBR ish	Just after 'storm'; intertidal rip links up with subtidal rip: generated by same event
ARTIF_BATHY_61	Extreme RBB	TBR ish	Months after 'storm'; intertidal rip have beer reshaped, subtidal rip still has same orientation: Subtidal still reminiscent of storm event, intertidal has been reshaped by more recent conditions
ARTIF_BATHY_62	Extreme RBB	TBR ish	Just after 'storm'; not as nice as 60
ARTIF_BATHY_63	TBR	TBR	

Table 15: Extra information about model bathymetries. First column: Model bathymetry ID. Second column: Visually discernible patterns in subtidal area. Third column: Visually discernible patterns in intertidal area. Fourth column: remarks